Interplay of ionizing radiation, oxygen, ROS and age-associated diseases

TECHNISCHE UNIVERSITÄT DARMSTADT

Vom Fachbereich Chemie

der Technischen Universität Darmstadt

zur Erlangung des akademischen Grades eines

Doctor rerum naturalium (Dr. rer. nat.)

genehmigte

Dissertation

vorgelegt von

Tamara Džinić, Magistra

aus Tuzla, Bosnien und Herzegowina

Referent: Prof. Dr. Norbert A. Dencher

Korreferent: PD Dr. Tobias Meckel

Tag der Einreichung: 15. März 2017

Tag der mündlichen Prüfung: 15. Mai 2017

Darmstadt 2017

D17

Interplay of ionizing radiation, oxygen, ROS and age-associated diseases

Vom Fachbereich Chemie
der Technischen Universität Darmstadt

zur Erlangung des Grades eines
Doctor rerum naturalium (Dr. rer. nat.)

genehmigte Dissertation
von Tamara Džinić, Magistra
aus Tuzla, Bosnien und Herzegowina

Referenten: Prof. Dr. Norbert A. Dencher
PD Dr. Tobias Meckel

Tag der Einreichung: 15.03.2017
Tag der mündlichen Prüfung: 15.05.2017

Darmstadt 2017
D17

Die vorliegende Arbeit wurde unter Leitung von Herrn Prof. Dr. Norbert A. Dencher in der Zeit von Mai 2014 bis März 2017 im Fachbereich Chemie am Clemens-Schöpf-Institut für Organische Chemie und Biochemie, Abteilung Physikalische Biochemie, der Technischen Universität Darmstadt angefertigt. Diese Arbeit wurde von der DFG im Rahmen des Graduiertenkollegs „Molekulare und zelluläre Reaktionen auf ionisierende Strahlung“ (GRK 1657) gefördert.

Publications

Parts of the doctoral thesis are published:

Džinić T, Hartwig S, Lehr S, Dencher NA. (2016). Oxygen and differentiation status modulate the effect of X-ray irradiation on physiology and mitochondrial proteome of human neuroblastoma cells. *Arch. Physiol. Biochem.*, 122: 257-265.

Manuscript submitted (March 2017):

Džinić T, Dencher NA. (2017). Oxygen concentration and oxidative stress modulate the influence of Alzheimer's disease $A\beta_{1\text{-}42}$ peptide on human neuroblastoma cells. (submitted to *PNAS*).

Manuscripts for submission in 2017:

Džinić T, Čavlović L, Dencher NA. (2017). Studying hypoxia in the cell culture: controlling oxygen concentration and incubation with the hypoxia mimetic $CoCl_2$.

Džinić T, Dencher NA. (2017). The requirement of physiological O_2 concentration in cell cultivation.

Džinić T, Decker V, Meckel T, Okhrimenko I, Dencher NA. (2017). Traffic and organelle targets of Alzheimer´s disease $A\beta_{1\text{-}42}$ peptide in human neuroblastoma cells and in rat oligodendrocytes.

Džinić T, Dencher NA. (2017). The effect of low/high dose fibrillized *versus* disaggregated $A\beta_{1\text{-}42}$ on cellular physiology.

Other publications:

Siegemund M, Seifert O, Zarani M, **Džinić T**, De Leo V, Göttsch D, Münkel S, Hutt M, Pfizenmaier K, Kontermann RE. (2016). An optimized antibody-single-chain TRAIL fusion protein for cancer therapy. *MAbs*, 8: 879-891.

Antunovic M, Matic I, Nagy B, Caput Mihalic K, Skelin J, StambukJ, Josipovic P, **Dzinic T**, Pavicic I. (2017). FADD protein acts as a turning point for diverse death fates after UVB radiation of mouse embryonic fibroblasts. (submitted to *BBA - Molecular Cell Research*).

Oral presentations at conferences and other events

GRK 1657 PhD-retreat, Annweiler am Trifels (2017), Germany
Title: *Interplay of ionizing radiation, oxygen, ROS and age-associated diseases*

International conference Dementia and Neuroscience, Los Angeles (2016), USA
Title: *Implication of oxidative stress in Alzheimer´s disease*

GRK 1657 PhD-retreat, Hirschegg im Kleinwalsertal (2014/15), Austria
Title: *Interplay of ionizing radiation, oxygen, ROS and age-associated diseases*

International conference Mitochondria at the Crossroad, Strasbourg (2015), France
Title: *Interplay of ionizing radiation, oxygen, ROS and age-associated diseases*

GRK 1657 PhD-workshop, Darmstadt (2014/15), Germany
Title: *Interplay of ionizing radiation, oxygen, ROS and age-associated diseases*

Poster presentations

68. Mosbacher Kolloquium "Cell Organelles-Origin, Dynamics, Communication", Mosbach (2017), Germany
Title: *Interaction of Alzheimer´s disease $A\beta_{1-42}$ peptide with human neuroblastoma cells and their organelles*

GRK 1657 PhD-networking event with GRK 1739, Höchst im Odenwald (2016), Germany
Title: *Interplay of ionizing radiation, oxygen, ROS and age-associated diseases*

GRK 1657 PhD-retreat, Hirschegg im Kleinwalsertal (2015/16), Austria
Title: *Interplay of ionizing radiation, oxygen, ROS and age-associated diseases*

GRK 1657 PhD-retreat, Annweiler im Trifels (2016), Germany
Title: *Interplay of ionizing radiation, oxygen, ROS and age-associated diseases*

PhD-workshop at the TU Darmstadt, Darmstadt (2015), Germany
Title: *Interplay of ionizing radiation, oxygen, ROS and age-associated diseases*

German Peptide Symposium, Darmstadt (2015), Germany
Title: *Interplay of ionizing radiation, oxygen, ROS and age-associated diseases*

EACR Conference Radiation Biology and Cancer, Essen (2015), Germany
Title: *Interplay of ionizing radiation, oxygen, ROS and age-associated diseases*

GRK 1657 PhD-networking event with GRK 1739, Bonn (2016), Germany
Title: *Interplay of ionizing radiation, oxygen, ROS and age-associated diseases*

Acknowledgement

- Thank you Prof. Dr. Norbert A. Dencher for giving me the opportunity to work on an interesting topic, for all discussions and motivation. I appreciate all your contributions of time and ideas to make my PhD experience productive and stimulating.
- Dr. Tobias Meckel for being my second reviewer and for interesting scientific conversations.
- Prof. Dr. Gerhard Thiel, Prof. Dr. Boris Schmidt and Dr. Tobias Meckel for precious discussions during the Thesis Committee meeting in the frame of the Graduate College (GRK 1657).
- Prof. Dr. Markus Löbrich, speaker of the GRK 1657, for providing equipment for radiation experiments.
- AG Cardoso, particularly M.Sc. Anne Ludwig for maintaining the flow cytometer and solving all technical issues during my sessions.
- AG Laube, thank you for providing a cell culture incubator in difficult times when our incubator was broken.
- AG Thiel, particularly Sebastian Fuck, my GRK colleague, for providing the HyPer sensor and for introducing the new method for ROS measurement to me. Also, I am thankful to M.Sc. Marina Kithil for the help with the confocal microscopy and for nice time during the flow cytometry sessions.
- AG Schmitz, for giving me the opportunity to use the plate reader.
- Dr. Stefan Lehr, Dr. Sonja Hartwig and co-workers from the German Diabetes Center (Deutsches Diabetes-Zentrum, DDZ) for MALDI MS/MS analyses and for contribution to the manuscript.
- Dr. Julius Hellmann-Regen for useful advices on differentiation of SH-SY5Y cells.
- Dr. Katarzyna Kuter, I will always remember the wonderful time in the lab and outside. Thank you for inspiration!
- M.Sc. Sarah Bothe for being a dedicated student during the practical course and Master thesis. Thank you for your interest in science and for numerous questions you had for me.
- German Research Foundation (Deutsche Forschungsgemeinschaft, DFG) for financial and educational support in the frame of Graduate College 1657 “Molecular and cellular responses to ionizing radiation”.
- Dr. Victoria Decker, Dr. Manuela Kratochwil and Dr. Sven Marx thank you for introducing the laboratory to me, for showing me the methods, for nice times in the lab and during our group activities. Also, thank you for reminding me to have an ice-cream break on the balcony.
- Dr. Lidija Cavlovic for being a wonderful, loving person and for conversations in “that strange language” (Bosnian/Croatian).
- Master Students in AG Dencher: Victoria Petermann, Olga Akundin, Stefanie Ascher for nice time in the laboratory and in our social events.
- Ivan Okhrimenko from the Moscow Institute of Physics and Technology (Russia) for the exchange of knowledge and ideas during a short stay in the laboratory at the TU Darmstadt.
- Christine Schröpfer, the heart of the lab, for all your support as a technical assistant, secretary, for your advices and for being there when no one else was. Thank you for have a faith in my experiments.
- Sabine Reinhold for the support with the documentation and all nice small talks in the kitchen.

- SciMento team of the TU Darmstadt (Laura Babel, Oxana Upir, Christine Groß and Meike Egert) for the exchange of experience, knowledge, information, and for fun times in our group meetings. With you I am always few steps forward and each "Zielsetzung" until the next meeting was a tremendous way to reach my aims.
- All colleagues from the GRK 1657 for sharing your knowledge and for nice times during the GRK events.
- My friends Patricia, Anita and Sandi, I am looking forward to our reunion anytime.
- Elham Abdolahi, my dear friend, our friendship has started in the first PhD retreat of the GRK and I hope it will never end.
- Rajvinder Kaur, our friendship has started in the last PhD retreat of the GRK of my generation and I am looking forward to all our future meetings.
- My parents and my sister Tatjana for all their love and encouragement. Thank you for supporting me in all my pursuits and for being my safe harbour for all these years. I am thankful to all other family members for the moral support.
- My dear Tobias thank you for your extraordinary love, support and patience and also for being my safe harbour. I am lucky to have you in my life.

Per aspera ad astra.

"If you're going to try, go all the way. Otherwise, don't even start. This could mean losing girlfriends, wives, relatives and maybe even your mind. It could mean not eating for three or four days. It could mean freezing on a park bench. It could mean jail. It could mean derision. It could mean mockery-isolation. Isolation is the gift. All the others are a test of your endurance, of how much you really want to do it. And, you'll do it, despite rejection and the worst odds. And it will be better than anything else you can imagine. If you're going to try, go all the way. There is no other feeling like that. You will be alone with the gods, and the nights will flame with fire. You will ride life straight to perfect laughter. It's the only good fight there is."

Charles Bukowski, Faktotum (1975)

Table of Contents

1. Summary

The aim of this doctoral thesis was to investigate and to understand the implication of oxidative stress, created by the interplay of ionizing (X-ray) radiation, oxygen and neurotoxic amyloid beta (Aβ) peptide, in age-associated diseases, with the focus on Alzheimer´s disease (AD), the most common dementia. Although AD has been known for more than hundred years, its mechanisms are still intriguing and there is no cure at the moment.

High doses of ionizing radiation (IR) lead to learning and memory impairment which is characteristic for AD as well. The cumulative doses of IR used in medical imaging procedures such as computed tomography (CT) and dental X-rays present a potential danger, particularly to children whose brains are not completely developed. Although single doses of radiation used for diagnostic purposes or therapeutic treatment are relatively low, small changes on the molecular and cellular level may accumulate upon repeated exposure and result in delayed long-term defects. Thus, the most important objective of this thesis was to reveal if there is an interplay of radiation and age-associated diseases through the effects of oxygen, reactive oxygen species (ROS) and Aβ peptide implicated in AD.

Aβ peptide monomers and small oligomers (one of the players in AD) are proposed to be involved in damage and death of neurons. Since IR causes oxidative stress and inflammation, occurring in AD as well, there is a concern that radiation exposure may be linked with neurodegeneration.

2 Gy X-rays presents a commonly used fractionated dose in radiotherapy of a variety of tumors and was used in this thesis as a single radiation dose alone or combined with the previous treatment with externally applied $A\beta_{1-42}$ peptide (the most toxic form) at two environmental oxygen concentrations.

The data provided in the thesis emphasize the importance of using the appropriate model system and conditions in the cell culture such as oxygen concentration that has to be considered in studies of cellular responses to oxidative stress, IR and neurotoxic peptides.

Changes in cellular responses of non-differentiated human neuroblastoma (SH-SY5Y) cells and/or cells pre-treated with retinoic acid (RA) for induction of differentiation, in order to obtain cells that resemble neurons, were investigated in parallel under standard condition of oxygen (~21%) used in cell culture incubators, but never found in tissues of human body, and 5% O_2 which resembles physiological oxygen concentration in human brain. For this purpose, home-made low O_2 incubators were setup using plastic containers able to retain a gas mixture containing 5% or 1% O_2, 5% CO_2 and 90% or 94% N_2.
Initially, two different low oxygen concentrations (1% and 5%) were tested in SH-SY5Y cells for cell proliferation and ATP concentration as a measure of the bioenergetic status. 5% O_2 was demonstrated to be more suitable for cultivation of SH-SY5Y cell since the proliferation activity and ATP concentration were higher than in cells at 1% O_2.

The starting hypothesis was that cells exposed to non-physiological oxygen concentration and/or in the presence of Aβ peptide react differently, more sensitive or less sensitive, due to the oxygen effect (i.e. increased sensitivity due to the increased formation of harmful ROS and modulation of signaling pathways or decreased sensitivity due to the previous adaptation to these processes).

A very important result was that the oxygen concentration in the cell culture and differentiation status of SH-SY5Y cells are modulators of cellular responses to X-ray radiation and Aβ peptide as shown employing cell and molecular biology as well as biochemistry methods and techniques.

Retinoic acid used for induction of differentiation leads to morphological changes of SH-SY5Y cells (i.e. flattening of the cell body and formation of long outgrowths that resemble axons of neurons) and increase in the sensitivity to radiation and/or to Aβ peptide depending on oxygen concentration. Moreover, oxygen plays a role in differentiation and proliferation of SH-SY5Y cells since the amount of neurofilament-M, a marker of differentiation, was dependent of oxygen concentration and was higher in cells cultivated at 5% O_2 which also showed increased cell number in the proliferation assay as compared to 21% O_2.
Intracellular oxygen concentration [O_2] differs from the oxygen concentration applied to the cell culture. Using an oxygen sensitive probe, intracellular [O_2] for SH-SY5Y cells cultivated at 21% O_2 was about 10% and for cells cultivated at 5% O_2 was 0.9% determined for the first time. However, 5% O_2 was not hypoxic for SH-SY5Y cells since no expression of hypoxia inducible factor (HIF-1α) was detected.

Changes in the mitochondrial proteome isolated from SH-SY5Y cells were investigated using a combination of blue-native/2D SDS-PAGE for protein separation, subsequent staining with the fluorescent dye SYPRO Ruby and quantitation of protein spot intensities from gel images. The protein amount of selected subunits of Oxidative Phosphorylation (OxPhos) complexes and other non-OxPhos mitochondrial proteins (identified by MALDI-TOF/TOF mass spectrometry and Western blot) did not change upon irradiation with the exception of the heat shock protein 70, which amount was increased depending on oxygen concentration and differentiation status.

Monomers and small oligomers of Aβ peptide interacted with SH-SY5Y cells as detected by flow cytometry. Compartments with low pH value (i.e. lysosomes and possibly late endosomes) were the main target and the peptide interacted only to a minor extent with mitochondria and endoplasmatic reticulum, respectively, as visualized by confocal scanning microscopy.
Although site and kinetics of interaction of Aβ peptide with SH-SY5Y cells cultivated at both 21% and 5% O_2 were similar, decreased lysosomal integrity after Aβ peptide treatment of SH-SY5Y cells was observed solely at 21% O_2.

Aβ peptide alone induced only a slight increase in ROS (up to 1.2 fold), a slight increase in mitochondrial membrane potential, and no changes in ATP concentration and in glutathione (GSH) level (used as an indicator of cell´s antioxidant capacity) regardless of oxygen concentration in the cell culture.

Radiation alone led to a significant increase in ROS (~1.5 fold) and a slight increase in ATP concentration (~1.2 fold) but solely in cells at 5% O_2. A slight increase in mitochondrial membrane potential was observed at both 21% and 5% O_2. Radiation caused a slight increase in GSH level at 21% O_2 and decrease at 5% O_2 (up to 1.2 fold).

Increase in protein carbonylation (~2.5 fold) induced by oxidative stress measured in the Oxyblot assay was specific for irradiated cells at 21% O_2.
A very important target of oxidative stress is DNA, particularly mtDNA that is less studied than nuclear DNA. MtDNA was assayed using primers specific for mtDNA in PCR methods for changes in its amount and for the presence of 4977 bp deletion. Aß peptide or radiation alone caused a change in mtDNA amount depending on O_2 concentration: up to 1.3 fold decrease at 21% O_2 and up to 1.5 fold increase at 5% O_2. The occurrence of the mtDNA deletion was specific for irradiated cells at both 21% and 5% O_2 but was more pronounced at 21% O_2.

For the first time, the combined effect of Aβ peptide and IR on cellular parameters and survival was studied. Radiation combined with Aβ peptide resulted in a statistically significant increase in ROS level at both 21% (~1.2 fold) and 5% O_2 (~1.4 fold); increase in ATP concentration (1.5 fold) at 5% O_2 solely; increase in GSH level at 21% O_2 and decrease at 5% O_2 (up to 1.2 fold) and no change in the mitochondrial membrane potential.

The results of the cell death assay (measurement of apoptotic and necrotic cells by flow cytometry) revealed that $A\beta_{1-42}$ peptide or 2 Gy X-rays alone resulted in a significant increase in cell death of SH-SY5Y cells at 5% O_2 and only in a minor increase at 21% O_2. Noteworthy, Aβ peptide restored the cell death of irradiated cells to the control level or below, particularly at 5% O_2. The combination of Aβ peptide and irradiation did not lead to a significant increase in protein carbonylation, mtDNA deletion and change in mtDNA amount. Therefore, the initial level of oxidative stress determines the point at which cellular defense mechanisms occur and it is possible that even neuroprotective mechanisms are triggered in such cases.

Furthermore, this study demonstrated that the incubation time together with concentration and state of the peptide (disaggregated *versus* aggregated to fibrils) is a crucial factor in Aβ peptide toxicity. High concentration (100 µM) of aggregated peptide (induced by storage at 37 °C overnight) caused an early response (after 1 day) of SH-SY5Y cells which underwent cell death. However, the effect of disaggregated Aß peptide (100 µM) after 3 days of incubation was more pronounced than of aggregated peptide. Aβ peptide treatment decreased the percentage of apoptotic and necrotic cells (2.5 fold) in irradiated cells after 1 day. However, after 3 days, a ~2.8 fold increase in cell death as compared to non-irradiated control cells was observed.
The observed traffic of Aβ peptide towards cellular organelles and the corresponding changes in cell physiology that were dependent on the level of oxidative stress are of relevance for AD pathology.

The results obtained require the use of more physiological 5% O_2 rather than of the non-physiological 21% O_2 for cultivation of SH-SY5Y cells and studies of their response to stress,

which is crucial for outcome and reliability of experiments. Cells cultivated at 5% O_2 have displayed higher total cellular ATP concentration (~1.3 fold), lower ROS level (1.5 fold), lower protein carbonlyation (2.5 fold), lower mtDNA deletion (2 fold) as compared to cells at 21% O_2.

1. Zusammenfassung

Ziel dieser Doktorarbeit war es den Einfluß von oxidativem Stress zu verstehen, der durch das Zusammenspiel von ionisierender Strahlung, Sauerstoff und neurotoxischem Amyloid beta (Aβ) Peptid der Alzheimer Demenz (AD) entstanden ist. Obwohl AD, die häufigste Form von Demenz, seit mehr als hundert Jahren bekannt ist, sind seine Mechanismen noch nicht verstanden und es gibt zur Zeit keine Heilung.

Hohe Dosen ionisierender Strahlung führen zu Lern- und Gedächtnisstörungen, die auch für AD charakteristisch sind. Die kumulativen Dosen von ionisierender Strahlung, die in medizinischen Bildgebungsverfahren wie Computertomographie und zahnärztlichen Untersuchungen verwendet werden, stellen eine potentielle Gefahr dar, insbesondere für Kinder, deren Gehirn nicht vollständig entwickelt ist. Obwohl einzelne Dosen von Strahlung, die für diagnostische Zwecke oder Behandlung verwendet werden, relativ niedrig sind, können kleine Schäden auf molekularer und zellulärer Ebene bei wiederholter Exposition akkumulieren und zu verzögerten Langzeitdefekten führen.
So war das wichtigste Ziel dieser Arbeit zu zeigen, ob es Wechselwirkungen von Strahlung und altersbedingten Erkrankungen durch die Effekte von Sauerstoff, reaktiver Sauerstoffspezies (ROS) und Aβ Peptid gibt, die an AD beteiligt sind.

Aβ Peptid Monomere und kleine Oligomere (Akteure in AD) sollen an Schäden und Tod von Neuronen beteiligt sein. Da ionisierende Strahlung oxidativen Stress und Entzündungen verursacht, die auch in AD auftreten, besteht die Möglichkeit, dass Strahlenbelastung mit Neurodegeneration verknüpft ist.

2 Gy Röntgenstrahlen ist eine häufig verwendete Dosis in der Strahlentherapie einer Vielzahl von Tumoren und wurde in dieser Arbeit als Strahlendosis alleine oder in Kombination mit der vorherigen Behandlung mit extern applizierten $A\beta_{1-42}$ Peptid (die schädlichste Form) bei zwei unterschiedlichen Sauerstoffkonzentrationen eingesetzt.

Die in der Arbeit erhaltenen Ergebnisse betonen die Bedeutung von geeigneten Zellkulturbedingungen, insbesondere der Sauerstoffkonzentration, die in Studien der zellulären Reaktionen auf oxidativen Stress, ionisierende Strahlung und neurotoxischem Peptid eingesetzt werden müssen.

Änderungen der zellulären Reaktionen von nicht-differenzierten menschlichen Neuroblastom (SH-SY5Y) Zellen und von mit Retinsäure (RA) zur Induktion der Differenzierung vorbehandelten Zellen, die Neuronen ähneln, wurden unter drei Sauerstoffkonzentrationen parallel untersucht. Bei ~21% Sauerstoff, was gewöhnlich in Zellkultur-Inkubatoren verwendet wird, aber nie in Geweben des menschlichen Körpers vorkommt und bei 5% bzw. 1% O_2, was der physiologischen Sauerstoffkonzentration im menschlichen Gehirn ähnelt. Zu diesem Zweck wurden O_2-Inkubatoren aus Kunststoffbehältern angefertigt, in denen die Zellen in einem Gasgemisch mit 5% oder 1% O_2, 5% CO_2 und 90% oder 94% N_2 kultiviert werden konnten.

Anfänglich wurden die Auswirkungen von zwei verschiedenen niedrigen Sauerstoffkonzentrationen (1% und 5%) in SH-SY5Y Zellen auf die Zellproliferation und ATP-Konzentration als Maß für den bioenergetischen Status getestet. 5% O_2 war für die Kultivierung der SH-SY5Y Zellen besser geeignet, da die Proliferationsaktivität und die ATP-Konzentration höher waren als bei den Zellen mit 1% O_2.

Die Ausgangshypothese war, dass Zellen, die einer nicht-physiologischen hohen Sauerstoffkonzentration ausgesetzt sind, gegenüber Strahlung und/oder dem Vorhandensein von Aβ Peptid aufgrund des Sauerstoffeffekts anders reagieren, empfindlicher oder unempfindlicher sind (d.h. erhöhte Empfindlichkeit aufgrund der erhöhten Bildung von schädlichem ROS und Modulation von Signalwegen oder aber unempfindlicher wegen vorheriger Adaptation dieser Prozesse).

Ein sehr wichtiges Ergebnis war, dass die Sauerstoffkonzentration in der Zellkultur und der Differenzierungsstatus von SH-SY5Y Zellen wichtige Modulatoren von zellulären Reaktionen auf Röntgenstrahlung und Aβ Peptid sind. Dies ergab sich aus den zell- und molekularbiologischen sowie aus den biochemischen Untersuchungen.

Die zur Induktion der Differenzierung verwendete Retinsäure führt zu morphologischen Veränderungen von SH-SY5Y Zellen (d.h. Abflachung des Zellkörpers und Bildung von langen Auswüchsen, die Axonen von Neuronen ähneln) und zu einer Erhöhung der Empfindlichkeit gegenüber Strahlung und Aβ Peptid in Abhängigkeit von der Sauerstoffkonzentration. Darüber hinaus spielt Sauerstoff eine Rolle bei der Differenzierung und Proliferation von SH-SY5Y Zellen, da die Menge an Neurofilament-M, ein Marker der Differenzierung, von der Sauerstoffkonzentration abhängig ist und bei 5% O_2 kultivierten Zellen höher war. Der Proliferationstest zeigte ebenfalls eine erhöhte Zellzahl im Vergleich zu den kultivierten Zellen bei 21% O_2.
Unter Verwendung einer sauerstoffempfindlichen optischen Sonde konnte nachgewiesen werden, dass die intrazelluläre Sauerstoffkonzentration [O_2] sich von der externen Sauerstoffkonzentration unterscheidet. Die intrazelluläre [O_2] von SH-SY5Y Zellen, die bei 21% O_2 kultiviert wurden, war 10%, die bei 5% O_2 kultivierten dagegen 0,9% O_2. 5% externe Sauerstoffkonzentration ist für SH-SY5Y Zellen nicht hypoxisch, da keine Expression von Hypoxie-induzierbarem Faktor (HIF-1α) nachgewiesen wurde.

Veränderungen des aus SH-SY5Y Zellen isolierten mitochondrialen Proteoms wurden unter Verwendung einer Kombination von blau-nativer/2D-SDS-PAGE zur Proteintrennung, anschließende Färbung mit dem Fluoreszenzfarbstoff SYPRO Ruby und Quantifizierung von Proteinspotsintensitäten aus Gelbildern untersucht. Die Proteinmenge ausgewählter Untereinheiten von Enzymkomplexen der oxidativen Phosphorylierung (OxPhos) und anderer nicht-OxPhos-mitochondrialer Proteine (identifiziert durch MALDI-TOF/TOF-Massenspektrometrie und Western Blot) änderte sich bei der Bestrahlung nicht. Nur die Menge des Hitzeschockproteins 70 erhöhte sich in Abhängigkeit von der Sauerstoffkonzentration und dem Differenzierungsstatus.

Monomere und kleine Oligomere des Aβ Peptids interagierten mit SH-SY5Y Zellen, wie durch Durchflusszytometrie nachgewiesen wurde. Kompartimente mit niedrigem pH-Wert (d.h. Lysosomen und möglicherweise späte Endosomen) waren der Hauptzielort (Target) des Peptids während es nur in geringem Maße mit Mitochondrien und dem endoplasmatischen Retikulum in Wechselwirkung tritt, wie durch konfokale Rastermikroskopie sichtbar gemacht wurde.
Obwohl der Ort und die Kinetik der Wechselwirkung von Aβ Peptid mit SH-SY5Y Zellen, die bei 21% oder bei 5% O_2 kultiviert wurden, ähnlich war, wurde eine verminderte lysosomale Integrität nach der Aβ Peptidbehandlung von SH-SY5Y Zellen allein bei 21% O_2 beobachtet.
Aβ Peptid allein induzierte nur eine leichte Erhöhung von ROS (bis zu 1,2-fach), eine leichte Zunahme des mitochondrialen Membranpotentials und keine Änderungen in der ATP Konzentration und in der Menge von Glutathion (GSH) (ein Indikator für die Antioxidationskapazität der Zelle), unabhängig von der Sauerstoffkonzentration in der Zellkultur.

Strahlung allein führte zu einem signifikanten Anstieg der ROS (~ 1,5-fach) und einer leichten Erhöhung der ATP-Konzentration (~1,2-fach), aber nur in Zellen bei 5% O_2. Eine leichte Zunahme des mitochondrialen Membranpotentials wurde bei 21% und 5% O_2 beobachtet. Strahlung bewirkte eine leichten Anstieg der GSH-Menge bei 21% O_2 und eine Abnahme bei 5% O_2 (bis zu 1,2-fach).

Die Zunahme der Proteincarbonylierung (~ 2,5-fach) durch oxidativen Stress, gemessen im Oxyblot-Assay, war für bestrahlte Zellen bei 21% O_2 spezifisch.
Ein sehr sensitiver Wirkungsort des oxidativen Stresses ist DNA, insbesondere mtDNA, die aber bis jetzt viel weniger untersucht wird als nukleare DNA. MtDNA wurde unter Verwendung von für mtDNA spezifischen Primern in PCR-Verfahren auf Änderungen in seiner Menge und auf das Vorhandensein von 4977 bp-Deletion untersucht. Aß Peptid oder Strahlung allein führen zu einer Veränderung der mtDNA Menge in Abhängigkeit von der O_2 Konzentration: bis zu 1,3-fache Abnahme bei 21% O_2 und bis zu 1,5-fachem Anstieg bei 5% O_2. Das Auftreten der mtDNA-Deletion war für bestrahlte Zellen sowohl bei 21% als auch bei 5% O_2 spezifisch, war aber bei 21% O_2 stärker ausgeprägt.

Zum ersten Mal wurde die kombinierte Wirkung von Aβ Peptid und ionisierender Strahlung auf zelluläre Parameter und Zellüberleben untersucht. Die mit Aβ Peptid kombinierte Strahlung führte zu einem statistisch signifikanten Anstieg der ROS-Menge bei 21% (~1,2-fach) und 5% O_2 (~1,4-fach), Erhöhung der ATP-Konzentration (1,5-fach) nur bei 5% O_2, Erhöhung der GSH-Menge bei 21% O_2 und Abnahme bei 5% O_2 (bis zu 1,2 fach) und zu keiner Veränderung des mitochondrialen Membranpotentials.

Die Ergebnisse des Zelltod-Assays (Messung von apoptotischen und nekrotischen Zellen durch Durchflusszytometrie) zeigten, dass $A\beta_{1-42}$ Peptid oder 2 Gy-Röntgenstrahlen allein zu einer signifikanten Zunahme des Zelltods von SH-SY5Y Zellen bei 5% O_2 führte und nur in einer geringfügigen Zunahme bei 21% O_2. Bemerkenswerterweise verringerte Aβ Peptid den Zelltod von bestrahlten Zellen auf das Kontrollniveau oder darunter, insbesondere bei 5% O_2. Im Gegensatz zu den individuellen Stressoren führte die Kombination von Aβ Peptid und Bestrahlung nicht zu einer signifikanten Zunahme der Proteincarbonylierung, der mtDNA Deletion und der Änderung der mtDNA Menge. Daher bestimmt der anfängliche Oxidationsstress den Punkt, an dem zelluläre Abwehrmechanismen auftreten, und es ist möglich, dass in diesem Fall auch neuroprotektive Mechanismen ausgelöst werden.

Darüber hinaus zeigte diese Studie, dass die Inkubationszeit zusammen mit der Konzentration und dem Zustand des Peptids (disaggregiert *versus* aggregiert zu Fibrillen) ein entscheidender Faktor für die Aβ Peptid-Toxizität ist. Eine hohe Konzentration (100 µM) des fibrillären Peptids (induziert durch Lagerung bei 37 °C über Nacht) führte zum Zelltod von SH-SY5Y Zellen nach einem Tag. Allerdings war die Wirkung des disaggregierten Aß Peptids (100 µM) nach 3 Tagen Inkubation stärker ausgeprägt als bei fibrillärem Peptid. Aβ Peptid Behandlung verringerte den Prozentsatz von apoptotischen und nekrotischen Zellen (2,5-fach) in bestrahlten Zellen nach 1 Tag. Nach 3 Tagen wurde jedoch ein ~2,8-facher Anstieg von apoptotischen und nekrotischen Zellen im Vergleich zu unbestrahlten Kontrollzellen beobachtet.
Der beobachtete Weg von Aβ Peptid zu zellulären Organellen und die induzierten Veränderungen der Zellphysiologie, die vom Oxidationsstress abhängen, könnten für die AD Pathologie von Bedeutung sein.

Die erhaltenen Ergebnisse fordern den Einsatz von mehr physiologischen 5% O_2 anstatt der nicht-physiologischen 21% O_2 für die Kultivierung von SH-SY5Y Zellen, insbesondere bei Studien ihrer Reaktion auf Stress. Dies ist die Zuverlässigkeit der experimentellen Aussagen entscheidend. Zellen, die bei 5% O_2 kultiviert wurden, zeigten eine höhere ATP Konzentration (~1,3-fach), eine niedrigere ROS Menge (1,5-fach), eine geringere Proteincarbonylierung (2,5-fach) und weniger mtDNA Deletion (2-fach) im Vergleich zu Zellen bei 21% O_2.

2. Introduction

The effect of radiation on cells is usually exerted through the formation of ROS in the radiolysis of water and through their high potential to react with other molecules creating more ROS in the cell. Although single doses of radiation used for diagnostic purposes or therapeutic treatment are relatively low, small changes on the molecular and cellular level may accumulate upon repeated exposure and result in delayed long-term defects.

Oxygen concentration in the cell culture is of crucial importance for the cellular response to oxidative stress caused by ionizing radiation or by presence of toxic peptides. The differentiation state is another important factor in cellular response to stress (Džinić et al., 2016). Differentiation state of the cell determines the gene expression which then regulates the sensitivity and cellular response to any treatment. The cell possesses different anti-oxidant mechanisms such as glutathione (GSH) (Dani et al., 2010) and repair mechanisms which are activated depending on the amount of oxidative stress.

Oxygen concentration and differentiation state are important in studies of disease mechanisms, particularly of multifactorial diseases such as neurodegenerative AD (Alzheimer´s disease). Although exact cause(s) of AD are still unknown, one of the players is Aβ peptide. However, the implication of different aggregation states of the peptide (fibrillized or disaggregated to monomers and oligomers) is largely debated. Monomers and small oligomers of Aβ peptide are recently proposed to be involved in damage of neurons, instead of extracellular Aβ peptide plaques, since they interact with and even intercalate in cellular membranes (Buchsteiner et al., 2010; Dante et al., 2011) and the peptide is found inside neurons of AD patients (Gouras et al., 2000). Lysosomal activity of sequestration and potential degradation of Aβ peptide is probably the first and most important defense mechanism of cells against Aβ peptide toxicity (Zheng et al., 2012).

Although effects of irradiation and Aβ peptide share some similarities, such as induction of inflammation linked with neurodegeneration, these two stressors probably affect different cellular pathways and result in different cellular responses.

2.1. Cellular responses to ionizing radiation

Absorption of radiation by tissue is a function of the electronic excitability of its constituent molecules. High energy radiation (α-, β-particles, neutrons, γ- and X-rays) sufficient for ejection of electrons from their orbital or collision with other energetic particles (e.g. α-particles, high energy electrons) results in **molecular ionization** leaving chemical entities with one or more electrons unpaired (Riley, 1994). The absorbed dose of radiation (D) is the fundamental dose quantity given by:

$$D = \frac{\Delta\varepsilon}{\Delta m}$$

where Δε is the mean energy imparted to matter of mass Δm by ionizing radiation. The SI unit for absorbed dose is joule per kilogram (J kg^{-1}) and its name is gray (Gy) (ICRP, 2007).

X-ray radiation is a type of electromagnetic radiation (photons with wavelenghts from 0.01 to 10 nm and energies in the range from 100 eV to 100 keV) (Waseda et al., 2011). The effect of ionizing radiation on biomolecules (i.e. nucleic acids, lipids and proteins) can be direct and indirect (e.g. through the radiolysis of water and formation of free radicals which then interact with biomolecules) (Figure 2.1).

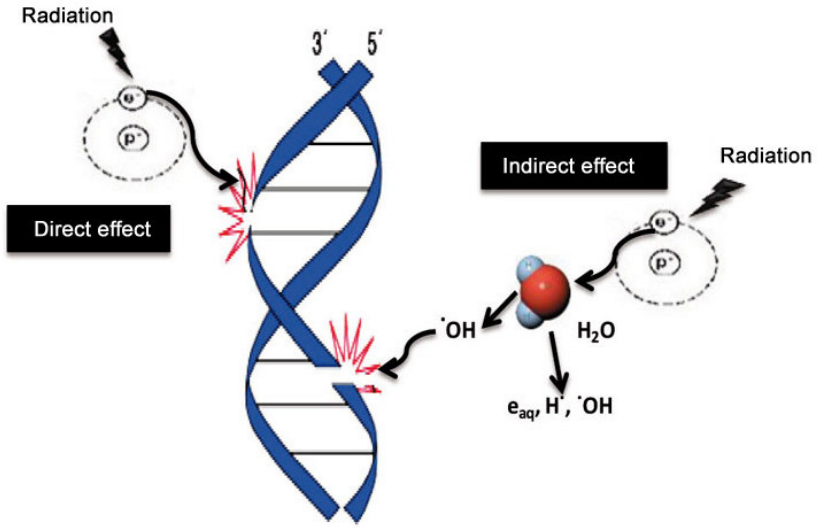

Figure 2.1. Representation of the direct and indirect effect of ionizing radiation on DNA. Ionizing radiation can directly damage a biomolecule by ionizing it or breaking its bonds, or by creating a hydroxyl radical, which in turn reacts with the biomolecule, causing damage indirectly.
(http://www.seguridadypromociondelasalud.com/n134/en/article2.html).

The most important electron acceptor in the biosphere is **molecular oxygen (O_2)** which readily accepts unpaired electrons to give rise to a series of partially reduced species collectively known as **reduced (or "reactive") oxygen species (ROS)** (Figure 2.2). These include superoxide radical anion ($•O_2^-$), hydrogen peroxide (H_2O_2), hydroxyl radical (•OH) and peroxyl (ROO•) and alkoxyl (RO•) radicals which may be involved in the initiation and propagation of free radical chain reactions and which are potentially highly damaging to cells (Riley, 1994). Furthermore, ROS are products of normal metabolic pathways too and serve as specific signaling molecules in both normal and pathological conditions, and their transient generation, within boundaries, is essential to maintain homeostasis (Gil del Valle, 2011). Endogenous sources of ROS include: mitochondrial oxidative phosphorylation, P450 metabolism, peroxisomes and activation of inflammatory cells as reviewed by Ames and colleagues (1993) and Franco (2008). Complex I of the electron transport chain (ETC) is thought to be the major source of ROS generation within mitochondria (Chen et al., 2007).

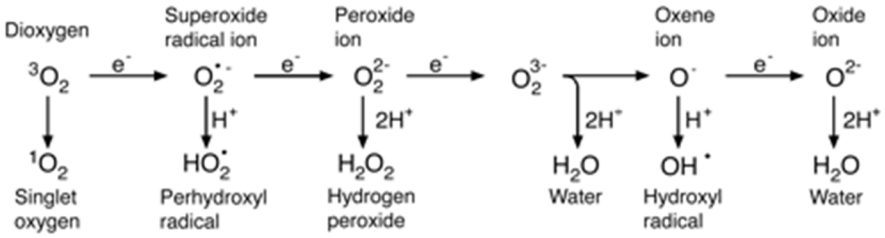

Figure 2.2. Generation of different ROS and oxygen radicals by energy transfer or sequential univalent reduction of ground-state triplet oxygen (Appel & Hirt, 2004).

Cellular responses to radiation depend on the absorbed dose of radiation, cell type, differentiation status and oxygen level in the cellular microenvironment or in the cell culture (Džinić et al., 2016). X-ray irradiation of human cells reduces their capability to divide and survive (Puck & Marcus, 1956). Clinically relevant doses of ionizing radiation (0 - 5 Gy) used in diagnostics and in therapeutic treatment cause increase of reactive oxygen and nitrogen species, apoptosis, inhibition of cell-cycle progression of human neural stem cells (hNSCs), which suggests that low-dose irradiation can cause long-lasting perturbations in the central nervous system (CNS) microenvironment due to radiation-induced oxidative stress (Acharya et al. 2010). Bauer (2011) showed that low dose gamma irradiation may lead to induction of apoptosis in nontransformed cells and protection of malignant cells or their destruction through the enhancement of peroxidase release and superoxide radical anion generation depending on the cellular signaling as well as certain situations with respect to the density of cells.

Proteins are due to their abundancy in the cell very common targets of oxidative stress. Their building blocks (i.e. cysteines, histidines and lysines) represent solvent exposed nucleophiles that are readily avaliable for adduction by reactive electrophiles formed primarly from lipid electrophiles generated under conditions of oxidative stress; 80% of all proteins can be modified at a single cysteine residue (Liebler et al., 2008). Depending on the amount and site of the damage, proteins may loose their functionality, e.g. adduction of HSP72 on cysteine 267 (located in the ATPase domain) by the cytotoxic aldehyde 4-HNE, leads to the inhibition of HSP72´s ATPase activity (Liebler et al., 2008). Since the protein turnover (i.e. synthesis and degradation) is a very dynamic process, damaged and non-functional proteins are easily replaced by newly synthesized (Goto et al., 1995) as long as there are functional transcription and translation.

DNA is another very important target of oxidative stress. ROS generated during oxidative phosphorylation or upon stress can damage both **mtDNA and nDNA** as reviewed by Kam & Banati (2013). However, mtDNA has a less efficient repair system (mostly base excision repair (BER (Alexeyev et al., 2015)), less protective protein structures and no introns compared to nDNA and the mutation frequency of mtDNA is ~10 fold higher (Brown et al., 1979). There are 2-10 copies of mtDNA per **mitochondrion** (Wiesner et al., 1992) and approximately 10^3 mitochondria per human cell (Alberts et al., 2015). Mitochondria form network-like structures which also get split into smaller mitochondrial compartments in the dynamic process of fusion and fission (Figure 2.3 A). The close proximity of the OxPhos machinery in the inner mitochondrial membrane makes

mtDNA vulnerable to damage by ROS in the „vicious cycle“ (Figure 2.3 B). ROS produced in the ETC, and during oxidative stress as well, can react with mtDNA and result in mutations. Due to these alterations in the functioning of OxPhos complexes more ROS is formed. Human mtDNA is a circular double-stranded 16569 bp molecule encoding 13 polypeptides all being subunits of OxPhos complexes, two rRNAs and 22 tRNAs (Anderson et al., 1981). Thus, damages in mtDNA, which has no introns and is less protected by accompanying proteins than nDNA, are more likely to cause functional changes such as respiratory chain dysfunction than those in nDNA.

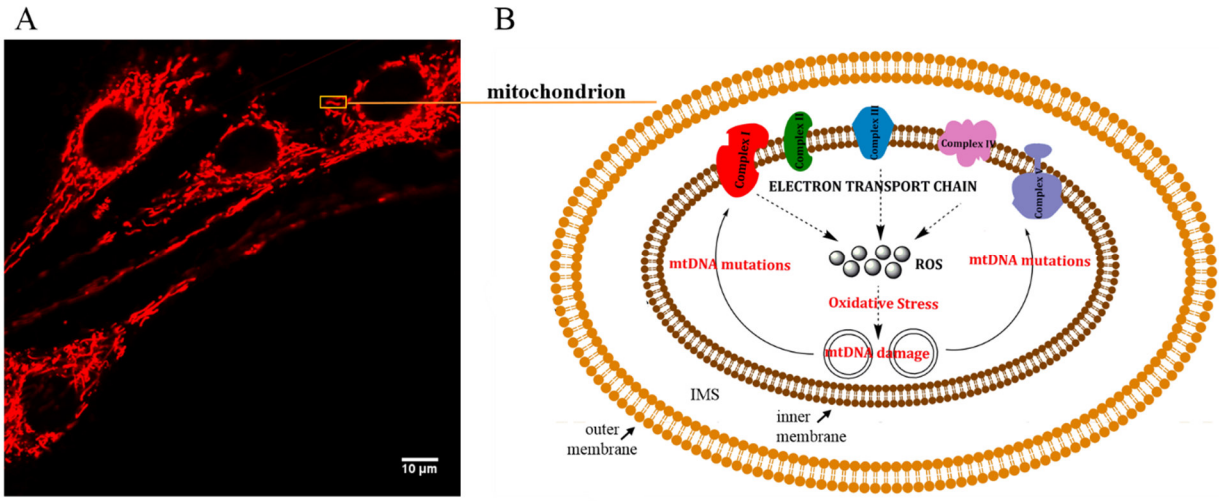

Figure 2.3. A) Microscopic image of mitochondria of SH-SY5Y cells taken by confocal scanning microscopy. Network-like structure of mitochondria and single mitochondrion (yellow box) stained by MitoTracker® Red CM-H2Xros ($\lambda_{EX}/\lambda_{EM}$ = 579/599 nm) dye. Magnification: 400×. Scale bar: 10 µm. B) Schematic representation of single mitochondrion with outer membrane, intermembrane space (IMS) and inner membrane with OxPhos complexes (I-V). Mitochondria are production sites of ROS in the electron transport chain. „Vicious cycle" of mtDNA damage by ROS: ROS can react with mtDNA, inducing mutations. These mutations cause a misfunctioning of the ETC in the mitochondria leading to more ROS, producing dysfunction in the mitochondria, which can lead to cell death. Figure B modified from: Zapico & Ubelaker, 2013.

It was found that oxidative modification of DNA, such as OH8dG, leads to mispairing of repetitive sequences which can result in deletions (Lezza et al., 1999). One of the best known damages in mtDNA is the 4977-bp deletion, known as the common deletion (Δ-mtDNA4977) that occurs upon oxidative stress, particulary after ionizing radiation. The site of this deletion is flanked by two 13-bp direct repeats at positions 13447-13459 and 8470-8482 (Figure 2.4) and DNA damage between these repeats can result in inappropriate pairing during DNA replication (slip-replication mechanism), causing the deletion (Prithivirajsingh et al., 2004). The 4977 bp long region that is deleted encodes several tRNAs and respiratory chain genes (Schilling-Tóth et al., 2011; Taylor et al., 2014) and is the common cause of diseases such as cancer and myopaties, and ocurrs during aging, hence the name „common“. Radiation results in many single-copy deletions and mutations in mtDNA, which are not practical to detect or quantify. However, the common deletion is more easily detected (e.g. using nested PCR and primers specific for mtDNA harboring the deletion)

because of its unique mechanism of formation, making it a very sensitive marker of mtDNA damage (Prithivirajsingh et al., 2004; Chen et al., 2011).

Since mitochondria are organelles in the center of different cellular pathways including energy conversion and metabolism, calcium homeostasis and apoptosis (Alberts et al., 2015), their dysfunction is linked with many diseases including neurodegenerations such as Parkinson´s or Alzheimer´ disease. More than 100 deletions found in mtDNA is associated with human diseases (http://www.mitomap.org/).

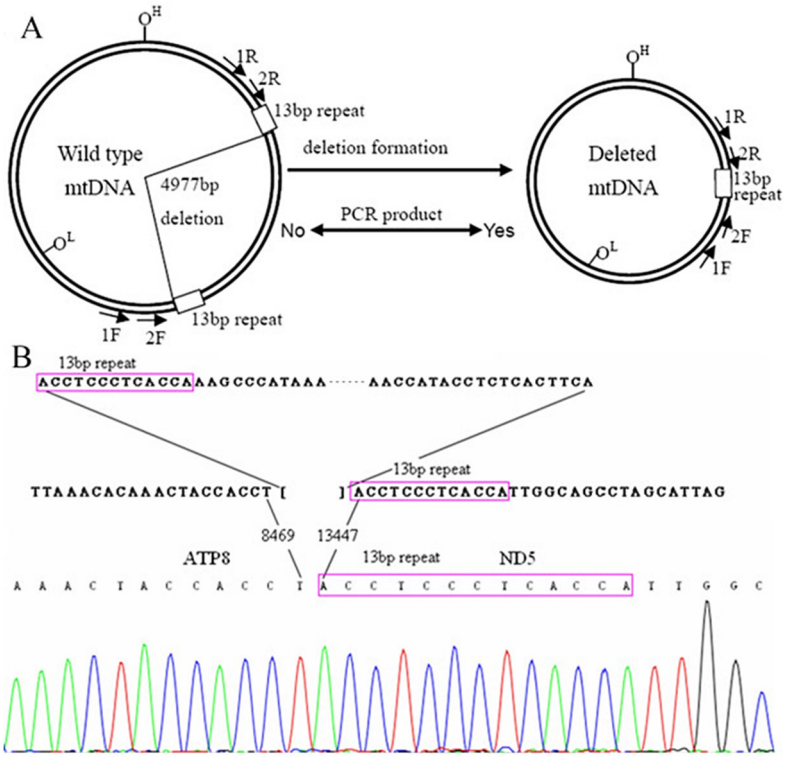

Figure 2.4. Detection of the mtDNA 4977-bp deletion. A) Human mitochondrial genome with or without the 4977-bp deletion; the positions of primers specific for mtDNA used in nested PCR for detecting the deletion are 1F (8192-8212), 1R (13663-13643), 2F (8261-8281) and 2R (13595-13575). PCR Conditions used in this approach are not appropriate for amplification of the wild type mtDNA since the fragment (>5 kb) is too large. B) Confirmation of the 4,977 bp deletion by sequencing. (Chen et al., 2011).

The cell uses a number of anti-oxidant defense and repair mechanisms (Riley, 1994) in Table 1. However, even small alterations in cell physiology if persistant can culminate in detrimental changes in the organism.

Table 1. Cellular antioxidant defense mechanisms (modified according to Riley (1994)).

(1) Compartmentation of `sensitive' material (e.g. DNA)
(2) Removal of ROS by antioxidant enzymes (SOD, catalase, GPX)
(3) Sequestration of transition metals (e.g. in ferritin)
(4) Radical scavengers such as cellular thiols (e.g. glutathione) and chain-breaking antioxidants (e.g. a-tocopherol, ascorbate)
(5) Inhibition of vulnerable processes (e.g. DNA replication)
(6) Monitoring and repair (e.g. excision repair of DNA lesions)
(7) Initiation of apoptosis

Furthermore, lysosomal activity of sequestration and degradation of damaged cellular components or harmful external stressors is another very important mechanism of cellular defense. For example, damaged mitochondria or their parts are targeted for endo/lysosomal degradation (Juhász, 2016) preventing further damage. **Lysosomes**, besides their digestive roles together with autophagosomes or late endosomes, are responsible for the repair of the plasma membrane by fusing locally with damaged sites. Lysosomes serve as a pool or storage of amino acids, phosphate, ions and intermediate metabolites and they are capable of sensing nutrients through the activation of kinases (e.g. mTORC1) and transcription factors, as reviewed by Lim and Zoncu (2016).

2.2. Oxygen concentration in the cell culture

O_2 is a molecule essential for life of aerobic organisms and proper function of most of the cells and tissues. Oxygen concentration in cells of the living organism or cells in the culture depends on the balance between its delivery and consumption by cellular processes. Intracellular oxygen concentration is usually much lower than in the atmosphere. Furthermore, varying concentrations of oxygen are present in tissues depending on their metabolism and functions. For example, lungs experience much higher oxygen concentration (~14.4% in the alveoli) than skin (1.1 ± 0.4% in superficial region). Oxygen concentration in arteries and veins of lungs is ~10-13% and ~5%, respectively, whereas brain tissues has ~3-5% O_2 (Carreau et al., 2011) (Figure 2.5).

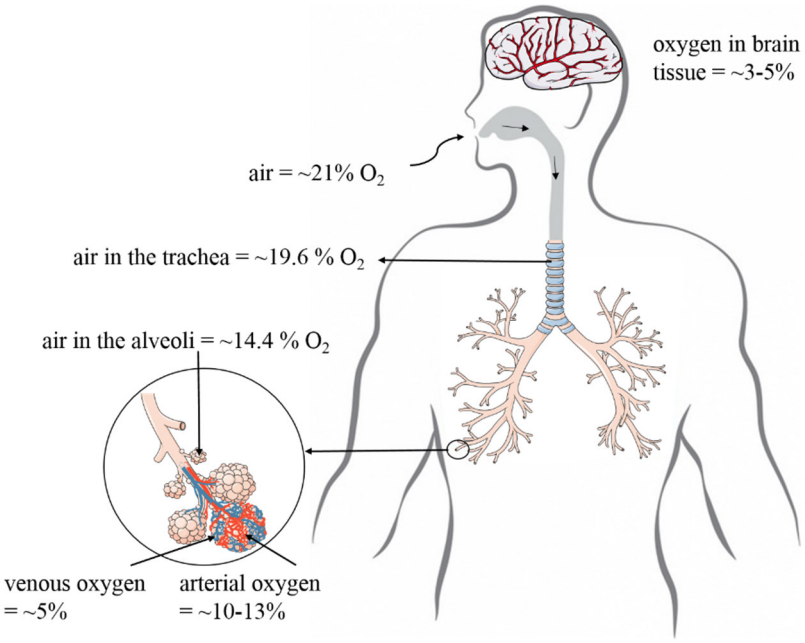

Figure 2.5. Oxygen concentrations in the human body. Gradual reduction of oxygen concentration (~21%) from the atmosphere after the delivery to trachea (~19.6% O_2) and alveoli (~14.4% O_2) of lungs. Further reduction of oxygen concentration in arteries (~10-13%) and veins (~5%). Brain tissue has oxygen concentration ranging from ~3-5% depending on the depth of the brain area. Oxygen concentration values according to: Carreau et al., 2011. Figure was created using Servier Medical Art (http://www.servier.com/).

Oxygen concentration in the cell culture is of crucial importance for cellular metabolism and for cellular response to oxidative stress. The most of cell culture nowadays is performed in 95% air which is ~21% O_2 by volume in 5% CO_2 controlled incubators (final O_2 concentration is ~20%). These conditions are often referred to as **normoxia**. However, the term „normoxic" does not describe the condition faithfully as it does not represent normal *in vivo* conditions and more appropriate term would be „hyperoxic". Meaning of terms used to describe oxygen levels is relative and often misinterpreted since atmospheric oxygen is often used as a reference point. **Physioxia** refers to the partial oxygen pressure in normal physiological conditions. On the other hand, changes in the homeostasis or pathological conditions may induce decrease in partial oxygen pressure which is called **hypoxia**. The term „hypoxia" refers to a condition of insufficient oxygen which can occur in tumors as well as in normal tissues and wounds (Hammond et al., 2014). Physioxia is sometimes misinterpreted as hypoxia (what is hypoxic for one cell type for others may not be and could represent a physioxia and *vice versa*).

The lifespan of human diploid cells in the culture is extended by incubation at oxygen concentrations lower than those used in the standard cell culture incubator (i.e. ~21% O_2) (Packer & Fuehr, 1977). It was shown that using 1-5% O_2 stimulates proliferation of neural stem cells through the activation of Wnt/β-catenin signaling involved in cell cycle regulation (Braunschweig et al., 2015). Cultivation of primary neurons isolated from the striatum of rat brains at 2% O_2 leads to increased mitochondrial membrane potential and decreased ROS production, changed ATP concentration, which is critical in replacement of damaged lipids and proteins (Tiede et al., 2011).

Interestingly, mitochondrial morphology or dynamics of mitoreticulum is affected by oxygen concentration, which leads to changes in cell bioenergetics (Willems et al., 2015). Plecitá-Hlavatá and colleagues (2016) observed expansion of mitochondrial IMS and rounding of a sharp cristae shape in hepatocellular carcinoma HepG2 cells adapted to 5% O_2, which resulted in profound changes in ATP production in glycolytic cells via disruption of ATP synthase dimers while OXPHOS cells (cultivated in aglycemic medium with galactose and glutamine) showed only non-significant changes in ATP production.

Furthermore, oxygen concentration affects gene expression. For example, transcription factor HIF-1 (hypoxia inducible factor 1) is a heterodimer consisting of HIF-1α protein (and of HIF-1β protein), which under conditions of high oxygen is rapidly degraded. HIF-1α has a half-life less than 10 min under normoxic conditions since PHDs (prolyl hydroxylases) hydroxylate prolyl residues of HIF-1-alpha making it a target for interaction with E3 ubiquitin-protein ligase complex. This leads to poly-ubiquitinilation and finally proteosomal degradation by 26 S proteasome. HIF-1 alpha is expressed in some cancer cell lines and in normal cell lines following stimulation or stress at non-hypoxic oxygen levels (Chun et al., 2002). When stabilized HIF-1α binds to HRE (Hypoxia Response Element) sequences in the DNA and then it is cabable to regulate (activation or inhibition) of more than 100 target genes involved in regulation of a variety of cellular processes (Horowitz and Simons, 2008).

Other cellular factors regulated by oxygen are microRNAs (miRNAs) (20-24 nucleotide non-coding RNAs) (Kulshreshtha et al., 2007) and cell adhesion molecules. Low oxygen induces switch from oxidative phosphorylation to anaerobic glycolysis, increased glucose uptake, and expression of stress proteins related to cell survival or death. Cell proliferation rates under conditions of low oxygen may increase as it was in the case of colon cancer HCT116 cells cultivated at 5% O_2 where HIF-1 alpha was upregulated and probably mediated by MAPK (Carrera et al., 2014).

Performing *in vitro* studies under appropriate oxygen conditions or at "physiologically-relevant oxygen concentrations" (Jež et al., 2015) is to be considered in tumor microenvironment studies but also in cellular therapies, regeneration medicine and identification of relevant biomarkers for diagnostic purposes. Furthermore, investigation of anti-oxidant properties of compounds under inappropriately high concentration of oxygen may contribute to false negative results as cell are exposed to high oxidative stress.

The **differentiation state** is another important factor in cellular response to stress. Differentiation state of the cell determines the gene expression which then regulates the sensitivity and cellular response to any treatment. All-*trans* retinoic acid (ATRA, tretinoin or vitamin A acid, RA), a ligand for both the retinoic acid receptor (RAR) and the retinoid X receptor (RXR) (Balmer & Blomhoff, 2002) is used alone or in combination with growth factors for differentiation of multipotent or oligopotent cells into more specialized cell types (Biedler et al., 1973). Activated RAR and RXR regulate the expression of genes involved in growth and differentiation of both

normal and malignant cells (Chiu et al., 1995, Korecka et al., 2013). Embryonic stem cells are primed to become neurons and human neuroblastoma (SH-SY5Y) cells resemble neurons after the treatment with RA (Rhinn & Dollé, 2012; Fagerström, 1996). Additionally, the oxygen concentration modulates the expression of neurofilament M, a marker of differentiation (Džinić et al., 2016) and is known to be implicated in differentiation (Cheng et al., 2014) and metabolic activity of neuronal cells (Zhu et al., 2012). Hematopoietic stem cells (HSC) important in clinical studies and in fundamental research come from the bone where levels of oxygen are very low (endosteal region next to the inside surface of the bone where blood vessels are small and the blood flow rate is slow). HSCs *in vitro* must be maintained at 3% O_2 since at higher oxygen concentrations these cells rather undergo differentiation and below 3% O_2 they do not proliferate (Ivanovic et al., 2004).

2.3. Implication of the Aβ peptide in Alzheimer´s disease

Alzheimer´s disease (AD) is one of many age-associated diseases (e.g. cancer, cardiovascular diseases, diabetes type 2) and the most common dementia in elderly (60-80% of all known dementias) (Alzheimer's Association, 2014). AD and related dementias affected about 47 million people worldwide (Alzheimer's Disease International, 2016). Despite the quantum leap in the progress of science and medicine, the cause(s) of AD and mechanisms involved in its pathology remain unresolved even more than 100 years after the disease was first described as a form of progessive, neurodegenerative and behavioral disorder (Alzheimer, 1907). Some researchers point out that AD is rather a systemic disorder than a brain-limited condition (Swerdlow et al., 2010; Querfurth et al., 2010).

AD is considered one of protein misfolding diseases (Sipe et al., 2010; Stefani et al., 2012) but it took until the mid to late 1980s to correlate **Aβ peptide** with AD symptoms (Masters et al., 1985; Tanzi et al., 1988) as processing of amyloid precursor protein (APP) peptide is altered in AD. Amyloid beta peptide is a metabolic product of the APP in cellular organelles (endoplasmatic reticulum, Golgi apparatus, endosomes and possibly in mitochondria) and is secreted predominantly as $A\beta_{1\text{-}40}$ or $A\beta_{1\text{-}42}$ peptide (Martin et al., 1995; Pagani & Eckert, 2011).

There is no direct correlation between the accumulation of Aβ peptide and cognitive decline (Soldano & Hassan, 2014), suggesting that the Aβ peptide is not a sole player in AD. Premature death of cholinergic neurons in the brain is caused by multiple genetic and environmental factors. In the early-onset AD with a familial pattern of inheritance (which accounts for only about 1% of all cases), autosomal dominant mutations in three nuclear genes: amyloid precursor protein (APP) at chromosome 21, presenilin 1 (PS-1) at chromosome 14 and apolipoprotein (ApoE) at chromosome 19 are involved in the pathogenesis. Risk factors for the late-onset and sporadic form of AD beside age, which is the most important factor, are the prevalence of ApoE4 allele among affected individuals and mutations in mitochondrial DNA (Scheffler, 1999, pg. 303).

APP is expressed at high levels in neurons and undergoes proteolytic processing by three different secretases: α-secretase, β-secretase, and γ-secretase (Soldano & Hassan, 2014) (Figure 2.6).

In amyloidogenic processing (i.e. in pathological conditions), the first cleavage is by β-secretase in the extracellular domain leading to the release of a soluble fragment (sAPPβ). The second cleavage is by γ-secretase in the transmembrane domain and results in the increased production of the Aβ peptide, a small peptide called p3 and the release of the APP intracellular domain (AICD) (Figure 2.6). On the other hand, under normal conditions, α-secretase cleaves APP releasing sAPPα and preventing the formation of Aβ peptide (Soldano & Hassan, 2014). Therefore, the cleavage of APP by α-secretase could be neuroprotective.

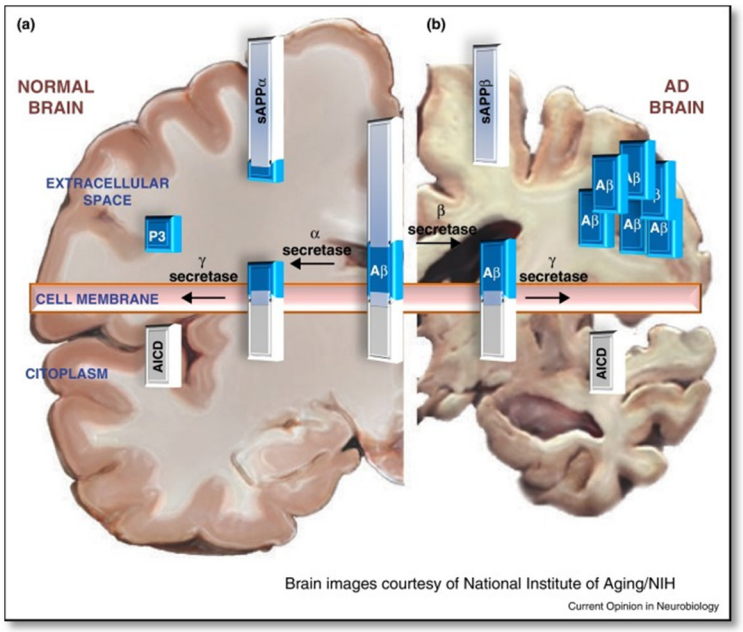

Figure 2.6. Proteolytic processing of the amyloid precursor protein (APP). a) In the non-amyloidogenic pathway, α-secretase cleaves APP on the cell surface and produces APPsα that is secreted and a membrane tethered fragment. This fragment is internalized and subsequently cleaved by γ-secretase to form the soluble p3 peptide and the APP intracellular domain (AICD). The P3 fragment is then eliminated via secretory pathway while location and function, if any, of AICD remain unclear. b) In the amyloidogenic pathway, APP is initially cleaved by β-secretase to form secreted APPsβ and a membrane tethered fragment. This fragment is also a substrate for γ-secretase and leads to the release of Aβ peptide and AICD (Soldano & Hassan, 2014).

Different mechanisms of the contribution of Aβ peptides in AD have been proposed and there are still discussions on whether Aβ fibrils, which form extracellular plaques, or amyloid beta monomers and small oligomers are the major contributor in the pathogenesis of AD.

According to the **amyloid hypothesis**, aggregates of amyloid fibrils that are deposited outside neurons in dense formations (senile or neuritic plaques) are the causative agent of AD and the neurofibrilary tangles (NFTs), neuron loss, vascular damage, and dementia follow Aβ peptide deposition (Hardy & Higgins, 1992). However, it was shown that plaque-independent Aβ toxicity plays an important role in the development of synaptic deficits in AD (Mucke et al., 2000). Moreover, cases of AD without plaques (Price & Morris, 1999) or their presence in non-demented people were documented (Crystal et al., 1988; Price & Morris, 1999). Plaque formation is correlated with other diseases and conditions as well. For example, brain amyloidosis is observed

in people with Down syndrome since they have an extra chromosome 21 where the gene coding APP, a protein from which β-amyloid peptides are derived, is located (Zigman et al., 2008).

Recent research put in focus smaller oligomers and/or monomers which have more potential to cause damages in neuronal cells in comparison to relatively inert fibrils (Ono et al., 2009). Studies showed that intracellular Aβ peptide in human neurons is implicated in Alzheimer´s disease before formation of extracellular plaques (Gouras et al., 2000; Friedrich et al., 2010). Aβ peptide is highly hydrophobic and has a great potential to interact with all cellular membranes and to cause structural perturbation, membrane fusion, changes in lipid diffusion and dynamics (Dante et al., 2003; Buchsteiner et al., 2010; Barrett et al., 2016). Lipid composition of cellular membranes is important in pathogenesis of AD. For example, cholesterol that prevents Aβ peptide insertion (Dante et al., 2006) can modulate lateral movements of proteins in the plasma membrane giving a preference either for nonamyloidogenic α-secretase cleavage of APP or β-secretase cleavage of APP in the plasma membrane (Bodovitz and Klein, 1996).

Both nonfibrillized and fibrillized microinjected $A\beta_{1-42}$ or cDNA-expressing $A\beta_{1-42}$ peptide are capable of apoptosis induction via p53-Bax pathway in primary human neurons *in vitro* (Zhang et al., 2002). Studies revealed that mitochondria are important targets of Aβ peptide (Selkoe, 1997). Mitochondrial dysfunction is broadly discussed to be implicated in late-onset and sporadic forms of Alzheimer´s disease. Aβ peptides are suggested to localize to mitochondrial membranes, to block the transport of nuclear-encoded proteins to mitochondria, disrupt the ETC, increase ROS production, cause mitochondrial damage and prevent neurons from functioning normally (Hansson Petersen et al., 2008; Sirk et al., 2007). Aβ peptides directly initiate free radical/ROS formation, cellular dysfunction, and subsequent neuronal death (Hensley et al., 1994). $A\beta_{1-42}$ peptide can induce reactive ROS production from cortical neurons through activation of NADPH oxidase (Shelat et al., 2008). Aβ peptide-induced „inflammatory“ changes lead to metabolic and cytoskeletal alterations, including changes in calcium homeostasis, and injury to mitochondrial functions (Scheffler, 1999; pg. 303). Hansson Petersen and colleagues (2008) showed that Aβ peptides are transported into mitochondria via the translocase of the outer mitochondrial membrane (TOM) and localizes within the mitochondrial cristae. MtDNA deletions, dysregulations of the fission and fusion events, mitochondrial autophagy have been linked to neurodegeneration (Villeneuve et al., 2013). Oxidative stress as one of the factors in AD leading to mtDNA mutations and deletions resulting in disturbance of ETC and leakage of ROS targeting mtDNA (Yoneda et al., 1995). Moreover, mtDNA damage in senescent cells results in apoptosis (Laberge et al., 2013) which can be induced by persistant single-stranded DNA breaks (Tann et al., 2011). Mutations in mitochondrial genes as well as changes in the activity of four OxPhos complexes (I-IV) are often related to AD. However, other studies did not prove respiratory chain enzyme activities below the normal range in AD patients (Scheffler, 1999, pg. 303). According to the mitochondrial cascade hypothesis, mitochondrial dysfunction is the primary event in sporadic AD. Inheritance determines mitochondrial baseline function and durability which influences how

mitochondria change with age and potentially governs AD histopathology (Swerdlow and Khan, 2009).

There is no direct link between exposure to ionizing radiation and Alzheimer´s disease. It is known that high doses of IR to the head (e.g. 20-50 Gy) lead to severe learning and memory impairment (Kempf et al., 2013) which are characteristic for AD as well. Both non-direct and direct effects of ionizing radiation may play important roles in the pathology of AD as well as of other age-associated diseases. For example, routine exposure of human head to dental X-rays can lead to direct DNA damage or cause increase in ROS that can later damage cellular structures such as telomeres of chromosomes. Cranial irradiation (3 Gy) used for the treatment of primary and metastatic brain tumors (Bauman et al., 1994) can impact cognition through the damage and depletion of neural progenitor stem cells found in hippocampus (Raber et al., 2004). Microglia, cells with a supportive role in the brain, and neuronal progenitor cells that keep dividing are more susceptible to radiation-induced damage such as telomere shortening leading to reduced cellular lifespan. Neurons deprived of the support by microglia, maintenance and nourishment undergo pathological changes resulting in cell death (Rodgers, 2011). Neurogenesis is a process which enables generation of new neural and glia cell not only during the development of the brain but also throughout life (Eriksson et al., 1998).

2.4. Motivation

Exposure to ionizing radiation (IR) regardless of the source and dose presents a potential danger to human health. Even low doses of radiation used in diagnostics or therapeutic treatment cause small changes on the molecular and cellular level (e.g. oxidation of biomolecules, mutations, cell death) which may accumulate upon repeated exposure. Thus, there is need to sentisize the society toward the risks of ionizing radiation. For example, patients are usually not given information about the risks, benefits, and radiation dose for a CT scan. Moreover, a study showed that patients, physicians, and radiologists are unable to provide accurate estimates of CT doses regardless of their experience level (Lee et al., 2004).
On the other hand, IR is an important tool in medicine, industry, agriculture and research, and its mechanisms of interaction with biological matter have to be elaborated.
In this thesis, in order to understand the molecular and cellular responses to IR, cells were irradiated with 2 Gy X-rays that represents a commonly used fractionated dose in radiotherapy of a variety of tumors (e.g. 50 Gy in 5 weeks, fractionated at 5 x 2 Gy/week) (Pedraza Muriel, 2007).

Age is an important factor in response to radiation. For example, children are more sensitive to radiation exposure since their brains are not completely developed. Differentiation state of the cell determines the sensitivity and cellular response to stress. Since it is difficult to study differences in the effect of radiation therapy between young and old patients, this thesis is focused on the interplay between IR and age-related diseases through the effects of oxygen in the cell culture and Aβ peptide implicated in Alzheimer´s disease. The effects of externally applied disaggregated $Aß_{1-42}$ peptide, which exact mechanisms of toxicity are still not resolved, were investigated alone or

combined with irradiation. Human neuroblastoma (SH-SY5Y) cells widely used to study mechanisms of neurodegeneration (Schlachetzki et al., 2013) served as a biological system in this thesis. Cellular responses of non-differentiated and/or SH-SY5Y cell pre-treated with retinoic acid for induction of differentiation were studied in parallel under 21% and 5% O_2, respectively. This approach enables comparison of different factors (i.e. IR, oxygen concentration, differentiation state and Aβ peptide) and their interplay.

Furthermore, most of studies on the molecular and cellular effects of ionizing radiation consider changes solely in the nuclear DNA (nDNA). The number of studies investigating the effects of ionizing radiation on mitochondria and mtDNA is far less than of those on the cell nucleus (Kam & Banati, 2013). Since mitochondrial DNA is highly susceptible to oxidative stress, changes in mitochondrial functioning can mediate oxidative damage of other cellular components including nDNA (e.g. by radiation-induced mitochondrial superoxide radical ions) (Kam & Banati, 2013).

The reliability of *in vitro* studies comes ever more into question as cell cultivation is performed under normoxic conditions meaning that cells are exposed to atmospheric air which is 21% oxygen by volume. Moreover, cultivated cells derived from different sources response differently to changes in oxygen tensions. For this reason, they should be cultivated under oxygen conditions which are similar to those found in tissues. Cell state, physiology and destiny are much influenced by oxygen.

The oxygen concentration in the cell culture can be regulated using „tri-gas“ incubators which function relies, besides usage of a standard CO_2 gas, on the application of nitrogen gas for regulation of oxygen concentration taken up from the atmospheric air. Although such incubators are available at the market, high cost required for providing a continuous source of nitrogen gas makes most of cell culture laboratories to continue work using standard incubators with high non-physiological oxygen concentrations. Ideally, performing cell culture in dedicated „hypoxia stations“, which represent a closed system for cultivation and handling of cells at desired oxygen concentration without exposure to atmospheric air, provides the most reliable results. Moreover, broken oxygen conditions, i.e. exposure of cells cultivated at low oxygen concentrations to atmospheric air for the purpose of subculturing or treatment, can change behavior of these cells and decrease their yield (Mantel et al., 2015). However „hypoxia stations“ are due to their very high costs not a favoured approach and most laboratories cannot afford such systems. On the other hand, simple home-made incubators for cultivation of cells at desired oxygen concentration, by using closed system and pre-mixed gas with a given oxygen concentration, were used in this thesis and can be set up by an average cell culture laboratory (Wright & Shay, 2006). Altering oxygen concentration is a useful tool in the modeling of metabolic disorders and neurodegeneration with a variety of different mitochondrial conditions (Villeneuve et al., 2013). Therefore, appropriate oxygen conditions were established and employed in this thesis in order to study not only the effects of Aβ peptide or radiation on cells but also their interplay the first time.

3. Materials

3.1. Equipment

Name	Manufacturer
Balance R 200 D	Sartorius AG, Göttingen, Germany
Balance U 4100 S	Sartorius AG, Göttingen, Germany
Cannula with Luer-Lock connector (1×200 mm)	neoLab Migge GmbH, Heidelberg, Germany
CCD camera system of Fujibox	Fujifilm Holdings K.K., Tokyo, Japan
Cell counting chamber Neubauer	Marienfeld, Lauda-Königshofen, Germany
Cell culture incubator CO_2-Auto-Zero Type B 50 61 EC O_2	Heraeus GmbH, Hanau, Germany
Centrifuge 5804 R	Eppendorf, Hamburg, Germany
Centrifuge Biofuge Primo R	Heraeus GmbH, Hanau, Germany
Centrifuge Micro V	Fisher Scientific, Schwerte, Germany
Confocal laser scanning microscope TCS SP5II	Leica Microsystems GmbH, Wetzlar, Germany
Electrophoresis power supply EPS301/ EPS601/EPS1001	Amersham pharmacia biotech Europe GmbH, Freiburg, Germany
Flow cytometer S3™ Cell Sorter	Bio-Rad Laboratories, Hercules, CA, USA
Gas bottle regulator HD 300-200-4-2	Airliquide, Kornwestheim, Germany
Glas/teflon homogenizer Potter-Elvehjem tight-fit (2 ml)	B. Braun, Melsungen, Germany
Gradient mixer (ø 18 mm chamber)	Mechanic workshop of Chemistry Department, TU Darmstadt
Handheld automated cell counter Scepter™	Merck Millipore, Billerica, MA, USA
Horizontal mini gel system PerfectBlue™	PEQLAB Biotechnologie GmbH, Erlangen, Germany
Laminar flow bench Lamin Air HLB 2448	Heraeus GmbH, Hanau, Germany
Light microscope Wilovert S	Helmut Hund GmbH, Wetzlar, Germany
Light microscope Zeiss Axio Observer.Z1	Carl-Zeiss Microscopy GmbH, Jena, Germany
Liquid nitrogen tank Locator 6 Plus	Thermo Scientific, Marietta, OH, USA
Magnetic stirrer IKAMAG® RET	IKA®-Werke GmbH, Staufen, Germany
Mass spectrometer MALDI-TOF/TOF MS Ultraflex I	Bruker Daltonik GmbH, Bremen, Germany
Mixer for homogenization EUROSTAR digita	IKA®-Werke GmbH, Staufen, Germany
Peristaltic pump Minipuls 3	Gilson, Middleton, WI, USA
pH-meter Blueline 14 pH/CG842	Schott AG, Mainz, Germany
Pipette 100/300 µl 8-channel	Eppendorf, Hamburg, Germany
Pipette PIPETMAN Classic™ P2/10/20/100/200/1000	Gilson, Middleton, WI, USA
Pipettor accu-jet®-pro	BRAND GmbH, Wertheim, Germany
Plate reader Infinite M1000	Tecan Group Ltd., Männedorf, Switzerland
Plate reader POLARstar Galaxy	BMG Labtech GmbH, Ortenberg, Germany

Scanner ViewPix 900	biostep® GmbH, Jahnsdorf, Germany
SE260 Mighty Small II Deluxe Mini Vertical Electrophoresis Unit	Hoefer, Holliston, MA, USA
Shaker for microtiterplates DSG Titertek 1	Flow Laboratories, Inglewood, CA, USA
Shaker Roto-Shake-Genie® type SI-1101	Scientific Industries, Bohemia, NY, USA
Shaker type 3016	Gesellschaft für Labortechnik (GFL), Burgwedel, Germany
Shaker with temperature regulation Vortemp	UniEquip GmbH, Planegg, Germany
Thermal cycler MyCycler™	Bio-Rad Laboratories, Hercules, CA
Trans-Blot® SD Semi-Dry Transfer Cell	Bio-Rad Laboratories, Hercules, CA, USA
Ultrasonic bath Sonorex TK 52 H	Bandelin electronic GmbH, Berlin, Germany
UV-VIS-scanning spektrophotometer UV-2102 PC	SCHIMADZU, Kyoto, Japan
Vortex mixer Reax 2000	Heidolf Instruments GmbH, Schwabach, Germany
Water bath RC 20/KWU R	mgw Lauda, Königshofen, Germany
Water bath type 1004	Gesselschaft für Labortechnik (GFL), Burgwedel, Germany
Water purification system D4000 distinction water still	Bibby Scientific Limited, Staffordshire, UK
Water purification system Simplicity®	Merck Millipore, Billerica, MA, USA
X-ray machine Pxi Precision X-rays x-rad 32(	Pxi Precision X-rays, North Brandford, CT, USA
X-ray tube Isovolt DS1 with wolfram anode	Seifert, Fairview Village, PA, USA

3.2. Software

Name	Manufacturer
Axio Vision 4.8.2. SP1 (for Axio Observer.Z)	Carl-Zeiss GmbH, Jena, Germany
BLAST (Basic Local Alignment Search Tool; for comparison of nucleotide or protein sequences)	National Center for Biotechnology Information, Bethesda MD, USA
Compass 1.3 (MS software)	Bruker Daltonik GmbH, Bremen, Germany
DELTA2D 4.3 (for analysis of gels)	DECODON GmbH, Greifswald, Germany
Epson Scan 3.81 DE (for ViewPix scanner)	biostep® GmbH, Jahnsdorf, Germany
FLUOstar-control 4.21-0 (for plate reader POLARstar Galaxy)	BMG Labtech GmbH, Ortenberg, Germany
i-control 1.9.17.0 (for plate reader Infinite M1000)	Tecan Group Ltd., Männedorf, Switzerland
Image J 1.48 (for analysis of images)	Wayne Rasband, National Institutes of Health, USA
Kaluza® 1.3 (for flow cytometry data analysis)	Beckman Coulter, Inc., Indianapolis, IN, USA

LAS-3000 2.1 (for imaging system LAS 3000)	Fujifilm Holdings K.K., Tokyo, Japan
LAS AF 2.60 (for confocal microscope TCS SP5 II)	Leica Camera, Wetzlar, Germany
Mascot search engine (for peptide mass fingerprint)	Matrix Science Inc., Boston, MA, USA
ProSort™ 1.1 (for S3™ Cell Sorter)	Bio-Rad Laboratories, Hercules, CA, USA
ProteinScape 3.1 (for the analysis of proteomics data)	Bruker Daltonik GmbH, Bremen, Germany
GraphPad Prism 7.01 (for statistical analysis)	GraphPad Software, Inc., La Jolla, CA, USA
UniProt (universal protein resource)	UniProt Consortium
UV-2102/3102 PC 3.0 (for UV-VIS-scanning spectrophotometer)	SCHIMADZU, Kyoto, Japan
ZEN 2 (blue and black edition; for analysis of microscopy images)	Carl-Zeiss GmbH, Jena, Germany

3.3. Chemicals

Name	Manufacturer
2-(4-(2-hydroxyethyl)-1-piperazineethanesulfonic acid (HEPES) >99%, tissue culture grade	Carl Roth GmbH, Karlsruhe, Germany
4´,6´-diamidino-2-phenylindole dihydrochloride (DAPI)	Molecular Probes Invitrogen, Eugene, OR, USA
4-Iodophenylboronic acid (4-IPBA) ≥95%	Sigma-Aldrich Life Science, Saint Louis, MO, USA
6-aminohexanoic acid >99%	Carl Roth GmbH, Karlsruhe, Germany
Acetic acid 100%, p.a.	Carl Roth GmbH, Karlsruhe, Germany
Ammonium persulfate (APS)	Fluka, Buchs, Switzerland
Antimycin A from *Streptomyces species*	Sigma-Aldrich Life Science, Saint Louis, MO, USA
Ascorbic acid (Na-salt) ≥98%	Sigma-Aldrich Life Science, Saint Louis, MO, USA
β-Mercaptoethanol, 99%, p.a.	Carl Roth GmbH, Karlsruhe, Germany
Bis-Tris ≥98%	Sigma-Aldrich Life Science, Saint Louis, MO, USA
Bovine serum albumin (BSA), fraction V	Carl Roth GmbH, Karlsruhe, Germany
Bromphenol blue	Fluka Chemie GmbH, Buchs, Switzerland
Calcium chloride ≥99.5%, p.a.	Carl Roth GmbH, Karlsruhe, Germany
Carbonyl cyanide 3-chlorophenyl-hydrazone (CCCP)	Sigma-Aldrich Life Science, Saint Louis, MO, USA
Carboxy-2,7-dichlorodihydrofluorescein diacetate (C-H2DCFDA)	Molecular Probes Invitrogen, Eugene, OR, USA
Dibasic potassium phosphate (K_2HPO_4) ≥99%, p.a.	Fluka Chemie GmbH, Buchs, Switzerland
Digitonin A1905	Applichem GmbH, Darmstadt, Germany

Dimethylsulfoxide (DMSO) ≥99.5%, for Molecular Biology	Carl Roth GmbH, Karlsruhe, Germany
Dithiothreitol (DTT), p.a.	Carl Roth GmbH, Karlsruhe, Germany
Disodium hydrogen phosphate (Na_2HPO_4 ≥98%, p.a.	Fluka Chemie GmbH, Buchs, Switzerland
ER-Tracker™ Red	Molecular Probes Invitrogen, Eugene, OR, USA
Ethanol, denatured	Chemistry department, TU Darmstadt
Ethylenediaminetetraacetic acid (EDTA) ≥99%, p.a.	Carl Roth GmbH, Karlsruhe, Germany
Ferric chloride hexahydrate ($FeCl_3$ x 6 H_2O) ≥98%, extra pure	Carl Roth GmbH, Karlsruhe, Germany
Formaldehyde 37%, p.a.	
Glacial acetic acid 99.5%, p.a.	Fluka Chemie GmbH, Buchs, Switzerland
Glucose oxidase from *Aspergillus niger* G7141	Sigma-Aldrich Life Science, Saint Louis, MO, USA
Glycerol ≥99.5%, p.a.	Carl Roth GmbH, Karlsruhe, Germany
Glycin, ≥99%, p.a.	Carl Roth GmbH, Karlsruhe, Germany
Hydrochloric acid (HCl) 37%, p.a.	Carl Roth GmbH, Karlsruhe, Germany
Hydrogen peroxide, 30% (H_2O_2)	Merck KGaA, Darmstadt, Germany
IGEPAL-CA630	Sigma-Aldrich Life Science, Saint Louis, MO, USA
Imidazole >99.5%, p.a.	Fluka Chemie GmbH, Buchs, Switzerland
Immersion oil	Sigma-Aldrich Life Science, Saint Louis, MO, USA
Isopropanol, denatured	Chemistry department, TU Darmstadt
Luminol	Fluka Chemie GmbH, Buchs, Switzerland
LysoTracker® Red	Molecular Probes, Invitrogen, Eugene, OR
Magnesium chloride hexahydrate ($MgCl_2$ x 6 H_2O) >98%, Ph.Eur.	Carl Roth GmbH, Karlsruhe, Germany
Methanol, denatured	Chemistry department, TU Darmstadt
MitoTracker® Red CM-H_2XRos	Molecular Probes, Invitrogen, Eugene, OR
Neutral red dye	Sigma-Aldrich Life Science, Saint Louis, MO, USA
Nitrogen (l)	Airliquide, Kornwestheim, Germany
N-(Tri(hydroxymethyl)methyl)glycin (Tricin) ≥99%	Sigma-Aldrich Life Science, Saint Louis, MO, USA
N, N, N´, N´-tetramethylethylenediamine (TEMED) ~99%	Sigma-Aldrich Life Science, Saint Louis, MO, USA
NuPAGE® LDS Sample Buffer	Life Technologies, Carlsbad, CA, USA
NuPAGE® MES SDS Running Buffer	Life Technologies, Carlsbad, CA, USA
NuPAGE® Reducing Agent	Life Technologies, Carlsbad, CA, USA
NuPAGE® Transfer Buffer	Life Technologies, Carlsbad, CA, USA
PeqFECT DNA transfection reagent	PEQLAB Biotechnologie GmbH, Erlangen, Germany
PeqGOLD universal agarose	PEQLAB Biotechnologie GmbH, Erlangen, Germany
PicoGreen dye	Molecular Probes, Eugene, OR, USA
Ponceau S	Sigma-Aldrich Life Science, Saint Louis, MO, USA

Potassium acetate >99%, p.a.	Carl Roth GmbH, Karlsruhe, Germany
Potassium dihydrogen phosphate (KH_2PO_4) ≥99%, p.a., ACS	Carl Roth GmbH, Karlsruhe, Germany
Pottasium hydroxide (KOH) ≥99.5%, p.a.	Carl Roth GmbH, Karlsruhe, Germany
Prolong Gold® antifade reagent	Molecular Probes Invitrogen, Eugene, OR, USA
Propidium iodide	Molecular Probes Invitrogen, Eugene, OR, USA
Protease inhibitor cocktail (PIC) for mammalian cell tissue	Sigma-Aldrich Life Science, Saint Louis, MO, USA
Retinoic acid ≥98%, HPLC grade	Sigma-Aldrich Life Science, Saint Louis, MO, USA
Roti®-Block 10×	Carl Roth GmbH, Karlsruhe, Germany
Roti®-Blue 5×	Carl Roth GmbH, Karlsruhe, Germany
Roti®-Nanoquant 5×	Carl Roth GmbH, Karlsruhe, Germany
Rotiphorese® Gel A	Carl Roth GmbH, Karlsruhe, Germany
Rotiphorese® Gel B (2%)	Carl Roth GmbH, Karlsruhe, Germany
Rotiphorese® Gel A/B 40 (29:1)	Carl Roth GmbH, Karlsruhe, Germany
Serva blue G (Coomassie-Brilliant blue G250)	SERVA Electrophoresis GmbH, Heidelberg, Germany
Silver nitrate ($AgNO_3$) ≥99.9%, p.a.	Carl Roth GmbH, Karlsruhe, Germany
Sodium carbonate (Na_2CO_3) ≥99.5%, p.a.	Carl Roth GmbH, Karlsruhe, Germany
Sodium chloride (NaCl) ≥99.5%, p.a.	Carl Roth GmbH, Karlsruhe, Germany
Sodium-deoxycholat (Na-deoxycholat)	Calbiochem, San Diego, CA, USA
Sodium dodecyl sulfate (SDS) ≥99.5%, ultra pure	Carl Roth GmbH, Karlsruhe, Germany
Sodium fluoride (NaF) ≥98%, technical	Sigma-Aldrich Life Science, Saint Louis, MO, USA
Sodium hydroxide (NaOH) ≥99%, p.a.	Carl Roth GmbH, Karlsruhe, Germany
Sodium thiosulfate pentahydrate >99.5%, p.a.	Merck KGaA, Darmstadt, Germany
Staurosporine >99%	Cell Signaling Technology, Danvers, MA, USA
Sucrose ≥99.5%, p.a.	Carl Roth GmbH, Karlsruhe, Germany
SYPRO® Ruby Protein Gel Stain 1×	Life Technologies, Carlsbad, CA, USA
Taq DNA Polymerase	New England Biolabs, Ipswich, MA, USA
Trifluoroacetic acid (TFA) ≥99.9%, for peptide synthesis	Carl Roth GmbH, Karlsruhe, Germany
Tris(hydroxymethyl)-aminomethan (Tris) >99.9%, p.a.	Carl Roth GmbH, Karlsruhe, Germany
Triton X-100 pure	Carl Roth GmbH, Karlsruhe, Germany
Trypan blue stain 0.4%	Gibco by Life Technologies, Paisley, UK
Tween® 20 Ph.Eur.	Carl Roth GmbH, Karlsruhe, Germany

3.4. Gases

Name	Manufacturer
Carbon dioxide (CO_2)	Airliquide, Kornwestheim, Germany
Gas mixture (1% O_2, 5% CO_2, 94% N_2)	Airliquide, Kornwestheim, Germany

Gas mixture (5% O_2, 5% CO_2, 90% N_2)	Airliquide, Kornwestheim, Germany
Nitrogen	Airliquide, Kornwestheim, Germany

3.5. Consumables

Name	Manufacturer
6, 12, 24, 96 (clear, black and white, F-bottom) well plates	Greiner bio-one GmbH, Frickenhausen, Germany
Cell culture flasks (T25,T75, T175)	Greiner bio-one GmbH, Frickenhausen, Germany
Chamber slides RS Glass 2/4 well	Nalge Nunc International, Naperville, IL, USA
Chamber slides CC2 Glass 2 well	Nalge Nunc International, Naperville, IL, USA
Cryovials with inner thread, 2 ml	Carl Roth GmbH, Karlsruhe, Germany
Dyalisis membrane, 12-16 kDa cut-off	Carl Roth GmbH, Karlsruhe, Germany
Eppendorf tubes (0.2, 0.5, 1 and 2 ml)	Eppendorf, Hamburg, Germany
Filters (0.22 µm)	Sarstedt, Nümbrecht, Germany
Flow cytometry vials (5 ml)	Sarstedt, Nümbrecht, Germany
Microscope slides	Carl Roth GmbH, Karlsruhe, Germany
Microscope slide coverslips	Carl Roth GmbH, Karlsruhe, Germany
Nitrocellulose membrane Roti®-NC	Carl Roth GmbH, Karlsruhe, Germany
NuPAGE® Novex® Bis-Tris Pre-Cast gels	Life Technologies, Carlsbad, CA, USA
Petri dishes (ø 35 mm; 10 cm^2)	Greiner bio-one GmbH, Frickenhausen, Germany
Pipette with tip, sterile (2, 5, 10, 25 ml)	Greiner bio-one GmbH, Frickenhausen, Germany
Pipette tips Gilson® (200, 1000 µl)	Greiner bio-one GmbH, Frickenhausen, Germany
Pipette tips Omnitip™ (10 µl)	ULPLAST, Warsaw, Poland
Rotilabo®-blotting paper, 1.5 mm thick	Carl Roth GmbH, Karlsruhe, Germany
Rotilabo®-stoppers (silicone rubber)	Carl Roth GmbH, Karlsruhe, Germany
Roti®-NC nitrocellulose membrane	Carl Roth GmbH, Karlsruhe, Germany
Rotisilon® B silicone grease	Carl Roth GmbH, Karlsruhe, Germany
Sensors (60 µm) for automated handheld cell counter Scepter™	Merck Millipore, Billerica, MA, USA
Tubes Cellstar® (15, 50 ml)	Greiner bio-one GmbH, Frickenhausen, Germany
Tygon® tube E-1000	Carl Roth GmbH, Karlsruhe, Germany
Plastic wide mouth jars (Nalgene® style)	Sigma-Aldrich, Taufkirchen, Germany
Sterile filters (0.22 and 0.45 µm)	Merck Millipore, Billerica, MA, USA

3.6. Cell culture

Name	Manufacturer
0.05% Trypsin- EDTA (1×)	Gibco by Life Technologies, Paisley, UK
Advanced DMEM (1×) Dulbecco's Modified Eagle Medium	Gibco by Life Technologies, Paisley, UK
DPBS (1×) Dulbecco's Phosphate Buffered Saline	Gibco by Life Technologies, Paisley, UK
Fetal Bovine Serum (FBS) Gold	PAA Laboratories GmbH, Pasching, Austria
L-glutamine (L-Gln)	Gibco by Life Technologies, Paisley, UK
Penicillin/Streptomycin	Gibco by Life Technologies, Paisley, UK

3.7. Kits/assays

Name	Manufacturer
Annexin V-FITC Apoptosis Detection Kit	Biotool, Houston, TX, USA
Blood & Cell Culture DNA Mini Kit	Qiagen, Hilden, Germany
EarlyTox Gluthatione Assay Kit	Molecular Devices, Sunnyvale, CA, USA
Luminescent ATP Detection Assay Kit	Abcam, Cambridge, UK
MitoXpress® Intra	Luxcel Biosciences, Cork, Ireland
OxyBlot™ Protein Oxidation Detection Kit	Merck Millipore, Billerica, MA, USA
Taq 2× Master Mix for PCR	New England Biolabs, Ipswich, MA, USA

3.8. Peptides

Name	Manufacturer
Amyloid-β 1-42 peptide ($A\beta_{1-42}$), human	China Peptides, Shanghai, China
FITC labelled amyloid-β 1-42 peptide (FITC-$A\beta_{1-42}$), human	Bachem, Bubendorf, Switzerland

3.9. Antibodies

Name and dilution in PBS-T	Manufacturer
Actin goat polyclonal antibody, 1:1000	Santa Cruz Biotechnology, Inc, Dallas, TX, USA
ATPB mouse monoclonal antibody, 1:1000	Abcam, Cambridge, UK
Bcl-2 mouse monoclonal antibody, 1:1000	Santa Cruz Biotechnology, Inc, Dallas, TX, USA
Caspase-9 mouse monoclonal antibody, 1:1000	Santa Cruz Biotechnology, Inc, Dallas, TX, USA
OxPhos Complex V subunit alpha polyclonal antibody, 1:1000	Molecular Probes, Eugene, OR, USA

Donkey anti-goat IgG-HRP, 1:2000	Santa Cruz Biotechnology, Inc, Dallas, TX, USA
Donkey anti-mouse IgG-HRP, 1:2000	Santa Cruz Biotechnology, Inc, Dallas, TX, USA
Donkey anti-rabbit IgG HRP antibody, 1:2000	Santa Cruz Biotechnology, Inc, Dallas, TX, USA
Hsp 60 mouse monoclonal antibody, 1:1000	Santa Cruz Biotechnology, Inc, Dallas, TX, USA
Hsp 70 mouse monoclonal antibody, 1:100	Abcam, Cambridge, UK
Hsp 90 mouse monoclonal antibody, 1:1000	Santa Cruz Biotechnology, Inc, Dallas, TX, USA
MTCO1 mouse monoclonal antibody, 1:1000	Abcam, Cambridge, UK
NDUFS1 rabbit polyclonal antibody, 1:1000	Proteintech Group, Chicago, IL, USA
OGG1/2 mouse monoclonal antibody, 1:500	Santa Cruz Biotechnology, Inc, Dallas, TX, USA
Rabbit Anti-DNP Antibody, 1:500	Merck Millipore, Billerica, MA, USA
VDAC1 goat polyclonal antibody, 1:2000	Santa Cruz Biotechnology, Inc, Dallas, TX, USA

3.10. Oligonucleotides

Name	Manufacturer
5’-CTGAGCCTTTTACCACTCCAG-3’	biomers.net GmbH, Ulm, Germany
5’-GGTGATTGATACTCCTGATGCG-3’	biomers.net GmbH, Ulm, Germany
5’-AACCACAGTTTCATGCCCATC-3’	biomers.net GmbH, Ulm, Germany
5’-TGTTAGTAAGGGTGGGGAAGC-3’	biomers.net GmbH, Ulm, Germany
5’- ACCCTATTGCACCCCCTCTAC’-3	biomers.net GmbH, Ulm, Germany
5’-CTTGTCAGGGAGGTAGCGATG-3’	biomers.net GmbH, Ulm, Germany

3.11. Gel markers/standards

Name	Manufacturer
Amersham™ HMW Calibration Kit for Native Electrophoresis (HMW)	GE Healthcare, Chalfont St Giles, UK
Amersham™ LMW Calibration Kit for SDS Electrophoresis (LMW)	GE Healthcare, Chalfont St Giles, UK
Lambda/HindIII DNA Digest	New England Biolabs, Ipswich, MA, USA
MagicMark™ XP Western Standard	Life Technologies, Carlsbad, CA, USA
PageRuler™ Plus Prestained Protein Ladder	Thermo Fisher Scientific, Waltham, MA, USA

4. Methods

4.1. Cell culture

Human neuroblastoma (SH-SY5Y) is a human derived cell line, a third subclone of SK-N-SH cells (Biedler et al., 1978) derived from the bone marrow of a 4-year old female with glioblastoma (Biedler et al, 1973). SH-SY5Y represents neural-like cells used for studies of proliferation and differentiation of neurons and is frequently used as a culture model for studying neurodegenerative diseases including Parkinson´s and Alzheimer´s disease (Schlachetzki et al., 2013).

4.1.1. Cell culture maintenance and oxygen adjustment

SH-SY5Y cell suspension in cryovials previously stored in gaseous phase of liquid nitrogen was thawed by warming in a water bath at 37° C for about 1 min. Cell suspension was added to 10 ml prewarmed cell culture medium and centrifuged at 700 x g for 5 min at RT. Cells were grown in DMEM supplemented with 10% FBS, 2% L-glutamine and 1% penicillin/streptomycin at 37°C, 5% CO_2, under two different oxygen conditions (~21% O_2 and 5% O_2, respectively). Low oxygen incubators were set up according to a previously described protocol (Wright and Shay, 2006). Premixed gas consisting of 5% O_2, 5% CO_2 and 90% N_2 was used to flush plastic wide mouth jars where cell culture flasks (T25) or Petri dishes (ø 35 mm) were placed (Figure 4.1).

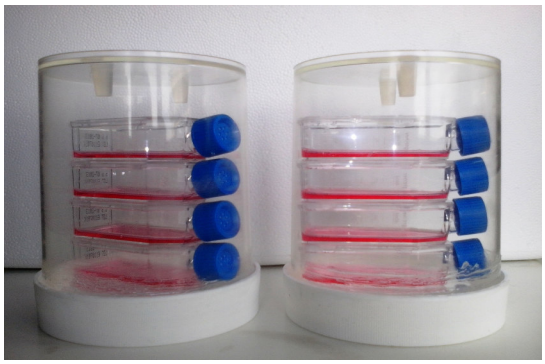

Figure 4.1. Home-made low O_2 incubators. Plastic wide mouth jars containing cell culture flasks were flushed with a gas mixture containing 5% O_2, 5% CO_2 and 90% N_2.

Home-made incubators with 1% or 5% O_2 were placed in the standard cell culture incubator for temperature regulation and cells were cultivated in parallel with cells at about atmospheric 21% O_2. In order to determine which of two different low oxygen concentrations (1% or 5% O_2) is more appropriate for cultivation of SH-SY5Y cells, cell proliferation and ATP concentration were tested in control experiments. The cell culture was checked regularly (after 24) hours under the light microscope to ensure that the cells were attached to the bottom of the flask. Once cells become confluent, i.e., when they cover all available substrate surface, their growth slows and cells have to be subcultured or passaged. Trypsin endopeptidase belonging to a family of serin proteases was used to break the cell-substrate connections. 0.05% EDTA added to trypsin was used to complex Ca^{2+} and Mg^{2+} to achieve the loss of cell-cell junctions of adherent cells. Cell culture media was

removed and cells were washed with PBS (Phosphate Buffer Saline) solution free of calcium and magnesium. Then, the cell monolayer was covered with trypsin-EDTA solution. Cells were incubated for 5 min at 37 °C. Thereafter, the complete medium was added to trypsinized cells which were resuspended in order to dislodge and dissociate cells which remained adherent. Cell suspension was centrifuged at 700 x g for 5 min at RT. The supernatant was removed after centrifugation, cells were resuspended in appropriate volume of media and distributed to new flasks. Cells were passaged every 3-4 days and incubation at 5% O_2 was performed at least 7 days before conducting experiments. Cell number was determined using either trypan blue exclusion of the dead cells or automated cell counter Scepter™ since both methods of counting were found to be similarly efficient in estimating cell number per ml of cell suspension when compared. Cells were maintained in the cell culture until they reached the passage number 20. Then, cells are harvested and cryopreserved. Cell culture medium was removed and cells were washed with PBS and dislodged by trypsin-EDTA at 37 °C for 5 min. Cells were re-suspended and the cell number was determined. Cell suspension was centrifuged at 700 x g for 10 min at 4 °C. The supernatant was removed and cells were re-suspended in freezing medium (cell culture medium with 10% DMSO). 1 ml aliquots of cell suspensions were transferred to cryovials and frozen gradually: 2 h at -20 °C, 1-2 days at -80 °C and then placed to the gaseous phase of liquid nitrogen for longer storage.

4.1.2. Cell differentiation

All-*trans* retinoic acid (ATRA, tretinoin or vitamin A acid) (Figure 4.2) is a bioactive small molecule and ligand for both the retinoic acid receptor (RAR) and the retinoid X receptor (RXR) (Balmer & Blomhoff, 2002) The bound RAR and RXR act as transcription factors that regulate the growth and differentiation of both normal and malignant cells (Chiu et al., 1995, Korecka et al., 2013). Retinoic acid primes embryonic stem cells to become neurons (Rhinn & Dollé, 2012). SH-SY5Y cells resemble neurons after the treatment with retinoic acid (Fagerström, 1996). Cytochromes P450 (CYPs) catalyze the 4-hydroxylation of ATRA (Nadin & Murray, 1999) making it inactive in the human body.

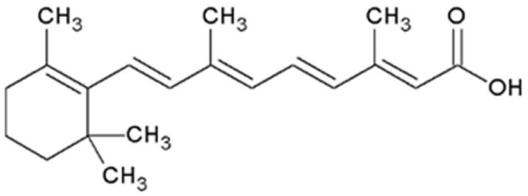

Figure 4.2. Structure of all-*trans* retinoic acid (ATRA).

10 mM ATRA was prepared in DMSO and was filter-sterilized and kept protected from light sources < 400 nm. Working solution (10 µM) was added in FBS-containing cell culture media (FBS is required as retinoic binding substrate) and cells were monitored for 3 days in 24 h intervals for morphological changes characteristic for differentiated cells.

4.1.3. Amyloid β peptide treatment

Cells were incubated with disaggregated externally applied $A\beta_{1-42}$ peptide according to the modified protocol of Jao and colleagues (1997). Briefly, 1 mg $A\beta_{1-42}$ peptide with or without attached fluorophore (FITC) was disaggregated in a glass vial using 1.5 ml distilled TFA (trifluoroacetic acid) in an ultrasonic bath for 15 min at RT, centrifuged at 3000 x g for 15 min at 16°C. The supernatant was transferred into a new glass vial and nitrogen was used to completely remove TFA. The peptide was dissolved in DMSO (1 mM stock solution was prepared for unlabeled and 200 µM for FITC-Aβ peptide) and stored at -20°C in aliquots to avoid repeated freeze-thaw cycles. Cells were incubated with 4 µM $A\beta_{1-42}$ peptide added to the cell culture medium and/or irradiated with 2 Gy X-rays. In the case when both Aβ peptide and irradiation were applied, cells were incubated with the peptide 6 h prior to irradiation and then incubated for the next 18 h. In order to test the effect of fibrillized Aβ peptide on SH-SY5Y cells, the peptide was aggregated by storage at 37 °C overnight ("aged" peptide) and applied in 4 µM and 100 µM concentration, respectively, to the cell culture.

4.1.4. X-ray irradiation

Irradiation of cells was performed using a X-ray tube with a metal-ceramic anode set to 250 kV (1keV/µm) with a current flow of 10 mA and 50 cm distance from a sample irradiated for 54 sec to obtain dose of 2 Gy. Alternatively, wolfram anode set to 90 kV, 19 mA and 30 cm distance from a sample for 40 sec was used to obtain a dose of 2 Gy. There was no difference in cellular responses when different anodes were used. Longer wavelenghts were excluded using a 2 mm aluminum filter. Cell culture vials were placed in the X-ray machine chamber in horizontal position at room temperature. After irradiation, cells remained in atmospheric condition of gases for approximately 10 min required for transportation back to the incubator with 21% and 5% O_2, respectively. Irradiation was performed in the group of Professor Markus Löbrich (Biology department, TU Darmstadt).

4.2. Cell culture experiments

4.2.1. Measurement of intracellular oxygen concentration

Intracellular oxygen concentration differs from the oxygen concentration applied usually to the cell culture. It is a marker of the metabolic activity of cells and it depends on surrounding O_2 concentration and temperature. The oxygen sensitive probe MitoXpress® Intra was used to measure intracellular oxygen concentrations ($[O_2]$). The probe emits photons (phosphorescence mechanism) and the signal intensity depends on the available oxygen which quenches the signal. Cells were seeded to black clear bottom plates with a density of ~4 x 10^4 cells per/well/200 µl cell culture medium. The next day, cells were washed with PBS and MitoXpress Intra probe diluted in medium (1:10 dilution) was added to cells (100 µl/well) and incubated at 37°C overnight. Addition of 150 µM antimycin which inhibits the electron transfer at complex III and removes the influence

of cellular O_2 consumption on intracellular oxygen concentration served as a negative control (increase in signal). 150 µM glucose oxidase which uses oxygen for its activity served as a positive control (decrease in signal). On the day of the assay, cells were washed twice with fresh medium and measured immediately for 30 minutes in 2 minute intervals using a plate reader with excitation at 390 nm and emission at 660 nm. Obtained intensity values were converted into oxygen scale (percentage of oxygen) using the following equation (given in the manual for MitoXpress® Intra Intracellular Oxygen assay):

$$[O_2]_t = \frac{[O2]a * Ia * (Io - It)}{It * (Io * Ia)}$$

where $[O_2]_a$ is oxygen concentration in atmospheric conditions (20.9%), I_o and I_a are signals measured after addition of glucose oxidase and antimycin, respectively, while I_t are experimental intensity values obtained during measurement.

4.2.2. Cell proliferation

Proliferation of SH-SY5Y cells was studied by determining cell number and doublig time (quantitative analysis) and by microscopic observation (qualitative analysis).

4.2.2.1. Determining the cell number

Cells were seeded in 10 cm^2 Petri dishes at density of ~4 x 10^3 cells/cm^2 and incubated at 21% O_2 and 5% O_2, respectively. Cell number and viability were determined every day during the period of 9 days.

$$viablity = \frac{number\ of\ viable\ cells}{total\ cell\ number} \times 100\%$$

Using Neubauer chamber cells were counted in a very small volume of cell suspension under the light microscope. A small aliquot of the cell suspension after trypsinization (20 µl) was mixed with the same volume of trypan blue, which stains only dead cells or cells with loss of the cell memebrane integrity, for the exclusion of dead cells. Unstained cells were counted in four large squares of the Neubauer chamber net indicated with A (Figure 4.3) each with the area of 1mm^2 and depth of 0.1 mm giving volume of 10^{-4} ml. Counted number of cells is divided by 2 and multiplied by 10^4 giving a the number of cells per ml (Pollard & Walker, 1997).

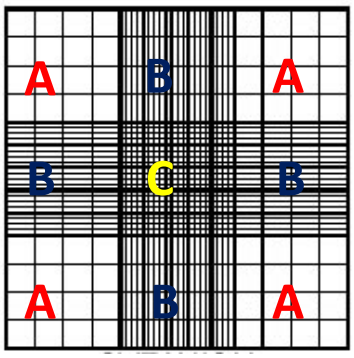

Figure 4.3. Schematic representation of Neubauer counting chamber. A, B and C represent large squares containing 16, 20 and 25 smaller squares, respectively. Every large square has an area of 1 mm^2 and depth of 0.1 mm giving a volume of 10^{-4} ml.

In addition to counting cells in Neubauer chamber and to confirm results, cell number was determined using Scepter™, a handheld automated cell counter with attached sensor (single use) with the 60 µm orifice (Figure 4.4). Number of cells passed through it creating resistance was measured as the number of electrical pulses. An aliquot of the cell suspension after trypsinization was diluted 1:3 in PBS and was drawn into the channel of the sensor and the cell concentration is calculated automatically. Then, the number was multiplied by dilution factor.

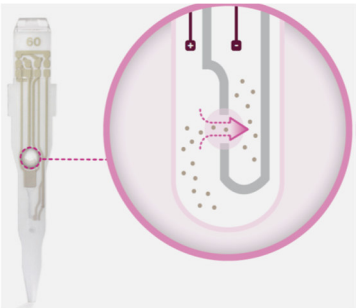

Figure 4.4. Sensor of the Scepter™ Handheld Automated Cell Counter (https://www.emdmillipore.com).

Population doubling time (DT) was calculated using the following equation:

$$DT = \frac{Tx\ log2}{\log(\frac{Xe}{Xb})}$$

where T is the incubation time in any units, Xb is the cell number at the beginning of the incubation time. Xe is the cell number at the time of the end of the exponential phase before the plateau phase was reached.

4.2.2.2. Fluorescence staining and microscopy

MitoTracker® Orange and DAPI staining of the adherent cells was applied for microscopic evaluation of proliferation and morphology of SH-SY5Y cells. MitoTracker Orange is a dye that freely enters mitochondria of healthy cells. The dye was prepared in DMEM without FBS. Media from the cells grown on glass slides in Petri dishes was removed and pre-warmed staining solution

containing 300 nM MitoTracker Orange was added. Cells are incubated for 30 min at 37°C and then washed with PBS with addition of 1 mM $CaCl_2$ and 0.5 mM $MgCl_2$. This solution allows cells to adhere to each other on the substrate. If cells are in the medium containing no Ca^{2+} or Mg^{2+}, they will round up and detach from the substrate. Cells were fixed using 3.7% formaldehyde for 10 min. Following fixation, cells were rinsed three times, 5 min each, in PBS. Cells were permeabilized by 0.2% Triton X-100 for 5 min and then rinsed three times, 5 min each, in PBS. For staining of the nuclei, DAPI was diluted 1:5000 in H_2O. Cells were incubated with DAPI solution 5 min at RT and then rinsed three times in PBS. Coverslips were mounted onto microscope slides using ProLong® Gold antifade reagent that prevents photobleaching. Cells were imaged using the fluorescence microscope with filters for DAPI (λ_{EX}/ λ_{EM} = 359 nm/461 nm) and MitoTracker Orange ((λ_{EX}/ λ_{EM} = 554 nm/576 nm).

4.2.3. Interaction of Aß$_{1-42}$ peptide with SH-SY5Y cells

4.2.3.1. Flow cytometry

In order to estimate whether Aβ peptide interacts with SH-SY5Y cells, ~1 x 10^5 cells/ml seeded in 35 mm Petri dishes were incubated with disaggregated 200 nM FITC-labelled Aβ_{1-42} peptide for 5, 10, 15, 30 min and 1, 3, 18, 24 h. Cells were harvested by trypsinization, washed and resuspended in PBS and the fluorescence signal was measured by flow cytometry using 488 nm laser for excitation. 5000 cells were analyzed and fluorescence signals were plotted in Kaluza software as FL1-area log against the signal count for detection of the shift of fluorescence signal compared to the unstained cells.

4.2.3.2. Confocal microscopy

In order to get information on the subcellular localization of disaggregated and externally added Aβ peptide, ~5 x 10^4 cells/ml were grown on 25 mm round glass coverslips and incubated 3, 8 and 18 h with 400 nM FITC-labelled Aβ_{1-42} peptide. Imaging was performed in PBS containing 5% FBS at room temperature using a confocal laser scanning microscope. Incubation with the endoplasmatic reticulum-specific dye ER-Tracker™ Red ($\lambda_{EX}/\lambda_{EM}$ = 587/615 nm), mitochondria-specific MitoTracker® Red CM-H2Xros ($\lambda_{EX}/\lambda_{EM}$ = 579/599 nm) and lysosomes-specific dye LysoTracker® Red ($\lambda_{EX}/\lambda_{EM}$ = 577/590 nm), respectively, was performed 15 or 5 min (for LysoTracker Red) prior to imaging. FITC and ER-Tracker/MitoTracker/LysoTracker Red were sequentially excited with an argon laser at 488 nm and with a yellow diode at 561 nm, respectively. Images (512 x 512 pixels) were acquired by sequential scannning between lines (line average 6) using 40x (1.3 NA) oil-immersion objective with a 12 bit HyD detector at the corresponding spectral range for each fluorophore. The background was subtracted from all images (rolling ball radius: 50 pixels) and images were overlayed in ImageJ software for putative detection of fluorescence signal colocalization.

4.2.4. Neutral red uptake assay

neutral red stock solution
4 mg/ml neutral red in PBS

neutral red medium
40 µg/ml neutral red stock solution i
cell culture medium

neutral red destain solution
50% (v/v) ethanol
49% (v/v) Milli-Q-water
1% (v/v) glacial acetic acid

Neutral red assay is one of the most used cytotoxictiy tests. It is based on the ability of viable cells to uptake take up neutral red, a weakly cationic dye that penetrates cell membranes by nonionic passive diffusion (Nemes et al., 1979). The dye is accumulated in lysosomes, where it becomes charged due to the lysosomal proton gradient necessary to maintain low pH. Charged neutral red is retained inside the lysosomes as it binds by electrostatic bonds to anionic groups of the lysosomal matrix (Winckler, 1974). Thus, the assay can provide valuable information on endocytotic activity of cells and lysosomal integrity. In order to get information on lysosomal integrity of SH-SY5Y cells upon oxidative stress caused by amyloid beta peptide and ionizing radiation, non-differentiated and cells treated with retinoic acid (~9 x 10^4 cells/ml) were seeded into 96-well plates in duplicates (n = 2). The next day, cells were treated with Aβ peptide and/or irradiated with 2 Gy X-rays and incubated for 24 hours. Neutral red working solution was prepared one day before the assay and kept at 37°C in the cell culture incubator as previously described (Repetto et al., 2008). On the day of the assay, cell culture medium was discarded and 100 µl neutral red medium was added to all wells containing cells and incubated 2 h at 21% and 5% O_2, respectively. Following incubation, neutral red medium was removed and cells were washed with 150 µl PBS per well. The dye was extracted from viable cells using acidified ethanol solution (100 µl/well) by shaking plates rapidly on a plate shaker for 15 minutes. Absorbance of extracted neutral red was measured at 540 nm using a plate reader.

4.2.5. Determination of cell death

4.2.5.1. Cell death detection by fluorescence microscopy

Apoptotic cells undergo rapid morphological alterations that indicate the progression of cell death. These include changes in the cytoskeleton and plasma membrane, condensation of the cytoplasm and nucleus and internucleosomal cleavage of DNA (Elmore, 2007). An early indicator of apoptosis is the rapid translocation and accumulation of the membrane phospholipid phosphatidylserine (PS) from the cytoplasm interface to the extracellular surface. This loss of membrane asymmetry can be detected by utilizing the binding properties of Annexin V. Annexin V is a calcium dependent phospholipid binding protein that preferentially binds to negatively charged phospholipids including PS. Cells progressing through apoptosis can be monitored according to their Annexin V and propidium iodide staining pattern. Early apoptotic cells will bind

extracellular Annexin V but are not sensitive to intracellular staining with propidium iodide (PI). As cells progress through apoptosis, the integrity of the plasma membrane is lost, allowing PI to penetrate, which results in a strong yellow-red fluorescence signal.
Cells were cultivated on chamber slides at a density of ~0.5 x 10^4 cells/ml/well of a 4-chamber slide at 21% and 5% O_2, respectively. Next day, cells were treated with $A\beta_{1-42}$ peptide and/or irradiated using 2 Gy X-rays. On the day of the assay, cells were rinsed with PBS and fixed using 3.7% formaldehyde for 10 min. Following fixation, cells were rinsed three times, 5 min each, in PBS. 1× Assay buffer (500 µl/well) from Annexin V-FITC Apoptosis Detection Kit was added and cells were incubated with 5 µl (1 µg) Annexin V-FITC and 10 µl of propidium iodide per 100 µl Assay Buffer for 15 minutes at room temperature in the dark. Cells were covered with coverslips and visualized under the fluorescence microscope using a dual filter set for FITC ($\lambda_{EX}/\lambda_{EM}$ = 495 nm/517 nm) and rhodamine ($\lambda_{EX}/\lambda_{EM}$ = 551 nm/573 nm).

4.2.5.2. Cell death detection by flow cytometry

FCS buffer
FBS in PBS (1:20)

Cells were grown in 10 cm^2 Petri dishes (~1 x 10^5 cells/ml) at 21% and 5% O_2, respectively. Next day, cells were treated with $A\beta_{1-42}$ peptide and/or irradiated using 2 Gy X-rays. Treatment with 1 µM staurosporine (ihnibits protein C kinase and other kinases) for 24 h was used as a positive control for apoptosis. On the day of the assay, cells were rinsed with PBS and harvested by trypisinization. Cells were resuspended in 300 µl FCS buffer and pelleted by centrifugation (700 x g for 5 min at 4 °C). Incubation of cells at 60 °C for 15 min served as a positive control for necrosis. Cells were resuspended in 200 µl 1× Assay Buffer and incubated with 0.5 µg (10 µl) propidium iodide (PI) and 0.4 µg (2 µl) Annexin V FITC for 15 min at room temperature in the dark. Positive control for apoptosis and necrosis were single (either Annexin V-FITC or PI) and double stained (both Annexin V-FITC and PI). Following incubation, 1× Assay Buffer (200 µl) was added to all samples and controls. Fluorescence emission was measured at 514 nm (FL1) for Annexin V-FITC and 617 nm (FL2/3) for PI. 10000 cells was analyzed and data were compensated in Kaluza software using single stained controls.

4.2.6. Cellular ATP concentration

The nucleotide ATP (adenosine-5'-triphosphate) generated mainly in mitochondria is a primary energy source of living cells and its amount can be influenced by pathological processes. For example, ATP supports synaptic vesicle recycling in axons and energy failure can contribute to neurodegeneration (Pathak et al., 2015). Thus, changes of cellular ATP concentration can indicate changes in cell viability and proliferation in response to cytotoxic compounds or other modifiers. In order to assess cellular ATP concentration depending on irradiation, differentiation status, treatment with $A\beta_{1-42}$ peptide and oxygen concentration in the cell culture, Luminiscent ATP

detection assay kit based on firefly (*Photinus pyralis*) luciferase was used. Reaction of ATP with luciferase and D-luciferin results in production of light which is proportional to the ATP concentration in the cell.

$$ATP + D\text{-}Luciferin + O_2 \xrightarrow[Luciferase]{Mg^{2+}} Oxyluciferin + AMP + PP_i + CO_2 + Light$$

About 1.5 x 10^5 cells were seeded in 10 cm^2 Petri dishes at least in duplicates. Cells were harvested and ~82.5 x 10^3 cells per well in reaction mix (final volume 200 µl/well) was added to a white flat-bottom 96 well-plate. Blank controls were prepared the same way as samples only without cells. Samples were incubated 10 min in the dark and luminescence was measured using a plate reader. ATP concentrations were determined using calibration line obtained by measuring luminescence of standard ATP dilutions (in a range of 0.5-15 µM/well). Background signal was subtracted from each signal measured and ATP concentrations per cell were presented. ATP concentrations were normalized to cell count and compared to corresponding controls.

4.2.7. Measurement of intracellular ROS level

Carboxy-H_2DCF-DA (2'7'-dichlorofluorescin diacetate) is a commonly used oxidative stress indicator and is used for detection of a range of ROS species such as H_2O_2 and reactive oxygen species derived from it (•OH and hydroperoxides). Non-fluorescent DCFH-DA enters cells and accumulates mostly in the cytosol (Halliwell & Whiteman, 2004) where it becomes converted by esterases and ROS to a fluorescent DCF (Figure 4.5). Carboxylated version of DCFDA (Figure 4.6) is better retained in cells (Hempel et al., 1999) due to the presence of two negative charges at physiological pH which prevent its leakage out of the cell. The intracellular level of reactive oxygen species (ROS) upon treatment with $A\beta_{1\text{-}42}$ peptide and/or ionizing radiation was monitored using carboxylated DCFDA in flow cytometric measurements. In addition, HyPer, a genetically encoded H_2O_2 sensor was used for monitoring intracellular H_2O_2 by confocal microscopy. Intracellular ROS measuement by flow cytometry gives the relative estimation of ROS level in cell suspension (cell population) in comparison to controls, while microscopic ROS measurement using HyPer provides relative estimation and analysis of H_2O_2 level in single cells in determined time interval (live cell imaging).

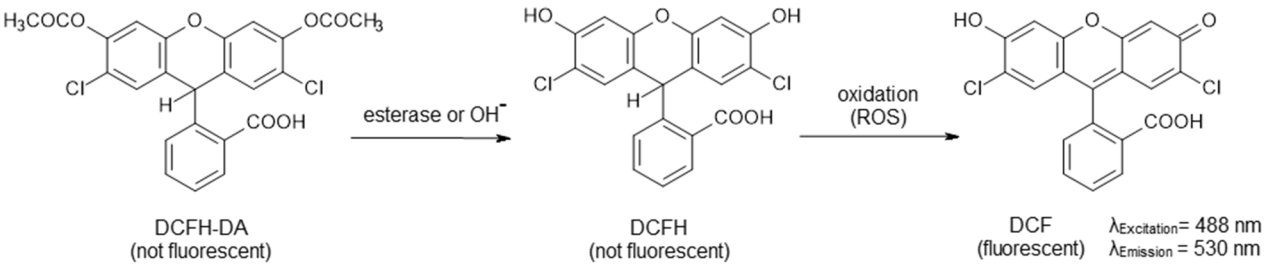

Figure 4.5. Mechanism of the conversion of non-fluorescent DCFH-DA to fluorescent DCF by intracellular enzymes (esterases) and ROS. The non-fluorescent DCFH-DA enters cells freely since the acetates help with effective loading into live cells. DCFH-DA is trapped after deacetylation by endogenous intracellular esterases inside the cells forming

the non-fluorescent 2', 7'-dichlorofluorescein (DCFH). DCFH is converted by peroxidases and ROS in several reaction steps to green fluorescent 2',7'-dichlorofluorescein (DCF). The excitation wavelength of DCF is 488 nm and the emission wavelength 530 nm. (https://tools.thermofisher.com)

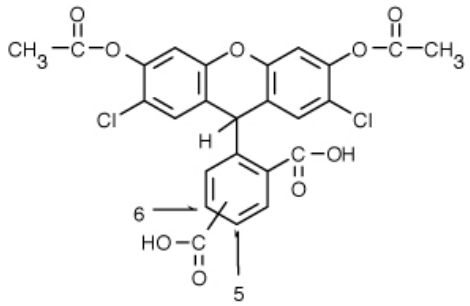

Figure 4.6. Structuture of carboxy-H_2DCF-DA (2'7'-dichlorofluorescin diacetate). (https://tools.thermofisher.com).

4.2.7.1. Intracellular ROS measurement by flow cytometry

carboxy-H_2DCF-DA
10 mM 2'7'-dichlorofluorescin diacetate in DMSO
aliqouted, flushed with $N_{2(g)}$
and stored at -20 °C in the dark

H_2O_2
10 mM in Milli-Q-water
prepared freshly

FCS buffer
FBS in PBS (1:20)

Cells were grown in 10 cm^2 Petri dishes (~1 x 10^5 cells/ml) at 21% and 5% O_2, respectively. Next day, cells were treated with $A\beta_{1-42}$ peptide and/or irradiated using 2 Gy X-rays. On the day of the assay, a sample of cells was treated with 1 mM H_2O_2 in FCS buffer for 30 min at RT (positive control for increse in ROS). Cells were harvested by trypsinization and incubated with 20 µM carboxy-H_2DCFH-DA in FCS buffer for 20 min at 37 °C. Folllowing incubation, cells were pelleted (700 x g for 5 min at RT), resuspended in 1 ml PBS and the fluorescence intensity of C-DCF ($(\lambda_{EX}/\lambda_{EM}$ = ~492–495 nm/517–527 nm) was measured by flow cytometry. Cell population was set as 10000 events in R2 channel using unstained sample. Data was analyzed in Kaluza software. Results were shown as the level (percentage) of ROS in samples compared to H_2O_2 treated cells (positive control).

4.2.7.2. Intracellular ROS measurement by confocal microscopy

HyPer
1 µg of DNA/2 ml serum free DMEM

H_2O_2
10 mM in Milli-Q-water
prepared freshly

Cells were seeded on 25 mm round glass coverslips in 6-well plates. 1 µg of Hyper was used per 2 ml of serum free cell culture media with 3 µl peqFECT transfection reagent added. The mixture was incubated 15 min at RT and 100 µl/well was added to the cells and then incubated for 48 h. Following incubation, cells were washed with PBS and observed using confocal laser scanning microscope with 40x (1.3 NA) oil-immersion objectives, 405 nm diode and 488 argon laser excitation. 100 µM H_2O_2 was used as a positive control for increase of the fluorescence signal. Images (512 x 512 px) were obtained using a 500-550 nm 12-bit HyD detector. Background was subtracted by choosing regions of interest (ROIs) at cell free positions). Ratio of signal obtained at 488 nm and 405 nm excitation was used to determine fluorescence signal ratio in Image J software.

4.2.8. Glutathione level

(2S)-2-amino-4-{[(1R)-1-[(carboxymethyl)carbamoyl]-2-sulfanylethyl]carbamoyl} butanoic acid (GSH9 or GSH) is a tripeptide and one of the antioxidants used by the cell. GSH is present in millimolar concentrations in the cell (Montero et al., 2013). The relative level of glutathione was measured using EarlyTox Gluthatione Assay Kit. About 2 x 10^4 cells were seeded per well (100 µl culture medium) of a 96-well black clear F-bottom plate and incubated at 37 °C and at 21% and 5% O_2, repsectively, overnight. Cells treated with 2 µM staurosporine served as a positive control for decrease in GSH level. The assay was performed 1 h and 18 h after irradiation or 6h and 24 h after Aβ peptide treatment by adding 40 µM monochlorbimane (MCB) from the kit directly to the cell culture media. Cells were incubated at 37 °C and fluorescence of the MCB-S-glutathione conjugate was measured using a plate reader with 394 nm excitation filter and 490 nm emission filter. The intensity of the fluorescence signal is directly proportional to the level of GSH in the cells.

4.2.9. Mitochondrial membrane potential

Electron transport in mitochondria drives pumping of H^+ out of the mitochondrial matrix across the inner membrane, which creates a pH gradient across the inner mitochondrial membrane (about 8 in the matrix and lower pH in the intermembrane space, about 7.4) and a voltage gradient across the inner mitochondrial membrane, creating a electrical membrane potential (V) with the matrix side negative and the cristae space side more positive. The mitochondrial membrane potential is about 150 mV and the pH gradient about 0.5 to 0.6 pH units (each unit is equivalent to a membrane potential of about 60 mV). Together, ΔpH and ΔV make up the electrochemical gradient of about 180 mV (inside negative) (Alberts, et al., 2015, pp.762-763). Relative changes in mitochondrial membrane potential (compared to the control) can be measured using dyes that have selectivity for mitochondria. MitoTracker® Red CM-H_2XRos (Figure 4.7) is a reduced, nonfluorescent probe that stains mitochondria in live cells where it fluoresces upon oxidation. The intensity of the fluorescence is proportional to the mitochondrial membrane potential.

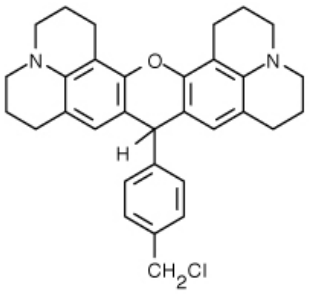

Figure 4.7. Structure of MitoTracker® Red CM-H_2Xros. (https://tools.thermofisher.com).

MitoTracker® Red CM-H_2Xros	**CCCP**
1 mM in DMSO	20 mM in DMSO
aliqouted, flushed with N_2 (g)	aliqouted and
and stored at -20 °C in the dark	stored at -20 °C in the dark

Cells were seeded to 10 cm^2 Petri dishes at a density of ~1 x 10^5 cells/ml. Next day, cells were treated with $A\beta_{1-42}$ peptide and 6 h later irradiated using 2 Gy X-rays. Cells were incubated for the next 18 h at 37 °C at 21% and 5% O_2, respectively. On the day of the assay, 1 µM MitoTracker Red ($\lambda_{EX}/\lambda_{EM}$ = 579/599 nm) was added to cells and incubated at 37 °C for 10 min. Cells are then harvested and washed in PBS at 700 x g for 5 min at RT, and cell pellet was resuspended in 300 µl PBS. The fluorescence was measured by flow cytometer. 10000 cells per sample were analyzed using 488 and 561 nm lasers for excitation of the dye in fluorescence channel FL3. Treatment with the proton gradient uncoupler CCCP (carbonyl cyanide m-chlorophenyl hydrazone) for 5 min served as a positive control for reduction of mitochondrial membrane potential. Data were analyzed by Kaluza software as FL3-area log against the signal count for detection of the fluorescence signal shift compared to control samples.

4.3. Protein analysis

4.3.1. Isolation of total cellular proteins

RIPA buffer for cell lysis
50 mM Tris-HCl (pH 7.4)
1% (v/v) IGEPAL®-CA630
0.5% Na-deoxycholat
0.1% SDS
150 mM NaCl
2 mM EDTA
50 mM NaF

In order to extract total cellular proteins, cells were lysed thoroughly using RIPA buffer. Medium was discarded and cells were harvested and re-suspended in PBS, counted and centrifuged at 700 x g for 5 min at 4 °C. The supernatant was discarded and the cell pellet was re-suspended in ice-cold RIPA buffer where ~2 x 10^5 cells per 24 µl RIPA-buffer was used. Samples were incubated on ice for 30 min and vortexed every 10 min for efficient release of the cellular content in the suspension. Afterwards, suspension was centrifuged at 14000 x g for 15 min at 4 °C. The supernatant containing the all proteins, both water soluble and solubilized membrane proteins, was transferred into pre-cooled Eppendorf tubes and stored at -20 °C. Small aliquot of the cell lysate was used for determination of the protein concentration by Bradford assay (Bradford, 1976).

4.3.2. Isolation of mitochondria

homogenisation buffer
10 mM HEPES (pH 7.4)
1.1 mM EDTA in
Milli-Q-water, stored at -20 °C

sucrose
2 M sucrose in
Milli-Q-water, stored at 4 °C

In order to extract „crude“ mitochondria for investigation of the mitochondrial proteome, cells were harvested and mechanically homogenized in 1.8 ml buffer with addition of protease inhibitor cocktail (PIC), preventing protein degradation, and using glas-teflon homogenizer (800 rpm, 15 strokes) on ice. 0.25 M sucrose preventing swelling of mitochondria was added to the homogenized suspension and centrifuged at 1900 x g for 10 min at 4 °C. Supernatant was kept on ice and pellet was resuspended in homogenisation buffer with 0.25 M sucrose and centrifuged at 1900 x g for 10 min at 4 °C three times to increase the yield of mitochondria. Supernatants from three centrifugation steps were merged and centrifuged at 14000 x g for 10 min at 4 °C. The pellet containing mitochondria (and partly other cellular compartments and components) was resuspended in homogenisation buffer with PIC and sucrose. Aliquots of isolates were quickly frozen in liquid nitrogen and then kept at -80 °C for longer storage. Small aliquots were used for determination of total protein concentration using Bradford assay (Bradford, 1976).

4.3.3. Bradford assay

In order to determine protein concentration either of isolated „crude“ mitochondria (4.3.2) or total cellular proteins from cell lysate (4.3.1), Bradford assay (Bradford, 1976) was employed. 1× Roti®-Nanoquant was prepared from 5× stock and used for colorimetric assay. The reagent Coomassie-Brilliant Blue G250 contained in Roti®-Nanoquant is red in its cathionic form (absorption maxiumum at about 465 nm) and green in its neutral form (absorption maxiumum at about 650 nm). In the presence of proteins, the neutral form of Coomassie-Brilliant blue G250 in acidic solution will be converted in the blue anionic form (Figure 4.8) with the decrease of absorption below 465 nm and the appearance of an additional peak at 595 nm.

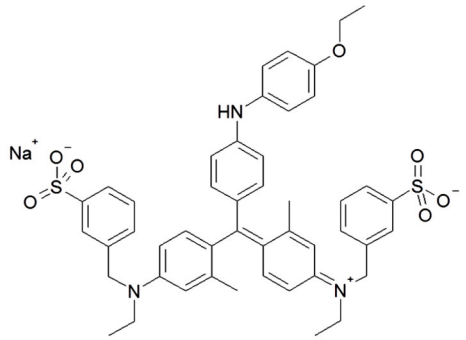

Figure 4.8. Structure of Coomassie-Brilliant Blue G250. (https://www.carlroth.com).

Bovine serum albumin (BSA) standard dilutions (Table 2) were prepared from BSA stock solution of concentration determined by UV-VIS spectrophotometer. Four protein dilutions per sample were prepared in 1.5 ml Eppendorf tubes (Table 3) and 640 µl of 1× Roti®-Nanoquant was added to each sample and standard and mixed well. Both, standard and protein dilutions were measured in triplicates (3 x 200 µl) in a clear 96-well plate. Samples and standard were incubated 10 min at RT and absorption was measured at 590 nm (protein and dye) and at 485 nm (dye) using a plate reader. The absorbance value of blank (water) was subtracted from all values and absorbance was calculated as 590 nm/480 nm ratio. Mean values of absorbances were ploted against concentrations. Slope and y-axis intercept were determined from the linear equation of the standard and used for determination of protein concentrations of samples multiplied with dilution factors.

Table 2. BSA-standard dilutions for Bradford assay.

Milli-Q-water [µl]	381.8 µg/ml BSA-stock[µl]	resulting BSA-concentration [ng/µl]	final BSA-concentration in 96-well [ng/µl]
160	0.0	0	0
158	2.0	4.77	0.95
156	4.0	9.54	1.90
152	8.0	19.09	3.82
144	16.0	38.18	7.64
136	24.0	57.27	11.45
130	30.0	71.58	14.32
120	40.0	95.45	19.09
110	50.0	119.31	23.86

Table 3. Protein sample dilutions for Bradford assay.

dilution	Milli-Q-water [µl]	sample [µl]	final dilution in 96-well
1:25	153.6	6.4	1:125
1:50	156.8	3.2	1:250
1:100	158.4	1.6	1:500
1:200	159.2	0.8	1:1000

4.3.4. Solubilisation of mitochondrial membranes

10% digitonin
in Milli-Q-water
dissolved for 30 min at 95 °C

1.1× solubilisation buffer
33.33 mM HEPES/KOH pH 7.4
166.67 mM potassium acetate
11.11% glycerol
in Milli-Q-water, stored at -20 °C

120 µg of protein from „crude" isolated mitochondria (4.3.2) per sample was centrifuged in 800 µl solubilisation buffer at 20800 x g for 8 min at 4 °C. Supernatant was removed and pellet was solubilized with the mild non-ionic detergent digitonin (3 g/g protein) at a final concentration of 1% (w/v) (3.6 µl of 10% digitonin) in solubilisation buffer (36.4 µl) 30 min on ice by vortexing samples every 10 min. Samples were centrifuged at 20000 x g for 10 min at 4 °C and supernatants were used immediately for further experiments.

4.3.5. Polyacrylamide gel electrophoresis

4.3.5.1. Blue-native polyacrylamide gel electrophoresis (BN-PAGE)

The blue native polyacrylamide gel electrophoresis (BN-PAGE) allows the separation of proteins in the mass range of 10 kDa to 10 MDa in their native form, i.e., protein complexes and supercomplexes remain both intact and active after separation (Neff and Dencher, 1999). In BN-

PAGE, the cathode buffer contains Coomassie Brilliant Blue G-250, a blue dye which binds to proteins almost proportional to their size, masking their intrinsic charge by its own net negative charge. Hence, separation of proteins occurs according to their molecular mass. Since interactions between Coomassie Brilliant Blue G-250 and proteins exhibit minor effects on protein structure or protein-protein interactions, secondary, tertiary and quaternary protein structures are preserved and enzyme activity can be determined in in-gel activity assays (Shagger & von Jagow, 1991). The separation of the proteins is carried out in a gradient polyacrylamide gel composed of a stacking gel with large pores and a separating gel with pores gradually decreasing in their size.

light BN-PAGE gel buffer (3×)
6-aminohexanoic acid 1.5 M
imidazole/HCl, pH 7.0 75 mM
in Milli-Q-H_2O, stored at 4 °C

heavy BN-PAGE gel buffer (3×)
6-aminohexanoic acid 1.5 M
imidazole/HCl pH 7.0 75 mM
glycerin 60 % (v/v)
in Milli-Q-H_2O, stored at 4 °C

BN-PAGE sample buffer
Bis-Tris/HCl pH 7.0 50 mM
Serva Blue G-250 5 % (w/v)
6-aminohexanoic acid 500 mM
in dest. H_2O stored at RT under light exclusion

10 % (w/v) ammonium persulfate (APS)
in Milli-Q-H_2O, stored up to 2 months at -20 °C, always used freshly thawed solution

BN-PAGE anode buffer
imidazole/HCl, pH 7.0 25 mM
in dest. H_2O, stored at 4 °C

BN-PAGE cathode buffer
tricine pH 7.0 50 mM
imidazole 7.5 mM
Serva Blue G-250 0.02 % (w/v)
in dest. H_2O, stored at RT, dye is resolved by stirring overnight, filtered

empty well solution (EMS)
buffer mix 180 µl
10 % digitonin 20 µl

HMW-marker protein	**molecular mass [kDa]**
thyroglobulin (pork)	669
ferritine (horse)	449
katalase (bovine)	232
lactate dehydrogenase (bovine)	140
albumin (bovine)	66

Solubilized proteins from isolations of mitochondria (4.3.4) were separated in the native and active state on a gradient (4-13%) BN-gel (Table 4) in the first dimension (Neff and Dencher, 1999). The linear gradient of the separating gel is established using a gradient mixer and a peristaltic pump (Krause & Seelert, 2008).

Table 4. Composition of BN- polyacrylamide gel.

	separating gel	**separating gel**	**stacking gel**
T [%]	13	4	3.5
C [%]	3	3	3
ml Rotiphorese® Gel A	0.357	0.719	0.728
ml Rotiphorese® Gel B	-	0.334	0.338
ml Rotiphorese® Gel A/B	2.140	-	-
ml 3xBN-gel buffer	-	2.470	2.500
ml 3xBN-gel buffer + glycerin	2.470	-	-
ml Milli-Q-H_2O	2.400	3.850	3.828
µl TEMED	2.050	3.400	10.000
µl 10 % APS	20.500	34.000	100.000
total volume [ml]	7.390	7.410	7.500

4.3.5.2. 2D-BN/SDS–PAGE

Following BN-PAGE, SDS PAGE can be performed in order to analyze proteins and their subunits in more detail as it enables high resolution separation of protein subunits, and combination of both methods can give insight into protein-protein interactions. SDS denatures proteins destroying protein-protein interactions and masks their intrinsic charge via formation of negatively charged SDS-protein complexes (aggregation is prevented by negative charges). SDS binds water-soluble proteins with a constant ratio of about 1.4 g SDS per g protein. Disulfide bonds are cleaved by β-mercaptoethanol or dithiothreitol (DTT).

denaturing solution
β-mercaptoethanol 1 % (v/v)
SDS 1 % (w/v)
in Milli-Q-H_2O, stored at -20 °C

SDS gel buffer (3×) for separating gels

Tris/HCl, pH 8.5	3 M
SDS	0.15 % (w/v)
glycerin	30 % (w/v)

in Milli-Q-H_2O, stored at room temperature, sterile-filtered

SDS gel buffer (3×) for stacking gels

Tris/HCl, pH 8.5	3 M
SDS	0.15 % (w/v)

in Milli-Q-H_2O, stored at RT, sterile-filtered

cathode buffer for 2D-Tricine-SDS gels

Tris	100 mM
Tricine	100 mM
SDS	0.05 % (w/v)

pH 8.25, in dest. H_2O, stored at 4 °C

anode buffer for 2D-Tricine-SDS gels

Tris/HCl	100 mM

pH 8.9, in dest. H_2O, stored at 4 °C

LMW-marker protein	**molecular mass [kDa]**
phosphorylase b	97
albumin	66
ovalbumin	45
carbonic anhydrase	30
trypsine inhibitor	20.1
α-lactalbumin	14.4

Lanes of the BN-gel were cut (about 1.5 cm wide) and proteins in the gel were denatured with 1% β-mercaptoethanol/1% SDS two times for 30 min each, and then washed with Milli-Q-water three times for 5 minutes each. Gel lanes were placed on top of a gel chamber and the separating gel and the two stacking gels (Table 5) were casted from bottom to top with the native stacking gel surrounding the BN-gel stripe. After the cast of the native stacking gel, a single well-former was clamped between the two glass plates where low molecular weight marker (LMW) (2 µl) was loaded after polymerization of the gel. Denatured proteins from BN-gel stripes were separated on the 13% SDS gel with 5% stacking gel in the second dimension over night applying 70 V and 40 mA.

Table 5. Composition of a 2D-Tricine-SDS gel.

	separating gel	**stacking gel (denature)**	**stacking gel (native)**
T [%], C [%]	13; 3	5; 3	5; 3
ml Rotiphorese® Gel A	0.650	0.405	0.405
ml Rotiphorese® Gel B	-	0.188	0.188
ml Rotiphorese® Gel A/B	4.400	-	-
ml 3× SDS-gel buffer (30 % glycerol)	5.000	-	-
ml 3× SDS-gel buffer	-	0.825	-
ml 3× BN-gel buffer	-	-	0.825
µl 20 % (w/v) SDS	-	-	25.000
ml Milli-Q-H_2O	4.875	1.070	1.033
µl TEMED	7.500	1.250	1.750
µl 10 % APS	75.00	12.500	17.500
total volume	15.000	2.500	2.490

4.3.5.3. 1D SDS polyacrylamide gel electrophoresis (SDS-PAGE)

stacking gel buffer
1 M Tris/HCl, pH 6.8
in dest. water, stored at RT

separating gel buffer
1.5 M Tris/HCl, pH 8.8
in dest. water, stored at RT

20% SDS solution
20% (w/v) SDS
in dest. water, stored at RT

electrophoresis buffer
400 mM glycerol
50 mM Tricine
0.1% (w/v) SDS
pH 8.5, in dest. water, stored at RT

4× SDS sample buffer
300 mM Tris (pH 6.8)
2.4% (w/v) SDS
60% glycerin
0.04% (w/v) bromphenol blue
30% (v/v) 2-mercaptoethanol

Separation of the proteins according to their mass was performed using one dimensional sodium dodecyl sulfate polyacrylamide gel electrophoresis (SDS-PAGE). In order to detect proteins with higher molecular mass, e.g. 200 kDa or higher, 9% acrylamide gel (Table 6) was used to assure appropriate pore size of the gel and hence effective protein separation. Separating gel was poured in a gel casting tray, covered with 1 ml ispopropanol and left to polymerize for 10-15 min. Isopropanol was removed and stacking gel was poured on top of the separating gel into which gel combs were inserted. Gel was left to polymerize at room temperature for ~30 min. Samples were mixed with equal volumes of 4× SDS-sample buffer and filled with Milli-Q-water up to 32 µl, heated at 95 °C for 5 min, spun down shortly and loaded onto the gel. 2 µl of marker was loaded in a separated well. Proteins on the gel were separated applying 50mA/gel and 100 V until proteins entered the separating gel. Then, the voltage was increased to 130 V and electrophoresis was performed until the dye front of samples reached the edge of the glass plate in the elecrophoresis unit.

Table 6. Composition of 1D SDS gel with 9% acrylamide separating and 4% acrylamide stacking gel.

	separation gel T = 9%, C = 4%	stacking gel T = 4%, C = 3%
Rotiphorese Gel A	1.44 ml	--
Rotiphorese Gel B	0.90 ml	--
Rotiphorese Gel 29:1	--	0.25 ml
1.5 M separating gel buffer	1.25 ml	--
1 M stacking gel buffer	--	0.31 ml
20% (w/v) SDS	25 µl	12.5 µl
Milli-Q-water	1.34 ml	1.89 ml
TEMED	3.75 µl	2.5 µl
APS	37.5 µl	25 µl
total volume	5 ml	2.5 ml

Alternatively, pre-casted SDS gels were used for protein analysis. 30 µg of protein sample in NuPAGE® LDS Sample Buffer with NuPAGE® Reducing agent (containing DTT) was heated at 70 °C, 10 min. Samples were loaded onto 4-12% NuPAGE® Novex® Bis-Tris Pre-Cast gels (1 mm thick, 10 cm x 10 cm in size) at the neutral operating pH (pH 7.0). MagicMark™ (MM) protein standard was used as a mass standard and control for Western blotting. PageRuler™ Plus Prestained Protein Ladder was used as an additional mass standard. Gels were run using NuPAGE® MES SDS Running Buffer at constant voltage (200 V), 110 mA, 35 min at RT.

4.3.6. Protein staining in gels

4.3.6.1. Colloidal Coomassie staining

Gels were incubated with Roti®-Blue staining solution containing Coommasie Brilliant Blue G250 which binds to proteins due to its colloidal qualities. The binding of the dye takes place non-specifically to basic and hydrophobic amino acid side chains of the proteins. This method enables detection of proteins ≥30 ng/band with low background staining. Gels were incubated in staining solution at least over night under gentle shaking. Following staining, gels were incubated in 25% (v/v) methanol in distilled water until proper background contrast was reached.

4.3.6.2. SYPRO Ruby staining

For proteome analysis with protein quantification in 2D-SDS polyacrylamide gels, the fluorescent dye SYPRO® Ruby was used. SYPRO® Ruby (Figure 4.9) possesses a large linear quantitation range of 3.3 orders of magnitude and a detection limit of 1 ng protein/spot (Berggren et al., 2000). SYPRO Ruby binds to alkaline amino acids and the polypeptide backbone with high sensitivity and without background signals with excitation peaks at 280 nm and 450 nm and an emission maximum near 610 nm. Compared to silver staining, SYPRO Ruby staining of proteins is quantitatively (proportional to the protein amount) and influences neither further protein staining nor protein identification by MALDI-MS (Lopez et al., 2000).

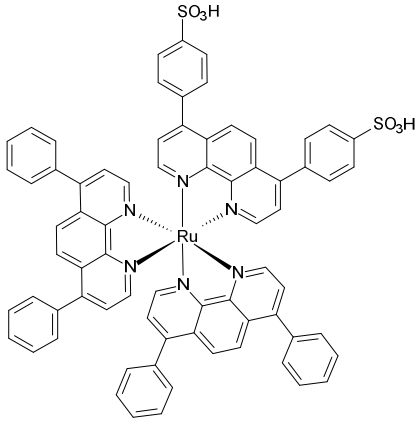

Figure 4.9. Structure of the fluorescent dye SYPRO® Ruby. (https://tools.thermofisher.com).

Following SDS-PAGE, gels were fixated in a solution containing 10% methanol/7% acetic acid for 3-4 h or overnight. Proteins in gels were stained using the fluorescent SYPRO Ruby protein stain for 3 h under light exclusion and then washed in the fixation solution 10 min following washing with Milli-Q-water for 5 min. Gel images were taken by the CCD camera system of Fujibox using LAS-3000 software in „Increment" mode, taking images using „standard sensitivity" every 10 sec until saturation was reached. 460 nm (blue diode) was used for excitation of the dye and 605 nm (band pass) filter with F 0.85 iris. Quantification of protein spots of interest was conducted using Delta2D software by determining their grey values (volumes) normalized to the grey value of all spots present on the gel. Normalization resulted in the value V % for each protein spot.

4.3.6.3. Silver staining according to Blum

Following SYPRO Ruby staining, proteins were silver-stained (Blum et al., 1987) for visualisation purposes only and gel images were taken using View Pix 900 scanner with Epson Scan software (Kratochwil, 2015; Decker, 2016).

4.3.7. Western blot

4.3.7.1. Semi-dry electro blotting and immunodetection of proteins

Towbin transfer buffer	**ECL-based detection solution**
0.025 M Tris	1 M Tris/HCl, pH 8.8
0.192 M glycine	250 mM luminol in DMSO
20 % methanol	90 mM 4-IPBA
deionized water, stored at RT	30% (v/v) hydrogen peroxide
	Milli-Q-water

Transfer of the electrophoresed proteins from the gel onto nitrocellulose membrane, which has binding capacity of 80-100 µg of proteins per cm^2, was performed employing the semi-dry Western

blotting technique. Blotting sandwich was prepared by cutting blotting paper (1.5 mm thick) and nitrocellulose membrane to appropriate size according to the size of the gel. For efficient blotting, the membrane was cut to be 0.5 cm larger then the gel and blotting paper was cut to be 0.5 cm larger than the membrane. After soaking the membrane and the paper in Towbin transfer buffer, blotting sandwich was assembled by placing blotting paper on the anode side of the blotting machine. The membrane was placed on the blotting paper, the gel was placed on the membrane and blotting paper was placed on top of the blotting sandwich on the cathode side (Figure 4.10). The air from the blotting sandwich was pressed out and the cathode of the blotting machine was placed on top. Blotting was performed at 20 V and 400 mA for 1 h and 20 min. Afterwards, the membrane was blocked in Roti®-Block blocking solution for 30 min at room temperature. Appropriate dilution of the primary antibody in 1× PBS-T was used for detection of the protein of interest and the membrane was incubated over night at 4 °C while gentle shaking. The next day, membrane was rinsed 3 times with 1× PBS-T buffer for 5 min each time. Then, membrane was incubated in dilution of HRP-conjugated secondary antibody in PBS-T for 2 h at 4 °C while gentle shaking. Following incubation, membrane was rinsed three times in 1× PBS-T buffer for 5 min each time. Proteins on membrane were detected using ECL-based detection system according to the method of Haan and Behrmann (2007) to ensure reduction in the background signal. Membrane was covered with ECL (enhanced chemiluminescence) solution and imaged using Fuji-Box detection system with Image Reader LAS-3000 software.

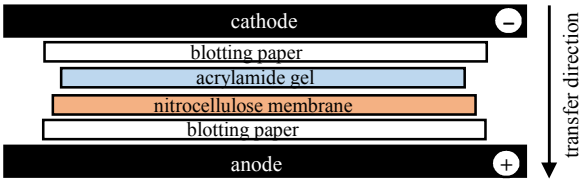

Figure 4.10. Blotting sandwich for Western blot (semi-dry transfer).

Similary, proteins separated on the NuPAGE® Novex® Bis-Tris Pre-Cast gels (4.3.5.3) were transferred onto nitrocellulose membrane. NuPAGE® Transfer Buffer was used for semi-dry transfer at 15 V, 400 mA, 15 min.

4.3.7.2. Oxyblot

In order to determine the overall degree of carbonylation (e.g. caused by oxidative damage by ROS) of mitochondrial proteins from „crude“ isolated mitochondria (4.3.2) or total isolated cellular proteins (4.3.1), the Oxyblot assay was performed using OxyBlot™ Protein Oxidation Detection Kit according to manufacturer protocol with modifications. Oxyblot assay is a specialized form of Western blot used for immunoblot detection of carbonyl groups introduced into protein side chains by oxidative reactions with reactive oxygen species. Carbonyl groups of the proteins are derivatized to 2,4-dinitrophenyhydrazone (DNP) by the reaction with 2,4-

dinitrophenylhydrazine (DNPH). An antibody directed against DNP was applied. New aliquots of samples were used for each experiment since subsequent freezing and thawing can introduce additional damage and lead to false positive results.

SDS solution
12% (w/v) SDS in Milli-Q-water, stored at RT

OxyBlot™ Protein Oxidation Detection Kit
1× 2,4-dinitrophenylhydrazine (DNPH) Solution
1× Derivatization-Control Solution
Neutralization Solution
rabbit anti-DNP antibody

buffer for positive control
25 mM HEPES
25 mM ascorbic acid (Na-salt)
100 µM $FeCl_3$ x 6 H_2O
pH 7.2, in bidest. water, stored at RT

BSA (positive control)
10 mg/ml BSA, incubated for 5h at 37 °C
in the buffer for positive control
dialyzed overnight (12-16 kDa cut-off membrane),
stored at 4 °C

dialysis buffer
50 mM HEPES
1mM EDTA
in bidest. water, stored at RT

Isolated mitochondria previously stored in solubilisation buffer containig sucrose and protease inhibitor cocktail at -80 °C were thawed on ice and appropriate volumes containing about 15 µg protein were centrifuged at 20800 x g for 8 min at 4 °C. Supernatant was carefully removed and pellet containing mitochondria was resuspended (5 µl) ice-cold solubilisation buffer. In the case when total cellular proteins from cell lysates were assessed, about 15 µg protein from cell lysates was used. BSA (15 µg) was used as a positive control. Each sample is denatured by adding 12% SDS to a final concentration of 6% SDS. Samples are derivatized by adding 10 µl of 1× DNPH Solution except for the negative control for immuno-binding (BSA) to which 10 µl 1× Derivatization-Control Solution was added instead of DNPH Solution. All samples were incubated at room temperature for 15 min. Derivatization reaction was stopped by adding 7.5 µl Neutralization Solution to all samples including controls. Samples were mixed with SDS sample loading buffer and loaded in duplicates into 9% SDS gel of 0.75 mm thickness. Electrophoresis was performed for 1.5 h at 50 mA/gel and 100 V until proteins entered the separating gel. Then, the voltage was increased to 130 V.
Following electrophoresis, gels were blotted on nitrocellulose membrane which was then blocked as described previously in this section. The membrane was incubated in primary rabbit anti-DNP antibody from the assay kit (1:500 in PBS-T) over night at 4 °C while gentle shaking. The membrane was rinsed three times with 1× PBS-T buffer for 5 min each time. Thereafter, the membrane was incubated in secondary anti-rabbit IgG HRP-conjugated antibody (1:2000 in PBS-

T) for 1 h at 4 °C and then washed three times with 1× PBS-T buffer for 5 min each time. Proteins on the membrane were detected using ECL-detection system as described above. Quantification of the oxidized proteins was performed with ImageJ software and data is expressed as a ratio of oxyblot lane average intensity and control (BSA positive control) band intensity. Data is expressed as a fold-change from control values.

4.4. DNA analysis

4.4.1. Total genomic DNA isolation and quantitation

Tris-EDTA (TE) buffer 20×
200 mM Tris
20 mM EDTA
in Milli-Q-water, autoclaved stored at RT

Total genomic DNA was isolated using Blood & Cell Culture DNA Mini Kit that enables mild purification of stable and high molecular weight DNA. Samples of cultured cells were harvested and prepared according to the manufacturer protocol for DNA isolation from tissue samples since protocol for cultured cells includes steps which remove mitochondrial DNA. Quantitation of isolated genomic DNA and PCR products, respectively, was performed using PicoGreen dye that binds to dsDNA. DNA samples (2 µl) and standard (Lambda/HindIII DNA Digest) were diluted in Milli-Q-water and loaded onto a black 96-well plate in duplicates. Lambda/HindIII DNA Digest was used for generating a standard curve (1.25-20 ng/µl DNA) (Table 7) for determining concentrations of samples. PicoGreen (5µl of reagent per milliliter of Milli-Q-water) was added into each well with DNA and incubated 10 min at room temperature in the dark. Quantitation of isolated DNA was performed to estimate the initial amount of DNA for preparing 100 ng DNA in each sample. Fluorescence of the dye was measured using a plate reader with the 485 nm excitation filter and 535 nm emission filter. Fluorescence readings (of the duplicate samples) were averaged and blank value (from no-DNA control) was subtracted.

Table 7. Lambda/HindIII DNA Digest standard dilutions for PicoGreen assay for determination of DNA concentrations.

λ/HindIII DNA standard [ng/µl]	**λ/HindIII DNA µl**	**1× TE buffer µl**
20	1.6	38.4
10	0.8	39.2
5	0.4	39.6
2.5	0.2	39.8
1.25	0.1	39.9
0	0	40

4.4.2. PCR analysis

4.4.2.1. Standard PCR for determination of mtDNA amount

To determine the mitochondrial DNA amount, short fragments of the mtDNA (up to 300 bps) were amplified as there is a low probability of damaged DNA in such fragments (Furda et al., 2014). In the wild-type mtDNA, forward (5'-CTGAGCCTTTTACCACTCCAG-3') and reverse (5'-GGTGATTGATACTCCTGATGCG-3') primers located within the deletion region (in order to ensure that only wild type and not DNA harboring a deletion is amplified) yield a PCR product of 142 bp (confirmed by BLAST for primers) (Soong and Arnheim, 1996). Standard PCR for determination of mitochondrial DNA copy number was setup according to Table 8 and was performed in a total volume of 50 µl and appropriate cycling conditions (Table 9). Different steps of the procedure (reaction setup, running and product investigation) were performed in physically separated laboratories to avoid cross-contamination or degradation of the template or inhibition of the polymerase.

Table 8. Standard PCR reaction setup.

Component	**Volume [µl]**
2× Taq Master Mix (1×)	25
10 µM forward primer (0.2 µM)	0.5
10 µM reverse primer (0.2 µM)	0.5
template DNA (200 ng)	Variable
Taq DNA Polymerase	0.5
sterile Milli-Q-water	Variable

Table 9. Cycling conditions for standard PCR.

Temperature [°C]	Time	Number of cycles
94	5 min	1
94	20 sec	
60	20 sec	35
72	20 sec	
72	2 min	1

PCR products were loaded on 2% agarose gels with addition of 0.25 µg/ml ethidium bromide for visualisation before performing quantitation of the DNA using PicoGreen dye as described above (4.4.1). Relative fluorescence values were obtained by subtracting the fluorescence value of the negative control (PCR assembly without DNA) from each sample.

4.4.2.2. Nested PCR for determination of a common deletion in mtDNA

Since levels of deletion in mtDNA can be very low and difficult to detect using standard PCR, a nested-PCR method was applied for detection of 4977 bp common deletion in mtDNA (Soong and Arnheim, 1996). This method is highly sensitive and allows discrimination between the few molecules of deleted mtDNA and the overhelming excess of wtDNA (Soong and Arnheim, 1996). In a first PCR step, a region outside the 13 bp repeats where the deletion occurs was amplified using first set of primers: forward (5'-ACCCTATTGCACCCCCTCTAC-3') and reverse (5'-TGTTAGTAAGGGTGGGGAAGC-3') in order to concentrate deleted molecules. In a second PCR step, 1 µl of this primary reaction was used as template for amplification of the abberant mtDNA using another set of primers: forward (5'- ACCCTATTGCACCCCCTCTAC-3') and reverse (5'-CTTGTCAGGGAGGTAGCGATG-3') (Chen et al., 2011).
Reaction setup was setup as decribed for standard PCR (Table 8) and cycling conditions for primary and secondary reaction were similar (Table 10). A PCR product in the form of 358-bp band was detected by electrophoresis on 2% agarose gel in the samples containing the common deletion and quantified using PicoGreen dye as described above (Section 4.4.1).

Table 10. Cycling conditions for nested PCR.

Temperature [°C]		Time		Number of cycles
step 1	step 2	step1	step 2	
94	94	5 min	5 min	1
94	94	20 sec	20 sec	
58	60	45 sec	40 sec	35
72	72	50 sec	45 sec	
72	72	5min	5 min	1

5. Results and discussion

The complex interplay of X-ray radiation, oxygen concentration in the cell culture, Alzheimer's $A\beta_{1-42}$ peptide and differentiation status were investigated in human neuroblastoma (SH-SY5Y) cells. Cellular responses were compared in cells cultivated at 21% O_2 commonly used in the cell culture and at more physiological 5% O_2. Intracellular oxygen concentration differed depending on the oxygen concentration applied. Moreover, it was shown to be a a potent modulator of cellular response to X-ray radiation and Aβ peptide.

This chapter is divided into many smaller chapters containing results of experiments combined together with discussion.

The difference in the cell proliferation depending on the oxygen concentration, differentiation status and X-ray radiation were explained. Study of the cellular physiology, mitochondrial proteome and expression pattern of subunits of OxPhos complexes and other mitochondrial proteins is presented in the published work (Džinić et al., 2016).

Furhermore, traffic of Aβ peptide toward cellular organelles and its kinetics were visualized. Cellular parameters and their changes such as lysosomal integrity, cell death, ATP concentration, GSH and ROS level, as well as mitochondrial membrane potential were elaborated. Carbonylation of total cellular and mitochondrial proteins, respectively, and changes in mtDNA (amount and ocurrence of the common deletion) were presented as an important markers of oxidative stress.

Parts of chapters 5.4, 5.6, 5.9, 5.10 and 5.11 are published:

Džinić T, Hartwig S, Lehr S, Dencher NA. (2016). Oxygen and differentiation status modulate the effect of X-ray irradiation on physiology and mitochondrial proteome of human neuroblastoma cells. *Arch. Physiol. Biochem.*, 122: 257-265.

Data described in chapters 5.3, 5.5, 5.6, 5.7, 5.8, 5.12, 5.13 and 5.14 are part of a manuscript submitted in March 2017:

Džinić T, Dencher NA. (2017). Oxygen concentration and oxidative stress modulate the influence of Alzheimer's disease $A\beta_{1-42}$ peptide on human neuroblastoma cells.

Abstract

Reactive oxygen species (ROS) generated e.g. after exposure to ionizing radiation (IR), toxic peptides as well as by mitochondrial metabolism and during aging contribute to damage of cell's structural and functional components and can lead to diseases. Monomers and small oligomers of amyloid beta (Aβ) peptide, one of the players in Alzheimer's disease (AD), and their intriguing mechanisms of action are recently thought to be involved in damage of neurons, instead of extracellular Aß plaques. We demonstrate that externally applied disaggregated $A\beta_{1-42}$ peptide interacts with SH-SY5Y cells, preferentially with acidic compartments (lysosomes). Oxygen concentration in the cell culture (5% *versus* 21%) and oxidative stress caused by IR modulate responses of differentiated SH-SY5Y cells to treatment with Aβ peptide. Cells did not exhibit dramatic increase in ROS and change in glutathione (GSH) level upon 4 µM Aβ peptide treatment, whereas exposure to 2 Gy X-rays increased ROS and changed GSH level and ATP concentration. Occurrence of the 4977 bp deletion in mtDNA and significant protein carbonlyation were specific effects of ionizing radiation and more pronounced at 21% O_2. Increase in cell death after Aβ peptide treatment or irradiation was unexpectedly restored to the control level or below when both Aβ peptide and irradiation were combined, particularly at 5% O_2. Therefore, Aβ peptide at low concentration can trigger neuroprotective mechanisms in cells exposed to ionizing radiation.

5.1. Intracellular oxygen concentration

In order to determine the intracellular oxygen concentration in SH-SY5Y cells cultivated at two different oxygen concentrations applied to the cell culture (21% and 5% O_2, respectively) in parallel, an oxygen sensitive probe loaded to cells overnight was used. The signal intensity measured depends on the oxygen concentration present in cells since oxygen quenches the signal. Cells were cultivated at least for 7 days before conducting measurements using fully confluent cells. Values of the signal intensities were converted into oxygen scale (Chapter 4.2.1). SH-SY5Y cells cultivated at 21% O_2 (blue dots) had about 10.5% O_2, whereas cells cultivated at 5% O_2 (red

squares) had about 0.9% O_2 intracellulary (Figure 5.1). The oxygen concentration in cells at 21% O_2 was stable during the measurement. Slight increase of intracellular oxygen concentration (~1.2% O_2) in cells cultivated at 5% O_2 was due to the exposure to atmospheric oxygen during measurement in the plate reader for 30 min in 2 min intervals.

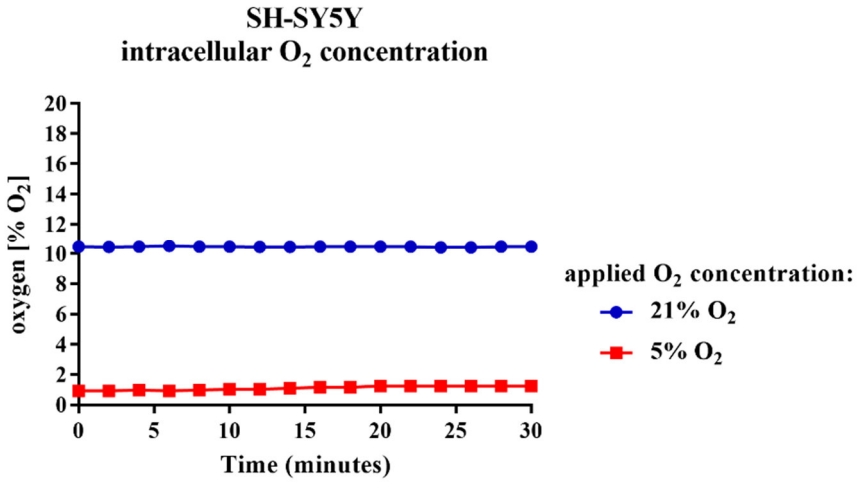

Figure 5.1. Intracellular O_2 concentration measured after SH-SY5Y cells were incubated at two different oxygen concentrations cultivated at least for 7 days before conducting measurements using an oxygen sensitive probe ($\lambda_{EX}/\lambda_{EM}$ = 587/615 nm) loaded to cells. Cells in a confluent monolayer (~4 x 10^4 cells/well of a 96-well plate) cultivated in a standard cell culture incubator at about 21% O_2 had about 10.5% O_2 (blue line), whereas cells cultivated at 5% O_2 had about 0.9% O_2 intracellulary (red line). Increase in the oxygen concentration (~1.2% O_2) in cells at 5% O_2 was due to the exposure to atmospheric oxygen during measurement in the plate reader for 30 min (2 min intervals).

The intracellular oxygen concentration depends not only on the oxygen concentration applied to the cell culture but also on the cell type. For example, human embryonic kindey (HEK29T) cells cultivated in 2D (monolayer) and measured at ~21% O_2 showed an intracellular O_2 concentration of ~14%. Reducing the oxygen concentration to 6% caused cellular oxygenation to drop to ~2% (manual for MitoXpress® Intra Intracellular Oxygen assay). Furthermore, human hepatoma (HepG2) cells cultivated at ~21% O_2 in 2D and 3D, respectively, showed an intracellular O_2 concentration of ~10% and ~9%, respectively (Krumm & Carey, 2016). For the first time measured intracellular O_2 concentration of SH-SY5Y cells cultivated at 21% O_2 was similar to that measured for HepG2 cells at 21% O_2. Intracellular oxygen concentration of ~1% for SH-SY5Y cells cultivated at 5% O_2 is comparable to the value (~2% O_2) obtained for HEK293T cells cultivated 6% O_2. Studies were performed using adherent cells. In the case of two different systems for cultivation of HepG2 cells (2D and 3D cell culture both at 21% O_2), there was no large difference in the intracellular O_2 concentration measured. However, it is possible that cells cultivated in a monolayer and cells in a suspension experience different intracellular O_2 concentrations since there are oxygen gradients between atmosphere and the medium or between medium and intracellular compartments (Krumm & Carey, 2016). The temperature was the same (37 °C) in both SH-SY5Y cells cultivated at 21% and 5% O_2. The oxygen concentration applied influences not only

intracellular oxygen concentration but it affects the metabolic activity of cells, proliferation and response to stress (Džinić et al., 2016).

5.2. Cell proliferation

Using dual staining of SH-SY5Y cells with DAPI (for the nuclei) and MitoTracker® Orange (for mitochondria), proliferation and morphology of cells were investigated by fluorescence microscopy. Qualitative analysis of microscopic images revealed that cells cultivated at both 21% and 5% O_2 proliferated similarly without a difference in morphology (Figure 5.2). Nuclei stained with DAPI were similar in size, shape and number at both oxygen conditions. Mitochondria stained with MitoTracker Orange showed similar fluorescence signal.

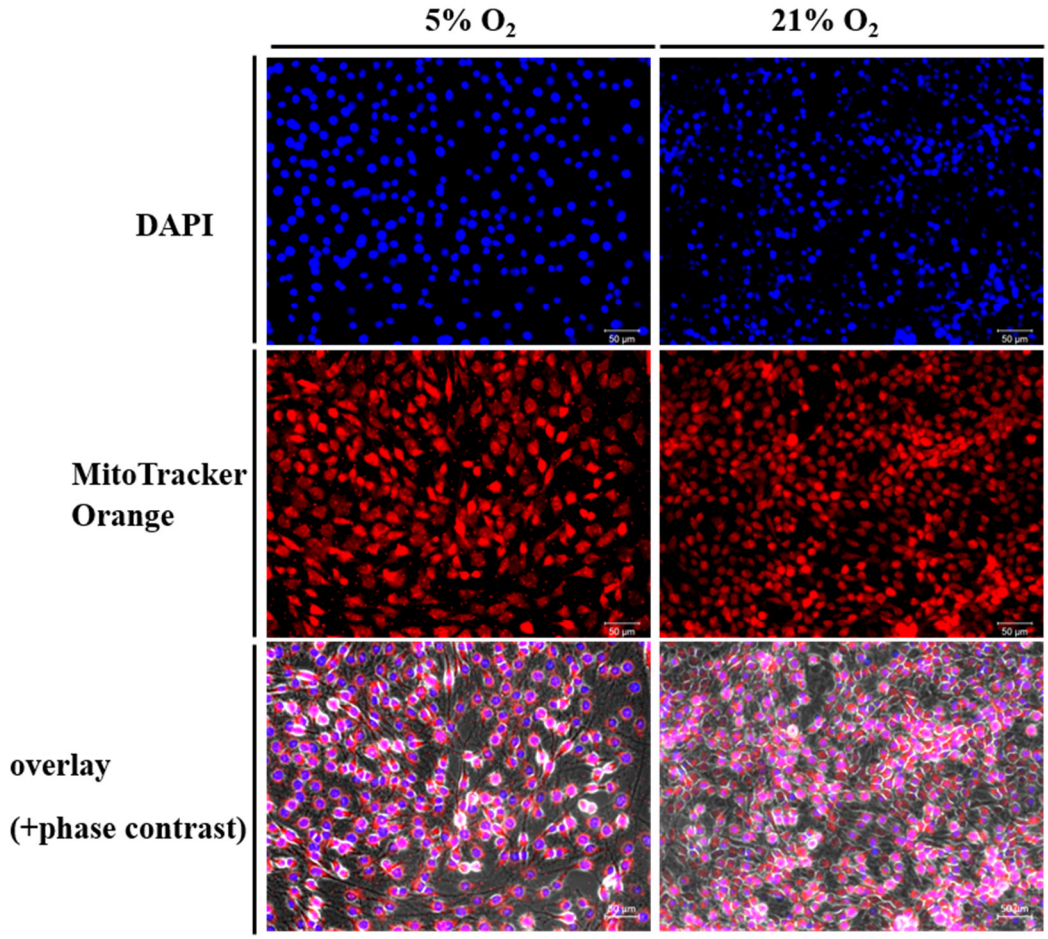

Figure 5.2. Cell proliferation and morphology of SH-SY5Y cells cultivated at 21% and 5% O_2, respectively. ~4 x 10^4 cells were grown on positively charged microscopic slides for 5 days. MitoTracker® Orange CMTMRos ($\lambda_{EX}/\lambda_{EM}$ = 554 nm/576 nm) that freely enters mitochondria of living cells was used to distinguish mitochondria (red fluorescence) located in the cytoplasm from the nuclei (blue fluorescence). Following fixation and permeabilization, nuclei were stained with DAPI ($\lambda_{EX}/\lambda_{EM}$ = 358nm/461 nm). Overlay of fluorescence images with phase contrast image. Scale bar: 50 µm. Magnification: 200×.

In order to quantitatively analyze cell proliferation, number of SH-SY5Y cells cultivated at 21% O_2 and 5% O_2, respectively, was monitored daily during a period of 9 days using the Trypan blue exclusion of the dead cells. The number of cells at 5% O_2 was higher than of cells at 21% O_2 observed as an increase in the cell number after day 1 which continued until day 7 when cells reached the plateau phase and then started to decrease in number (Figure 5.3 A). Cells cultured at 21% O_2 did not reach the plateau phase during 9 days. The viability of the cells at both oxygen conditions exceeded 90% during the experiment. Population doubling time (DT) for SH-SY5Y cells at 21% O_2 was about 49 h and for cells at 5% O_2 about 46 h. Calculated DT of SH-SY5Y cells were close to 48 h, a doubling time for this cells line published by American Type Culture Collection (ATCC) (www.lgcstandards-atcc.org). Additionally, lower cell proliferation activity of cells cultivated at 1% O_2 as compared to 21% O_2 (Figure 5.3 B) measured in an independent experiment was decisive for using 5% O_2 instead of 1% O_2 for cultivation of SH-SY5Y cells.

A

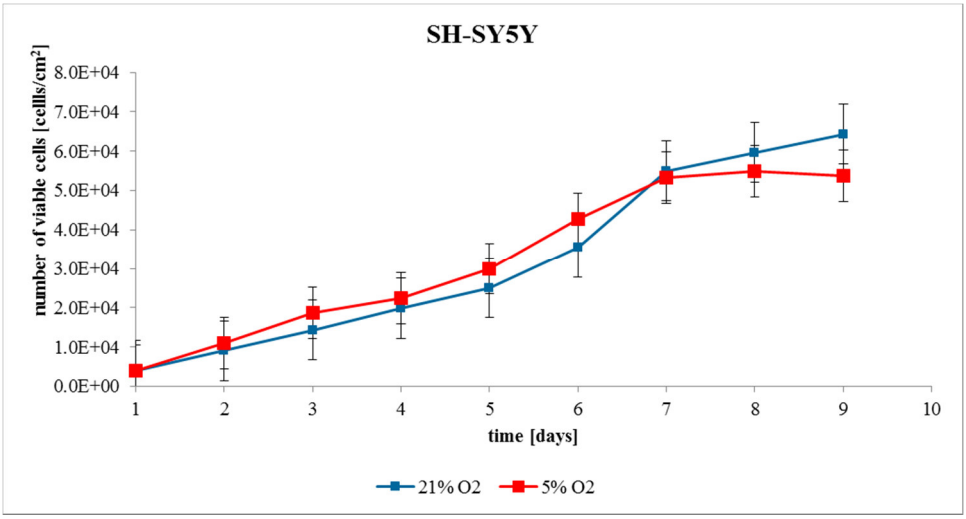

B

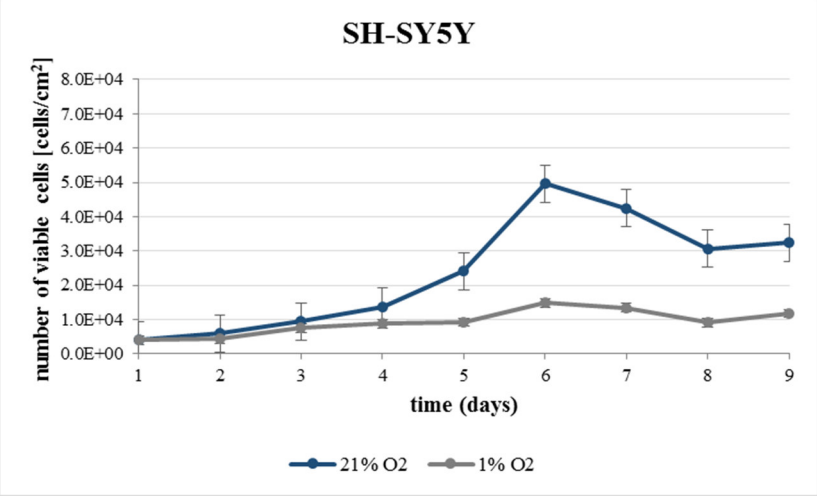

Figure 5.3. A) Cell proliferation of SH-SY5Y cells at 21% O_2 and 5% O_2, respectively. ~4 x 10^4 cells were grown in 10 cm^2 Petri dishes in advanced DMEM supplemented with 10% FBS, 2% L-glutamine and 1% penicillin/streptomycin without changing the medium. Cell number was determined microscopically every day during the 9-day period (n = 3) using Neubauer chamber for cell counting and Trypan blue for the exclusion of the dead cells. Accuracy of the cell numbers was confirmed by automated cell counter Scepter™. The number of cells at 5% O_2 was significantly higher during the first 6 days compared to cells at 21% O_2 and cells at 5% O_2 reached the plateau phase on the day 7 in comparison to the cells cultured at 21% O_2 where the plateau phase was not observed. The viability of the cells was exceeded 90% during the experiment. Samples were analyzed in three independent experiments (N = 3) and data is presented as mean ± SEM analyzed by two-way ANOVA. $p<0.05$. B) Cell proliferation of SH-SY5Y cells at 21% O_2 and 1% O_2, respectively. The experiment was performed solely to test cell proliferation at 1% O_2. Significantly lower cell proliferation in cells at 1% O_2 as compared to 21% O_2.

In order to study the effect of radiation on cell proliferation, cells were irradiated using 2 Gy X-rays on day 1 and cell number was monitored during the period of 9 days as decribed above. Cell morphology and proliferation were not affected one day after irradiation (Figure 5.4 and 5.6). However, the effect of X-ray radiation on cell proliferation was observed after day 3-4 from the begining of the experiment as a decrease in number of cells cultivated at both of 21% O_2 and 5% O_2 (Figure 5.6). Furthermore, induction of differentiation with 10 µM retinoic acid (added on day 1) resulted in changed morphology of SH-SY5Y cells which showed overall elongation and flattening of the cell body with long protrusions (neurites-like) characteristic for the process of differentiation compared to non-differentiated neuroblastoma cells (control cells) with more rounded cell body and short outgrowths (Figure 5.5). SH-SY5Y cells with induced differentiation morphologically resemble neurons (Hellmann-Regen et al., 2012). Furthermore, reduced cell proliferation of these cells was observed after day 2-3 (Figure 5.6). The viability of the cells at both O_2 conditions exceeded 90% during the experiment. Furthermore, oxygen plays a role in differentiation of SH-SY5Y cells. For example, the expression of neurofilament M, a marker of differentiation was affected by the oxygen concentration and it was increased in cells cultivated at 5% O_2 in comparison to cells at 21% O_2 (Džinić et al., 2016).

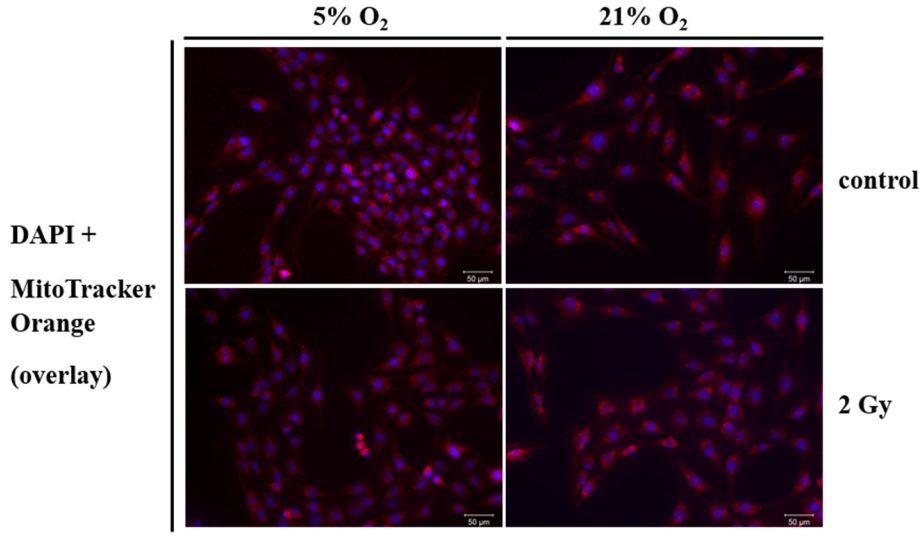

Figure 5.4. Cell proliferation and morphology after X-ray irradiation of SH-SY5Y cells cultivated at 21% and 5% O_2, respectively. ~4 x 10^4 cells were grown on positively charged microscopic slides and irradiated on day 1 and imaged on day 2. MitoTracker® Orange CMTMRos and DAPI staining (see Figure 5.2). No difference in morphology and proliferation of SH-SY5Y cells was observed 1 day after irradiation. Scale bar: 50 µm. Magnification: 200×.

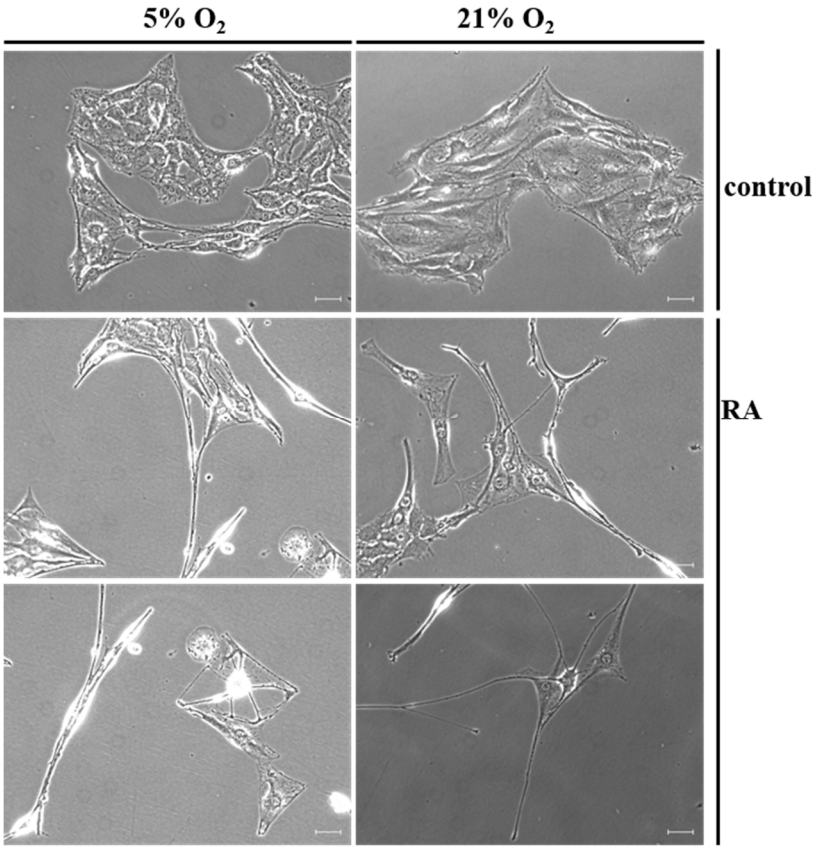

Figure 5.5. Cell proliferation and morphology after induction of differentiation of SH-SY5Ycells cultivated at 21% and 5% O_2, respectively. ~4 x 10^4 cells were grown in 10 cm^2 Petri dishes and 10 µM RA was added on day 1. Images of non-fixated cells (PBS only) were taken on day 3. Reduced proliferation of cells treated with RA and change of the morphology: elongation, flattening and presentation of long protrusions (neurite-like) compared to non-differentiated neuroblastoma cells with more round body and shorts protrusions. Scale bar: 100 µm. Magnification: 200×.

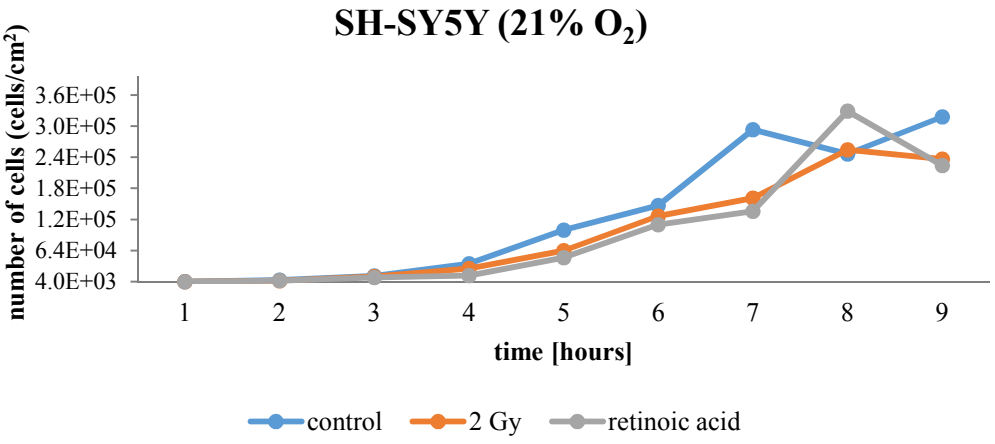

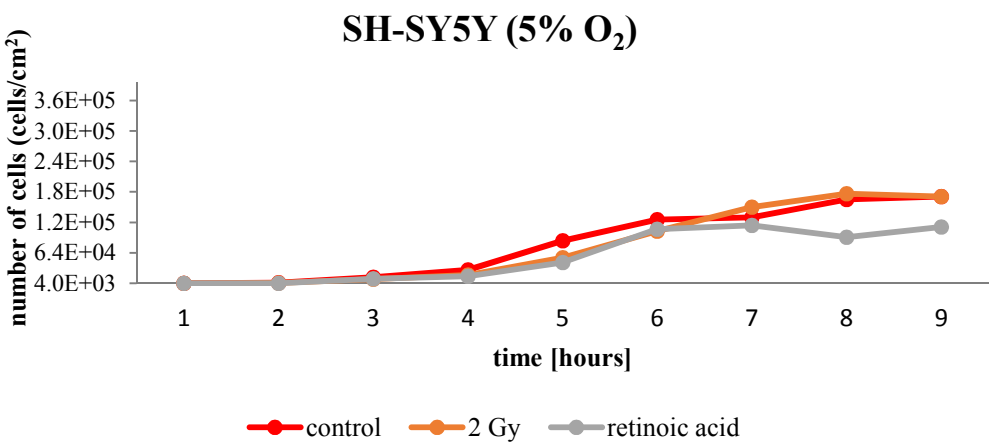

Figure 5.6. Cell proliferation of retinoic acid-treated and irradiated SH-SY5Y cells at 21% O_2 and 5% O_2, respectively. ~4 x 10^4 cells were grown in 10 cm^2 Petri dishes in advanced DMEM supplemented with 10% FBS, 2% L-glutamine and 1% penicillin/streptomycin without changing the medium. Cells were irradiated with 2 Gy X-rays or treated with 10 µM retinoic acid on day 1. Cell number was determined microscopically every day during the 9-day period (n = 3) using Neubauer chamber for cell counting and Trypan blue for the exclusion of the dead cells. Accuracy of the cell numbers was confirmed by automated cell counter Scepter™. Control cells at 5% O_2 and at 21% O_2 proliferated similar. However, cells at 5% O_2 reached the plateau phase on the day 8 in comparison to the cells cultured at 21% O_2 where no real plateau phase was observed. Irradiation led to a decrease in cell proliferation after day 3-4 at both oxygen concentrations. Induction of differentiation reduced cell proliferation after day 2-3. The viability of the cells at both O_2 conditions exceeded 90% before the plateau phase was reached.

5.3. Intracellular localization of externally applied $A\beta_{1-42}$ peptide

Interaction of the amyloid beta peptide with SH-SY5Y cells was assayed using flow cytometry for detection of the fluorescence signal of FITC-labelled $A\beta_{1-42}$ peptide after 5, 10, 15, 30 min and after 1, 3, 18, 24 h. $A\beta_{1-42}$ peptide was interacting with SH-SY5Y cells indicated by a progressive increase (shift) in the fluorescence signal after 15 min, 1h, 3h and 18 h of incubation compared to control (unstained) cells (Figure 1 5.7 A). Maximum fluorescence signal was observed after 18 h, thereafter a slight decrease of the signal occurred after 24 h. Fig. 5.7 A depicts the data for cells cultivated at 21% O_2 and similar results were obtained for cells at 5% O_2 (data not shown). In order to determine the site(s) and kinetics of interaction, subcellular localization of externally added $A\beta_{1-42}$ peptide was investigated using confocal microscopy by measuring colocalization of FITC-labelled peptide with organelles (lysosomes, mitochondria and endoplasmatic reticulum) stained with appropriate specific dyes. Aβ peptide strongly interacted with acidic organelles (lysosomes and possibly endosomes) (Yapici et al., 2015), stained by LysoTracker Red dye, at both 21% and 5% O_2 with progress in the signal after 3, 8 and 18 h (Figure 5.7 B). Very weak colocalization was found with other organelles of the SH-SY5Y cells examined here (endoplasmatic reticulum and mitochondria, respectively) at both 21% and 5% O_2 (Figure 5.7 C-D).

A

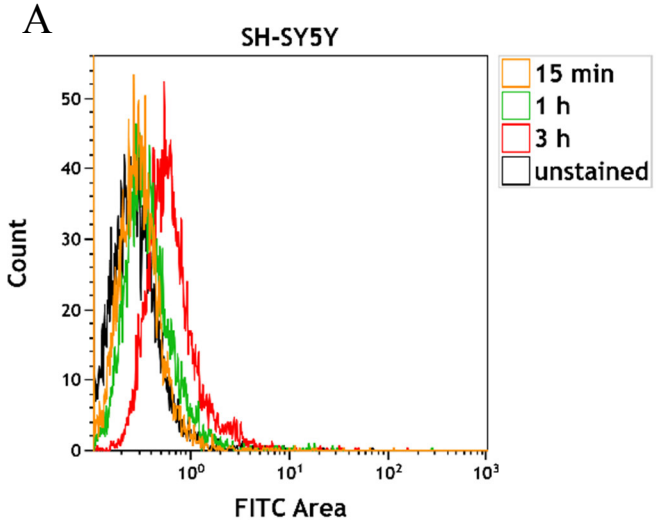
SH-SY5Y
15 min
1 h
3 h
unstained
Count
FITC Area

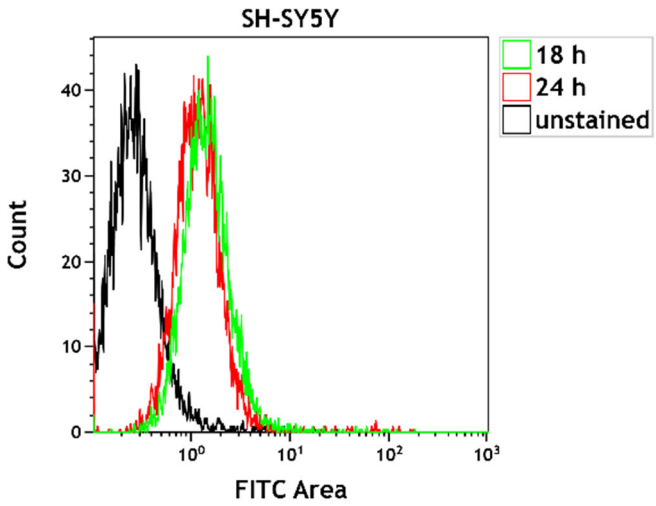
SH-SY5Y
18 h
24 h
unstained
Count
FITC Area

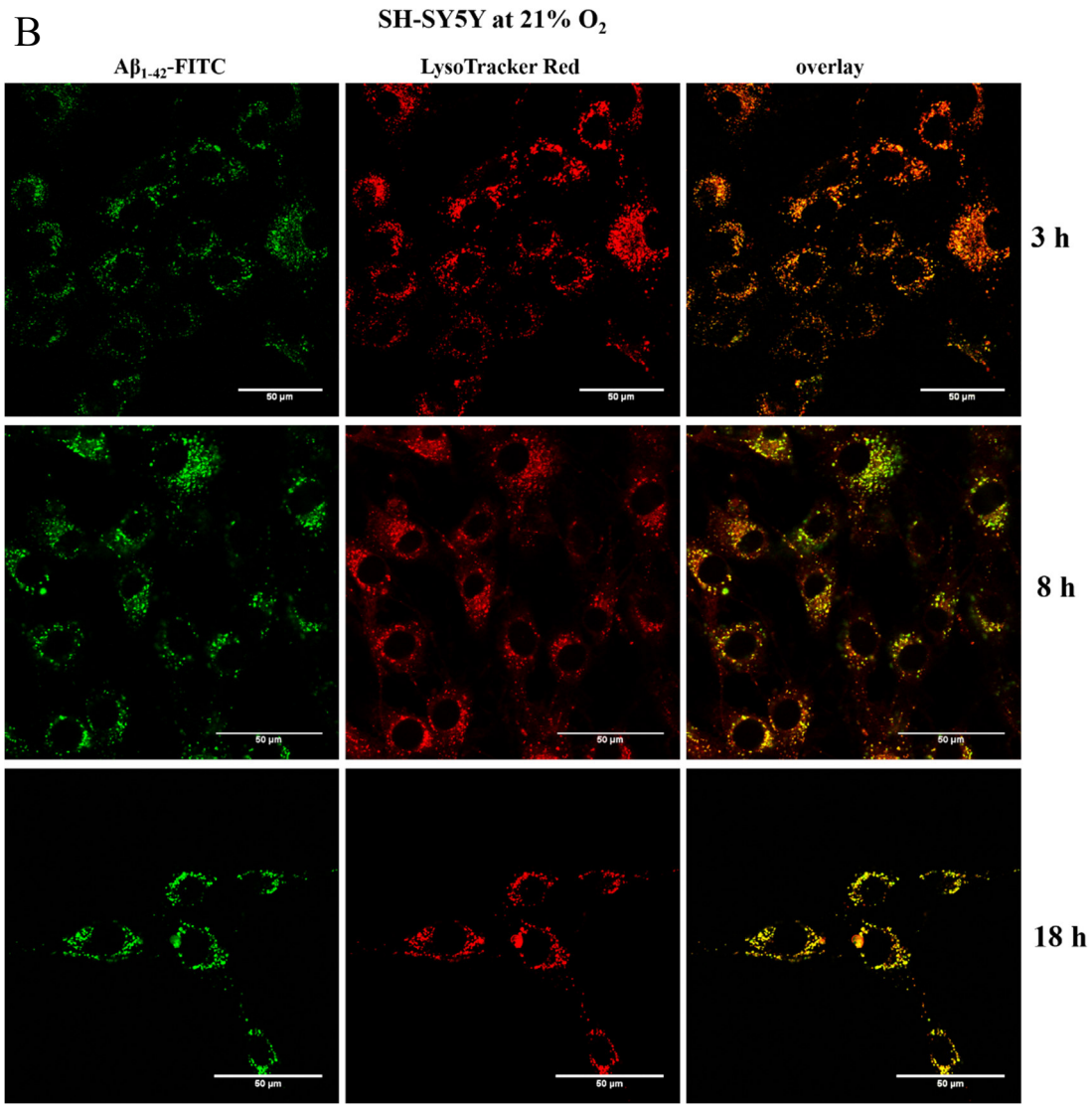
B
SH-SY5Y at 21% O2
Aβ1-42-FITC
LysoTracker Red
overlay
3 h
8 h
18 h
50 µm

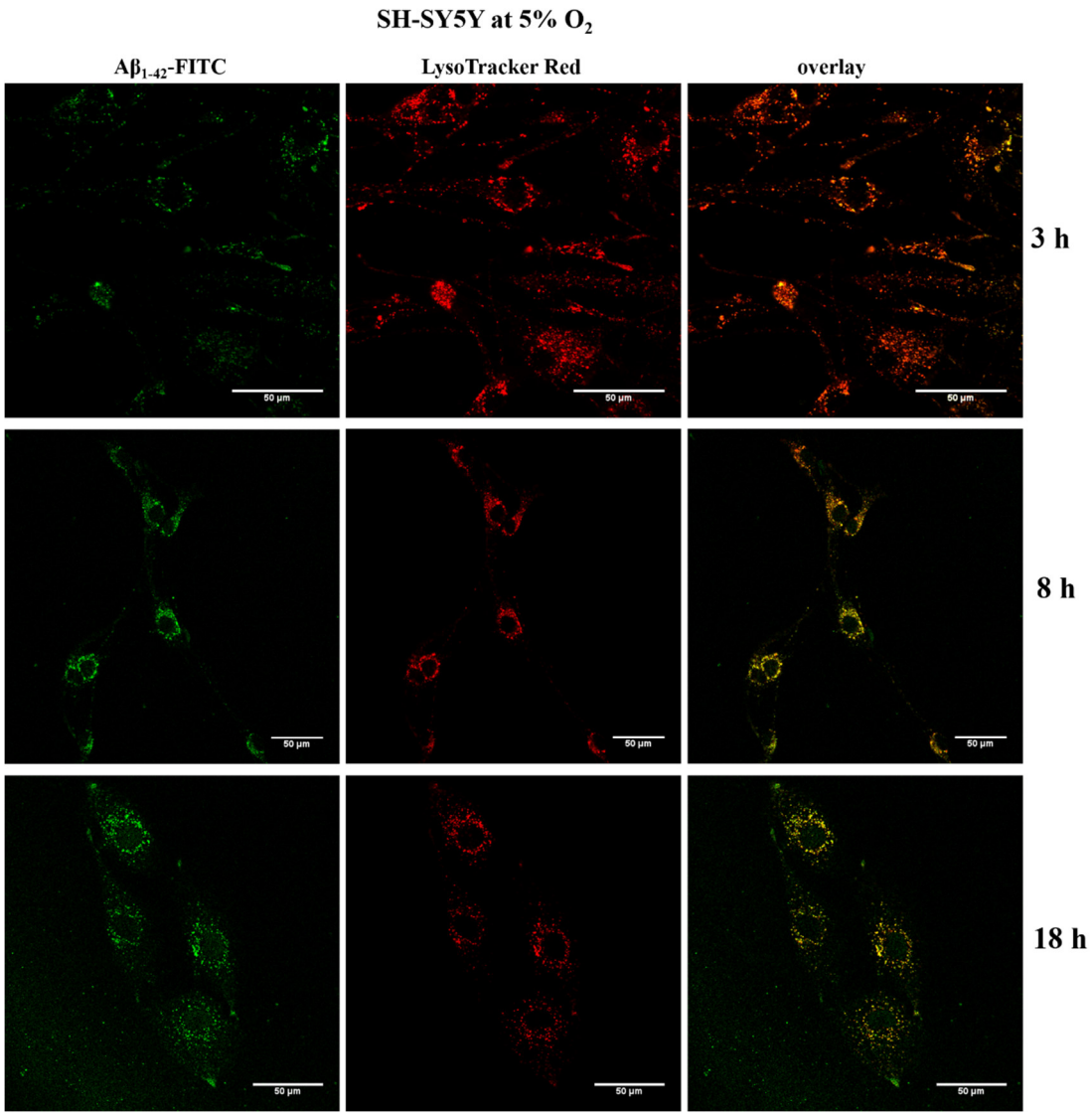
SH-SY5Y at 5% O2
Aβ1-42-FITC
LysoTracker Red
overlay
3 h
8 h
18 h
50 µm

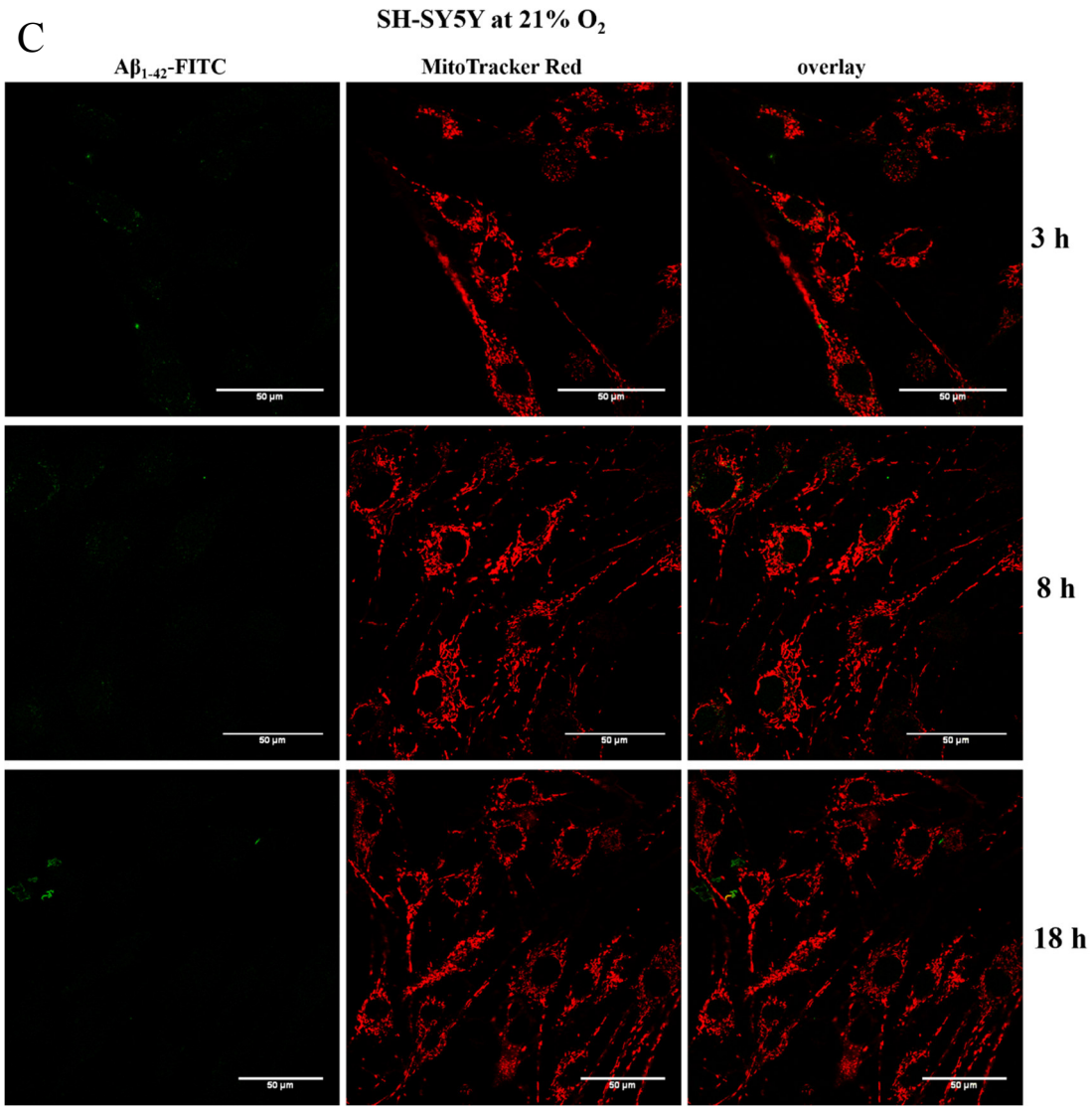
C
SH-SY5Y at 21% O2
Aβ1-42-FITC
MitoTracker Red
overlay
3 h
8 h
18 h
50 µm

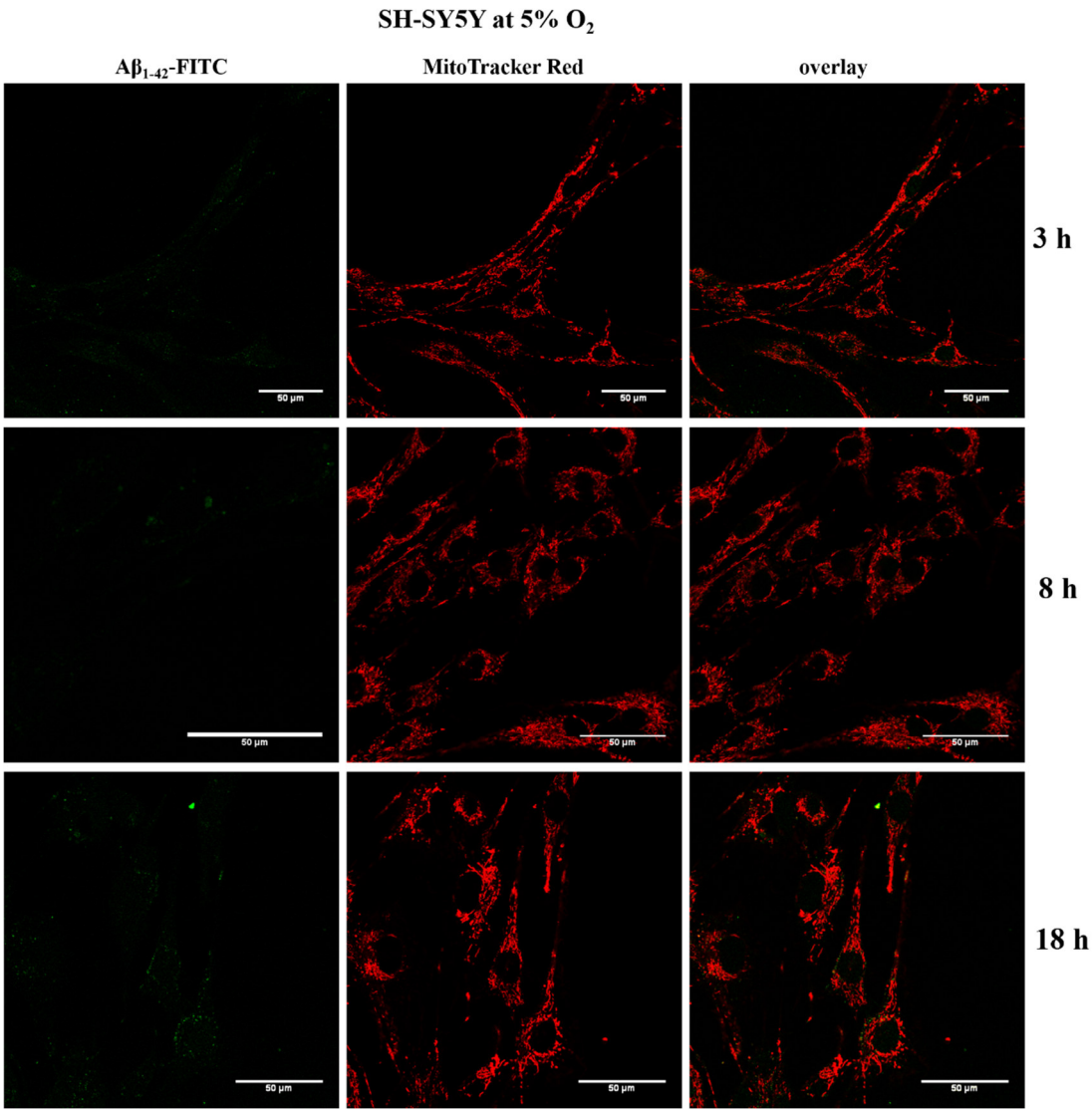
SH-SY5Y at 5% O2
Aβ1-42-FITC
MitoTracker Red
overlay
3 h
8 h
18 h
50 µm

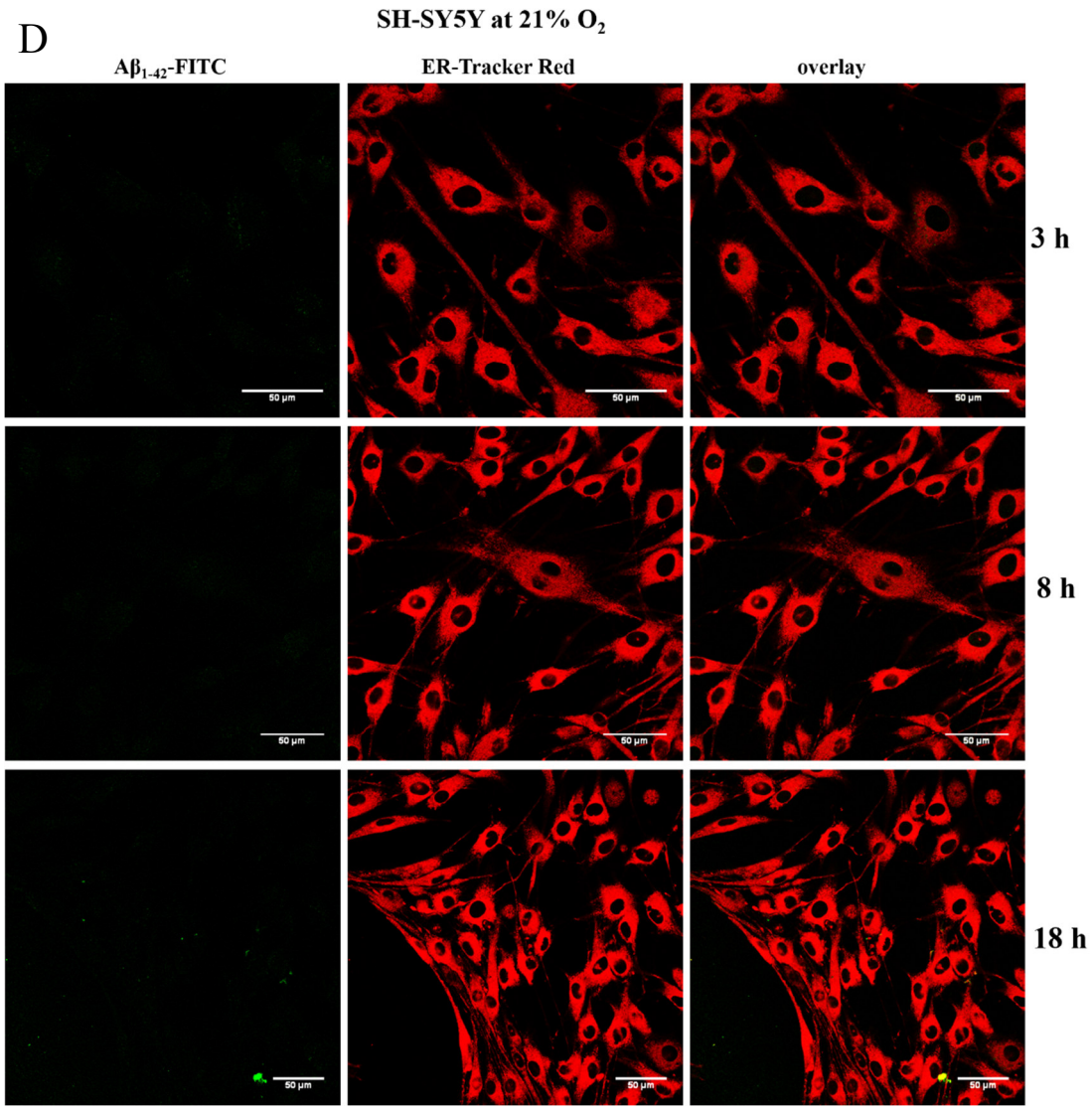
D
SH-SY5Y at 21% O_2
$A\beta_{1-42}$-FITC
ER-Tracker Red
overlay
3 h
8 h
18 h
50 µm

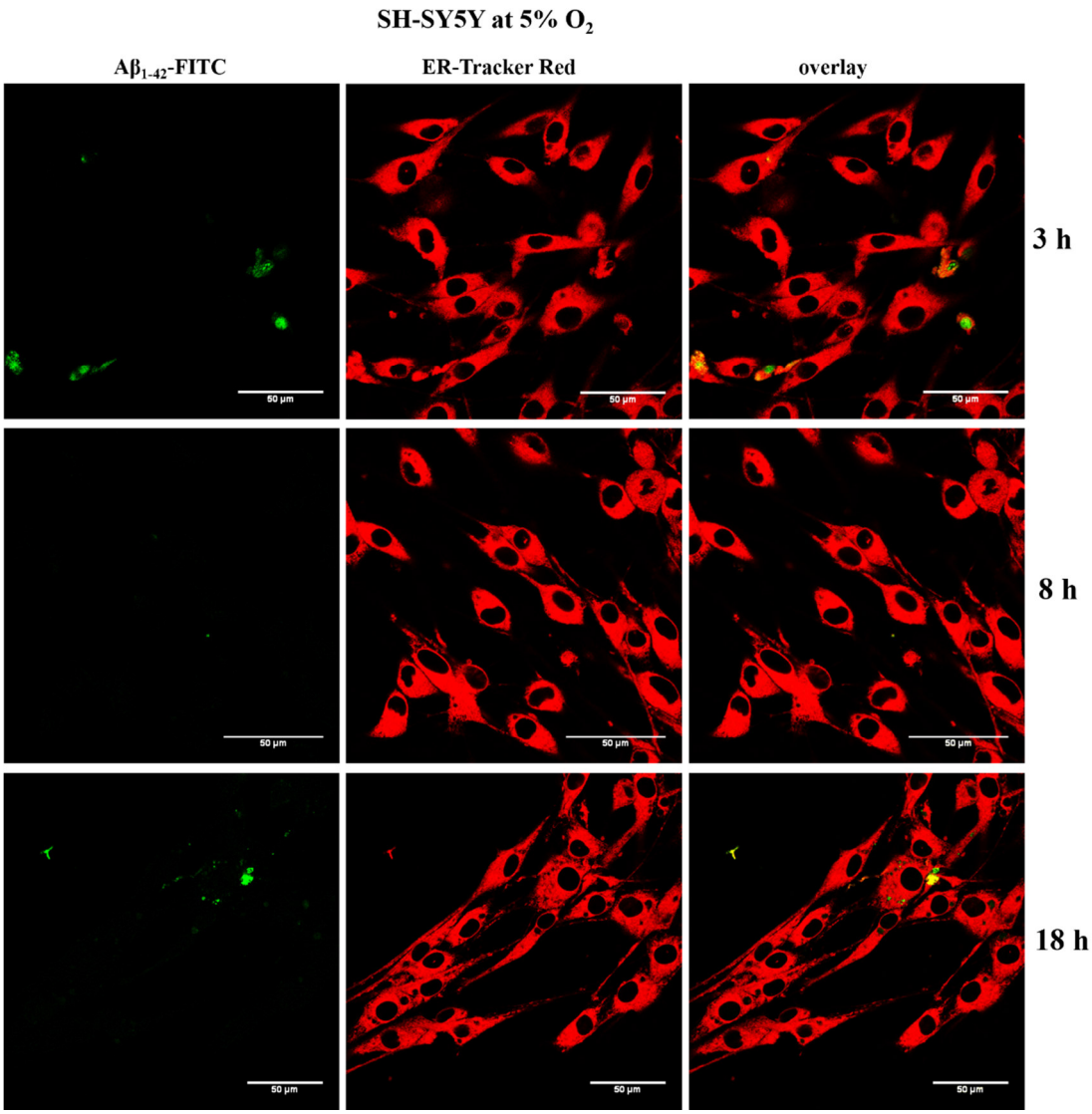

Figure 5.7. FITC-labelled $A\beta_{1-42}$ peptide interacts with SH-SY5Y cells. A) Flow cytometry analysis: shift in the fluorescence signal in SH-SY5Y cells cultivated at 21% O_2 incubated with FITC-$A\beta_{1-42}$ peptide after 15 min, 1, 3, 18 and 24 h compared to unstained cells. Maximum in the fluorescence signal occurred after 18 h, whereas a slight decrease of the signal was detected after 24 h. Very similar results were obtained for cells cultivated at 5% O_2 (data not shown). B) Confocal microscopy: FITC-$A\beta_{1-42}$ peptide (green fluorescence) colocalizes with acidic organelles (lysosomes; endosomes) stained by LysoTracker Red dye (red fluorescence) at both 21% and 5% O_2; progressive interaction after: 3, 8 and 18 h. C-D) FITC-Aβ peptide showed very weak colocalization with mitochondria (C) and endoplasmatic reticulum (D) stained by MitoTracker Red and ER-Tracker Red dye (red fluorescence), respectively, at both 21% and 5% O_2, documented after 3, 8 and 18 h. 400× magnification. 50 µm scale bar.

Externally applied disaggregated $A\beta_{1-42}$ peptide (initially monomers and small oligomers) interacts with SH-SY5Y cells within minutes and the peak in the signal of fluorescently labeled peptide was reached after 18 h of incubation with cells (Figure 5.7 A). Slight decrease of the signal after 24 h suggests the peptide gets degraded or exported. In order to get more information into subcellular localization of externally added Aß peptide, its colocalization with cellular organelles (i.e. with endoplasmatic reticulum, mitochondria and lysosomes) was studied. The peptide interacted

preferentially with acidic organelles (lysosomes and possibly late endosomes) of SH-SY5Y cells cultivated at both 21% and 5% O_2, respectively (Figure 5.7 B), and only at minor extent in other organelles (mitochondria and endoplasmatic reticulum) which showed only very weak colocalization with the peptide (Figure 5.7. C-D). It was previously demonstrated that cellular uptake of $A\beta_{1-42}$ is independent from the attached fluorophore and non-attached fluorophore does not go into the cell (Hu et al., 2009). The confocal scanning microscopy used in this study proved Aβ peptide localization inside the cell, but due to the limited resolution it cannot distinguish if the peptide only attaches to the membrane or it penetrates in the membrane and enters cellular organelles. The peptide has a great potential to intercalate in all cellular membranes due to its hydrophobicity (Dante et al., 2003) and to cause structural perturbation, membrane fusion, changes in lipid diffusion and dynamics (Buchsteiner et al., 2010; Dante et al., 2011; Barrett et al., 2016). Therefore, colocalization of Aβ peptide with mitochondria or endoplasmatic reticulum was expected as well. However, it was primarily found colocalized with lysosomes (Figure 5.7 B).
These organelles present a powerful defense of the cell through its capability to digest unwanted compounds or damaged cellular structures. It seems that lysosomes represent very important defense against intracellular Aß peptide toxicity (Zheng et al., 2012). Possibly, damaged parts of mitochondria are packed in mitochondria-derived vesicles and are targeted to late endosomes and lysosomes for degradation and this process, although it shares similarities with bulk macrophagy and mitophagy, is specific for oxidative damage (Juhàsz, 2016).

5.4. Lysosomal integrity

Information on lysosomal integrity as well as on endocytotic activity of SH-SY5Y cells upon Aβ peptide treatment and/or X-ray irradiation was obtained using Neutral red assay based on the ability of viable cells to uptake neutral red dye which accumulates in lysosomes. The absorbance of the dye extracted from lysosomes is an indicator of lysosomal integrity, the larger the uptake of neutral red dye, the larger lysosomal integrity and absorbance measured. 4 μM $A\beta_{1-42}$ peptide or 2 Gy X-ray irradiation resulted in a lower absorbance of the neutral red (less lysosomal integrity) in cells cultivated at 21% O_2, whereas combination of both resulted in an increase of the absorbance in both RA-treated and non-treated cells (Figure 5.8 A). On the other hand, Aβ peptide and/or irradiation did not cause changes in the absorbance of neutral red dye in cells at 5% O_2 (Figure 5.8 B). Induction of differentiation with RA made SH-SY5Y cells more sensitive, observed as a decrease of the neutral red absorbance compared to non-treated cells at both 21% and 5% O_2.

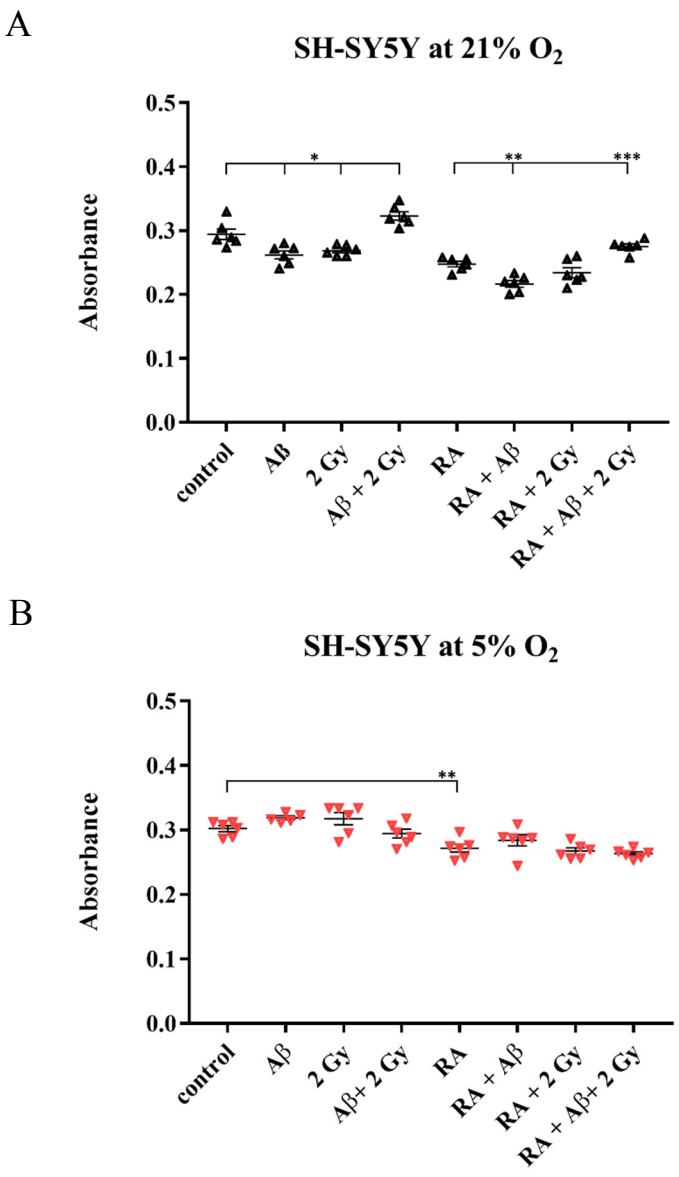

Figure 5.8. Neutral red assay of the lysosomal integrity of SH-SY5Y cells with and without pre-treatment with retinoic acid (RA) and after treatment with 4 μM $A\beta_{1-42}$ peptide, X-ray irradiation with the dose of 2 Gy and combination of both. Absorbance of the neutral red dye extracted from viable cells was measured. A) In cells cultivated at 21% O_2 the absorbance of the neutral red (lysosomal integrity) was significantly lower after Aβ peptide treatment or irradiation, whereas combination of both resulted in an increase of the absorbance in both RA-treated and non-treated cells. B) In cells at 5% O_2 Aβ peptide treatment and/or irradiation did not cause change in the absorbance of neutral red dye. RA treatment resulted in a significant decrease of the neutral red absorbance compared to non-treated cells at both 21% and 5% O_2. Samples were analyzed in duplicates (n = 2) in three independent experiments (N = 3) and data is analyzed by t test with Welch's correction. (*p<0.05; **p<0.01; ***p<0.001).

Although site and kinetics of interaction of the Aβ peptide with SH-SY5Y cells cultivated at both 21% and 5% O_2 were similar (Figure 5.7) and the peptide accumulated preferentially in lysosomes, there was difference in the response (i.e. lysosomal integrity) to Aβ peptide depending on the oxygen concentration applied to the cell culture. Lower lysosomal integrity after Aβ peptide

treatment or irradiation of SH-SY5Y cells cultivated at 21% O_2 suggests that cultivation at non-physiological oxygen concentration makes cells more susceptible to oxidative stress in comparison to cells cultivated at 5% O_2. Interestingly, combination of Aβ peptide and radiation resulted in an increased lysosomal integrity, but solely in cells cultivated at 21% O_2, in both retinoic-acid treated and non-treated cells. This is in line with already published data which show that oxygen concentration modulates cellular response to stress (Tiede et al., 2011; Džinić et al., 2016). General decline of lysosomal integrity was observed in RA-treated cells compared to non-treated cells at both 21% and 5% O_2, which indicates that differentiation status of cells is another important factor in response to stress.

5.5. Cell death

In order to determine the level of cell death (apoptosis and necrosis) after treatment of SH-SY5Y cells with externally applied disaggregated $A\beta_{1-42}$ peptide and/or X-ray irradiation, Annexin V-FITC, for detection of apoptotic cells, together with propidium iodide (PI) staining, for detection of late apoptotic and necrotic cells, was used. Qualitative analysis of the cell death was performed using microscopy for visualization of the fluorescence signal (Figure 5.9). In this assay, non-differentiated SH-SY5Y cells were analyzed.

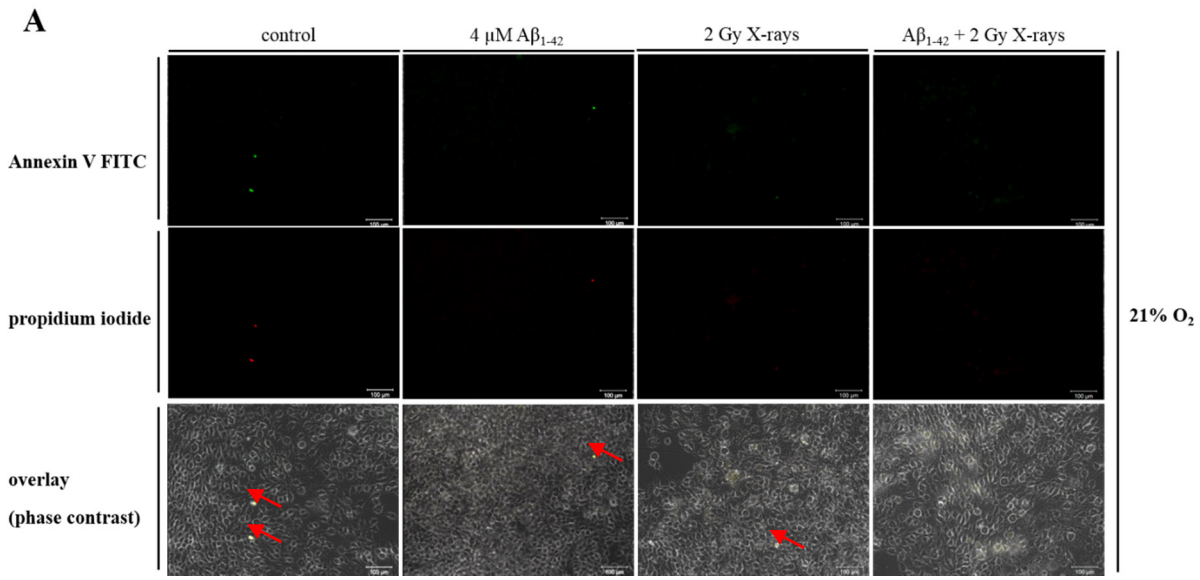

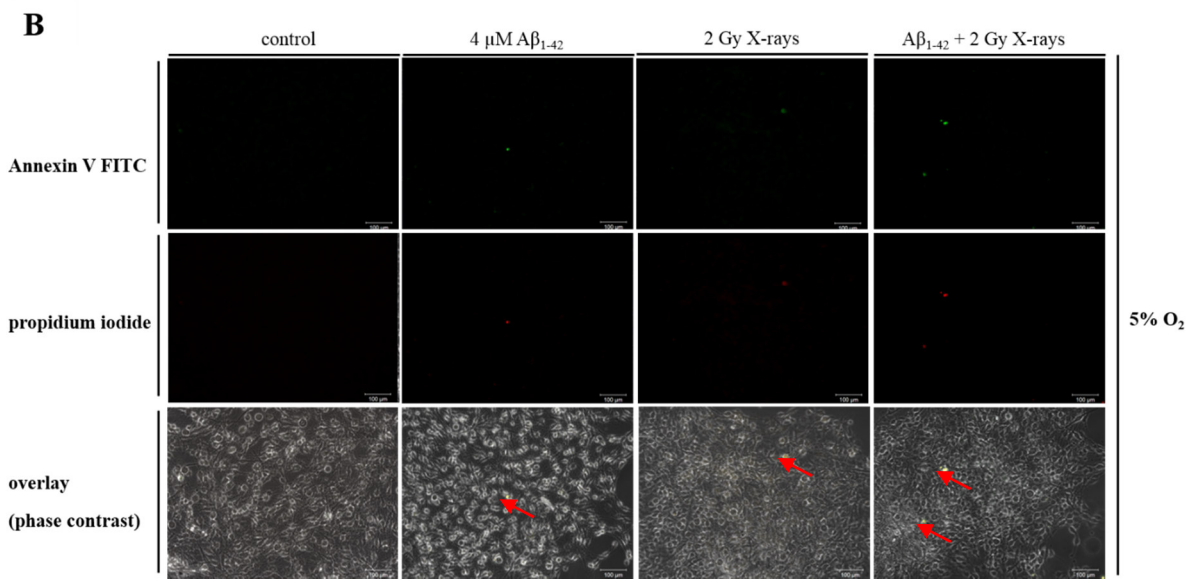

Figure 5.9. Detection of cell death (apoptosis and necrosis) in non-differentiated SH-SY5Y cells after treatment with 4 µM $A\beta_{1-42}$ peptide and/or 2 Gy X-ray irradiation by fluorescence microscopy. A) In cells cultivated at 21% O_2 no increase in the fluorescence signal of Annexin V-FITC (green) and/or of propidium iodide (PI) (red fluorescence) was observed compared to control cells. B) In cells cultivated at 5% O_2 only minor increase in the fluorescence signal (green and red) was observed. Green fluorescence: cells stained with Annexin V-FITC-measure of early apoptosis. Red fluorescence: cells stained with propidium iodide-measure of late apoptosis and necrosis. Bright yellow signal on phase contrast images (indicated with red arrows): overlay of green and red signal. Magnification: 200×. Scale bar: 100 µm. Presented overlayed images are one typcal example of many other comparable images.

Analysis of cell death (apoptosis and necrosis) by fluorescence microscopy did not reveal increase in cell death of non-differentiated SH-SY5Y cells cultivated at 21% and 5% O_2, respectively. Fluorescence signals indicating the presence of apoptosis and/or necrosis (Figure 5.9) was rarely present in all samples analyzed. Since the method includes washing of the excess of Annexin V-FITC and PI after incubation, it is possible that dead cells (apoptotic and necrotic), which detach from the glass slide, are washed away. Therefore, another technique which minimizes the signal loss, i.e. flow cytometry was employed for quantitative cell death analysis.

Statistically significant increase (~1.4 fold) in the number of apoptotic and necrotic cells upon irradiation of non-differentiated SH-SY5Y cells with 2 Gy X-rays was observed in cells cultivated at 5% O_2, whereas 4 µM Aβ peptide treatment alone did not lead to significant changes in cell death at 5% O_2 as compared to control cells (Figure 5.10 B). In non-differentiated cells cultivated at 21% O_2, there was no change in cell death after irradiation. Aβ peptide treatment resulted in a minor decrease (~1.2 fold) in percentage of apoptotic and necrotic cells compared to control cells (Figure 5.10 A). Aβ peptide treatment of irradiated cells resulted in a decrease (~1.3 fold) of cell death to the level in control cells or below at 21% O_2 and 5% O_2, respectively.

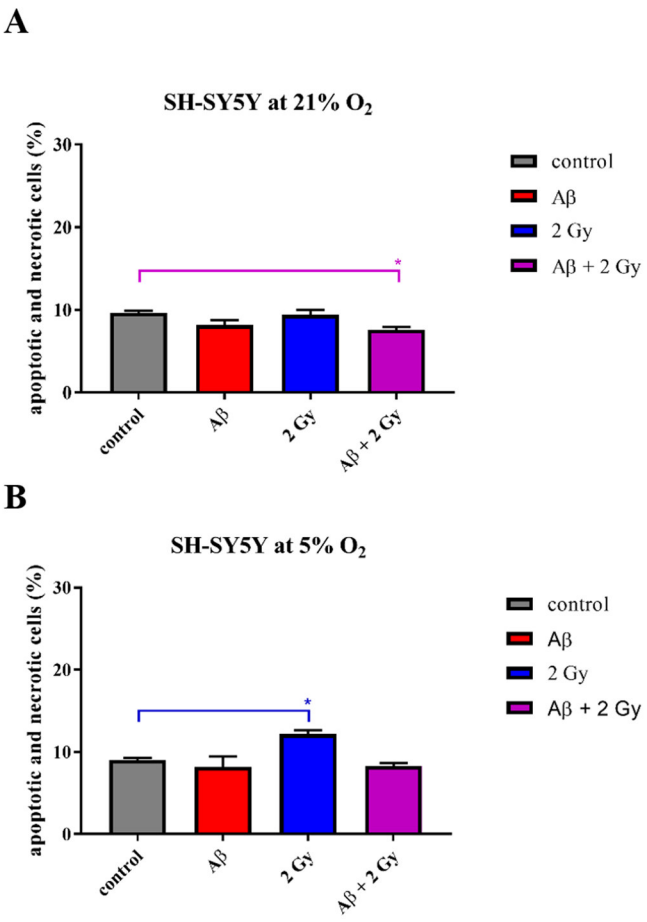

Figure 5.10. The percentage of apoptotic and necrotic cells in non-differentiated SH-SY5Y cells after treatment with 4 μM $Aβ_{1-42}$ peptide, X-ray irradiation with the dose of 2 Gy and combination of both. A). In cells cultivated at 21% O_2 there was a minor decrease (~1.2 fold) in percentage of apoptotic and necrotic cells after Aβ peptide treatment and no change after irradiation, whereas combination of both resulted in a statistically significant decrease (~1.3 fold) in cell death compared to control cells. B) In cells at 5% O_2 Aβ peptide treatment did not lead to significant changes in cell death, whereas irradiation led to a significant increase (~1.4 fold) in percentage of apoptotic and necrotic cells. The combination of both amyloid beta peptide treatment and irradiation resulted in a decrease of cell death to its level in control sample. Samples were analyzed at least in duplicates (n = 2-6) in three independent experiments (N = 3) and data is analyzed by two-way ANOVA followed by Tukey post-tests. (*$p<0.05$).

In the case of retinoic acid-treated SH-SY5Y cells, cultivation at 21% O_2 resulted in an increase (~1.2 fold) in apoptosis and necrosis compared to cells at 5% O_2. Aβ peptide or ionizing radiation led to increase (~1.3 or 1.5 fold) in the number of early and late apoptotic as well as necrotic cells when cells were cultivated at 5% O_2 (Figure 5.11 B), whereas non-significant increase (up to 1.2 fold for both stressors) in apoptotic and necrotic cells was observed at 21% O_2 compared to control cells (Figure 5.11 A). Interestingly, combination of two stressors reduced cell death below the level present in control cells at both 21% and 5% O_2.

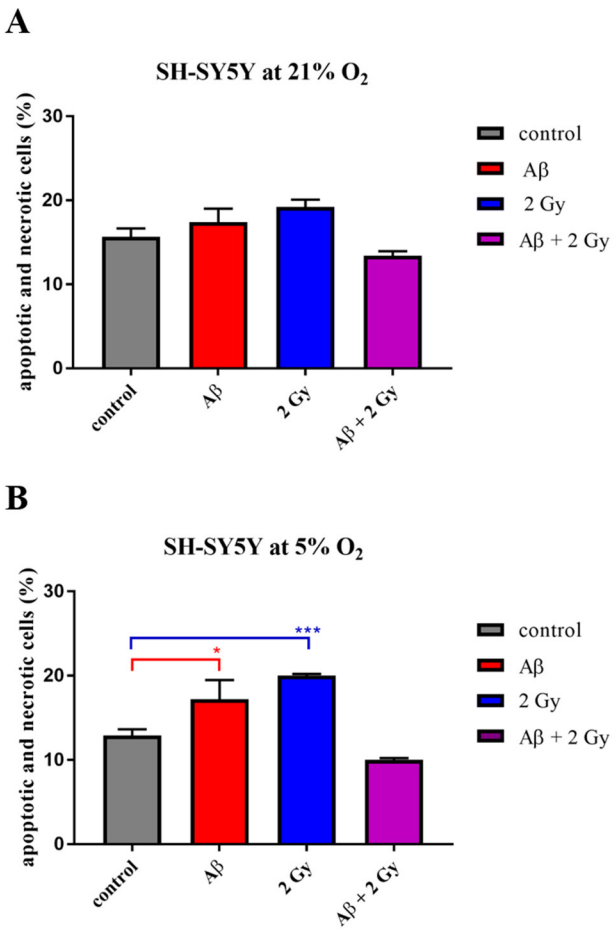

Figure 5.11. The percentage of apoptotic and necrotic cells after treatment with 4 µM $A\beta_{1-42}$ peptide, X-ray irradiation with the dose of 2 Gy and combination of both. A) In cells cultivated at 21% O_2 percentage of apoptotic and necrotic cells was only slightly increased (~1.1 or 1.2 fold) after Aβ peptide treatment or irradiation, whereas combination of both resulted in a slight decrease in cell death (apoptosis and necrosis) compared to control cells. B) In cells at 5% O_2 Aß peptide treatment or irradiation led to a significant (~1.3 or 1.5 fold) increase in percentage of apoptotic and necrotic cells. The combination of both Aβ peptide treatment and irradiation resulted in a decrease (up to 1.3 fold) of cell death below its level in control sample. Samples were analyzed at least in duplicates (n = 2-6) in three independent experiments (N = 3) and data is analyzed by two-way ANOVA, followed by Tukey post-tests. (*p<0.05; **p<0.01; ***p<0.001).

Aß peptide did not harm SH-SY5Y cells to a great extent. The 4 µM peptide applied in this work probably represents a sub-lethal concentration for SH-SY5Y cell as reported previously for 10 µM Aß peptide applied to differentiated PC12 cells as well (Sirk et al., 2007). Additionally, cells were incubated with the peptide for 1 day, which is a short time compared to the many years that are necessary for action of the peptide in human brain. However, many non-lelthal alterations in cell physiology such as slight increase in protein carbonlyation and interaction of Aß peptide with lysosomes (in line with studies performed on the same cell line at 21% O_2 (Decker, 2016)) if persistant, may induce detrimental changes. Moreover, observed accumulation of Aß peptide in lysosomes probably leads to degradation of the most of the applied peptide and protects cells

against its harmful effects as long as lysosomal integrity and functions are preserved. Lysosomes, besides their digestive roles, have numerous other functions for maintenance of cell integrity (Lim and Zoncu, 2016). However, it is possible that continuous accumulation of the peptide harm the integrity and normal function of lysosomes. In some cases the peptide even had protective functions, which requires further investigation. Possibly, aromatic amino acid residues of Aß peptide act as ROS scavengers (Stadtman, 1993). Furthermore, Aβ peptide toxicity is cell-specific and depends on their metabolism; basal metabolism and its rate affects the level of endogenous oxidants and other mutagens (Ames et al., 1993; Decker, 2016). For example, picomolar concentrations of intracellular $Aß_{1-42}$ (both non-fibrillized and fibrillized) induce cell death of primary neurons through p53-Bax pathway (Zhang et al., 2002) but not of other neuronal and non-neuronal cell types.

Very high concentration of the peptide (100 µM) did not harm SH-SY5Y cells after 1 day (Figure 5.12). However, incubation for 3 days was sufficient to cause a massive cell death (~5.3 fold increase as compared to control). Additionally, 100 µM of aged (aggregated by storage at 37 °C overnight) peptide led to a significant increase (up to 3.4 fold) in cell death after 1 and 3 days as well (i.e. earlier response than disaggregated peptide but less cell death after 3 days). On the other hand, the effect of 4 µM aged peptide was very similar to that of disaggregated peptide (data not shown). Irradiation with 10 Gy X-rays increased the percentage of apoptotic and necrotic cells (1.6 and 1.7 fold) after 1 and 3 days, respectively. Interestingly and in accordance with data described above, Aβ peptide treatment decreased the percentage of apoptotic and necrotic cells (2.5 fold) in irradiated cells after 1 day. However, after 3 days, a ~2.8 fold increase in cell death as compared to control cells was observed. Data in Figure 5.12 is presented for RA-treated cells cultivated at 5% O_2 only. Incubation time together with concentration and aggregation state of the peptide (disaggregated or aggregated to fibrils) is a crucial factor in Aβ peptide toxicity. Aged peptide caused earlier response of SH-SY5Y cells which underwent cell death. However, the effect of disaggregated Aß peptide after 3 days of incubation was more pronounced than of aged peptide. Although not used in this work, the reverse peptide ($Aβ_{42-1}$) tested on SH-SY5Y cells cultivated at 21% O_2 behaved as a negative control and did not induce changes in cell death, ATP and ROS level (Decker, 2016).

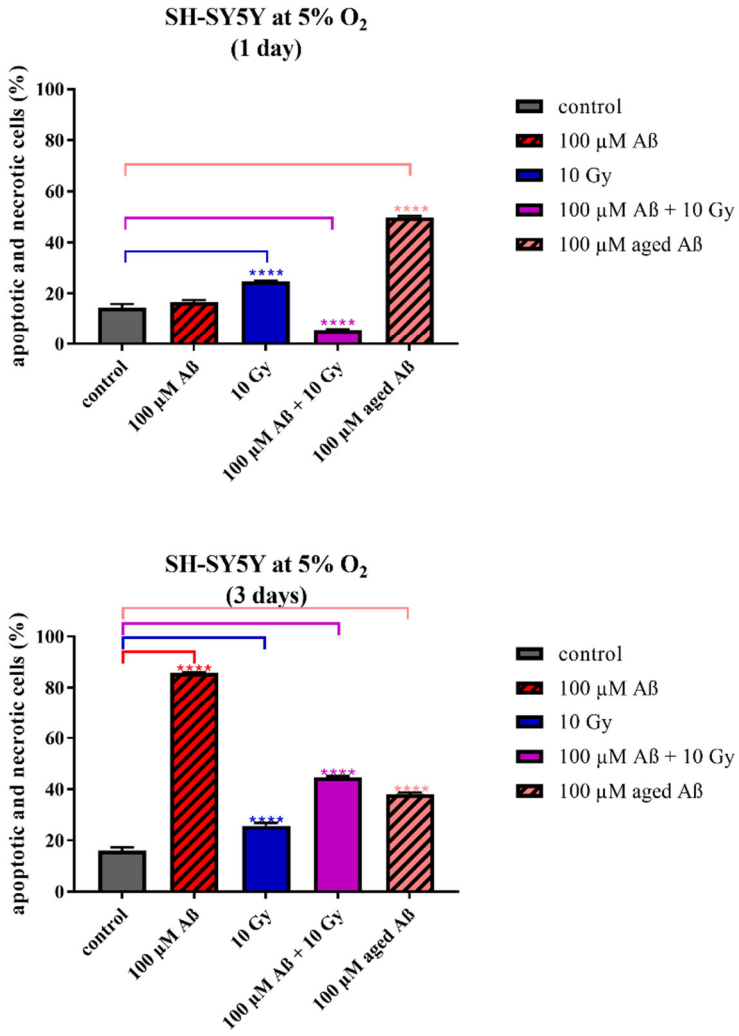

Figure 5.12. The percentage of apoptotic and necrotic cells in retinoic acid-treated SH-SY5Y cells after treatment with 100 µM disaggregated $A\beta_{1\text{-}42}$ peptide and/or 10 X-ray irradiation; "aged" $A\beta_{1\text{-}42}$ peptide (incubated at 37 °C overnight for aggregation) in cells cultivated at 5% O_2. A) 1 day incubation with disaggregated Aβ peptide did not lead to significant changes in cell death; irradiation led to a significant (~1.7 fold) increase in cell death, whereas combination of both resulted in a significant (~2.5 fold) decrease in cell death; aggregated (aged) peptide led to a significant (~3.4 fold) increase in cell death. B) 3 days incubation with disaggregated Aβ peptide resulted in a massive cell death (~5.3 fold increase); irradiation, combination of both and treatment with "aged" Aβ peptide all led to a significant (~1.6, 2.8 and 2.3 fold, respectively) increase in cell death. Samples were analyzed at least in duplicates (n = 2-6) in three independent experiments (N = 3) and data is analyzed by two-way ANOVA, followed by Tukey post-tests. (****p<0.0001).

5.6. Intracellular ATP concentration

ATP concentration is an indicator of change in cell viability and proliferation. ATP concentration upon treatment of RA-treated SH-SY5Y cells with Aβ peptide and/or ionizing irradiation was assayed by luminescence-based measurement of total cellular ATP.

Higher (~1.3 fold) cellular ATP concentration was observed in SH-SY5Y control cells cultivated at 5% O_2 in comparison to cells at 21% O_2 (Figure 5.13 A). Whereas Aβ peptide did not affect the ATP concentration at these two different oxygen conditions, irradiation alone led to a slight (~1.2 fold) but non-significant increase in ATP and a significant (~1.5 fold) increase when combined with Aβ peptide treatment in cells at 5% O_2 only.

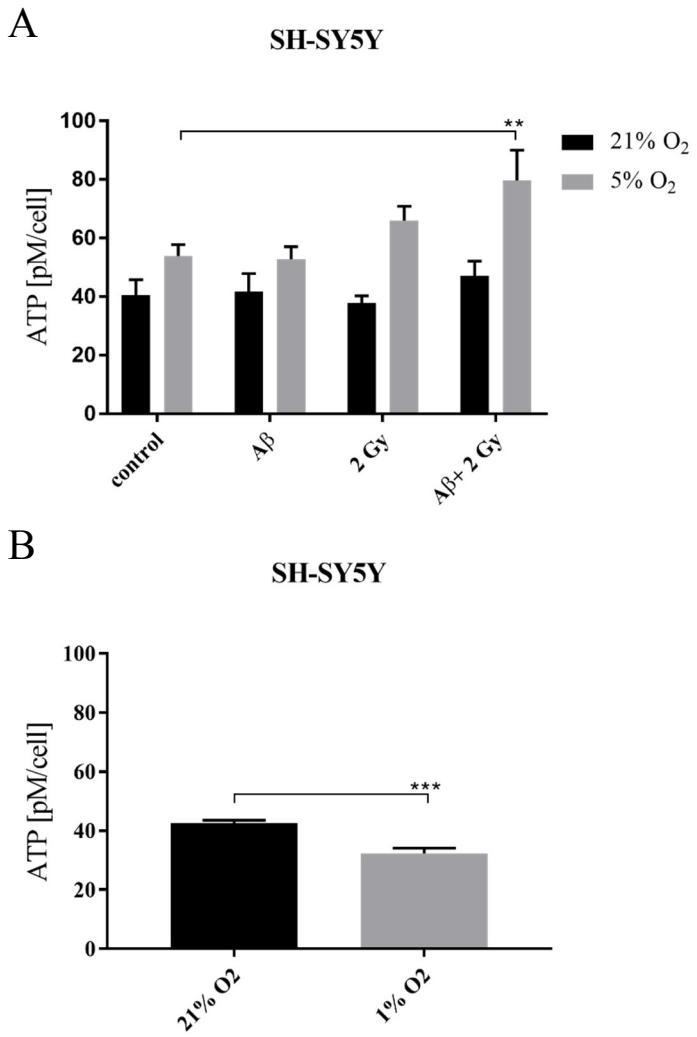

Figure 5.13. A) Total cellular ATP concentration of SH-SY5Y cells cultivated at 21% and 5% O_2, respectively, after treatment with Aβ peptide and/or X-ray irradiation, normalized to cell count and compared to respective controls. ATP concentration was about 1.3-1.8 fold higher at all conditions in cells cultivated at 5% O_2 compared to 21% O_2. Combination of Aβ peptide treatment and irradiation resulted in a significantly increased (~1.5 fold) ATP concentration at 5% O_2 compared to the control. Samples were measured at least in duplicates (n = 2-4) in three independent experiments (N = 3). Mean ± SEM analyzed by two-way ANOVA with Tukey´s multiple comparison test with $p<0.05$ considered as a significant. (**$p<0.01$). B) Total cellular ATP concentration of SH-SY5Y cells cultivated at 21% and 1% O_2, respectively. The experiment was performed solely to test ATP concentration at 1% O_2. Significantly lower (~1.3 fold) ATP concentration in cells at 1% O_2 as compared to 21% O_2. Mean ± SEM analyzed by t-test. (***$p<0.001$).

ATP is required for repair processes upon stress such as irradiation or presence of toxic peptides. The ATP concentration in the cell is balanced by its generation and consumption. The ATP concentration reflects the activity of the respiratory chain complexes and proliferation activity depending on irradiation and oxygen concentration. In addition, ATP is utilized for repair processes after oxidative stress or under other unfavorable conditions. For example, observed increase in ATP concentration upon irradiation of Aβ peptide treated cells cultivated at 5% O_2 is in accordance with this. Oxygen affects bioenergetic status of the cell since cells at 5% O_2, which is more physiological, showed higher ATP concentration compared to cells at non-physiological 21% O_2. Additionally, decreased (~1.3 fold) ATP concentration in cells cultivated at 1% O_2 as compared to 21% O_2 (Figure 5.13 B) measured in an independent experiment was one of the reasons to use 5% O_2 instead of 1% O_2 for cultivation of SH-SY5Y cells.

5.7. ROS level

Changes of the intracellular ROS level upon irradiation, treatment with $A\beta_{1-42}$ peptide, and combination of both were monitored using carboxy-H_2DCF-DA for detection of different ROS species such as H_2O_2, •OH and hydroperoxides. Intracellular ROS measurement by flow cytometry reflects the ROS level (shift in the fluorescence signal) in comparison to respective controls (Aß peptide non-treated and non-irradiated cells and H_2O_2 positive control) (Figure 5.14 A). Noteworthy, the ROS level in non-treated control cells was significantly higher (~1.5 fold) in cells cultivated at 21% O_2 compared to cells cultivated at more physiological (5%) O_2 concentration (Figure 5.14 B). Treatment with Aβ peptide only slightly increased ROS level at both 21% and 5% O_2 (up to 1.2 fold). 2 Gy X-ray irradiation led to a significantly larger (~1.8 fold) increase in ROS but solely in cells at 5% O_2. Radiation combined with Aβ peptide treatment resulted in a statistically significant increase in ROS level at both 21% (~1.2 fold) and 5% O_2 (~1.4 fold) compared to respective controls. Data in Figure 5.14 is presented for RA-treated SH-SY5Y cells.

A

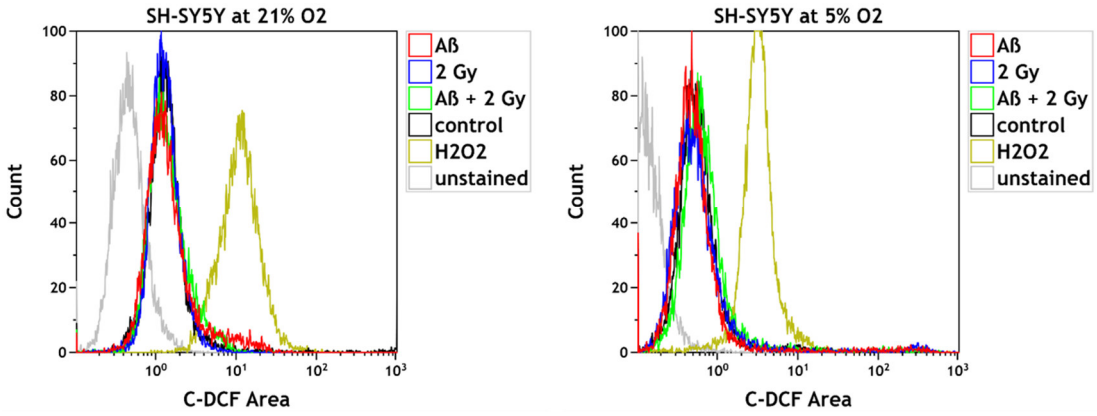

B

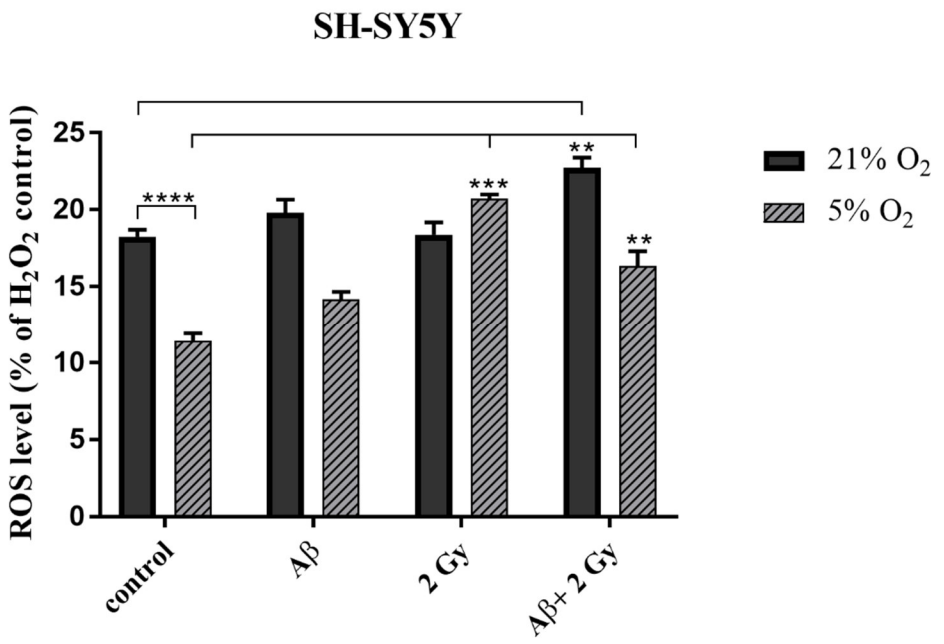

Figure 5.14. Modulation of intracellular ROS level in SH-SY5Y cells by oxygen concentration, treatment with $A\beta_{1-42}$ peptide and/or 2 Gy X-rays. A) Shift in the fluorescence signal of 2'7'-dihydrofluorescein in comparison to the signal of the positive control (H_2O_2 treated cells) and to the non-treated cells detected after irradiation, Aβ peptide treatment or combination of both in SH-SY5Y cells depending on the oxygen concentration (21% and 5% O_2, respectively). B) Generally higher (~1.5 fold) ROS level was detected in cells cultivated at 21% O_2 compared to 5% O_2. Slight (~1.1 fold) increase of ROS level after Aβ peptide treatment at 21% O_2 and about 1.3 fold at 5% O_2 in comparison to the non-treated control cells. Significant (1.8 fold) increase of ROS level after irradiation at 5% O_2 only and after irradiation of Aβ peptide treated cells at both 21% (~1.2 fold) and 5% O_2 (~1.4 fold). Samples were measured at least in duplicates (n = 2) in at least three (N = 3) independent experiments and relative fluorescence values are presented as percentages (%) of the fluorescence value of the H_2O_2 control (100%). Mean ± SEM analyzed by two-way ANOVA with Tukey´s test. (*p<0.05; **p<0.01; ***p<0.001; ****p<0.0001).

Although it is generally assumed that cytotoxic effects of Aβ peptides are exerted through the induction of ROS generation, similar to ionizing radiation, the observed increase in ROS level was not as high as expected. ROS generated after irradiation alone or combined with Aß peptide was more pronounced in cells at 5% O_2 as compared to atmospheric concentration. Control cells cultivated at 21% O_2 had higher ROS level than cells at 5% O_2 (Figure 5.14 B). Probably cultivation at non-physiological 21% O_2 already presents oxidative stress for cells. The treatment with Aβ peptide for 1 day and/or single dose of 2 Gy X-ray irradiation is an acute stress, which can be compensated by a variety of natural antioxidant mechanism (such as glutathione and different dismutases and catalases) that prevent ROS imbalance in the cell and cell death. In addition, the concentration of the peptide (4 µM) is a sub-lethal dose as showed in the assay of cell death (Chapter 5.5), where only minor increase in the number of apoptotic and necrotic cells was observed.

Furthermore, the ROS level depends on the dose of irradiation applied. 8 Gy X-rays irradiation resulted in more pronounced increase in ROS level than 2 Gy X-rays as compared to controls for

5% *versus* 21% O_2 cultivation (Figure 5.15). Data in Figure 5.15 is presented for non-differentiated SH-SY5Y cells.

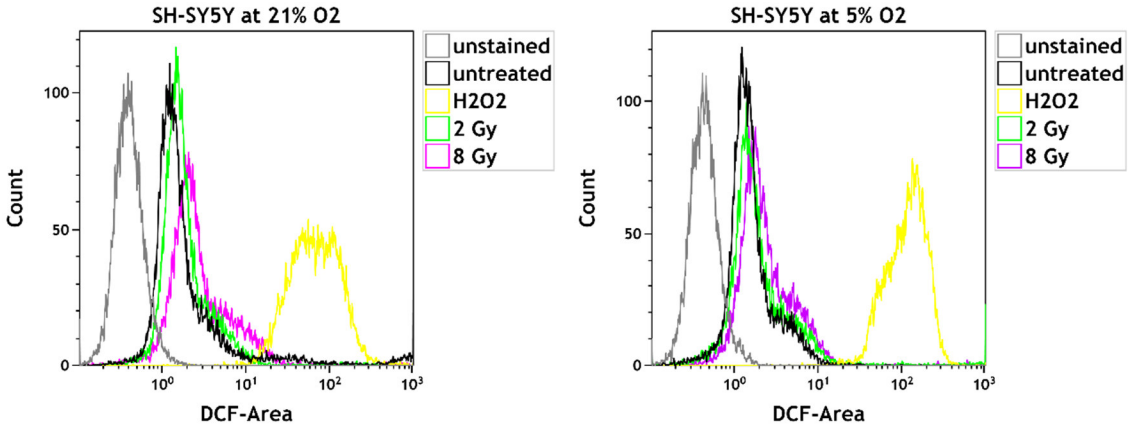

Figure 5.15. Modulation of intracellular ROS level in SH-SY5Y cells by oxygen concentration and irradiation dose. Shift in the fluorescence signal of 2'7'-dihydrofluorescein in comparison to the signal of the positive control (H_2O_2 treated cells) and to the control (non-treated) cells detected after 2 Gy and 8 Gy X-ray irradiation of cells cultivated at 21% and 5% O_2, respectively. Irradiation with 8 Gy X-rays resulted in more pronounced increase of ROS as compared to 2 Gy which led only to a minor increase in ROS compared to the control (untreated) cells which at both 21% and 5% O_2; samples from a single measurements by flow cytometry and data for non-differentaited cells were presented.

Observed changes in ROS induced by Aβ peptide and/or radiation were measured at least 18 h later (Figure 5.14 and 5.15), which is a long time compared to short half-lives (10^{-9}–10^{-4} s) of ROS (Powers et al., 2011). Changes in ROS might be immediate and transient and one approach to detect such changes is the use of HyPer, a genetically encoded H_2O_2 sensor (Belousov et al., 2006). For example, immediately after adding 100 µM H_2O_2 to SH-SY5Y cells transfected with the construct containing the sensor, maximum in the fluorescence signal representing increase in ROS occurred but then the signal started to decrease in seconds (Figure 5.16). Data is presented for non-differentiated SH-SY5Y cells cultivated at 21% O_2 solely as an example for transient and fast change in ROS level in the cell induced by the stressor H_2O_2. It was prevously demonstrated, using Hyper, that irradiation of HEK293 cells using ≥1 Gy X-rays causes a rapid rise of H_2O_2 in the cell and subsequent decrease (Gibhardt et al., 2015), which is in line with results obtained here. However, Aβ peptide induced changes in ROS may be different from those induced by H_2O_2 or radiation.

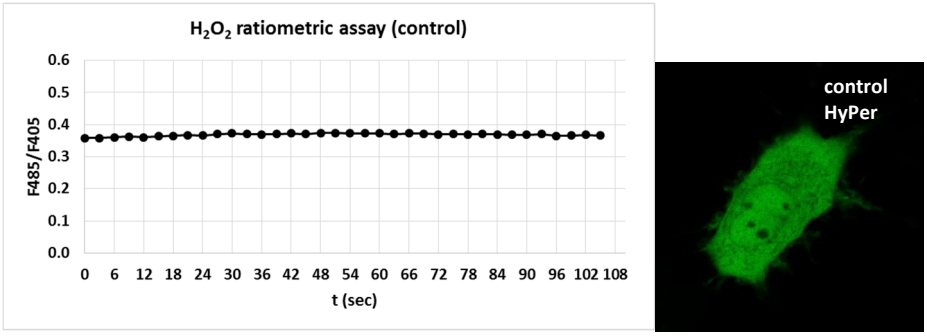

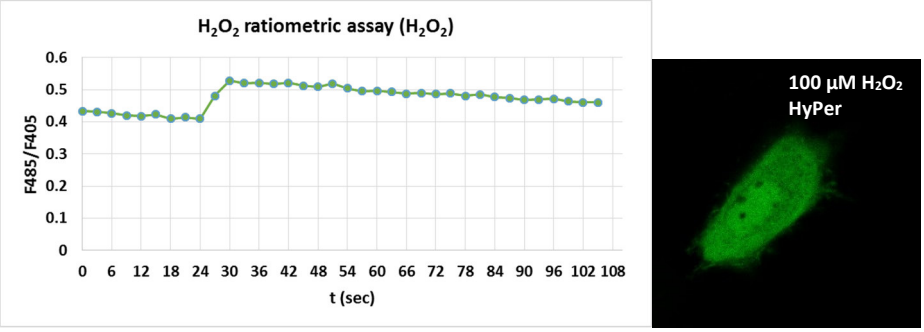

Figure 5.16. Ratiometric assay of ROS level in SH-SY5Y cells observed using a confocal laser scanning microscope. HyPer, a H_2O_2 sensor, in control cells and cells treated with 100 µM H_2O_2 (positive control for oxidative stress) was excited with a 405 nm diode and a 488 nm argon laser. Ratio of fluorescence signal for single cells obtained for each time point (every 3 sec during 110 sec) at 488 nm and 405 nm excitation was used to determine fluorescence signal ratio in Image J software. Control cells showed stable ROS level during the measurement (upper graph). Cells treated with 100 µM H_2O_2 at the time point 24 sec from the beginning of the measurement showed maximum in the fluorescence signal at the time point 30 sec and subsequent decrease of the signal (lower graph). Microscopic images of control cells (above) and H_2O_2 treated cells (below) transfected with HyPer. Images taken at the time point 30 sec were presented. Magnification: 400×.

5.8. Glutathione level

GSH level is an indicator of cell´s antioxidant capacity (Dani et al., 2010) and was measured in SH-SY5Y cells cultivated at 21% and 5% O_2 after treatment with Aβ peptide (6 and 24 h, respectively) and/or X-ray irradiation (after 1 h and 18 h, respectively). Varying levels of GSH were detected depending on different duration of Aß peptide incubation and/or X-ray irradiation (Figure 5.17). Aß peptide alone resulted in a statistically significant (~1.2 fold) decrease in GSH level after 6 h of incubation but only in cells cultivated at 5% O_2, whereas the small decrease at 21% O_2 was non-significant. 24 h after Aβ peptide treatment, GSH level was at the level of GSH in corresponding non-treated controls at both 21% and 5% O_2. 2 Gy X-rays led to an increase in the GSH level only at 5% O_2 assayed 1 h post-irradiation followed by a decrease 18 h later. On the other hand, at 21% O_2 irradiation did not lead to change in GSH level after 1 h, whereas an increase was observed 18 h later. Combination of both Aβ peptide and irradiation resulted in a decrease in the GSH level on the first day and then to an increase on the next day in cells at 21% O_2. Contrary, this combination in cells at 5% O_2 resulted in no change on the first day and then in a significant decrease (~1.2 fold) in the GSH level on the next day. Notable, GSH level measured on the second day was significantly ($p<0.0001$) higher in control cells cultivated at 5% O_2 compared to that at 21% O_2. In summary, Aß peptide by itself did not significantly change the GSH level after 1 day, no matter of oxygen concentration in the cell culture. Irradiation alone or in combination with Aβ peptide treatment had opposite effects depending on the oxygen concentration: significantly increased (up to 1.1 fold) GSH level at 21% O_2 and decreased (up to 1.2 fold) at 5% O_2, as compared to respective non-treated controls.

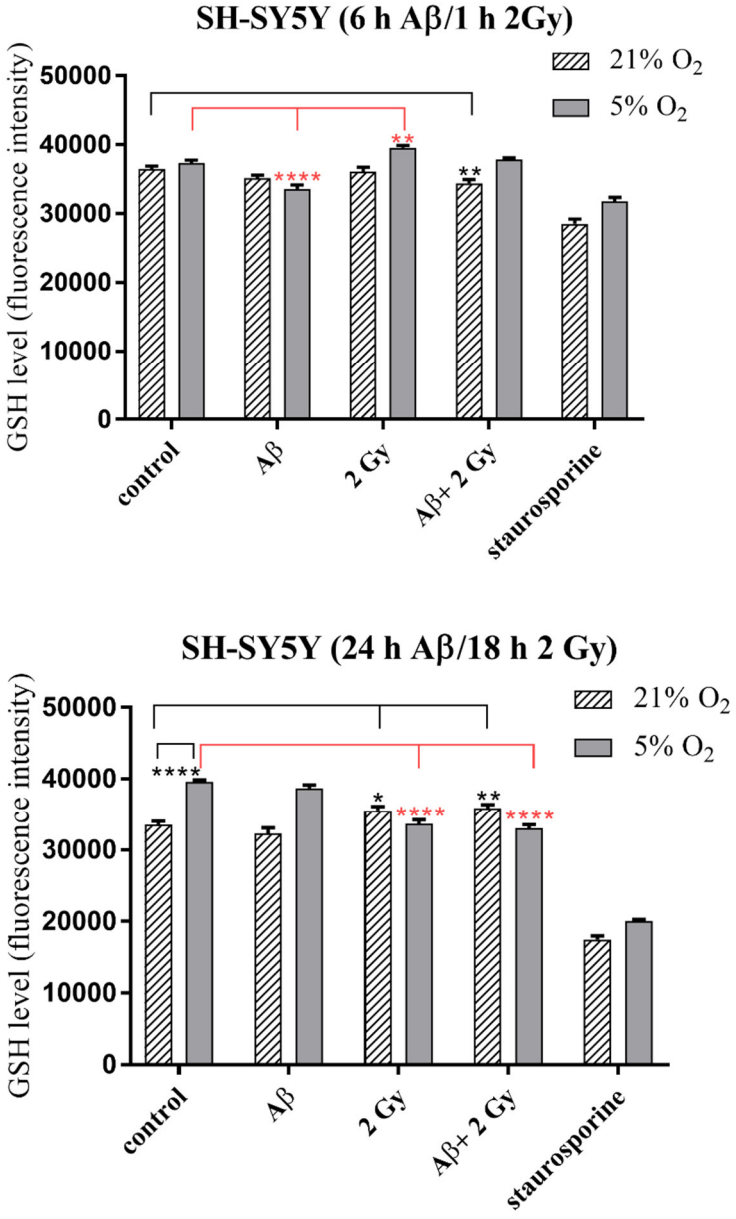

Figure 5.17. The level of glutathione in SH-SY5Y cells cultivated at 21% and 5% O_2, respectively after treatment with Aβ peptide and/or X-ray irradiation compared to non-treated controls. Measurements were performed 6 h after incubation with Aβ peptide and/or 1 h after irradiation and 24 h after incubation with Aβ peptide and/or 18 h after irradiation (2 Gy X-rays), respectively. Aβ peptide treatment alone for 6 h resulted in a small but significant decrease (~1.2 fold) of GSH level only at 5% O_2, whereas irradiation alone elevated GSH level in those cells after 1 h. Cells at 21% O_2 showed significantly decreased (up to 1.2 fold) GSH level only 1 h after irradiation of Aß peptide treated cells. GSH level of Aß peptide treated cells cultivated at 5% O_2 was restored almost to the level in control cells after 1 day, whereas GSH level of irradiated cells (with and without Aß peptide) decreased significantly. Contrary, GSH level of irradiated cells (with and without Aß peptide) was elevated (up to 1.1 fold) at 21% O_2 compared to control. Control cells at 5% O_2 showed higher GSH level (~1.2 fold) on the second day of the assay compared to control cells

at 21% O_2. Treatment of cells with 2 µM staurosporine served as an experimental control for a pronounced decrease in GSH level. Samples were measured at least in octaplicates (n = 8) in four independent experiments (N = 4). Mean ± SEM analyzed by two-way ANOVA with Dunnet´s multiple comparison test. (*p<0.05; **p<0.01; ***p<0.001, ****p<0.0001).

GSH is the primary defense mechanism against free radicals (Dani et al., 2010). Control cells cultivated at 5% O_2 had a higher GSH level than cells at 21% O_2 and it was dependent on the incubation duration with Aß peptide and irradiation. Irradiation alone or in combination with Aβ peptide treatment had opposite effects depending on the oxygen concentration in the cell culture: significantly increased GSH level at 21% O_2 and decreased at 5% O_2, as compared to respective controls. Although GSH level decrease is used as an early indicator of apoptosis (Coppola et al., 2000), in this thesis in most cases it could not be correlated with cell death, particularly not in cells at 5% O_2. Probably, cells employ other antioxidant and repair mechanisms depending on the starting level of oxidative stress.

5.9. Mitochondrial membrane potential

The mitochondrial membrane potential was measured using MitoTracker® Red dye that freely enters healthy mitochondria. Increase in mitochondrial membrane potential of differentiated SH-SY5Y cells was observed after the treatment with 4 µM $Aβ_{1-42}$ peptide or 2 Gy X-ray irradiation at both 21% and 5% O_2 as compared to respective controls (Figure 5.18). Combination of Aβ peptide and irradiation did not lead to a significant change in mitochondrial membrane potential.

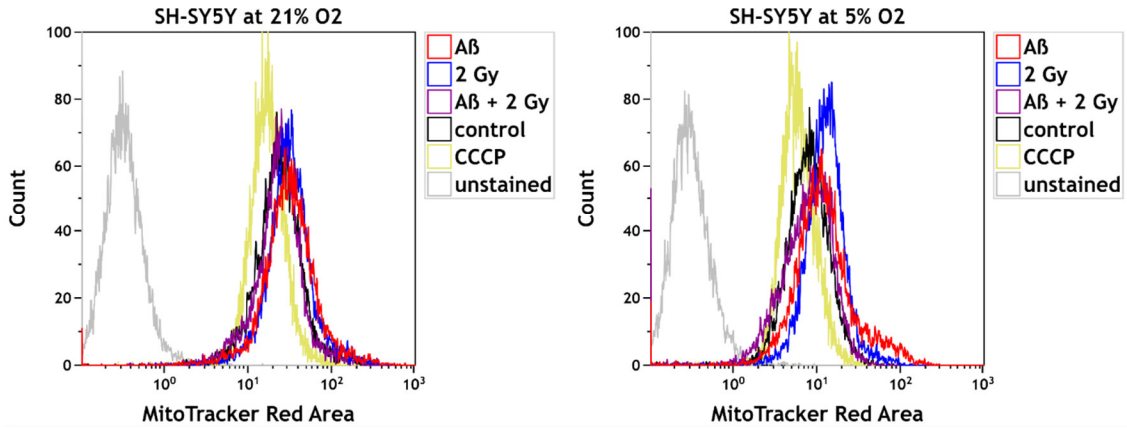

Figure 5.18. Modulation of mitochondrial membrane potential of SH-SY5Y cells by oxygen concentration, treatment with $Aβ_{1-42}$ peptide and/or irradiation measured using MitoTracker® Red CM-H2Xros ($λ_{EX}/λ_{EM}$ = 579/599 nm) by flow cytometry. Increase in mitochondrial membrane potential upon treatment with 4 µM Aβ peptide or 2 Gy X-ray irradiation was observed as a shift (increase) in the fluorescence signal compared to controls (non-treated and non-irradiated cells and cells incubated with 100 µM CCCP (carbonyl cyanide m-chlorophenyl hydrazone) used as a positive control for the abolishment of the mitochondrial membrane potential)) at both 21% and 5% O_2. Combination of Aβ peptide and irradiation did not result in change of mitochondrial membrane potential.

Increase in the mitochondrial membrane potential after treatment with Aβ peptide or irradiation was not dramatic and probably represents a transient change and one of the mechanisms that cells employ in the presence of stressors. These results are in accordance with already published data,

where increase in mitochondrial membrane potential of differentiated cells at both oxygen concentrations upon 2 Gy X-ray irradiation was observed (Džinić et., 2016).

5.10. Effects of X-ray radiation on cellular physiology and mitochondrial proteome

The influence of X-ray radiation on human neuroblastoma (SH-SY5Y) cells, their physiology and mitochondrial proteome was studied depending on the oxygen concentration in the cell culture and differentiation status. Cells were in parallel cultivated at 21% and 5% O_2 for comparison of cellular responses to stress at high oxygen concentration used in standard cell culture incubators and at concentration of 5% which resembles physiological oxygen concentration in human brain. Retinoic acid was used for induction of differentiation to obtain cells that resemble neurons.
Specific cellular parameters such as mitochondrial membrane potential, ATP concentration and cell viability were investigated.
Complex interplay of oxygen and differentiation status modulated the cellular response to oxidative stress upon ionizing radiation as discussed in the published work:

Džinić T, Hartwig S, Lehr S, Dencher NA. (2016). Oxygen and differentiation status modulate the effect of X-ray irradiation on physiology and mitochondrial proteome of human neuroblastoma cells. *Arch. Physiol. Biochem.*, 122: 257-265.

Published data are not separately discussed in the thesis.

Archives of Physiology and Biochemistry

http://informahealthcare.com/arp
ISSN: 1381-3455 (print), 1744-4160 (electronic)

Arch Physiol Biochem, Early Online: 1–9
 DOI: 10.1080/13813455.2016.1218518

Taylor & Francis
Taylor & Francis Group

ORIGINAL ARTICLE

Oxygen and differentiation status modulate the effect of X-ray irradiation on physiology and mitochondrial proteome of human neuroblastoma cells

Tamara Džinić[1], Sonja Hartwig[2,3], Stefan Lehr[2,3], and Norbert A. Dencher[1]

[1]*Physical Biochemistry, Department of Chemistry, Technische Universität Darmstadt, Darmstadt, Germany,* [2]*Institute of Clinical Biochemistry and Pathobiochemistry, German Diabetes Center at the Heinrich-Heine-University Düsseldorf, Leibniz Center for Diabetes Research, Düsseldorf, Germany, and* [3]*German Center for Diabetes Research (DZD), München, Neuherberg, Germany*

Abstract

Cytotoxic effects, including oxidative stress, of low linear energy transfer (LET)-ionizing radiation are often underestimated and studies of their mechanisms using cell culture models are widely conducted with cells cultivated at atmospheric oxygen that does not match its physiological levels in body tissues. Also, cell differentiation status plays a role in the outcome of experiments. We compared effects of 2 Gy X-ray irradiation on the physiology and mitochondrial proteome of nondifferentiated and human neuroblastoma (SH-SY5Y) cells treated with retinoic acid cultivated at 21% and 5% O_2. Irradiation did not affect the amount of subunits of OxPhos complexes and other non-OxPhos mitochondrial proteins, except for heat shock protein 70, which was increased depending on oxygen level and differentiation status. These two factors were proven to modulate mitochondrial membrane potential and the bioenergetic status of cells. We suggest, moreover, that oxygen plays a role in the differentiation of human SH-SY5Y cells.

Keywords

Ionizing radiation, retinoic acid, human neuroblastoma cells, differentiation, mitochondria

History

Received 12 April 2016
Revised 27 June 2016
Accepted 26 July 2016
Published online 17 August 2016

Introduction

Humans get exposed to ionizing radiation occupationally or accidentally and from different sources such as natural or man-made. However, only catastrophes, such as Fukushima nuclear disaster in 2011, are reminder of its detrimental effects since the level of awareness of low LET (linear energy transfer) ionizing radiation, for example X- and γ-rays used in diagnostics and therapy, is still quite low in general population (Lee *et al*., 2004). Indirect cytotoxic effects of radiation include activation of inflammatory cytokines and oxidative stress leading to up-regulation of apoptotic protein expression and DNA damage (Saeed *et al*., 2014; Tann *et al*., 2011), which are risks of not only cancer but also cognitive deficits (Kalm *et al*., 2009) and neurodegenerative diseases (Kempf *et al*., 2013). Oxygen is an important factor that modulates sensitivity to radiation due to the oxygen effect (Riley, 1994), that is an increased sensitivity to radiation in the presence of oxygen. Furthermore, knowledge of effects of oxidative stress on cell physiology and performance has raised the importance of the usage of appropriate oxygen conditions in cell culture incubators comparable to levels ranging from 1% to 11% O_2 in human body tissues (Carreau *et al*., 2011). Although beneficial effect of oxygen levels lower than 21% on proliferation of normal human diploid cells was observed almost 40 years ago (Packer & Fuehr, 1977), cultivation of cells continued being performed at inappropriately high atmospheric oxygen level in most laboratories. However, there is strong evidence that differences in oxygen concentrations can alter the outcome of experiments (Brewer & Cotman, 1989; Tiede *et al*., 2011; Villeneuve *et al*., 2013). Considering this, it is important particularly when it comes to study of oxidative metabolism in both health and disease such as neurodegenerative diseases (e.g. Alzheimer's and Parkinson's disease) and cancer in which mitochondrial function gets impaired and subsequently affects cell maintenance and survival. Expression level of mitochondrial proteins is crucial for cell performance and health of the whole organism (Dencher *et al*., 2006; Reifschneider *et al*., 2006) since the prime function of mitochondria is generation of ATP (adenosine triphosphate) with balanced production of reactive oxygen species (ROS) as by-products. It was already observed that physiological oxygen level reduces oxidative stress and ROS level and improves mitochondrial function of cultivated cells (Tiede *et al*., 2011; Zhu *et al*., 2012). In order to establish oxygen conditions in the cell culture to resemble physiological conditions found in respective tissues of the human body, home-made low-cost incubators can be set up by the average cell culture laboratory (Wright & Shay,

Correspondence: Tamara Džinić, Physical Biochemistry, Department of Chemistry, Technische Universität Darmstadt, Alarich-Weiss-Str.4, D-64287 Darmstadt, Germany. Tel: +49 6151 16-21243. E-mail: dzinic.tamara@physbiochem.tu-darmstadt.de

2006) to avoid high costs of specialized incubators or dedicated low oxygen stations. We have established such simple system for cultivating cells with the aim to understand effects of 2 Gy X-ray irradiation, which is a standard dose per fraction used in tumor treatment (McBride & Withers, 2004), on the mitochondrial proteome and physiology of human neuroblastoma (SH-SY5Y) cells. Neuroblastoma accounts for 15% of childhood cancer fatalities (Lonergan *et al*., 2002) remaining the major therapeutic challenge in pediatric oncology (Modak & Cheung, 2010; Quaglia, 2014). Furthermore, SH-SY5Y derived from human neuroblastoma is widely used to study mechanisms of neurodegeneration, especially of Alzheimer's disease (Schlachetzki *et al*., 2013). In parallel to cultivating cells at 21% O_2, we used 5% O_2 as a physiological oxygen concentration, which is close to 4.6% O_2, the level at which normal oxygenation of the brain tissue is assured (Carreau *et al*., 2011). Since susceptibility to radiation and oxidative stress are largely determined by differentiation status of the cell (Acharya *et al*., 2010; Schneider *et al*., 2011), we compared cellular response of nondifferentiated human SH-SY5Y and cells treated with *all-trans* retinoic acid (RA), for the induction of differentiation, to X-rays at two different oxygen levels. We observed that the expression of subunits of mitochondrial oxidative phosporylation (OxPhos) protein complexes and non-OxPhos mitochondrial proteins, except for heat-shock protein 70 (CH70), was not affected by 2 Gy X-ray radiation at both oxygen levels and states of differentiation. The amount of CH70 was increased upon irradiation in both nondifferentiated and differentiated cells at both 21% and 5% O_2. Furthermore, the bioenergetic status of the cell was affected by oxygen level as the total cellular ATP level was higher in cells cultivated at 5% O_2 as compared to cells at nonphysiological 21% O_2, particularly in differentiated cells compared to respective controls but was not affected by irradiation. Cell viability was affected by irradiation and treatment with retinoic acid at both 21% and 5% O_2. Although responses to single-dose radiation studied here were acute, they were modulated by oxygen level in the cell culture and differentiation status, factors that should be considered in studies of both acute and long-term molecular and cellular responses to stress.

Methods

Cell culture

Human neuroblastoma (SH-SY5Y) cells were cultivated in DMEM (Gibco, Life Technologies, Paisley, UK) supplemented with 10% FBS (PAA Laboratories GmbH, Pasching, Austria), 2% L-glutamine and 5 U/mL penicillin/5 µg/mL streptomycin (Gibco, Life Technologies, Paisley, UK) at 37 °C, 5% CO_2, under two different oxygen conditions. In parallel to cultivating cells in a standard cell culture incubator (Heraeus Instruments, Hanau, Germany) with atmospheric air of about 21% O_2 by volume, cells were cultivated in simple home-made incubators (Wright & Shay, 2006) flushed with premixed gas consisting of 5% O_2, 5% CO_2 and 90% N_2 (Air Liquide GmbH, Krefeld, Germany) in order to obtain more physiological condition of oxygen as described previously. Briefly, premixed gas was used to flush plastic wide mouth jars, where cell culture dishes were placed, for 1 min and regassed after 1 h and each time when opened for cell handling. Sealed home-made incubators were placed in the standard cell culture incubator for temperature regulation. Cells were adapted to 5% O_2 for one week before conducting experiments and passaged according to their confluency (every 3–4 days).

Induction of differentiation and radiation exposure

Cells at both 5% and 21% O_2 were differentiated using 10 µM *all-trans* retinoic acid (Sigma-Aldrich, Taufkirchen, Germany), prepared as a 10 mM filter-sterilized stock solution in DMSO (Carl Roth GmbH, Karlsruhe, Germany) kept protected from light, added to 1×10^4 cells/mL on the passage day 0 and incubated 3 days to induce differentiation (Hellmann-Regen *et al*., 2012). Cells were monitored for 3 days in 24 h intervals for morphological changes, that is, neurite outgrowths. Media were changed after 3 days and cells were harvested or subcultured for assays using 0.05% trypsin-EDTA (Gibco, Life Technologies, Paisley, UK). One day after subculturing, cells were irradiated once using X-ray tube (x-rad 320, Pxi Precision X-rays, North Brandford, CT) with a metal ceramic anode set to 250 kV (1 keV/µm) with a current flow of 10 mA and 50 cm distance from a sample for 54 s to obtain a dose of 2 Gy. Longer wavelengths (above 0.2 nm) were excluded using 2-mm aluminum filter. Cell culture dishes were placed in the X-ray machine chamber in a horizontal position at room temperature and remained about 10 min at atmospheric condition of gases for the purpose of irradiation exposure before placing them back to the incubator with appropriate oxygen level as described previously. Cells were incubated for the next 18 h post irradiation before conducting experiments.

Cell lysis for immunoblotting against differentiation markers

For the analysis of the expression of total cellular proteins, cells were harvested using 0.05% trypsin-EDTA (Gibco, Life Technologies, Paisley, UK), counted microscopically using Neubauer chamber (Marienfeld, Lauda-Königshofen, Germany) and Trypan blue (Gibco, Life Technologies, Paisley, UK) exclusion of the dead cells and washed with 1X DPBS (Gibco, Life Technologies, Paisley, UK) at 700 × g, 4 °C for 5 min. In order to extract total cellular proteins, cell pellet was lysed thoroughly using RIPA buffer (50 mM Tris-HCl (pH 7.4), 1% (v/v) IGEPAL®-CA630 detergent, 0.5% Na-deoxycholat, 0.1% SDS, 150 mM NaCl, 2 mM EDTA, 50 mM NaF) using 24 µL RIPA-buffer per 2×10^5 cells. Samples were incubated on ice for 30 min and vortexed every 10 min followed by centrifugation at 14 000 × g, 4 °C, 15 min. Supernatants containing proteins were used immediately or stored at −20 °C. Protein concentrations were determined by Bradford assay using Roti®-Nanoquant (Carl Roth GmbH, Karlsruhe, Germany). About 30 µg of protein per lane was loaded for samples in duplicates onto polyacrylamide SDS gel (4% stacking, 8% separation) and used for immunoblotting.

Isolation of mitochondria and solubilization of mitochondrial proteins

Equal number of cells cultivated at both 5% and 21% O_2 were washed with PBS and harvested for isolation of crude mitochondrial fraction. Cells were homogenized (10 mM

HEPES/NaOH, pH 7.4, 1.1 mM EDTA, with the addition of 0.5% protease inhibitor cocktail (Sigma-Aldrich, Life Science, St. Louis, MO) on ice using a motor driven pistill homogenizer (IKA-Werke GmbH, Staufen, Germany) applying 15 strokes at 800 rmp. Homogenized suspension with sucrose added to a final concentration 0.25 M was centrifuged (1900×*g*, 10 min, 4 °C). Supernatants were collected by washing pellets twice in homogenization buffer with sucrose and finally centrifuged at 14 000×*g*, 10 min, 4 °C. Pellets were resuspended in homogenization buffer with sucrose and stored at −80 °C. Protein concentrations were determined using Bradford assay and aliquots were shock-frozen in liquid nitrogen and stored at −80 °C. About 120 µg of protein from ''crude'' isolated mitochondria per sample were solubilized with the mild nonionic detergent digitonin (3 g/g protein) (Applichem GmbH, Darmstadt, Germany) at a final concentration of 1% (w/v) in solubilization buffer (33.33 mM HEPES/KOH pH 7.4, 166.67 mM potassium acetate, 11.11% glycerol) 30 min on ice by vortexing samples every 10 min. Samples were centrifuged at 20 000×*g*, 4 °C, 10 min and supernatants were used immediately for further experiments.

Blue native (BN) and 2D-BN/SDS-PAGE

Solubilized proteins from isolations of mitochondria were separated in the native and active state on a gradient (4–13%) BN-gel in the first dimension (Neff & Dencher, 1999). Lanes of the BN-gel were cut and proteins in the gel were denatured with 1% β-mercaptoethanol/1% SDS two times for 30 min each and then washed with Milli-Q water three times for 5 min each. Denatured proteins from BN-gel stripes were separated on the 13% SDS gel with 5% stacking gel in the second dimension overnight applying 70 V and 40 mA, following fixation in a solution containing 10% methanol/7% acetic acid for 1 h. Proteins on 2D gels were stained using the fluorescent SYPRO® Ruby protein stain (Life Technologies, Carlsbad, CT) for 3 h and then washed in the fixation solution 10 min following washing with Milli-Q for 5 min. Gel images were taken by the CCD camera system of Fujibox using LAS-3000 software (Fujifilm Holdings K.K., Tokyo, Japan). Quantification of protein spots of interest was conducted using Delta2D (DECODON GmbH, Greifswald, Germany) software by determining their gray values (volumes) normalized to the gray value of all spots present on the gel. Following SYPRO Ruby staining, proteins were silver-stained (Blum *et al.*, 1987) for visualization purposes only and gel images were taken using View Pix 900 scanner with Epson Scan (biostep® GmbH, Jahnsdorf, Germany) software.

Protein identification with (LC)-MALDI-TOF/TOF analysis

Protein bands were cut out of the BN-gel and gel pieces were washed three times alternating with 25 mM ammonium bicarbonate (NH_4HCO_3) and 25 mM ammonium bicarbonate within 50% acetonitril (ACN). Neat ACN was added and removed to dehydrate the gel pieces. A solution of 65 mM DTT (10 mg/mL) in 25 mM ammonium bicarbonate was added and incubated 15 min at 50 °C and 300 rpm (Thermomixer, Eppendorf, Hamburg, Germany). The reduction solution was removed and neat ACN was added and removed after 10 min to dehydrate the gel piece again. For alkylation, a solution of 216 mM iodacetamid in 25 mM ammonium bicarbonate was added followed by an incubation of 10 min at RT in the dark. Afterwards, gel pieces were washed again twice alternating with 25 ammonium bicarbonate and 25 mM ammonium bicarbonate/50% ACN and gel pieces were dehydrated again with neat acetonitrile. For protein digestion, the dry gel pieces were rehydrated in 50 µL ice-cold solution of trypsin (5 ng/µL in 25 mM NH_4HCO_3 and 2% ACN resulting in 250 ng/band, trypsin-sequencing grade, Promega). Proteins were digested at 37 °C overnight. Peptides were extracted for 1 h with 50 µL of 1% trifluoroacetic acid (TFA). For protein identification from 1D-gel bands with off-line LC-MALDI-MS, peptides from tryptic digest were separated using an Ultimate 3000 (Dionex/Thermo Scientific, Germering, Germany) nanoflow HPLC system. Peptides were concentrated on a trap column, Acclaim® PepMap 100 (C18, 3 µm particle size, 100 Å pore size, 7.5 µm inner diameter, 20 mm length (Thermo Scientific, Sunnyvale, CA), flow rate 6 µL/min) followed by separation on a Acclaim PepMap 100 column (C18, 3 µm, 100 Å, 75 µm × 150 mm (Thermo Scientific, Sunnyvale, CA)) using a linear gradient 4–50% eluent (80% ACN containing 0.1% TFA) over 48 min. The flow rate was maintained at 300 nL/min. About 192 HPLC-fractions were spotted onto an AnchorChip™ MALDI target (Bruker Daltonics, Bremen, Germany) using a Proteineer-FC II (Bruker Daltonics, Bremen, Germany) spotter. For MALDI sample preparation, HPLC fractions (75 nL) were automatically mixed with matrix solution (420 nL; (348 µL 95:5 (v/v) acetonitrile: 0.1% TFA, 36 µL of saturated solution of HCCA in 90:10 (v/v) acetonitrile: 0.1% TFA, 8 µL of 10% TFA and 8 µL of 100 mM ammonium phosphate monobasic)). The instruments were controlled using HyStar 3.2 software (Bruker Daltonics, Bremen, Germany). Subsequently, samples were analyzed in a time-of-flight Ultraflex-TOF/TOF mass spectrometer (Bruker Daltonics, Bremen, Germany). Acquired mass spectra were automatically calibrated and annotated using LC-Warp/Compass 1.3 software (Bruker Daltonics, Bremen, Germany) and XML-formatted peak lists were transferred to Proteinscape 3.1 (Bruker Daltonics, Bremen, Germany). Because all experiments were performed on human SH-SY5Y cells MS spectra from each individual LC-MALDI run were used to search a human subset of Swiss-Prot (SwissProt 2015_08, Homo sapiens (human), 20204 sequences) nonredundant database using Mascot search engine (Version 2.5.1, Matrix Science Ltd, London, UK) in consideration of the following settings: enzyme ''trypsin,'' species ''human,'' fixed modifications ''carbamidomethyl,'' optional modifications ''Methionine oxidation'' and missed cleavages ''1.'' Mass tolerance was set to 100 ppm for peptide and 0.9 Da for fragment spectra. Using these settings, a combined Mascot score of greater than 80 was set to accept proteins (significance threshold $p < 0.05$). Calculated pI and molecular mass data were obtained by Mascot and only proteins were reported where we identified at least two significant peptides.

Immunoblotting

In order to confirm the identity of protein spots on 2D-BN/SDS gels in addition to LC-MALDI-TOF/TOF analysis,

following primary antibodies were used for immunoblotting of mitochondrial proteins on the nitrocellulose membrane: NDUFS1 rabbit polyclonal (dilution 1:1000) (Proteintech Group, Inc, Chicago, IL); ATPA mouse monoclonal (1:1000) (Molecular Probes, Eugene, OR); UQCRC2 mouse monoclonal (1:1000), MTCO1 mouse monoclonal (1:2000), CH60 rabbit polyclonal (1:20000), CH70 mouse monoclonal (1:100) (Abcam plc, Cambridge, UK); ACO2 rabbit polyclonal (1:1000), VDAC1 goat polyclonal (1:500), SDHA mouse monoclonal (1:1000) (Santa Cruz Biotechnology, Inc, Dallas, TX). Primary antibodies used for the detection of cytoplasmic proteins from cell lysates: neurofilament-M mouse monoclonal antibody (1:1000) (Cell Signaling Technology, Inc., Danvers, MA) and actin goat polyclonal antibody (1:1000) (Santa Cruz Biotechnology, Inc, Dallas, TX). Secondary antibodies used are: donkey anti-mouse IgG-HRP, donkey anti-goat IgG-HRP, donkey anti-rabbit IgG-HRP (1:2000) (Santa Cruz Biotechnology, Inc, Dallas, TX).

Mitochondrial membrane potential measurement

Cells were seeded to 35-mm dishes at a density of 1×10^5 cells/mL. The next day, cells were irradiated with 2 Gy X-rays and incubated 18 h under different oxygen conditions. On the day of the assay, 1 μM MitoTracker® Red CM-H_2Xros (λ_{EX}/λ_{EM} = 579/599 nm) (Molecular Probes, Invitrogen, Eugene, OR) was added to cells and incubated at 37 °C for 10 min. Cells are then harvested and washed in PBS at 700×*g*, RT, 5 min and cell pellet was resuspended in 300 μL PBS and fluorescence was measured by flow cytometer (S3 Cell Sorter, Bio-Rad Laboratories, Inc., Hercules, CA). About 10 000 cells per sample were analyzed using 488 and 561 nm lasers for the excitation of the dye in fluorescence channel FL3. Treatment with proton gradient uncoupler CCCP (carbonyl cyanide m-chlorophenyl hydrazone) for 5 min served as a positive control for the reduction of mitochondrial membrane potential. Data were analyzed by Kaluza software (Beckman Coulter, Inc., Indianopolis, IN) as FL3-area log against the signal count for detection of the fluorescence signal shift compared to control samples.

ATP assay

Luminiscent ATP detection assay kit (ab113849; Abcam plc, Cambridge, UK) was used to assess ATP levels depending on irradiation, differentiation status and oxygen level in the cell culture. Cells were harvested and 82.5×10^3 cells per well of a 96-well plate was used immediately for the cell lysis and assay according to manufacturer protocol. Luminiscence was determined by M1000 Infinite plate reader (Tecan Group, Ltd., Männedorf, Switzerland). ATP levels were normalized to cell count and compared to corresponding controls.

Cell viability assay

Neutral red uptake assay was used for the analysis of cell viability or lysosomal integrity according to the modified protocol by Repetto *et al.* (2008). Briefly, 9×10^4 cells/mL was seeded into a 96-well plate. Cells were washed with PBS and incubated with 40 μg/mL neutral red (Sigma-Aldrich, St. Louis, MO) in DMEM with 10% FBS for 2 h at 37 °C in the cell culture incubator with appropriate oxygen conditions, that is, 5% and 21% O_2. Cells were washed and neutral red destain solution (50% ethanol + 50% mL Milli-Q water + 1% glacial acetic acid) was added and incubated for 15 min in order to extract neutral red dye taken up by cells with healthy lysosomes. Absorbance of neutral red extract was measured at 540 nm using M1000 Infinite plate reader (Tecan Group, Ltd., Männedorf, Switzerland).

Statistical analysis

Statistical analyses of protein expression profiles and ATP level measured in three independent experiments were performed using two-way analysis of variance (ANOVA) with Tukey's or Dunnet's multiple comparisons test and unpaired *t*-test for cell viability assay in Prism (GraphPad Software, Inc., La Jolla, CA).

Results

Differentiation of human SH-SY5Y cells

We compared effects of 2 Gy X-ray irradiation on human neuroblastoma (SH-SY5Y) cells cultivated at 21% and 5% O_2, respectively, and cells treated with 10 μM retinoic acid (RA). After three-day treatment with retinoic acid, cells at both oxygen levels showed pronounced morphological changes, that is, outgrowth of long protrusions (neurites) characteristic for cells with induced differentiation, compared to corresponding control cells with fine short processes and compact morphology (Figure 1A). Expression of neurofilament-M (NFM) was not significantly affected by RA. Only a slight increase in its amount was observed in RA-treated cells at 21% O_2. The expression of NFM at 5% O_2 was similar in nondifferentiated cells and after treatment with RA and was increased in comparison to cells at 21% O_2 as revealed by Western blot (Figure 1B).

Expression of mitochondrial proteins upon 2 Gy X-ray irradiation

Expression levels of mitochondrial proteins upon 2 Gy X-ray irradiation were investigated in both nondifferentiated and in human SH-SY5Y cells with RA-induced differentiation which are in parallel cultivated at 21% and 5% O_2. Identity of proteins of interest (NDUFS1, SDHA, UQCRC2, MTCO1, ATPA, ACO2, VDAC1, CH60, CH70) upon separation by 2D-BN/SDS–PAGE on SYPRO Ruby-stained gels (Figure 2) was confirmed by Western blot (Figure S2) and their expression levels were evaluated by the analysis of SYPRO Ruby-stained gel images only using Delta 2D (DECODON GmbH, Greifswald, Germany) software by determining gray values (volumes) of each selected spot normalized to the gray value of all spots present on the gel. Identity of 97 different proteins and protein subunits in selected bands of BN-gel was revealed by nLC-MALDI-TOF/TOF (Table S1), which confirmed identifications of protein subunits of OxPhos complexes (NDFUS1, QCRC2, ATPA) and other non-OxPhos proteins (CH60, VDAC1) by Western blot for proteins present in higher molecular weight bands of BN-gel (shaded in Table S1). Amounts of five subunits (NDUFS1, SDHA, UQCRC2, MTCO1, ATPA) of OxPhos complexes (I-V) (Figure 3A) and

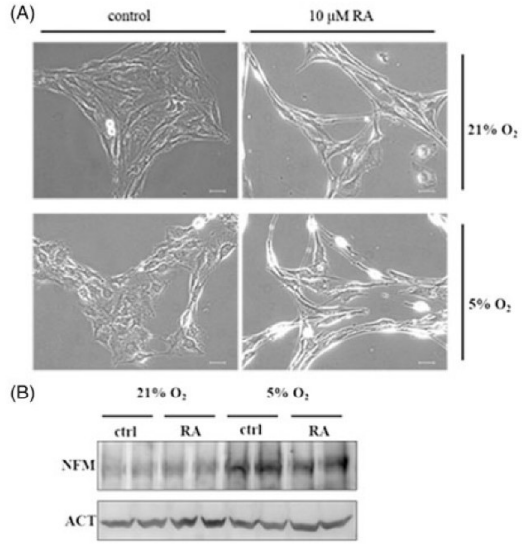

Figure 1. (A) Phase contrast micrographs of nondifferentiated human neuroblastoma (SH-SY5Y) (control) and cells treated with 10 µM retinoic acid (RA) for 3 days for the induction of differentiation at 21% and 5% O_2, respectively. Cells with induced differentiation presented long protrusions (neurites) in comparison to controls at corresponding oxygen levels. 200× magnification. 50 µm scale bar. (B) Western blot detection of neurofilament-M (NFM) in SH-SY5Y cells. Increased expression of NFM was observed in SH-SY5Y cells treated with 10 µM RA for 3 days when cultivated at 5% O_2 in comparison to cells at 21% O_2 which showed only minor increase in NFM expression after treatment with RA. Actin (ACT) was used as loading controls for immunoblotting of cell lysates (30 µg protein per lane) of samples in duplicates separated by SDS-PAGE (4% stacking gel, 7% separation gel).

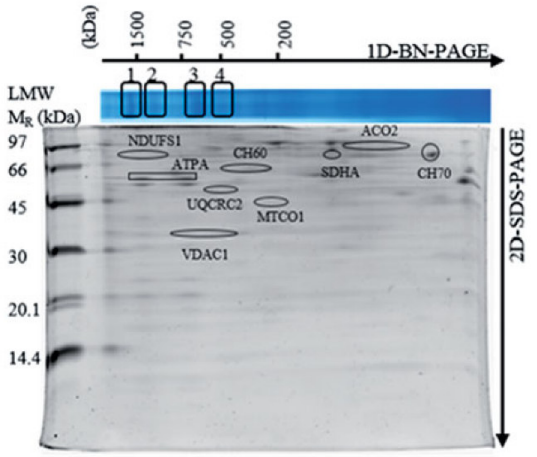

Figure 2. Mitochondrial proteome analysis of human SH-SY5Y depending on oxygen level in the cell culture, differentiation status and irradiation. About 120 µg of protein from ''crude'' isolated mitochondria was solubilized with the mild nonionic detergent digitonin (3 g/1 g protein) and separated in the native and assembled state on blue native (BN)-gel in the first dimension and then on SDS gel in the second dimension following SYPRO Ruby staining of protein spots for the evaluation of protein expression (Figure 3) and subsequent silver staining for protein visualization only (Figure S1). For the identification of proteins in bands, control sample at 5% O_2 was used and selected bands (1, 2, 3 and 4) were cut from BN-gel and separated by nLC following MALDI-TOF/TOF (Table S1). Denatured proteins of interest (encircled) separated on the 2D SDS-PAGE identified/confirmed by Western blotting (Figure S2) were used for the evaluation of protein expression in mitochondria depending on 2 Gy X-ray irradiation, treatment with 10 µM retinoic acid and oxygen level in the cell culture (21% O_2 and 5% O_2, respectively). LMW (low molecular weight) standard was used for mass calibration. [NDUFS1: NADH dehydrogenase (ubiquinone) Fe-S protein 1 (complex I), SDHA: succinate dehydrogenase complex flavoprotein subunit A (complex II), UQCRC2: ubiquinol-cytochrome-c reductase complex core protein 2 (complex III), MTCO1: mitochondrially encoded cytochrome c oxidase I (complex IV), ATPA: ATP synthase subunit alpha (complex V), ACO2: aconitase 2, CH60: 60 kDa heat-shock protein, CH70: heat shock protein 75 kDa, VDAC1: voltage-dependent anion-selective channel protein 1].

of three non-OxPhos mitochondrial proteins (ACO2, CH60 and VDAC1) (Figure 3B) were not affected by the irradiation of cells, regardless of their differentiation status and oxygen level of the cell culture. On the other hand, amount of heat-shock protein CH70 was significantly increased (Figure 3B) in irradiated cells treated with 10 µM retinoic acid at 21% and 5% O_2, respectively, as well as in nondifferentiated cells at 5% O_2 18 h after 2 Gy X-ray irradiation.

Changes of mitochondrial membrane potential and total ATP amount

The mitochondrial membrane potential increased after 2 Gy X-ray irradiation of RA-treated human SH-SY5Y cells cultivated at both oxygen levels (21% and 5% O_2) as compared to respective controls (Figure 4). A shift in the fluorescence signal of cells incubated with MitoTracker® Red was particularly pronounced in RA-treated cells at physiological oxygen (5%) 18 h post irradiation (Figure 4B). Total cellular ATP level was significantly higher under all conditions in cells at 5% O_2 in comparison to cells at 21% O_2 (up to 1.5- to 2-fold increase) (Figure 5). Irradiation did not affect ATP level of cells at 21% O_2 and only a slight increase was observed after RA treatment in nonirradiated cells.

Changes of cell viability

Irradiation of human SH-SY5Y cells with 2 Gy X-rays resulted in significantly decreased cell viability (lysosomal integrity) for both nondifferentiated and RA-treated cells at 21% O_2 compared to corresponding control cells (Figure 6A) as measured using neutral red dye which is taken up and stored in lysosomes of healthy cells. Cells cultivated at 5% O_2 showed significantly decreased viability after irradiation and particularly after treatment with RA alone or in combination with irradiation in comparison to control cells (Figure 6B).

Discussion

We have performed a quantitative study of changes in the mitochondrial proteome and of mitochondrial parameters caused by ionizing radiation depending on the oxygen level in the cell culture and on the differentiation status of human neuroblastoma (SH-SY5Y) cells. Surprisingly, the protein pattern and the amount of selected OxPhos and non-OxPhos mitochondrial proteins were statistically unchanged after irradiation, except for the heat shock protein CH70 which was upregulated (Figure 3). Furthermore, changes in the bioenergetic status (mitochondrial membrane potential and ATP concentration) and cell viability upon irradiation were

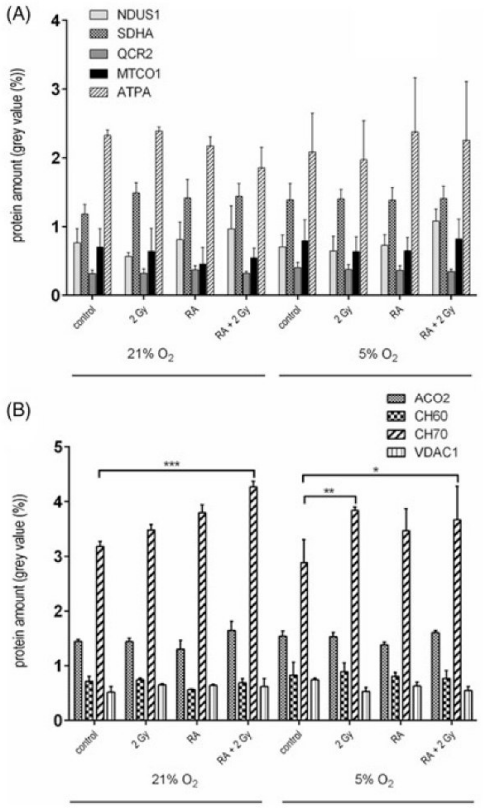

Figure 3. Dependence of expression levels of mitochondrial proteins on oxygen concentration, X-ray irradiation and differentiation analyzed using SYPRO Ruby-stained gel images using Delta2D software. Nonaffected protein amounts of five studied subunits (NDUS1, SDHA, QCR2, MTCO1 and ATPA) of oxidative phosphorylation complexes (A) and three non-OxPhos mitochondrial proteins (ACO2, CH60 and VDAC1) (B) were observed after 2 Gy X-ray irradiation regardless of differentiation status of SH-SY5Y cells and oxygen concentration in the cell culture. Increase in the amount of heat-shock protein CH70 was detected in irradiated cells treated with 10 μM retinoic acid at 21% and 5% O_2, respectively, and in nondifferentiated cells at 5% O_2 after irradiation. Quantifications are presented as mean ± SEM of $N = 3$ independent experiments of $n = 2$ samples per group, $*p < 0.5$, $**p < 0.01$, $***p < 0.001$, analyzed by two-way ANOVA with Tukey's test.

modulated by oxygen level as well as by RA used for the induction of differentiation. Indirect and long-term damaging effects of low LET ionizing radiation such as 2 Gy X-rays applied as a standard dose per single treatment in fractionated treatment of many tumors (McBride & Withers, 2004) and used in our studies, are often underestimated. However, oxidative stress caused by ionizing radiation is a potential trigger for the development of a variety of diseases including cancer, cognitive deficits and neurodegenerative diseases (Kalm *et al*., 2009; Kempf *et al*., 2013). Neuroblastoma still represents a therapeutic challenge (Quaglia, 2014) due to its high recurrence and lethality rates (Modak & Cheung, 2010). Furthermore, SH-SY5Y cell line derived from human neuroblastoma, model in cytotoxicity research and studies of neurodegenerative diseases, is often used in nondifferentiated state and cultivated mostly at atmospheric oxygen level, which is far above physiological conditions in the human brain, and in most of other tissues, and can result in misleading outcomes of experiments. Cultivation of cells at 5% O_2 provides a significant improvement over 21%, but it is at the upper range of partial pressure in tissues (Wright & Shay, 2006). Also, cells in our study were handled under discontinued conditions of oxygen, that is, exposing cells to atmospheric oxygen for the purpose of subculturing, treatment or irradiation for a short period (5–10 min). Nevertheless, there is an increase in data supporting cultivation of cells using physiological tissue oxygen concentrations, that is, much lower than that present in the atmospheric air. This is very important in revealing mechanisms of oxidative stress in health and disease where mitochondria are implicated as organelles at the crossroad of many cellular pathways, including those involved in ageing (Dencher *et al*., 2006). Tiede *et al*. (2011) reported that cultivating primary neurons at physiological oxygen level found in the human brain (5% O_2) resulted in higher mitochondrial membrane potential, lower rates of ROS production, greater cytoplasmic fractions of mitochondria and larger mitochondrial networks than in cells at atmospheric oxygen. Observation of the higher bioenergetic status of cells at 5% O_2 in our studies (i.e. increase in mitochondrial membrane potential (Figure 4) and ATP concentration (Figure 5) are consistent with these findings. Furthermore, according to our and previous data of others, it is probable that oxygen level plays an important role in the decision of the differentiation status of the cell, which is dependent on the specific cell type and context (Cheng *et al*., 2014; Redshaw & Loughna, 2012). For example, low oxygen (5%) in combination with a chemical cocktail induced generation of neural progenitor cells (NPCs) from mouse embryonic fibroblasts (Cheng *et al*., 2014). Oxygen regulated conversion of somatic cells to NPCs opens the possibility for treatment of neural diseases. In the present study, we observed oxygen level affected expression of neurofilament-M (NFM), a structural constituent of the cytoskeleton, which is used as a marker of differentiation. Interestingly, its expression at 5% O_2 was more pronounced than at 21% O_2 (Figure 1B). On the other hand, the expression of NFM was nonresponsive to retinoic acid-induced differentiation (Figure 1B) as also reported previously for P19 embryonal carcinoma cells (Chiu *et al*., 1995). Retinoic acid is used alone or in combination for the treatment of a variety of tumors including neuroblastoma (Matthay *et al*., 1999) and it is known to regulate expression of numerous genes (Balmer & Blomhoff, 2002) as a signaling molecule during development. We observed increase in mitochondrial membrane potential of RA-treated cells at both oxygen levels upon irradiation (Figure 4), which was in accordance with the increased ATP level at 5% O_2 (1.5- to 2-fold increase), whereas the level of ATP of RA-treated cells was only slightly increased at 21% O_2 and was not affected by irradiation (Figure 5). Previous findings revealed that RA increases the oxygen consumption and enhances the respiratory capacity of mitochondria in SH-SY5Y cells without affecting the composition of the electron transport chain or number of mitochondria (Xun *et al*., 2012). Our data also showed nonaffected amounts of mitochondrial OxPhos complexes subunits and other mitochondrial proteins such as VDAC1 (Figure 3) which is a marker for the amount of mitochondria in the cell (Yamamoto *et al*., 2006). Changes in the total ATP

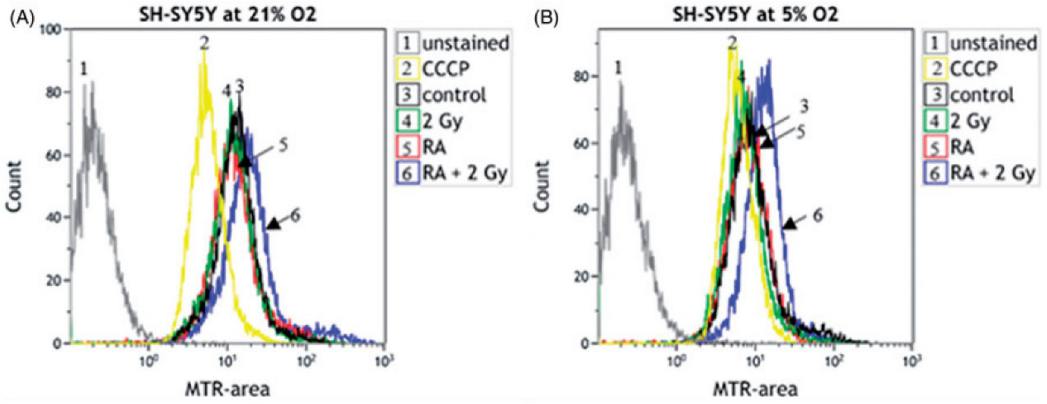

Figure 4. Increase in mitochondrial membrane potential after irradiation (2 Gy) of retinoic acid (RA)-treated SH-SY5Y at 21% (A) and at 5% O_2 (B) 18 h post irradiation, measured using MitoTracker® Red CM-H2Xros ($\lambda_{EX}/\lambda_{EM} = 579/599$ nm), observed as a shift in the fluorescence signal (peak) to the right on overlayed plots compared to corresponding control samples. Incubation with 100 µM CCCP (carbonyl cyanide m-chlorophenyl hydrazone) for 5 min was used as a positive control for the reduction in the mitochondrial membrane potential.

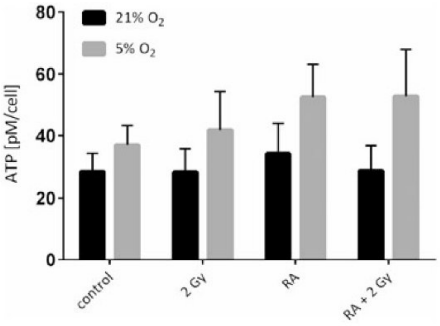

Figure 5. Total cellular ATP levels of human SH-SY5Y cells cultivated at 5% and 21% O_2, respectively, upon induction of differentiation with 10 µM retinoic acid and/or irradiation with 2 Gy X-rays, normalized to cell count for $N = 3$ independent measurements of samples from at least $n = 2$ independent biological replicates compared to corresponding controls. ATP level was significantly ($p < 0.05$) higher in cells cultivated at 5% O_2 in comparison to 21% O_2. Increase of ATP level was observed in both nonirradiated and irradiated RA-treated cells at 5% O_2. Quantifications are presented as mean ± SEM analyzed by two-way ANOVA with Dunnett's test.

level (Figure 5) reflect changes in ATP generated by the OxPhos machinery and cellular ATP consumption. For example, increased demand for ATP after external stress such as irradiation may lead to such changes since ATP is required for repair processes in the cell. Increased amount of heat shock protein CH70 upon irradiation in both nondifferentiated and differentiated cells at both 21% and 5% O_2 (Figure 3B) could be due to the oxidative stress (Hall & Martinus, 2013). CH70 is known to facilitate proteolytic degradation of damaged proteins and folding of newly synthesized proteins, mechanisms that rely on the ATP-regulated association of CH70 with substrate polypeptides (Flynn *et al.*, 1991; Hartl, 1996). It is also possible that heat shock proteins possess differentiation controls, at least induction, independent of RA (Balmer & Blomhoff, 2002), but further studies are required. Responses to single-dose irradiation studied by us were acute and short term. However, we observed decreased lysosomal integrity, particularly after

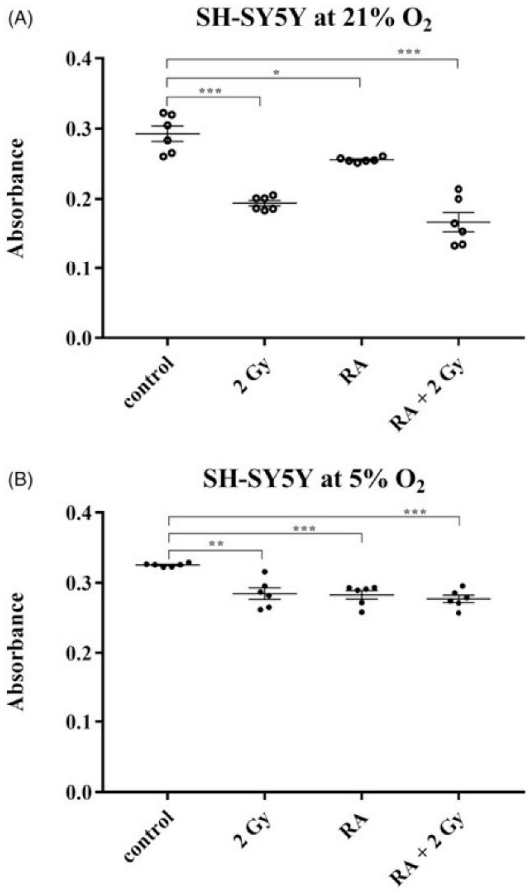

Figure 6. Neutral red uptake assay for the analysis of cell viability upon irradiation of human SH-SY5Y cells with 2 Gy X-rays and induction of differentiation with 10 µM retinoic acid. Cell viability was significantly decreased after RA-treatment alone and particularly 18 h after irradiation of both nondifferentiated and RA-treated cells cultivated at 21% (A) and at 5% O_2 (B). Quantifications are presented as mean ± SEM of $N = 3$ independent experiments of $n = 2$ samples per group, $^*p < 0.5$, $^{**}p < 0.01$, $^{***}p < 0.001$, analyzed by unpaired *t*-test with Welch's correction.

irradiation, which is a sensitive indicator of cell viability. Cells cultivated at 5% O_2 were in general less affected by irradiation and/or induction of differentiation than cells at 21% O_2. Condition of 5% O_2, which is considered more physiological, provides an environment where more ATP (Figure 5) and less damaging ROS is generated than at 21% O_2. Furthermore, induction of differentiation had only a minor effect on cell viability at 21% O_2, whereas irradiation significantly decreased cell viability. Treatment of cells with nontoxic concentration of RA for 3 days resulted in only induction of differentiation, that is, cells were not terminally differentiated and they retained their ability to proliferate and as such are still susceptible to damaging effects of radiation to a greater extent than terminally differentiated cells. At 5% O_2, irradiation and/or induction of differentiation with RA led to a significant decrease of cell viability in comparison to the respective control. Additionally, oxygen may play a role in differentiation status as we demonstrated that cells at 5% O_2 showed increased expression of NFM in comparison to cells at 21% O_2. The difference in the bioenergetic status and metabolism of cells cultivated at two different oxygen levels (different starting levels of oxidative stress) determines their response to stress (or any other treatment) and their fate. For example, time-dependent regulation of heat-shock response proteins and apoptotic response machinery may determine the relationship between the level of induced apoptosis and radiosensitivity in human neuroblastoma cells (Aravindan *et al.*, 2008) and further investigation of apoptotic markers is needed. Nevertheless, we demonstrated that these responses were modulated by oxygen level in the cell culture and differentiation status, factors important to be considered in future investigation of oxidative stress mechanism modulated by, for example, ionizing radiation.

Conclusions

Oxidative stress caused by ionizing radiation may alter protein amounts and mitochondrial functioning. These changes are modulated by the oxygen level and differentiation status of cells, two very important factors that should be taken into account in studies of mechanisms of oxidative stress in the cell culture. In order to translate knowledge gained in fundamental research on neurons, using physiological oxygen level present in the brain and choosing appropriate cell culture model, or adapting it according to the aim of the study, are crucial. We showed that this is relevant for human neuroblastoma cells that can be differentiated into neuron-like cells and used as a model for investigation of cytotoxic effects of, for example, radiation or chemicals providing more insight into mechanisms of diseases and developing potential therapeutics.

Acknowledgements

This work was supported by the DFG in the framework of GRK 1657 (Molecular and cellular responses to ionizing radiation). The authors thank Dr. Katarzyna Kuter (Polish Academy of Sciences, Krakow and Technische Universität Darmstadt) for fruitful discussions, Dr. Julian Hellmann-Regen for valuable suggestion for differentiation of human SH-SY5Y cells, Christine Schröpfer (Technische Universität Darmstadt), Waltraud Passlack and Ulrike Nitzgen (German Diabetes Center, Düsseldorf) for the excellent technical assistance. This article is part of the doctoral thesis of Tamara Džinić at the Technische Universität Darmstadt.

Declaration of interest

The authors declare no conflicts of interest. The authors alone are responsible for the content and writing of this article.

References

Acharya MM, Lan ML, Kan VH, *et al.* (2010). Consequences of ionizing radiation-induced damage in human neural stem cells. *Free Radic Biol Med*, 49:1846–55.

Aravindan N, Madhusoodhanan R, Natarajan M, Herman TS. (2008). Alteration of apoptotic signaling molecules as a function of time after radiation in human neuroblastoma cells. *Mol Cell Biochem*, 310: 167–9.

Balmer JE, Blomhoff R. (2002). Gene expression regulation by retinoic acid. *J Lipid Res*, 43:1773–808.

Blum H, Beier H, Gross HJ. (1987). Improved silver staining of plant proteins, RNA and DNA in polyacrylamide gels. *Electrophoresis*, 8: 93–9.

Brewer GJ, Cotman CW. (1989). Survival and growth of hippocampal neurons in defined medium at low density: Advantages of a sandwich culture technique or low oxygen. *Brain Res*, 494:65–74.

Carreau A, El Hafny-Rahbi B, Matejuk A, *et al.* (2011). Why is the partial oxygen pressure of human tissues a crucial parameter? Small molecules and hypoxia. *J Cell Mol Med*, 15:1239–53.

Cheng L, Yang W, Hu W, *et al.* (2014). Generation of neural progenitor cells by chemical cocktails and hypoxia. *Cell Res*, 24:665–79.

Chiu F-C, Feng L, Chan S-O, *et al.* (1995). Expression of neurofilament proteins during retinoic acid-induced differentiation of P19 embryonal carcinoma cells. *Mol Brain Res*, 30:77–86.

Dencher NA, Goto S, Reifschneider NH, *et al.* (2006). Unraveling age-dependent variation of the mitochondrial proteome. *Ann N Y Acad Sci*, 1067:106–15.

Flynn GC, Chappell TG, Rothman JE. (1991). Peptide binding and release by proteins implicated as catalysts of protein assembly. *Science*, 245:385–90.

Hall RD, Martinus L. (2013). Hyperglycaemia and oxidative stress upregulate HSP60; HSP70 expression in HeLa cells. *SpringerPlus*, 2:431. doi:10.1186/2193-1801-2-431.

Hartl FU. (1996). Molecular chaperones in cellular protein folding. *Nature*, 381:571–80.

Hellmann-Regen J, Gertz K, Uhlemann R, *et al.* (2012). Retinoic acid as target for local pharmacokinetic interaction with modafinil in neural cells. *Euro Arch Psychiatry Clin Neurosci*, 262:697–704.

Kalm M, Lannering B, Björk-Eriksson T, Blomgren K. (2009). Irradiation-induced loss of microglia in the young brain. *J Neuroimmunol*, 206:70–5.

Kempf SJ, Atkinson MJ, Azimzadeh O, Tapio S. (2013). Long-term effects of ionising radiation on the brain: Cause for concern? *Radiat Environ Biophys*, 52:5–16.

Lee CI, Haims AH, Monico EP, *et al.* (2004). Diagnostic CT scans: assessment of patient, physician, and radiologist awareness of radiation dose and possible risks. *Radiology*, 231:393–8.

Lonergan GJ, Schwab CM, Suarez ES, Carlson CL. (2002). Neuroblastoma, ganglioneuroblastoma, and ganglioneuroma: radiologic-pathologic correlation. *Radio Graphics*, 22:911–34.

Matthay KK, Villablanca JG, Seeger RC, *et al.* (1994). Treatment of high-risk neuroblastoma with intensive chemotherapy, radiotherapy, autologous bone marrow transplantation, and 13-cis-retinoic acid. *N Engl J Med*, 341:1165–73.

McBride WH, Withers HR. (2004). Biologic basis of radiation therapy. In: Perez CA, Brady LW, Halperin EC, Schmidt-Ullrich RK, eds. Principles and practice of radiation oncology. Philadelphia: Lippincott Williams Wilkins, 96–136.

Modak S, Cheung N-KV. (2010). Neuroblastoma: therapeutic strategies for a clinical enigma. *Cancer Treat Rev*, 36:307–17.

Neff D, Dencher NA. (1999). Purification of multisubunit membrane protein complexes: Isolation of chloroplast FoF1-ATP-synthase, CFo

and CF1 by blue native electrophoresis. *Biochem Biophys Res Commun*, 259:569–75.
Packer L, Fuehr K. (1977). Low oxygen concentration extends the lifespan of cultured human diploid cells. *Nature*, 267:423–5.
Quaglia MP. (2014). State of the art in oncology: high risk neuroblastoma, alveolar rhabdomyosarcoma, desmoplastic small round cell tumor, and POST-TEXT 3 and 4 hepatoblastoma. *J Pediatr Surg*, 49: 233–40.
Riley PA. (1994). Free radicals in biology: oxidative stress and the effects of ionizing radiation. *Int J Radiat Biol*, 65:27–33.
Redshaw Z, Loughna PT. (2012). Oxygen concentration modulates the differentiation of muscle stem cells toward myogenic and adipogenic fates. *Differentiation*, 84:193–202.
Reifschneider NH, Goto S, Nakamoto H, *et al.* (2006). Defining the mitochondrial proteomes from five rat organs in a physiologically significant context using 2D blue-native/SDS-PAGE. *J Proteome Res*, 5:1117–32.
Repetto G, del Peso A, Zurita JL. (2008). Neutral red uptake assay for the estimation of cell viability/cytotoxicity. *Nat Protoc*, 3:1125–31.
Saeed Y, Wang H, Hong M, *et al.* (2014). Indirect effects of radiation induce apoptosis and neuroinflammation in neuronal SH-SY5Y cells. *Neurochem Res*, 39:2334–42.
Schlachetzki JCM, Saliba SW, Pinheiro de Oliveira AC. (2013). Studying neurodegenerative diseases in culture models. *Rev Bras Psiquiatr*, 35:92–100.
Schneider L, Giordano S, Zelickson BR, *et al.* (2011). Differentiation of SH-SY5Y cells to a neuronal phenotype changes cellular bioenergetics and the response to oxidative stress. *Free Radic Biol Med*, 51:2007–17.
Tann AW, Boldogh I, Meiss G, *et al.* (2011). Apoptosis induced by persistent single-strand breaks in mitochondrial genome, Critical role of exog (5-exo/endonuclease) in their repair. *J Biol Chem*, 286: 31975–83.
Tiede LM, Cook EA, Morsey B, Fox HS. (2011). Oxygen matters: tissue culture oxygen levels affect mitochondrial function and structure as well as responses to HIV viroproteins. *Cell Death Dis*, 2:e246. doi:10.1038/cddis.2011.128.
Villeneuve L, Tiede LM, Morsey B, Fox HS. (2013). Quantitative proteomics reveals oxygen-dependent changes in neuronal mitochondria affecting function and sensitivity to rotenone. *J Proteome*, 12: 4599–606.
Wright WE, Shay JW. (2006). Inexpensive low-oxygen incubators. *Nat Protoc*, 1:2088–90.
Xun Z, Lee D-Y, Lim J, *et al.* (2012). Retinoic acid-induced differentiation increases the rate of oxygen consumption and enhances the spare respiratory capacity of mitochondria in SH-SY5Y cells. *Mech Ageing Dev*, 133:176–85.
Yamamoto T, Yamada A, Watanabe M, *et al.* (2006). VDAC1, having a shorter N-terminus than VDAC2 but showing the same migration in an SDS-polyacrylamide gel, is the predominant form expressed in mitochondria of various tissues. *J Proteome Res*, 5:3336–44.
Zhu J, Aja S, Kim E-K, *et al.* (2012). Physiological oxygen level is critical for modeling neuronal metabolism in vitro. *J Neurosci Res*, 90: 422–34.

Supplementary material available online

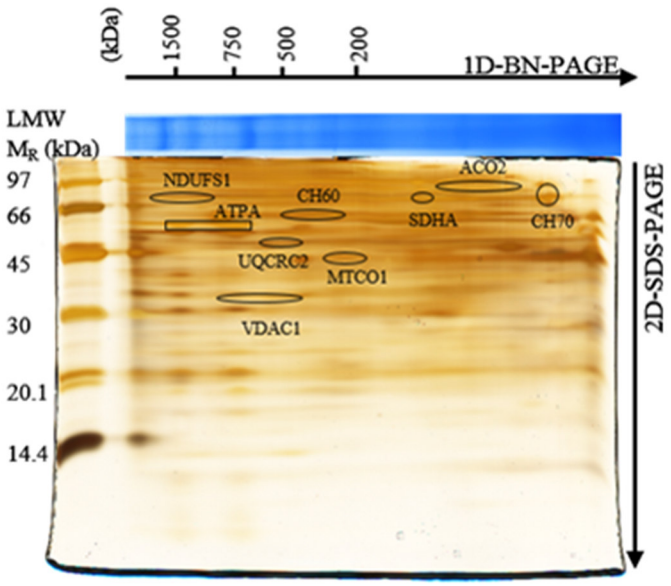

Figure S1. **Silver-stained 2D-BN/SDS gel.** Following SYPRO Ruby staining of gels used for analysis of protein expression levels, 2D-BN/SDS gels were stained with silver for visualization of protein spots and gel documentation only.

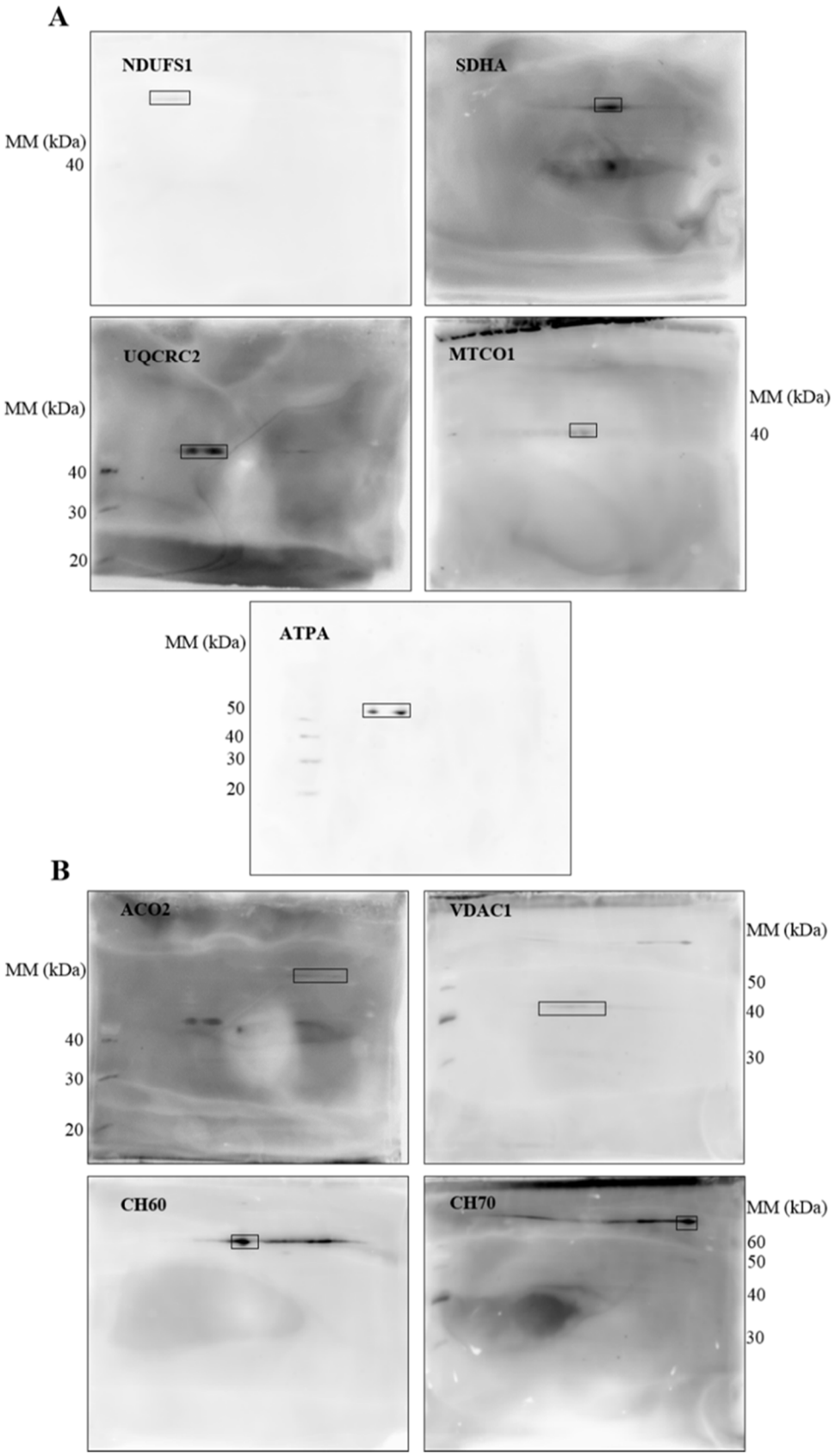
A
NDUFS1
SDHA
MM (kDa)
40
UQCRC2
MTCO1
MM (kDa)
40
30
20
MM (kDa)
40
ATPA
MM (kDa)
50
40
30
20
B
ACO2
VDAC1
MM (kDa)
MM (kDa)
40
30
20
50
40
30
CH60
CH70
MM (kDa)
60
50
40
30

Figure S2. Western blot. Western blot detection of oxidative phosphorylation protein subunits **(A)** and other mitochondrial proteins **(B)** after separation of 120 µg of protein from "crude" isolated mitochondria solubilized with the mild non-ionic detergent digitonin (3 g/1 g protein) using 2D-BN/SDS-PAGE. MagicMark™ (MM) protein standard was used for mass calibration. [NDUFS1: NADH dehydrogenase (ubiquinone) Fe-S protein 1 (79.4 kDa) of complex I, SDHA: succinate dehydrogenase complex flavoprotein subunit A (70 kDa) of complex II, UQCRC2: ubiquinol-cytochrome-c reductase complex core protein 2 (48.4 kDa) of complex III, MTCO1: mitochondrially encoded cytochrome c oxidase I (40 kDa) of complex IV, ATPA: ATP synthase subunit alpha (59.7 kDa) of complex V, ACO2: aconitase 2 (82 kDa), CH60: 60 kDa heat shock protein (60.1 kDa), CH70: heat shock protein 70 (75 kDa) , VDAC1: voltage-dependent anion-selective channel protein 1 (30.8 kDa] [Additional signals appeared on membranes that were re-used for immunoblotting after regeneration with mild stripping buffer (200 mM glycin, 0.1 (w/v) SDS, 1% (v/v) Tween 20)].

Table S1. Mitochondrial and other proteins of human SH-SY5Y cells identified in bands from 1D BN-gel using LC-MALDI-TOF/TOF*

Band	Protein identification	Accession	MW [kDa]	pI	Mascot score	No. of peptides	SC [%]
2	NADH dehydrogenase [ubiquinone] 1 alpha subcomplex subunit 9, mitochondrial	NDUA9	42.5	10.3	137.6	3	6.9
2	NADH dehydrogenase [ubiquinone] 1 alpha subcomplex subunit 12	NDUAC	17.1	10	149.4	3	31
1, 2	**NADH-ubiquinone oxidoreductase 75 kDa subunit, mitochondrial**	**NDUS1**	**79.4**	**5.8**	**176.8**	**4**	**5.1**
1, 2	NADH dehydrogenase [ubiquinone] iron-sulfur protein 2, mitochondrial	NDUS2	52.5	7.9	132.7	3	5.8
2	NADH dehydrogenase [ubiquinone] iron-sulfur protein 3, mitochondrial	NDUS3	30.2	7.8	371.4	6	17.4
1, 2	NADH dehydrogenase [ubiquinone] iron-sulfur protein 7, mitochondrial	NDUS7	23.5	10.8	81.3	2	4.7
2	NADH dehydrogenase [ubiquinone] iron-sulfur protein 8, mitochondrial	NDUS8	23.7	6	145.5	3	12.4
1, 2	NADH dehydrogenase [ubiquinone] flavoprotein 1, mitochondrial	NDUV1	50.8	9.5	212.4	4	9.3
2	NADH dehydrogenase [ubiquinone] flavoprotein 2, mitochondrial	NDUV2	27.4	9.2	156.8	3	14.9
4	Cytochrome b-c1 complex subunit 1, mitochondrial	QCR1	52.6	5.9	410.2	6	9.4
4	**Cytochrome b-c1 complex subunit 2, mitochondrial**	**QCR2**	**48.4**	**9.3**	**169.9**	**3**	**6.2**
4	Cytochrome b-c1 complex subunit 7	QCR7	13.5	9.2	240.8	4	29.7
4	Cytochrome b-c1 complex subunit 8	QCR8	9.9	10.4	211.9	4	35.4
4	Cytochrome b-c1 complex subunit Rieske, mitochondrial	UCRI	29.6	9.4	107.1	2	7.3
2, 4	Cytochrome c1, heme protein, mitochondrial	CY1	35.4	9.8	80.7	2	8
1, 2, 3	**ATP synthase subunit alpha, mitochondrial**	**ATPA**	**59.7**	**9.6**	**1114.3**	**19**	**25.1**
1, 2, 3	**ATP synthase subunit beta, mitochondrial**	**ATPB**	**56.5**	**5.1**	**1419.9**	**17**	**28**
1, 3	ATP synthase subunit gamma, mitochondrial	ATPG	33	9.7	128.2	2	5.7
3	ATP synthase subunit d, mitochondrial	ATP5H	18.5	5.1	108.2	2	8.1
3	ATP synthase subunit epsilon, mitochondrial	ATP5E	5.8	10.5	81.9	2	31.4
1, 3	ATP synthase subunit O, mitochondrial	ATPO	23.3	10.5	127.8	2	11.7
3	ATP synthase F(0) complex subunit B1, mitochondrial	AT5F1	28.9	9.8	108.2	2	3.5
3, 4	ATP-citrate synthase	ACLY	120.8	7.1	211	5	6.4
3	Peroxisomal multifunctional enzyme type 2	DHB4	79.6	9.6	100.1	2	3.4
3	Trifunctional enzyme subunit alpha, mitochondrial	ECHA	82.9	9.8	139.4	4	4.2
3	Extended synaptotagmin-1	ESYT1	122.8	5.5	148.7	2	2.6
3, 4	Glutamate dehydrogenase 1, mitochondrial	DHE3	61.4	8.5	140.2	3	9
4	Pyruvate carboxylase, mitochondrial	PYC	129.6	6.4	363.6	8	9.1
2, 4	Aspartate aminotransferase, mitochondrial	AATM	47.5	9.8	160.3	2	5.6
3, 4	Dolichyl-diphosphooligosaccharide--protein glycosyltransferase 48 kDa subunit	OST48	50.8	6.1	509.9	8	22.6
2, 3, 4	Dolichyl-diphosphooligosaccharide--protein glycosyltransferase subunit 1	RPN1	68.5	5.9	126.6	2	2.6
3, 4	Dolichyl-diphosphooligosaccharide--protein glycosyltransferase subunit 2	RPN2	69.2	5.4	164.8	4	7.9
3, 4	Dolichyl-diphosphooligosaccharide--protein glycosyltransferase subunit DAD1	DAD1	12.5	7.5	132.7	2	19.5
3, 4	Dolichyl-diphosphooligosaccharide--protein glycosyltransferase subunit STT3A	STT3A	80.5	8.9	221	4	7.1
4	Dolichyl-diphosphooligosaccharide--protein glycosyltransferase subunit STT3B	STT3B	93.6	9.6	402.8	9	11
2, 3, 4	Fructose-bisphosphate aldolase A	ALDOA	39.4	9.2	85.7	2	7.1
3, 4	Magnesium transporter protein 1	MAGT1	38	10.4	126	3	7.2
4	Malectin	MLEC	32.2	5.2	257.7	5	17.5
4	UTP--glucose-1-phosphate uridylyltransferase	UGPA	56.9	8.9	182.8	4	12.2
4	Peroxiredoxin-4	PRDX4	30.5	5.8	217.4	5	23.2
4	Solute carrier family 12 member 2	S12A2	131.4	6	402.5	7	6.8
4	Sodium bicarbonate cotransporter 3	S4A7	136	6.3	85.6	2	1.5
3, 4	**Voltage-dependent anion-selective channel protein 1**	**VDAC1**	**30.8**	**9.2**	**175**	**3**	**21.9**
2	V-type proton ATPase 116 kDa subunit a isoform 1	VPP1	96.4	6	181.9	4	5.4
2	V-type proton ATPase catalytic subunit A	VATA	68.3	5.2	615	10	18.2
2,3	V-type proton ATPase subunit B, brain isoform	VATB2	56.5	5.5	380.7	9	16.8
4	V-type proton ATPase subunit d 1	VA0D1	40.3	4.7	174.1	4	13.7
4	MICOS complex subunit MIC60	MIC60	83.6	6.1	170.8	3	5.1
2, 3, 4	Annexin A2	ANXA2	38.6	8.5	232.7	5	17.1
2, 3, 4	Calnexin	CALX	67.5	4.3	158.2	3	8.3

3	Alpha-2-macroglobulin	A2MG	163.2	6	124	2	1.2
2, 4	Sarcoplasmic/endoplasmic reticulum calcium ATPase 2	AT2A2	114.7	5.1	282.9	5	6.8
3, 4	78 kDa glucose-regulated protein	GRP78	72.3	4.9	179.2	5	9.2
3, 4	Protein disulfide-isomerase A6	PDIA6	48.1	4.8	188.9	3	8.6
3,4	Transitional endoplasmic reticulum ATPase	TERA	89.3	5	147.4	2	4.8
4	Endoplasmin	ENPL	92.4	4.6	103	3	3.6
4	**60 kDa heat shock protein, mitochondrial**	**CH60**	**61**	**5.6**	**255.1**	**4**	**10.8**
3	Proteasome subunit alpha type-1	PSA1	29.5	6.2	181.7	4	20.2
3	Proteasome subunit alpha type-2	PSA2	25.9	7.7	189.9	4	18.4
3	Proteasome subunit alpha type-4	PSA4	29.5	8.7	129.3	2	12.6
3	Proteasome subunit alpha type-6	PSA6	27.4	6.4	179.4	3	16.7
3	Proteasome subunit alpha type-7	PSA7	27.9	9.3	218.5	4	27
3	Proteasome subunit beta type-2	PSB2	22.8	6.6	161.9	4	25.9
3	Proteasome subunit beta type-4	PSB4	29.2	5.6	92.6	2	6.8
4	Keratin, type II cytoskeletal 1	K2C1	66	8.8	223.7	2	10.9
4	Integrin alpha-6	ITA6	126.5	6.2	176.9	2	2.6
4	Integrin alpha-7	ITA7	128.9	5.4	96.4	2	2.3
4	Integrin beta-1	ITB1	88.4	5.1	288.3	3	3.8
3	Laminin subunit alpha-3	LAMA3	366.4	7.2	82.2	2	0.6
2, 3, 4	Moesin	MOES	67.8	6	296.3	6	8.5
2, 3, 4	Tubulin alpha-1C chain	TBA1C	49.9	4.8	232.2	4	13.1
2,4	Tubulin beta chain	TBB5	49.6	4.6	428.3	11	20.9
3	Tubulin beta-4B chain	TBB4B	49.8	4.6	232.7	5	15.1
2	T-complex protein 1 subunit alpha	TCPA	60.3	5.7	813.1	15	23.2
2	T-complex protein 1 subunit beta	TCPB	57.5	6	812.8	14	27.1
2	T-complex protein 1 subunit gamma	TCPG	60.5	6.1	1074.4	19	37.2
2	T-complex protein 1 subunit delta	TCPD	57.9	9	1085.9	20	35.8
2	T-complex protein 1 subunit epsilon	TCPE	59.6	5.3	495	9	15.7
2	T-complex protein 1 subunit zeta	TCPZ	58	6.2	738.5	13	23.2
2	T-complex protein 1 subunit eta	TCPH	59.3	8.6	824.9	12	20.4
2	T-complex protein 1 subunit theta	TCPQ	59.6	5.3	938.9	15	31.6
2	Cytoplasmic dynein 1 heavy chain 1	DYHC1	532.1	6	822.9	18	4.5
2, 3, 4	Filamin-A	FLNA	280.6	5.7	891.9	21	12.2
4	Filamin-B	FLNB	278	5.4	256	5	2.1
3, 4	Cytoplasmic FMR1-interacting protein 1	CYFP1	145.1	6.5	344.3	9	8.5
3	Rho-associated protein kinase 2	ROCK2	160.8	5.7	246.5	7	4.8
2	Myosin-9	MYH9	226.4	5.4	570.7	12	7.7
3, 4	Septin-2	SEPT2	41.5	6.1	280.6	4	16.1
3, 4	Septin-7	SEPT7	50.6	9.4	370.7	7	21.1
3, 4	Septin-9	SEPT9	65.4	9.7	115.6	3	7.8
4	Septin-11	SEP11	49.4	6.4	94.5	2	4.4
2	Elongation factor 1-alpha 1	EF1A1	50.1	9.7	83.1	2	5
3, 4	Neuroblast differentiation-associated protein AHNAK	AHNK	628.7	5.7	211.9	4	0.9
4	Renin receptor	RENR	39	5.7	99	2	8.3
1, 3	Up-regulated during skeletal muscle growth protein 5	USMG5	6.5	10.3	125.1	2	19
1, 2	Prohibitin	PHB	29.8	5.5	98.7	3	11.8
1, 2	Prohibitin-2	PHB2	33.3	10.2	141.8	4	12.7

*Identified proteins by the LC-MALDI-TOF/TOF with their related accession code of Swiss-Prot (SwissProt 2015 08, Homo sapiens (human)) data-base. Band number refers to marked bands of Figure 2. MW shows molecular weights of identified proteins and SC is the sequence coverage. Proteins of interest present in gel bands are shaded in the table.

5.11. Expression of cytoplasmic proteins

The expresion of hypoxia inducible factor-1 alpha (HIF-1α) that gets expressed under conditions of low oxygen (hypoxia) was investigated in SH-SY5Y cells upon treatment with 4 μM $A\beta_{1-42}$ peptide and/or 2 Gy X-ray irradiation at 21% and 5% O_2, respectively. Full lenght HIF-1α with the size of about 120 kDa representing a factor induced in hypoxia (Wang & Semenza, 1995) was not observed in cell lysates of SH-SY5Y (Figure 5.19). Instead, multiple lower molecular mass bands suggesting the degradation of the protein were observed using an antibody against full lenght HIF-1α, particularly in SH-SY5Y cells cultivated at 21% O_2. Aβ peptide and/or irradiation contributed to the increased appearance of such bands.

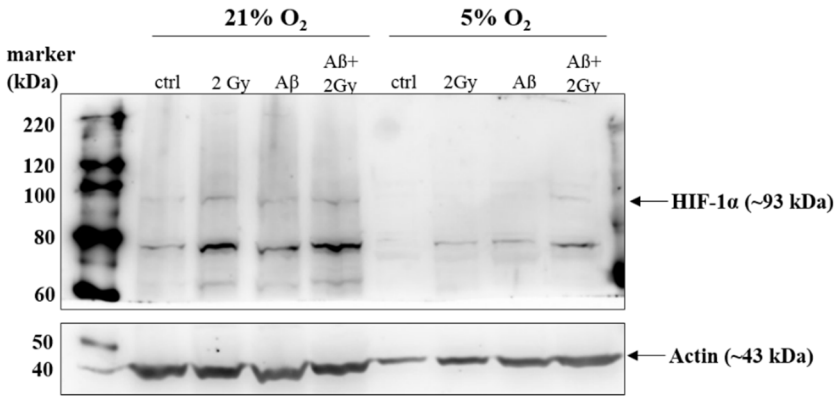

Figure 5.19. Western blot detection of hypoxia inducible factor-1 alpha (HIF-1α) after treatment with 4 μM $A\beta_{1-42}$ peptide and/or 2 Gy X-ray irradiation of SH-SY5Y cells pre-treated with 10 μM retinoic acid and cultivated at 21% and 5% O_2, respectively. No HIF-1α (~120 kDa) representing a factor expressed in hypoxia was observed 1 day after the treatment and/or 18 h after irradiation. Multiple lower molecular mass bands detected with the specific antibody suggesting the degradation of the protein. Actin was used as a loading control for immunoblotting of cell lysates (about 30 μg protein per lane) of samples separated by SDS-PAGE (4% stacking gel, 9% separation gel).

HIF-1α is not stable under conditions which are non-hypoxic and even if induced it gets degraded in some minutes (Gultice et al., 2009). Previous studies showed that HIF-1α is induced by ROS in hypoxia (Chandel et al., 1998) and upon treatment with $CoCl_2$ (Kallio et al., 1997). Observed degradation of HIF-1α upon the treatment with Aβ peptide and/or irradiation suggests that ROS other than those produced in hypoxia could affect its expression for a short time. Cells at 21% O_2 experienced more ROS as compared to cells at 5% O_2 (Chapter 5.7) and this is in correlation with such transient increase in HIF-1α expression and then more intense degradation bands in Western blot.

The expression of heat shock protein 60 (Hsp60) was observed in all samples and was increased after the treatment with Aβ peptide in cells at 21% O_2 only (Figure 5.20).

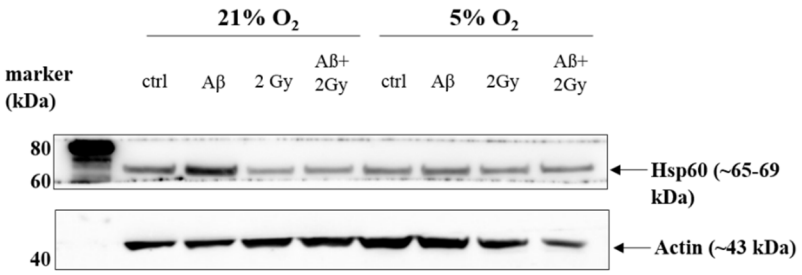

Figure 5.20. Western blot detection of heat shock protein 60 (Hsp60) after treatment with 4 µM $A\beta_{1-42}$ peptide and/or 2 Gy X-ray irradiation of SH-SY5Y cells differentiated with 10 µM retinoic acid and cultivated at 21% and 5% O_2, respectively. Elevated expression of Hsp60 protein was observed after treatment with Aβ peptide in cells at 21% O_2 only. Actin was used as a loading control for immunoblotting of cell lysates (about 30 µg protein per lane) of samples separated by SDS-PAGE (4-12% gradient gel).

Hsp60 protein is necessary for proper folding of proteins (Hartl, 1996) and for removal of damaged or non-functional proteins as well. Its expression can be elevated under the cellular stress (Hall & Martinus, 2013) such as presence of Aβ peptide. Its expression under the stress is probably regulated by the oxygen concentration in the cell culture. Cells exposed to 21% O_2 experience more ROS (Chapter 5.7) and increased protein carbonylation (Chapter 5.12) as compared to cells at 5% O_2.

5.12. Level of protein carbonylation

The level of protein carbonylation upon Aβ peptide treatment and/or irradiation with 2 Gy X-rays was assayed for the total cellular proteins (Chapter 4.3.1) or mitochondrial proteins from „crude" isolated mitochondria (Chapter 4.3.2) of SH-SY5Y cell cultivated at 21% and 5% O_2, respectively. Intensities of bands in the oxyblot were correlated to the degree of protein carbonylation (assessed using DNP antibody against carbonyl groups) (Stadtman 1993; Stankowski et al., 2011); the more intense the bands are, the higher is the degree of protein oxidation. About 1.8-2.5 fold higher protein carbonylation was detected in cells cultivated at 21% O_2 compared to cells at 5% O_2 at all experimental conditions (Figure 5.21). Irradiation at 21% O_2 caused increase in protein carbonylation, whereas Aβ peptide treatment or combination of two stressors did not lead to a significant increase in protein carbonylation. Increase (~1.6 fold) in protein carbonylation in cells cultivated at 5% O_2 was observed after amyloid beta peptide treatment alone and when combined with irradiation (~1.4 fold), whereas irradiation alone did not affect the level of protein carbonylation.

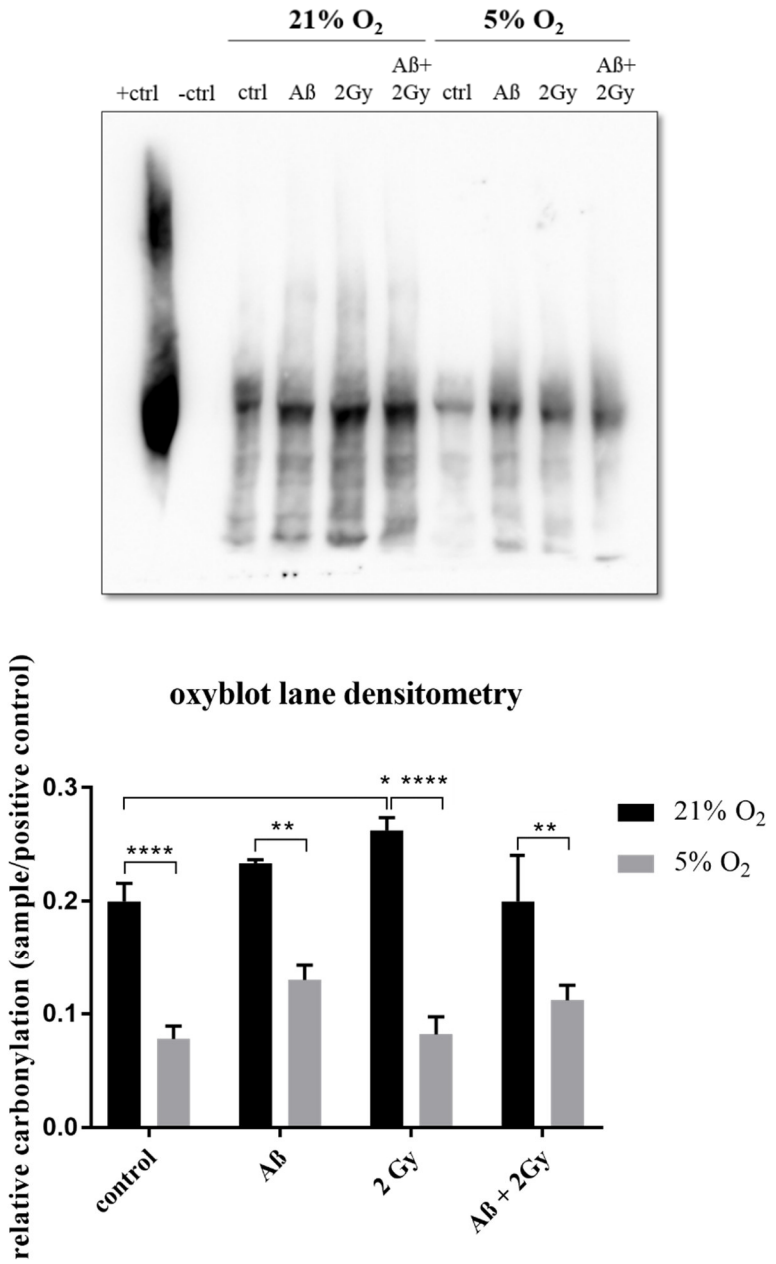

Figure 5.21. Determination of the level of protein carbonylation by Oxyblot upon $A\beta_{1-42}$ treatment and/or irradiation (2 Gy X-rays) in SH-SY5Y cells cultivated at 21% and 5% O_2, respectively. Oxidized and derivatized (+) bovine serum albumin (BSA, 15 µg, 60 kDa) served as a positive control and mass standard and non-derivatized (-) BSA was used as a negative control for immuno-binding. Mean gray values of Oxyblot lanes (~15 µg protein/lane) were normalized to the gray value of BSA positive control lane (mean grey value = 1). Cells cultivated at 21% O_2 showed significantly increased (about 1.8-2.5 fold) protein carbonylation compared to cells at 5% O_2 and this increase at 21% O_2 only was significantly pronounced after irradiation. Aβ peptide treatment alone or combined with irradiation resulted in an increase (~1.6 and 1.4 fold, respectively, not significant) in protein carbonylation in cells at 5% O_2, whereas only minor increase (1.15 fold) after Aβ peptide only was observed at 21% O_2. Combination of two stressors did not lead further increase in protein carbonylation at 21% O_2. Samples were measured at least in three independent experiments. Mean ± SEM analyzed by two-way ANOVA with Dunnet´s multiple comparison test. (*$p<0.05$;****$p<0.0001$).

Mitochondrial proteins from „crude“ isolated mitochondria showed no significant difference in protein carbonlyation when cell were cultivated at 21% and 5% O_2. About 1.5 fold higher protein carbonylation of mitochondrial proteins was detected after irradiation of cells cultivated at 21% O_2 compared to control cells at 21% O_2 and irradiated cells at 5% O_2 as well (Figure 5.22).

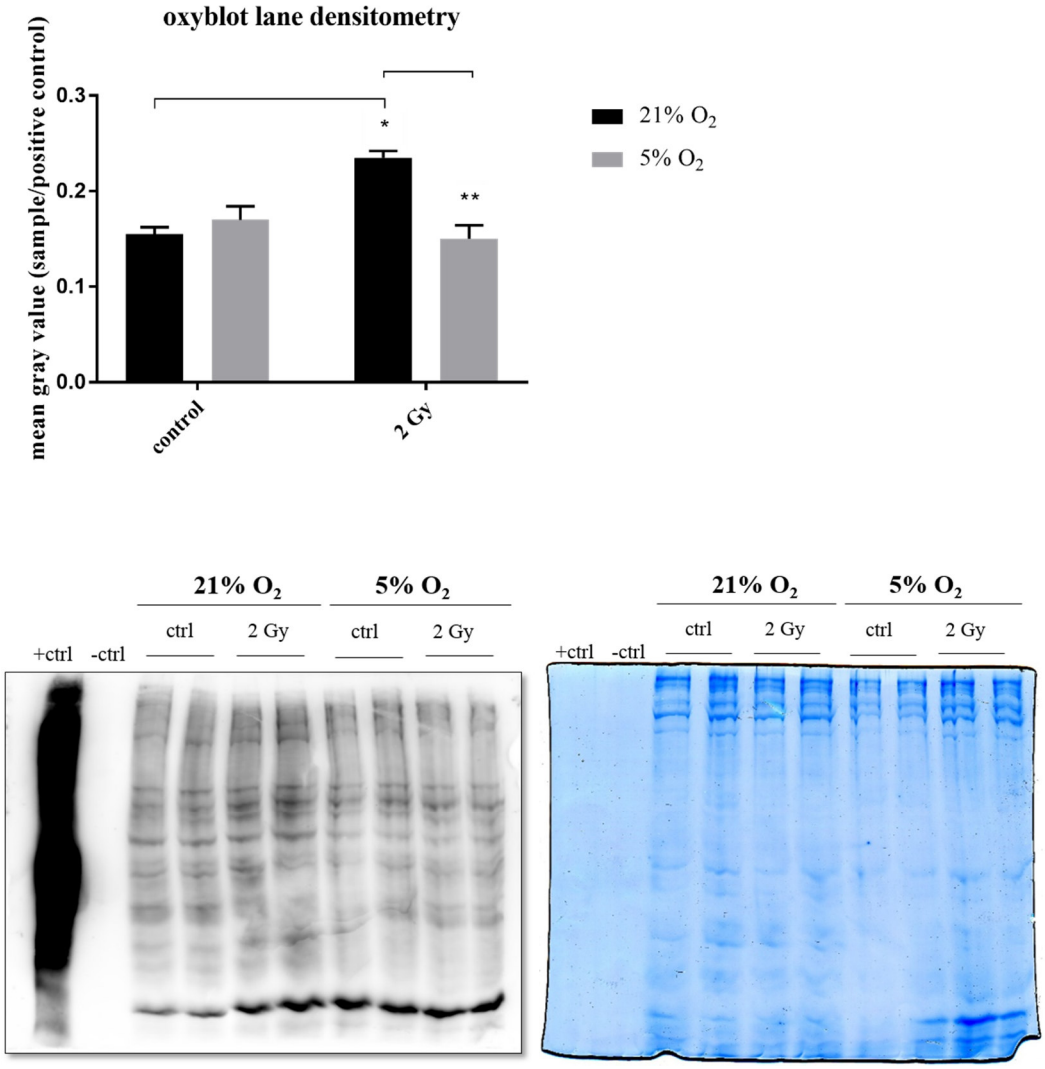

Figure 5.22. Determination of the level of protein carbonylation of mitochondrial proteins from „crude“ isolated mitochondria by Oxyblot upon 2 Gy X-ray irradiation of SH-SY5Y cells cultivated at 21% and 5% O_2, respectively. Oxidized and derivatized (+) bovine serum albumin (BSA, 15 µg, 60 kDa) served as a positive control and mass standard and non-derivatized (-) BSA was used as a negative control for immuno-binding (left) after separation of DNPH (2,4-dinitrophenylhydrazine)-derivatized mitochondrial proteins on 9% SDS gel that was Coomassie-stained to determine blotting efficiency (right). Mean gray values of Oxyblot lanes were normalized to the gray value of BSA positive control lane (mean grey value = 1). Cells cultivated at 21% O_2 showed significantly increased (~1.5 fold) protein carbonylation after irradiation as compared to control cells at 21% O_2 and irradiated cells at 5% O_2. Each mitochondria sample was loaded in a duplicate. Mean ± SEM analyzed by two-way ANOVA with Sidak multiple comparison test. (*$p<0.05$; **$p<0.01$).

Important target of ROS in the cell, beside DNA, are proteins. Reactive electrophiles and other reactive oxygen species may induce irreversible alterations of protein structure and function leading to cellular dysfunction. For example, carbonyl groups are being introduced to proteins in reaction with ROS (Liebler et al., 2008). Carbonyl group (aldehyde or keton) formation on protein side chains, mostly on prolines, arginines, lysines and threonines, is a general biochemical marker of oxidative stress (Stankowski et al., 2011). Generally higher (2.5 fold) level of protein carbonylation was observed in total cellular proteins from cells cultivated at 21% O_2 as compared to 5% O_2. A significantly pronounced further increase in protein carbonylation was detected only after irradiation of cells cultivated at 21% O_2, whereas Aß peptide alone or in combination with irradiation led only to a minor increase in protein carbonylation at both 21% and 5% O_2 (Figure 5.21). This is in accordance with the assumption that protein damage at physiological oxygen concentration is less pronounced than at 21% O_2. Also, protein repair and degradation systems are probably more efficient at 5% O_2 compared to that 21% O_2. There was no significant change in the level of protein carbonylation of mitochondrial proteins between cells cultivated at 21% and 5% O_2. Irradiation resulted in ~1.5 fold increase in carbonylation of mitochondrial proteins solely at 21% O_2 (Figure 5.22). Different level of protein carbonylation may be due to the heterogenous distribution of ROS and anti-oxidant enzymes in the cell (i.e. different ROS level and ROS scavengers/ROS protective enzymes in the cytosol and mitochondria) (Noori, 2012).

5.13. Mitochodrial DNA amount

Amount of mitochondrial DNA was determined by PCR 24 h and 72 h upon $A\beta_{1-42}$ peptide treatment or 18 h and 54 h after X-ray irradiation of SH-SY5Y cells cultivated at atmospheric oxygen (~21% O_2) and at 5% O_2, respectively. Effect of Aß peptide or irradiation alone on mtDNA amount was dependent on O_2 level in the cell culture: about 1.2 and 1.3 fold, respectively, decrease of mtDNA amount at 21% O_2 and up to 1.3 and 1.5 fold, respectively, increase at 5% O_2 compared to respective controls (Figure 5.23 A-B). The combined effect of Aß peptide and irradiation led to 1.8 and 1.4 fold, respectively, decrease in mtDNA amount at 21% and 5% O_2, particularly at 21% O_2 after 1 day or 18 h. However, no significant change in mtDNA amount at this oxygen concentration was observed 3 days after Aβ peptide treatment combined with irradiation, whereas at 5% O_2 it was restored to the level of control sample. The presence of 142 bp PCR products in samples was a confirmation for a successful amplification (Figure 5.23 C).

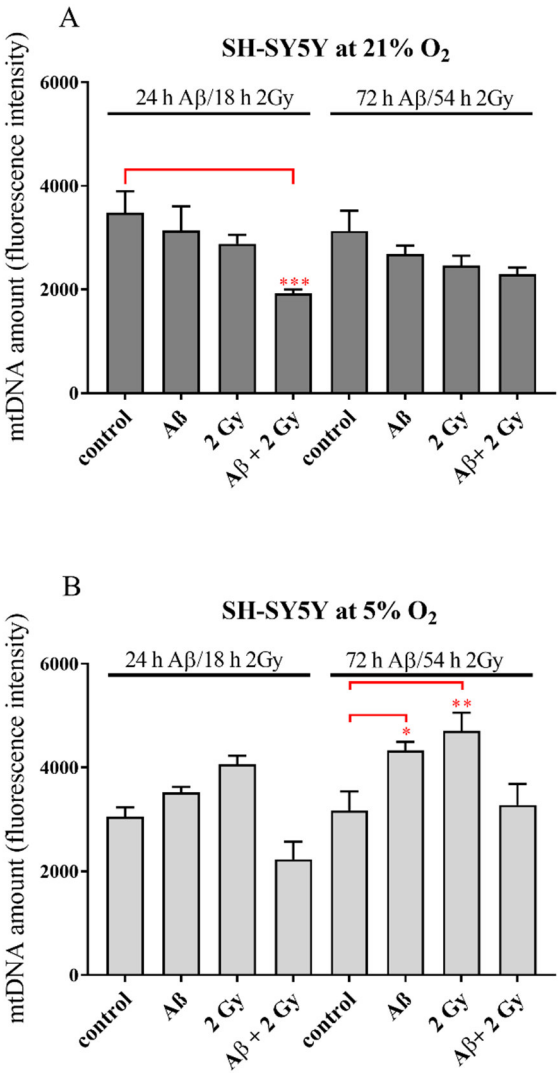
A
SH-SY5Y at 21% O2
mtDNA amount (fluorescence intensity)
6000
4000
2000
0
24 h Aβ/18 h 2Gy
72 h Aβ/54 h 2Gy
***
control
Aß
2 Gy
Aβ + 2 Gy
control
Aß
2 Gy
Aβ+ 2 Gy
B
SH-SY5Y at 5% O2
mtDNA amount (fluorescence intensity)
6000
4000
2000
0
24 h Aβ/18 h 2Gy
72 h Aβ/54 h 2Gy
*
**
control
Aß
2 Gy
Aβ + 2 Gy
control
Aß
2 Gy
Aβ+ 2 Gy

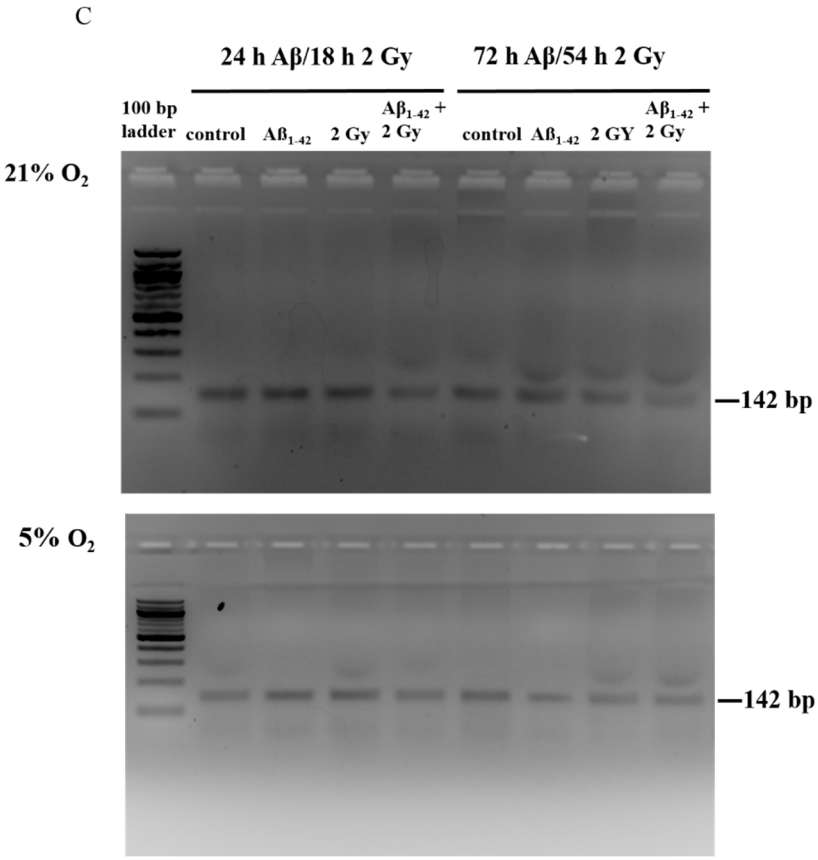

Figure 5.23. Mitochondrial DNA amount 24 h and 72 h upon $A\beta_{1-42}$ peptide treatment or 18 h and 54 h after irradiation (2 Gy X-rays) in SH-SY5Y cells cultivated at 21% and at 5% O_2, respectively. DNA amounts were quantified using PicoGreen dye. A-B) Aß peptide or irradiation alone affected mtDNA amount depending on O_2 level in the cell culture: about 1.2 and 1.3 fold, respectively, decrease at 21% O_2 and up to 1.3 and 1.5 fold, respectively, increase at 5% O_2 compared to respective controls. The combined effect of Aß peptide and irradiation led to decrease in mtDNA amount at both oxygen concentrations, particularly at 21% O_2 (1.8 fold) after 1 day/18 h with almost no change observed after 3 days/54 h, whereas at 5% O_2 it was restored to the level of control sample. C) The presence of a 142 bp bands after PCR was evaluated by agarose gel electrophoresis on a 2% agarose gel with addition of ethidium bromide for visualization of the DNA; 100 bp ladder was used as a molecular mass standard. Mean ± SEM analyzed by two-way ANOVA with Dunnet´s multiple comparison test. (*$p<0.05$; **$p<0.01$; ***$p<0.001$).

5.14. Mitochondrial DNA deletion

Mitochondrial DNA common deletion (4977 bp) was assayed using nested PCR for detection of a very small amount of aberrant molecules in the sample and for discrimination between the few molecules of deleted mtDNA and the overwhelming excess of wild type DNA (Soong and Arnheim (1996). The occurrence of the deletion can serve as an indicator of the increase in oxidative damage of mtDNA (Prithivirajsingh et al., 2004; Schilling-Tóth et al., 2011), which may lead to changes in ATP concentration in the cell and results in cell death. Samples were amplified 24 h and 72 h upon $A\beta_{1-42}$ peptide treatment or 18 h and 54 h after irradiation (2 Gy X-rays) in SH-SY5Y cells cultivated at 21% and at 5% O_2, respectively. DNA amounts were quantified using PicoGreen dye. A significant increase (~1.6 and ~2 fold, respectively) in mtDNA deletion was

observed only upon irradiation (2 Gy X-rays) after 54 h at both 21% and 5% O_2 compared to corresponding controls (Figure 5.24 A-B). Aβ peptide did not cause significant changes in mtDNA deletion measured at these two time points whereas combination of Aß peptide and irradiation resulted in a decreased mtDNA deletion at both oxygen concentrations (about 1.5 and 1.2 fold, respectively). The presence of the deletion was confirmed by agarose gel electrophoresis of PCR products in the form of 358 bp band (Figure 5.24 C).

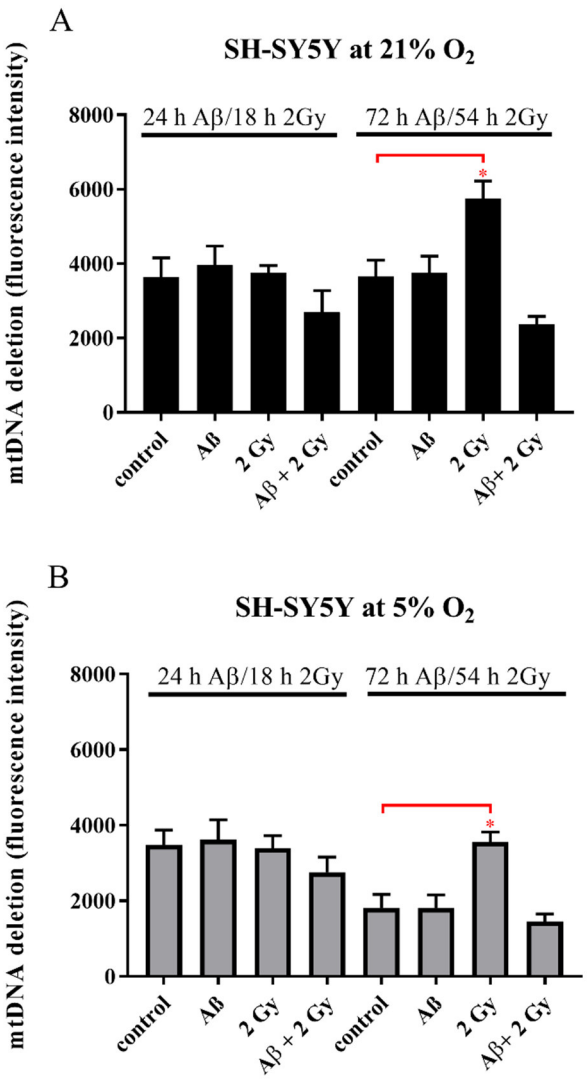

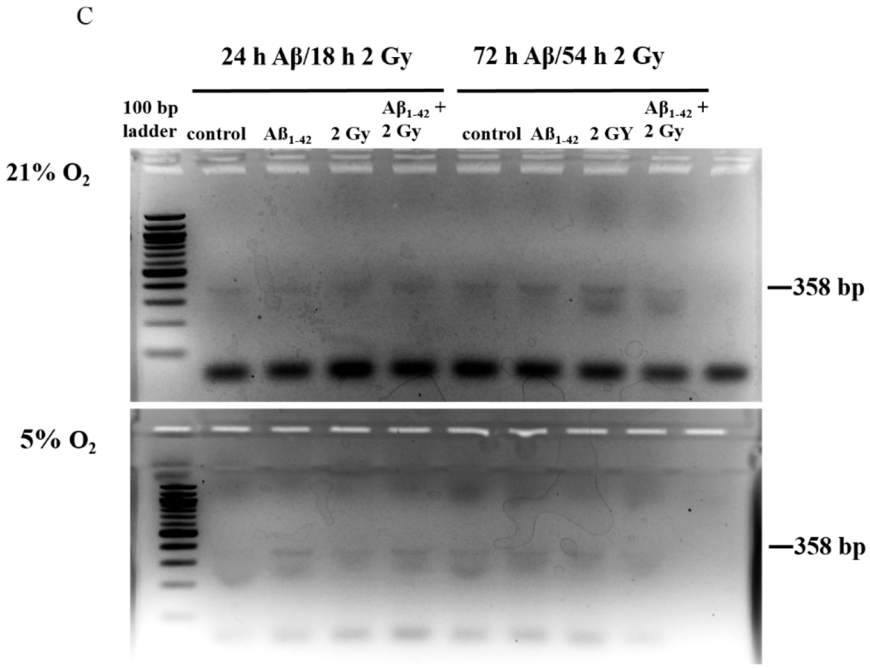

Figure 5.24. Mitochondrial DNA common (4977 bp) deletion 24 h and 72 h upon $A\beta_{1-42}$ peptide treatment or 18 h and 54 h after irradiation (2 Gy X-rays) in SH-SY5Y cells cultivated at 21% and at 5% O_2, respectively. Amounts of DNA were quantified using PicoGreen dye. A-B) 2 Gy X-rays led to a significant increase in mtDNA deletion after 54 h at both 21% and 5% O_2 compared to corresponding controls. Combination of Aß peptide and irradiation resulted in less mtDNA deletion at both oxygen concentrations. C) The presence of a 358 bp band, which represents amplification of mtDNA harboring deletion bands after PCR, was evaluated by agarose gel electrophoresis on 2% agarose gel with addition of ethidium bromide; 100 bp ladder was used as a molecular mass standard. Samples were measured triplicates (n = 3) in four independent experiments (N = 4). Mean ± SEM analyzed by two-way ANOVA with Tukeys´s multiple comparison test. (*$p<0.05$).

Nucleic acids, particularly mtDNA are very prone to oxidative damage by ROS causing mutations and larger rearrangements. The relative amount of mtDNA and the occurrence of mtDNA common (4977 bp) deletion which occurs in diseases, aging, after irradiation was measured and is related to oxidative damage (Prithivirajsingh et al., 2004; Schilling-Tóth et al., 2011). It was suggested that the degeneration of neurons and synapses in AD may be associated with oxidative damage to nuclear DNA and more severe damage to mtDNA (Wang et al., 2005) leading to its degradation, a process unique to the mitochondrial compartment (Shokolenko et al., 2009). Although mtDNA common (4977 bp) deletion was proposed as one of the hallmarks in AD (Ito et al., 1999), another study correlated its presence with oxidative damage that occurs during aging but not with AD (not found in brains of AD patients) (Lezza at al., 1999). A significantly increased level of the common mtDNA deletion (4977 bp) which was specific for irradiated cells only was observed (Figure 5.24). Aß peptide treatment alone did not result in increase in amount of this deletion. Interestingly, in Aβ peptide treated cells which were subsequently irradiated its amount was restored to the control level at both 21% and 5% O_2. The amount of mtDNA detected by standard PCR was not significantly changed by Aß peptide treatment alone or combined with irradiation at both 21% and 5% O_2 (measured 72 h after treatment and 54 h after irradiation) (Figure 5.23). Noteworthy,

irradiation of cells at 5% O_2 resulted in a significant increase of mtDNA amount after 54 h (Figure 5.23). In general, cells at 5% O_2 showed higher mtDNA amount after Aβ peptide treatment or after irradiation than cells at 21% O_2. Probably, increase in mtDNA amount is a compensatory mechanism after stress and damage and it is dependent on the oxygen concentration in the cell culture. Although effects of irradiation and Aβ peptide share some similarities, such as induction of inflammation, these two stressors probably affect different cellular pathways and result in different cellular responses. Mitochondrial DNA deletions could be responsible for triggering compensatory mechanisms such as increase in mtDNA amount (observed in cells at 5% O_2) and improvement in mitochondrial respiration, which allows normal functioning of cells and may have neuroprotective effect (Perier et al., 2013). Also, balanced mitochondrial fission and fusion processes enable maintenance of their proper function and integrity including mtDNA quality (Busch et al., 2014) and it was reported that mitochondria of cells cultivated at 5% O_2 show larger mitochondrial networks, greater cytoplasmic fractions of mitochondria (area occupied by the mitochondria) and larger mitochondrial perimeters than those cultured at higher oxygen concentrations (Tiede et al., 2011). It was shown previously that Aß peptide can induce oxidative-mediated autophagic cell death in vitro after damage of mtDNA in AD (Wang et al. 2010). In addition, hyperoxic conditions (e.g. 95% O_2) induce rapid cell death with fragmentation of mtDNA (Yoneda et al., 1995). Overexpression of mitochondrial transcription factor A (Tfam) is one of the mechanisms to compensate mitochondrial dysfunction, protect mtDNA from oxidative stress and to maintain mtDNA amount in SH-SY5Y cells treated with Aß peptide (Xu et al., 2009).

6. General discussion

The complex interplay of ionizing radiation (IR), oxygen in the cell culture, differentiation status of cells and Alzheimer´s disease (AD) $A\beta_{1-42}$ peptide were presented and discussed in this thesis.

Oxygen concentration in the cell culture is of crucial importance for the cellular response to oxidative stress, which was compared between cells cultivated at 21% O_2 commonly used in the cell culture and at more physiological 5% O_2.

It was demonstrated that the intracellular oxygen concentration was about 2-5 fold lower than the concentration applied to the cell culture. For human neuroblastoma (SH-SY5Y) cells cultivated at 21% O_2 the measured intracellular oxygen concentration was ~10%, and for cells cultivated at 5% O_2 was ~1% (Figure 5.1). Although no previous measurements for SH-SY5Y cells were performed, data obtained in this thesis are in line with published data for adheherent 2D culture of HepG2 cells at 21% O_2 (~10% O_2 intracellularly) (Krumm & Carey, 2016), and for HEK293T cells cultivated 6% O_2 (~2% O_2 intracellulary) (manual for MitoXpress® Intra Intracellular Oxygen assay).

5% O_2 was considered more physiological for SH-SY5Y cells as compared to 21% O_2 and the term „hypoxia“ (i.e. lack of oxygenation or O_2 concentration lower than that measured in different organs in a physiological condition) (Carreau et al., 2011) could not be attributed to this concentration. Moreover, no hypoxia inducible factor (HIF-1α), which is usually expressed in hypoxia, was detected in the studied system (Figure 5.19). Furthermore, proliferation activity of cells cultivated at 5% O_2 was higher than at 21% O_2 (Figure 5.3), which was in accordance with published data showing that lower O_2 concentrations are beneficial for cell proliferation (Packer and Fuehr, 1977; Brewer and Cotman, 1989; Parinello et al., 2003).

Oxygen affects bioenergetic status of the cell since cells at 5% O_2, which is more physiological, revealed higher ATP concentration (~1.3 fold) (Figure 5.13 A) and less mtDNA deletion (up to 2 fold) (Figure 5.24) compared to cells at non-physiological 21% O_2. Furthermore, lower ROS level (~1.5 fold) (Figure 5.14 B) and less protein carbonylation (~2.5 fold) in total cellular proteins (Figure 5.21) were observed at 5% O_2. This is in accordance with the assumption that the protein damage at physiological oxygen concentration is less pronounced than at 21% O_2. Also, protein repair and degradation systems are probably more efficient at 5% O_2 compared to that at 21% O_2. However, no significant change in the level of protein carbonylation of mitochondrial proteins between cells cultivated at 21% and 5% O_2 was observed (Figure 5.22). This may be due to the heterogenous distribution of ROS and anti-oxidant enzymes in the cell (i.e. different ROS level and ROS scavengers/ROS protective enzymes in the cytosol and mitochondria) (Noori, 2012).

The **differentiation state** is another important factor in cellular response to stress. Treatment of cells with retinoic acid (RA) for 3 days used for induction of differentiation resulted in changed morphology of SH-SY5Y cells (i.e. elongation of the cell body and presentation of long outgrowths) (Figure 5.5). Furthermore, RA reduced cell proliferation at both of 21% O_2 and 5%

O_2 (Figure 5.6). Differentiation state of the cell determines the gene expression which then regulates the sensitivity and cellular response to any treatment. Noteworthy, SH-SY5Y cells in this study, due to the limited time frame, were not terminally differentiated to homogenous human neuronal cultures as described by Shipley and colleagues (2016) where the differentiation is based on sequential removal of serum from media with introduction of extracellular matrix proteins and neurotrophic factors. In this work, only RA was used to induce differentiation (Hellmann-Regen et al., 2012) and this resulted in rather heterogenous population where most, but not all cells, were at a similar differentiation state.
Additionally, oxygen concentration modulated the expression of neurofilament M, a marker of differentiation (Džinić et al., 2016) and is known to be implicated in differentiation (Cheng et al., 2014) and metabolic activity of neuronal cells (Zhu et al., 2012).

Oxygen concentration and differentiation state are important in studies of disease mechanisms, particularly of multifactorial diseases e.g. neurodegenerative AD. Although exact cause(s) of AD are still unknown, one of the players is Aβ peptide. However, the implication of different aggregation states of the peptide (fibrillized or disaggregated to monomers and oligomers) is largely debated. Monomers and small oligomers of Aβ peptide are recently proposed to be involved in damage of neurons, instead of extracellular Aβ plaques, since they interact with cellular membranes (Buchsteiner et al., 2010; Dante et al., 2011) and the peptide is found inside neurons of AD patients (Gouras et al., 2000).

In this thesis, externally applied disaggregated **Aß$_{1-42}$ peptide** was found to interact preferentially with lysosomes of SH-SY5Y cells at both 21% and 5% O_2 (Figure 5.7 B). Thus, the peptide interacted only to a minor extent with mitochondria and endoplasmatic reticulum (Figure 5.8 C-D). Flow cytometric analysis revealed increase in cell death after Aβ peptide treatment solely in RA-treated cells, particularly at 5% O_2 (~1.3 fold) (Figure 5.11). However, the effect of 4 μM Aβ peptide on cell survival was not dramatic. Similar results were obtained for 10 μM Aß peptide applied to differentiated PC12 cells as well (Sirk et al., 2007). In studies of Aβ peptide toxicity, it is important to consider the **concentration and aggregation state** of the peptide and the **cell type**. For example, picomolar concentrations of intracellular Aß$_{1-42}$ peptide (both non-fibrillized and fibrillized) induced cell death of primary neurons through p53-Bax pathway (Zhang et al., 2002) but not of other neuronal and non-neuronal cell types.

In order to test the effect of high concentration of two different aggregation states of the peptide, 100 μM disaggregated and the same concentration of fibrillized Aβ peptide, respectively, was applied to SH-SY5Y cells for 1 and 3 days, respectively. Interesting finding was that the aged peptide caused earlier response of SH-SY5Y cells which underwent cell death (~3.4 fold increase compared to control cells) (Figure 5.12). This may indicate that aggregated peptide is more harmful and that the monomer/oligomer theory does not apply here. However, the effect of disaggregated Aß peptide after 3 days of incubation was much more pronounced (~5.3 fold increase in cell death as compared to control cells) than of fibrillized peptide (~2.3 fold increase

in cell death as compared to control cells). Therefore, **time** of incubation, together with all other factors mentioned above, is a crucial factor in Aβ peptide toxicity.

Aβ peptide did not dramatically affect mitochondrial-related parameters. There was only a slight increase in ROS (up to 1.2 fold) (Figure 5.14), a slight increase in mitochondrial membrane potential (Figure 5.18), and no changes in ATP concentration at both 21% and 5% O_2 (Figure 5.13 A). Although mtDNA common (4977 bp) deletion was proposed as one of the hallmarks in AD (Ito et al., 1999), another study correlated its presence with oxidative damage that occurs during aging but not with AD (not found in brains of AD patients) (Lezza at al., 1999). Also, in this thesis, no change in the mtDNA deletion could be detected in Aβ peptide treated cells (Figure 5.24). Change in mtDNA amount after Aβ peptide treatment depended on O_2 concentration: up to 1.3 fold decrease at 21% O_2 and up to 1.5 fold increase at 5% O_2 (Figure 5.23).

Aβ affected lysosomal integrity in oxygen dependent manner: decreased lysosomal integrity was measured after Aβ peptide treatment in SH-SY5Y cells cultivated at 21% O_2 (Figure 5.8). Therefore, oxygen concentration was confirmed to be an important modulator of cellular response to stress (Tiede et al., 2011; Džinić et al., 2016). Additionaly, RA-treated cells were more sensitive than non-differentiated cells reflected in overall decline of lysosomal integrity in the former.

Many non-lethal alterations in cell physiology such as slight increase in protein carbonlyation (Figure 5.21) and interaction of Aß peptide with lysosomes (in line with studies performed at 21% O_2 (Decker, 2016)) if persistant, may induce detrimental changes. Important to note, the reverse peptide ($Aβ_{42-1}$), which was not used in this work, tested previously on SH-SY5Y cells cultivated at 21% O_2 behaved as a negative control and did not induce changes in cell death, ATP concentration and ROS level (Decker, 2016).

Lysosomal activity of sequestration and potential degradation of Aβ peptide is probably the first and most important defense mechanism of SH-SY5Y cells against Aβ peptide toxicity, as described by Zheng and colleagues (2012) as well. Other acidic compartments such as endosomes may be involved in the mechanism against Aβ peptide toxicity as well. Beside the observed interaction of Aβ peptide with lysosomes, which suggests their degradation, an increased expression of heat shock protein 60 (Hsp60), necessary for proper folding of proteins (Hartl, 1996) and for removal of damaged or non-functional proteins as well, was observed after the treatment with Aβ peptide, but solely in cells at 21% O_2 (Figure 5.20).

Ionizing X-ray radiation in general affected SH-SY5Y cells more than Aβ peptide. 2 Gy X-rays caused a significant increase in ROS (~1.5 fold) (Figure 5.14), and a slight increase in ATP concentration (~1.2 fold) (Figure 5.13 A) but solely in cells at 5% O_2. A slight increase in mitochondrial membrane potential observed upon irradiation at both 21% and 5% O_2 (Figure 5.18) was as similar as the effect of Aβ peptide. This is probably a transient change and one of the mechanisms that cells employ in the presence of stressors (Džinić et al., 2016).

Cell proliferation activity of irradiated cells was reduced after 3-4 days, observed as a decrease in the number of cells cultivated at both of 21% O_2 and 5% O_2 (Figure 5.6). This suggests that the effect of radiation on cells is not immediate but exerted through the formation of ROS in the radiolysis of water and through their high potential to react with other molecules creating more ROS in the cell. 2 Gy applied does not present a high dose (commonly used as a fractionated dose in tumor treatment as well) of radiation compared to 8 Gy that resulted in more pronounced increase in ROS level at both 21% and 5% O_2 (Figure 5.15). Since half-lives (10^{-9}–10^{-4} s) of ROS are short (Powers et al., 2011), and changes in ROS were measured after at least 18 h, another approach to measure immediate and transient changes in ROS, as suggested and tested in this thesis, is the use of HyPer, a genetically encoded H_2O_2 sensor (Belousov et al., 2006).

The cell possesses its own anti-oxidant mechanisms such as glutathione (GSH) (Dani et al., 2010) which is activated depending on the amount of oxidative stress. For example, radiation caused a slight increase in GSH level at 21% O_2 and decrease at 5% O_2 (up to 1.2 fold) (Figure 5.17). The level of GSH, although used as an indicator of cell viability or of apoptosis (Coppola et al., 2000), studied here was varying and in most cases it could not be correlated with cell death; an increase of cell death after irradiation was observed in non-differentiated cells solely at 5% O_2 (~1.4 fold) (Figure 5.10) but in RA-treated cells at both 21% (~1.2 fold) and 5% O_2 (~1.5 fold) (Figure 5.11). Since GSH is not the only anti-oxidant in the cell, it is probable that the cell employs other antioxidant (e.g. dismutases and catalases) and repair mechanisms depending on the starting level of oxidative stress. For example, the observed increase in ATP that is utilized for repair processes under unfavorable conditions is one of the ways to cope with oxidative stress.

Increase in carbonyl groups in proteins induced by oxidative stress (Liebler et al., 2008) was specific for both total isolated (Figure 5.21) and mitochondrial proteins (Figure 5.22) of irradiated cells at 21% O_2. Furthermore the occurrence of the mtDNA deletion after 3 days was specific for irradiated cells at both 21% and 5% O_2 and was more pronounced at 21% O_2 (Figure 5.24). The presence of the deletion after irradiation is in accordance with previously published data (Prithivirajsingh et al., 2004; Schilling-Tóth et al., 2011). A significant increase of mtDNA amount in irradiated cells at 5% O_2 (Figure 5.23) is probably a compensatory mechanism after stress and damage and may have neuroprotective effect (Perier et al., 2013) depending on oxygen concentration in the cell culture. Damaged mtDNA, if not repaired, is usually degraded and this process is unique to the mitochondrial compartment (Shokolenko et al., 2009).

Similar to Aβ peptide, X-ray radiation reduced the lysosomal integrity in both RA-treated and non-treated cells solely at 21% O_2 (Figure 5.8). Increase in Hsp60 detected after treatment with Aβ peptide was not observed in irradiated cells (Figure 5.20). However, another heat shock protein (Hsp70) was found to be increased upon irradiation of SH-SY5Y cells (Džinić et al., 2016).

Although effects of irradiation and Aβ peptide share some similarities, such as induction of inflammation, these two stressors probably affect different cellular pathways and result in different

cellular responses. For the first time studied **combined effects of Aß peptide and X-ray radiation** revealed interesting cellular responses of SH-SY5Y cells.

Mitochondrial membrane potential (Figure 5.18), mtDNA amount (Figure 5.23), mitochondrial deletion (Figure 5.24) and cell death (Figure 5.10 and 5.11) were restored to their levels in control cells at both 21% and 5% O_2 in irradiated cells which were previously treated with Aβ peptide. Furthermore, there was an increase in ATP concentration upon irradiation of Aβ treated cells cultivated at 5% O_2 (~1.5 fold). Lysosomal integrity, which was decreased in cells at 21% O_2 upon Aβ treatment or irradiation, was restored to its level in control cells when both stressors were combined (Figure 5.8). Although the level of ROS was significantly increased at both 21% and 5% O_2 (up to 1.4 fold) (Figure 5.14), only minor increase in protein carbonylation was detected at both 21% and 5% O_2 (Figure 5.21).

It seems that Aβ peptide in lower concentration (4μM) has a protective effect on irradiated SH-SY5Y cells and the final cellular response is modulated by the starting level of oxidative stress (i.e. oxygen concentration) and differentiation state. Possibly, aromatic amino acid residues of Aß peptide act as selective ROS scavengers (Stadtman, 1993) but not for all ROS since there was a slight increase in ROS after Aβ peptide treatment alone or combined with radiation measured in this work. This demands further investigation of cellular responses to Aβ peptide.

7. References

Acharya MM, Lan ML, Kan VH, Patel NH, Giedzinski E, Tseng BP, Limoli CL. (2010). Consequences of ionizing radiation-induced damage in human neural stem cells. *Free Radic. Biol. Med*., 49: 1846-1855.

Alberts B, Johnson A, Lewis J, Morgan D, Raff M, Roberts K, Walter P. (2015). Molecular Biology of the cell. New York: Garland Science.

Alexeyev M, Shokolenko I, Wilson G, LeDoux S. (2015). The maintenance of mitochondrial DNA integrity-critical analysis and update. *Cold. Spring Harb. Perspect. Biol*., 5: a012641. doi: 10.1101/cshperspect.a012641.

Alzheimer A. (1907). Über eine eigenartige Erkrankung der Hirnrinde. *Allgemeine Zeitschrift für Psychiatrie und Psychisch-gerichtliche Medizin*, 64: 146-148.

Ames B, Shigenaga MK, Hagen TM. (1993). Oxidants, antioxidants, and the degenerative diseases of aging. *Proc. Natl. Acad. Sci. USA*, 90: 7915-7922.

Anderson S, Bankier AT, Barrell BG, de Bruijn MH, Coulson AR, Drouin J, Eperon IC, Nierlich DP, Roe BA, Sanger F, Schreier PH, Smith AJ, Staden R, Young IG. (1981). Sequence and organization of the human mitochondrial genome. *Nature*, 290: 457-465.

Apel K, Hirt H. (2004). Reactive oxygen species: metabolism, oxidative stress, and signal transduction. *Annu. Rev. Plant. Biol*., 55: 373-399.

Balmer JE, Blomhoff R. (2002). Gene expression regulation by retinoic acid. *Journal of Lipid Research*, 43: 1773-1808.

Barrett MA, Trapp M, Lohstroh W, Seydel T, Ollivier J, Ballauff M, Dencher NA, Hauß T. (2016). Alzheimer's peptide amyloid-β, fragment 22–40, perturbs lipid dynamics. *Soft Matter*, 12: 1444-1451.

Bauer G. (2011). Low dose gamma irradiation enhances defined signaling components of intercellular reactive oxygen-mediated apoptosis induction. *Journal of Physics Conference Series*, 261: 012001.

Bauman GS, Gaspar LE, Fisher BJ, Halperin EC, Macdonald DR, Cairncross JG. (1994). A prospective study of short-course radiotherapy in poor prognosis glioblastoma multiforme. *Int. J. Radiat. Oncol. Biol. Phys*., 29: 835-839.

Belousov VV, Fradkov AF, Lukyanov KA, Staroverov DB, Shakhbazov KS, Terskikh AV, Lukyanov S. (2006). Genetically encoded fluorescent indicator for intracellular hydrogen peroxide. *Nature Methods*, 3: 281-286.

Berggren K, Chernokalskaya E, Steinberg TH, Kemper C, Lopez MF, Diwu Z, Haugland RP, Patton WF. (2000). Background-free, high sensitivity staining of proteins in one- and two-dimensional sodium dodecyl sulfate-polyacrylamide gels using a luminescent ruthenium complex. *Electrophoresis*, 21: 2509-2521.

Biedler JL, Helson L, Spengler BA. (1973). Morphology and growth, tumorigenicity, and cytogenetics of human neuroblastoma cells in continuous culture. *Cancer Res*., 33: 2643-2652.

Biedler JL, Roffler-Tarlov S, Schachner M, Freedman LS. (1978). Multiple neurotransmitter synthesis by human neuroblastoma cell lines and clones. *Cancer Res*., 38: 3751-3757.

Blum H, Beier H, Gross H. (1987). Improved silver staining of plant proteins, RNA and DNA in polyacrylamide gels. *Electrophoresis*, 8: 93-99.

Bodovitz S, Klein WL. (1996). Cholesterol modulates alpha-secretase cleavage of amyloid presursor protein. *J. Biol.Chem*. 271: 4436-4440.

Bradford MM. (1976). Rapid and sensitive method for the quantitation of microgram quantities of protein utilizing the principle of protein-dye binding. *Anal. Biochem*., 72: 248–254.

Braunschweig L, Meyer AK, Wagenführ L, Storch A. (2015). Oxygen regulates proliferation of neural stem cells through Wnt/β-catenin signaling. *Molecular and Cellular Neuroscience*, 67: 84-92.

Brewer GJ, Cotman CW. (1989). Survival and growth of hippocampal neurons in defined medium at low density: advantages of a sandwich culture technique or low oxygen. *Brain Res*., 494: 65-74.

Brown WM, George M Jr, Wilson AC. (1979). Rapid evolution of animal mitochondrial DNA. *Proc. Natl. Acad. Sci. USA*, 76: 1967-1971.

Buchsteiner A, Hauss T, Dante S, Dencher NA. (2010). Alzheimer's disease amyloid-beta peptide analogue alters the ps-dynamics of phospholipid membranes. *Biochim. Biophys. Acta*, 1798: 1969-1976.

Busch KB, Kowald A, Spelbrink JN. (2014). Quality matters: how does mitochondrial network dynamics and quality control impact on mtDNA integrity? *Philos. Trans. R. Soc. Lond. B. Biol. Sci*., 369: 20130442.

Carreau A, El Hafny-Rahbi B, Matejuk A, Grillon C, Kieda C. (2011). Why is the partial oxygen pressure of human tissues a crucial parameter? Small molecules and hypoxia. *Journal of Cellular and Molecular Medicine,* 6: 1239-1253.

Carrera S, Senra J, Acosta MI, Althubiti M, Hammond EM, de Verdier PJ, Macip S. (2014). The role of the HIF-1a transcription factor in increased cell division at physiological oxygen tensions. *PLOS ONE*, 9: e97938.

Chandel NS, Maltepe E, Goldwasser E, Mathieu CE, Simon MC, Schumacker PT. (1998). Mitochondrial reactive oxygen species trigger hypoxia-induced transcription. *Cell Biology*, 95: 11715-11720.

Chen C-L, Zhang L, Yeh A, Chen C-A, Green-Church KB, Zweier JL, Chen Y-R. (2007). Site-specific S-glutathiolation of mitochondrial NADH ubiquinone reductase. *Biochemistry,* 46: 5754–5765.

Chen T, He J, Shen L, Fang H, Nie H, Jin T, Wie X, Xin Y, Jiang Y, Li H, Chen G, Lu J, Bai Y. (2011). The mitochondrial DNA 4,977-bp deletion and its implication in copy number alteration in colorectal cancer. *BMC Medical Genetics*, 12: 1-8.

Cheng L, Yang W, Hu W, Pei G, Qiu B, Zhao J, Yu Y, Guan W, Wang M. (2014). Generation of neural progenitor cells by chemical cocktails and hypoxia. *Cell Research*, 24: 665-679.

Chiu F-C, Feng L, Chan S-O, Padin C, Federoff HJ. (1995). Expression of neurofilament proteins during retinoic acid-induced differentiation of P19 embryonal carcinoma cells. *Molecular Brain Research*, 30: 77-86.

Chun Y-S, Kim M-S, Park J-W. (2002). Oxygen-dependent and -independent regulation of HIF-1 alpha. *J. Korean. Med. Sci*., 17: 581-588.

Coppola S, Ghibelli L. (2010). GSH extrusion and the mitochondrial pathway of apoptotic signaling. *Biochem. Soc. Trans.*, 28: 56-61.

Crystal H, Dickson D, Fuld P, Masur D, Scott R, Mehler M, Masdeu J, Kawas C, Aronson M, Wolfson L. (1988). Clinico-pathologic studies in dementia: nondemented subjects with pathologically confirmed Alzheimer's disease. *Neurology*, 38: 1682-1687.

Dani D, Shimokawa I, Komatsu T, Higami Y, Warnken U, Schokraie E, Schnölzer M, Krause F, Sugawa MD, Dencher NA. (2010). Modulation of oxidative phosphorylation machinery signifies a prime mode of anti-ageing mechanism of calorie restriction in male rat liver mitochondria. *Biogerontology*, 11: 321-334.

Dante S, Hauß T, Dencher NA. (2003). Insertion of externally administered amyloid beta peptide 25-35 and perturbation of lipid bilayers. *Biochemistry*, 42: 13667-13672.

Dante S, Hauss T, Dencher NA. (2006). Cholesterol inhibits the insertion of the Alzheimer's peptide Abeta(25-35) in lipid bilayers. *Eur. Biophys. J.*, 35: 523-531.

Decker V. (2016). Beeinflussung von Zellphysiologie und mitochondrialer Funktion durch Alzheimer Demenz-assoziiertes Amyloides-β Peptid (Doctoral dissertation). Technische Universität Darmstadt, Darmstadt. http://tuprints.ulb.tu-darmstadt.de/5731/.

Džinić T, Hartwig S, Lehr S, Dencher NA. (2016). Oxygen and differentiation status modulate the effect of X-ray irradiation on physiology and mitochondrial proteome of human neuroblastoma cells. *Arch. Physiol. Biochem.*, 122: 257-265.

Elmore S. (2007). Apoptosis: A review of programmed cell death. *Toxicol. Pathol*., 35: 495–516.

Eriksson PS, Perfilieva E, Björk-Eriksson T, Alborn AM, Nordborg C, Peterson DA, Gage FH. (1998). Neurogenesis in the adult human hippocampus. *Nat. Med*., 4: 1313-1317.

Fagerström S, Påhlman S, Gestblom C, Nånberg E. (1996). Protein kinase C-epsilon is implicated in neurite outgrowth in differentiating human neuroblastoma cells. *Cell Growth Differ*., 7:775-785.

Franco R, Schoneveld O, Georgakilas AG, Panayiotidis MI. (2008). Oxidative stress, DNA methylation and carcinogenesis. *Cancer Letters*, 266: 6-11.

Friedrich RP, Tepper K, Rönicke R, Soom M, Westermann M, Reymann K, Kaether C, Fändrich M. (2010). Mechanism of amyloid plaque formation suggests an intracellular basis of Abeta pathogenicity. *Proc. Natl. Acad. Sci. USA*, 107: 1942-1947.

Furda A, Santos JH, Meyer JN, Van Houten B. (2014). Quantitative PCR-based measurement of nuclear and mitochondrial DNA damage and repair in mammalian cells. *Methods Mol. Biol.*, 1105: 419-437.

Gibhardt CS, Roth B, Schroeder I, Fuck S, Becker P, Jakob B, Fournier C, Moroni A, Thiel G. (2015). X-ray irradiation activates K+ channels via H2O2 signaling. *Sci. Rep.,* 5: 13861. doi: 10.1038/srep13861.

Gil del Valle L. (2011). Oxidative stress in aging: Theoretical outcomes and clinical evidences in humans. *Biomedicine & Aging Pathology*, 1: 1–7.

Goto S, Hasegawa A, Nakamoto H, Nakamura A, Takahashi R, Kurochkin IV. (1995). Age-associated changes of oxidative modification and turnover of proteins. Oxidative Stress and Aging. Basel: Birkhäuser Basel, pp. 151-158.

Gouras GK, Tsai J, Naslund J, Vincent B, Edgar M, Checler P, Greenfield JP, Haroutunian V, Buxbaum JD, Xu H, Greengard P, Relkin NR. (2000). Intraneuronal Aβ42 accumulation in human brain. *Am. J. Pathol*., 156: 15-20.

Gultice AD, Kulkarni-Datar K, Brown TL. (2009). Hypoxia-inducible factor 1alpha (HIF1A) mediates distinct steps of rat trophoblast differentiation in gradient oxygen. *Biol. Reprod.*, 80: 184-193.

Haan C, Behrmann I. (2007). A cost effective non-commercial ECL-solution for Western blot detections yielding strong signals and low background. *J. Immunological Methods*, 318: 11-19.

Hall RD, Martinus L. (2013). Hyperglycaemia and oxidative stress upregulate HSP60; HSP70 expression in HeLa cells. *SpringerPlu*s, 2:431. doi:10.1186/2193-1801-2-431.

Halliwell B, Whiteman M. (2004). Measuring reactive species and oxidative damage in vivo and in cell culture: how should you do it and what do the results mean? *British Journal of Pharmacology*, 142: 231-255.

Hammond EM, Asselin MC, Forster D, O' Connor JP, Senra JM, Williams KJ. (2014). The meaning, measurement and modification of hypoxia in the laboratory and the clinic. *Clinical Oncology*, 26: 277-288.

Hansson Petersen CA, Alikhani N, Behbahani H, Wiehager B, Pavlov PF, Alafuzoff I, Leinonen V, Ito A, Winblad B, Glaser E, Ankarcrona M. (2008). The amyloid β-peptide is imported into mitochondria via the TOM import machinery and localized to mitochondrial cristae. *PNAS,* 105: 13145-13150.

Hardy JA, Higgins GA. (1992). Alzheimer's disease: the amyloid cascade hypothesis. *Science*, 256: 184-185.

Hartl FU. (1996). Molecular chaperones in cellular protein folding. *Nature*, 381: 571–580.

Hellmann-Regen J, Gertz K, Uhlemann R, Colla M, Endres M, Kronenberg G. (2012). Retinoic acid as target for local pharmacokinetic interaction with modafinil in neural cells. *Euro. Arch. Psychiatry. Clin. Neurosci.*, 262:697–704.

Hempel SL, Buettner GR, O'Malley YQ, Wessels DA, Flaherty DM. (1999). Dihydrofluorescein diacetate is superior for detecting intracellular oxidants: comparison with 2',7'-dichlorodihydrofluorescein diacetate, 5 (and 6)-carboxy-2',7'-dichlorodihydrofluorescein diacetate, and dihydrorhodamine 123. *Free Radic. Biol. Med.*, 27: 146-59.

Hensley K, Carney JM, Mattson MP, Aksenova M, Harris M, Wu JF, Floyd RA, Butterfield DA. (1994). A model for beta-amyloid aggregation and neurotoxicity based on free radical generation by the peptide: relevance to the Alzheimer's disease. *Proc. Natl. Acad. Sci. USA*, 91: 3270-3274.

Horowitz A, Simons M. (2008). Branching morphogenesis. *Circulation research*, 103: 784-795.

Hu X, Crick SL, Bu G, Frieden C, Pappu RV, Lee J-M. (2009). Amyloid seeds formed by cellular uptake, concentration, and aggregation of the amyloid-beta peptide. *PNAS*, 106: 20324–20329.

ICRP, 2007. The 2007 Recommendations of the International Commission on Radiological Protection. ICRP Publication 103. *Ann. ICRP,* 37 (2-4).

Ivanovic Z, Hermitte F, Brunet de la Grange P, Dazey B, Belloc F, Lacombe F, Vezon G, Praloran V. (2004). Simultaneous maintenance of human cord blood SCID-repopulating cells and expansion of committed progenitors at low O_2 concentration (3%). *Stem Cells*, 22: 716-724.

Ito S, Ohta S, Nishimaki K, Kagawa Y, Soma R, Kuno SY, Komatsuzaki Y, Mizusawa H, Hayashi J. (1999). Functional integrity of mitochondrial genomes in human platelets and autopsied brain tissues from elderly patients with Alzheimer's disease. *Proc. Natl. Acad. Sci. USA*, 96: 2099-2103.

Jao S, Ma K, Talafous J, Orlando R, Zagorski MG. (1999). Trifluoroacetic acid pretreatment reproducibly disaggregates the amyloid β-peptide. *Amyloid: Int. J. Exp. Clin. Invest*., 4: 240-252.

Jež M, Rožman P, Ivanović Z, Bas T. (2015). Concise review: the role of oxygen in hematopoietic stem cell physiology. *J. Cell Physiol.,* 230: 1999-2005.

Juhàsz G. (2016). A mitochondrial-derived vesicle HOPS to endolysosomes using Syntaxin-17. *J.Cell Biol*., 214: jcb.201603105.

Kallio PJ, Pongratz I, Gradin K, McGuire J, Poellinger L. (1997). Activation of hypoxia-inducible factor 1alpha: posttranscriptional regulation and conformational change by recruitment of the Arnt transcription factor. *Proc. Natl. Acad. Sci. USA*, 94: 5667-5672.

Kam W W-Y, Banati RB. (2013). Effects of ionizing radiation on mitochondria. *Free Radical Biology and Medicine*, 65: 607–619.

Kempf SJ, Azimzadeh O, Atkinson MJ, Tapio S. (2013). Long-term effects of ionising radiation on the brain: cause for concern? *Radiat. Environ. Biophys*., 52: 5-16.

Korecka JA, van Kesteren RE, Blaas E, Spitzer SO, Kamstra JH, Smit AB, Swaab DF, Verhaagen J, Bossers K. (2013). Phenotypic characterization of retinoic acid differentiated SH-SY5Y cells by transcriptional profiling. *PLOS ONE*, 8: e63862.

Kratochwil M. (2015). Effects of ageing, calorie restriction and ageing-associated diseases on themitochondrial proteome (Doctoral dissertation). Technische Universität Darmstadt, Darmstadt. http://tuprints.ulb.tu-darmstadt.de/id/eprint/5217.

Krause F, Seelert H. (2008). Detection and analysis of protein-protein interactions of organellar and prokaryotic proteomes by blue native and colorless native gel electrophoresis. *Curr. Protoc. Protein Sci.,* Chapter 14: Unit 14 11.

Krumm A, Carey C. (2016). Real-time monitoring of cellular metabolic activity: intracellular oxygen. Nature Methods., 13. 10.1038/nmeth.f.396.

Kulshreshtha R, Ferracin M, Wojcik SE, Garzon R, Alder H, Agosto-Perez FJ, Davuluri R, Liu CG, Croce CM, Negrini M, Calin GA, Ivan M. (2007). A microRNA signature of hypoxia. *Mol. Cell. Biol*., 27: 1859-1867.

Laberge R-M, Adler D, DeMaria M, Mechtouf N, Teachenor R, Cardin GB, Desprez P-Y, Campisi J, Rodier F. (2013). Mitochondrial DNA damage induces apoptosis in senescent cells. *Cell Death Dis*., 4: e727.

Lee CI, Haims AH, Monico EP, Brink JA, Forman HP. (2004). Diagnostic CT scans: assessment of patient, physician, and radiologist awareness of radiation dose and possible risks. *Radiology,* 231: 393–398.

Lezza AMS, Mecocci P, Cormio A, Beal MF, Cherubini A, Cantatore P, Senin U, Gadaleta MN. (1999). Mitochondrial DNA 4977 bp deletion and OH8dG levels correlate in the brain of aged subjects but not Alzheimer's disease patients. *FASEB J.*, 13: 1083–1088.

Liebler DC. (2008). Protein damage by reactive electrophiles: targets and consequences. *Chem. Res. Toxicol.,* 21: 117–128.

Lim C-Y, Zoncu R. (2016). The lysosome as a command-and-control center for cellular metabolism. *J. Cell Biol*., 214: 653–664.

Lopez MF, Berggren K, Chernokalskaya E, Lazarev A, Robinson M, Patton WF. (2000). A comparison of silver stain and SYPRO Ruby Protein Gel Stain with respect to protein detection in two-dimensional gels and identification by peptide mass profiling. *Electrophoresis*, 21: 3673-3683.

Mantel CR, O'Leary HA, Chitteti BR, Huang X, Cooper S, Hangoc G, Brustovetsky N, Srour EF, Lee MR, Messina-Graham S, Haas DM, Falah N, Kapur R, Pelus LM, Bardeesy N, Fitamant J, Ivan M, Kim KS, Broxmeyer HE. (2015). Enhancing hematopoietic stem cell transplantation efficacy by mitigating oxygen shock. *Cell*, 161: 1553-1565.

Martin BL, Schraeder-Fischer G, Busciglio J, Duke M, Paganetti P, Yankne BA. (1995). Intracellular accumulation of β-amyloid in cells expressing the Swedish mutant amyloid precursor protein. *J. Biol. Chem*., 270: 26727-26730.

Masters CL, Simms G, Weinman NA, Multhaup G, McDonald BL, Beyreuther K. (1985). Amyloid plaque core protein in Alzheimer disease and Down syndrome. *PNAS*, 82: 4245–4249.

Montero D, Tachibana C, Rahr Winther J, Appenzeller-Herzog C. (2013). Intracellular glutathione pools are heterogeneously concentrated. *Redox Biol*., 28: 508-513.

Mucke L, Masliah E, Yu GQ, Mallory M, Rockenstein EM, Tatsuno G, Hu K, Kholodenko D, Johnson-Wood K, McConlogue L. (2000). High-level neuronal expression of abeta 1-42 in wild-type human amyloid protein precursor transgenic mice: synaptotoxicity without plaque formation. *J. Neurosci*., 20: 4050-4058.

Nadin L, Murray M. (1999). Participation of CYP2C8 in retinoic acid 4-hydroxylation in human hepatic microsomes. *Biochem Pharmacol*., 58: 1201-1208.

Neff D, Dencher NA. (1999). Purification of multisubunit membrane protein complexes: Isolation of chloroplast FoF1-ATP-synthase, CFo and CF1 by blue native electrophoresis. *Biochem. Biophys. Res. Commun*., 259: 569-575.

Nemes Z, Dietz R, Lüth JB, Gomba S, Hackenthal E. Gross F. (1979). The pharmacological relevance of vital staining with neutral red. *Experientia,* 35: 1475-1476.

Noori S. (2012). An overview of oxidative stress and antioxidant defensive system. *Scientific Reports*, 1: 413. doi:10.4172/scientificreports.413.

Ono K, Condron MM, Teplow DB. (2009). Structure-neurotoxicity relationships of amyloid beta-protein oligomers. *PNAS*, 106: 14745–14750.

Packer L, Fuehr K. (1977). Low oxygen concentration exends the lifespan of cultured human diploid cells. *Nature*, 267: 423-425.

Pagani L, Eckert A. (2011). Amyloid-beta interaction with mitochondria. *International Journal of Alzheimer's Disease*, 2011: 1-9.

Parrinello S, Samper E, Krtolica A, Goldstein J, Melov S, Campisi J. (2003). Oxygen sensitivity severely limits the replicative lifespan of murine fibroblasts. *Nat. Cell Biol*., 5: 741-747.

Pathak D, Shields LY, Mendelsohn BA, Haddad D, Lin W, Gerencser AA, Kim H, Brand MD, Edwards RH, Nakamura K. (2015). The role of mitochondrially derived ATP in synaptic vesicle recycling. *J. Biol. Chem*., 290: 22325-22336.

Pedraza Muriel V. (2007). Hypofractionation in radiotherapy. *Clin. Transl. Oncol*., 9: 21-27.

Perier C, Bender A, García-Arumí E, Melià MJ, Bové J, Laub C, Klopstock T, Elstner M, Mounsey RB, Teismann P, Prolla T, Andreu AL, Vila M. (2013). Accumulation of mitochondrial DNA deletions within dopaminergic neurons triggers neuroprotective mechanisms. *Brain*, 136: 2369–2378.

Plecitá-Hlavatá L, Engstová H, Alán L, Špaček T, Dlasková A, Smolková K, Špačková J, Tauber J, Strádalová V, Malínský J, Lessard M, Bewersdorf J, Ježek P. (2016). Hypoxic HepG2 cell adaptation decreases ATP synthase dimers and ATP production in inflated cristae by mitofilin down-regulation concomitant to MICOS clustering. *FASEB J.*, 30: 1941-1957.

Pollard JW, Walker JM. (1997). Basic cell culture protocols. Methods in Molecular Biology, 75. New Jersey: Humana Press.

Powers SK, Ji LL, Kavazis AN, Jackson MJ. (2011). Reactive oxygen species: impact on skeletal muscle. *Compr. Physiol.,* 1: 941-969.

Price JL, Morris JC. (1999). Tangles and plaques in nondemented aging and "preclinical" Alzheimer's disease. *Ann. Neurol*., 45: 358-368.

Prithivirajsingh S, Story MD, Bergh SA, Geara FB, Ang KK, Ismail SM, Stevens CW, Buchholz TA, Brock WA. (2004). Accumulation of the common mitochondrial DNA deletion induced by ionizing radiation, *FEBS Letters*, 571: 227-232.

Puck TT, Marcus PI. (1956). Action of X-rays on mammalian cells. *J. Exp. Med*., 103: 653-666.

Querfurth HW, LaFerla FM. (2010). Alzheimer's disease. *N. Engl. J. Med*., 362: 329-344.

Raber J, Rola R, LeFevour A, Morhardt D, Curley J, Mizumatsu S, VandenBerg SR, Fike JR. (2004). Radiation-induced cognitive impairments are associated with changes in indicators of hippocampal neurogenesis. *Radiat. Res*., 162: 39-47.

Repetto G, del Pesso A, Zurita JL. (2008). Neutral red uptake assay for the estimation of cell viability/cytotoxicity. *Nature Protocols,* 3: 1125-1131.

Riley PA. (1994). Free radicals in Biology: oxidative stress and the effects of ionizing radiation. *International Journal of Radiation Biology*, 65: 27-33.

Rhinn M, Dollé P. (2012). Retinoic acid signalling during development. *Development*, 138: 843-858.

Rodgers CC. (2011). Dental X-ray exposure and Alzheimer´s disease: A hypothetical etiological association. *Medical Hypotheses*, 77: 29-34.

Scheffler IE. (1999). Mitochondrion. New York: Wiley-Liss Inc., pp.304-304.

Schilling-Tóth B, Sándor N, Kis E, Kadhim M, Sáfrány G, Hegyesi H. (2011). Analysis of the common deletions in the mitochondrial DNA is a sensitive biomarker detecting direct and non-targeted cellular effects of low dose ionizing radiation. *Mutation Research*, 716: 33-39.

Shipley MM, Mangold CA, Szpara ML. (2016). Differentiation of the SH-SY5Y human neuroblastoma cell line. *J. Vis. Exp.*, 108: e53193, doi: 10.3791/53193.

Schlachetzki J CM, Saliba SW, de Oliveira ACP. (2013). Studying neurodegenerative diseases in culture models. *Revista Brasileira de Psiquiatria*, 35: 92-100.

Schagger H, von Jagow G. (1991). Blue native electrophoresis for isolation of membrane protein complexes in enzymatically active form. *Anal. Biochem*., 199: 223-231.

Shokolenko I, Venediktova N, Bochkareva A, Wilson GL & Alexeyev MF. (2009). Oxidative stress induces degradation of mitochondrial DNA. *Nucleic Acids Research*, 37: 2539–2548.

Selkoe DJ. (1991). The molecular pathology of Alzheimer's disease. *Neuron*, 6: 487–498.

Shelat PB, Chalimoniuk M, Wang JH, Strosznajder JB, Lee JC, Sun AY, Simonyi A, Sun GY. (2008). Amyloid beta peptide and NMDA induce ROS from NADPH oxidase and AA release from cytosolic phospholipase A2 in cortical neurons. *J. Neurochem*., 106: 45-55.

Sipe JD, Benson MD, Buxbaum JN, Ikeda S, Merlini G, Saraiva MJ, Westermark P. (2010). Amyloid fibril protein nomenclature: recommendations from the nomenclature committee of the International Society of Amyloidosis. *Amyloid*, 17: 101–104.

Sirk D, Zhu Z, Wadia JS, Shulyakova N, Phan N, Fong J, Mills LR. (2007). Chronic exposure to sub-lethal beta-amyloid (Ab) inhibits the import of nuclear-encoded proteins to mitochondria in differentiated PC12 cells. *Journal of Neurochemistry*, 103: 1989–2003.

Soldano A, Hassan BA. (2014). Beyond pathology: APP, brain development and Alzheimer's disease. *Curr. Opin. Neurobiol*., 27: 61-67.

Soong N-W, Arnheim N. (1996). Detection and quantification of mitochondrial DNA deletions. *Methods in Enzymology*, 264: 421-431.

Stankowski JN, Codreanu SG, Liebler DC, McLaughlin BA. (2011). Analysis of protein targets by oxidative stress using the oxyblot and biotin-avidin-capture methodology. *Neuromethods,* 56: 365-381.

Stefani M. (2012). Structural features of cytotoxicity of amyloid oligomers: Implications in Alzheimer's disease and other diseases with amyloid deposits. *Prog. Neurobiol*., 99: 226–245.

Swerdlow RH, Burns JM, Khan SM. (2010). The Alzheimer's disease mitochondrial cascade hypothesis. *J. Alzheimers Dis*., 20: 265-279.

Swerdlow RH, Khan SM. (2009). The Alzheimer's disease mitochondrial cascade hypothesis: an update. *Exp. Neurol.*, 218: 308-315.

Tann AW, Boldogh I, Meiss G, Qian W, Van Houten B, Mitra S, Szczesny B. (2011). Apoptosis induced by persistent single-strand breaks in mitochondrial genome: critical role of EXOG (5'-EXO/endonuclease) in their repair. *J. Biol. Chem.*, 286: 31975-31983.

Tanzi RE, McClatchey AI, Lamperti ED, Villa-Komaroff L, Gusella JF, Neve RL. (1988). Protease inhibitor domain encoded by an amyloid protein precursor mRNA associated with Alzheimer's disease. *Nature*, 331: 528–530.

Taylor SD, Ericson NG, Burton JN, Prolla TA, Silber JR, Shendure J, Bielas JH. (2014). Targeted enrichment and high-resolution digital profiling of mitochondrial DNA deletions in human brain. *Aging Cell*, 13: 29-38.

Tiede LM, Cook EA, Morsey B, Fox HS. (2011). Oxygen matters: tissue culture oxygen levels affect mitochondrial function and structure as well as responses to HIV viroproteins. *Cell Death and Disease*, 2. 10.1038/cddis.2011.128.

Villeneuve L, Tiede LM, Morsey B, Fox HS. (2013). Quantitative proteomics reveals oxygen-dependent changes in neuronal mitochondria affecting function and sensitivity to rotenone. *J. Proteome*, 12: 4599–4606.

Wang GL, Semenza GL. (1995). Purification and characterization of hypoxia-inducible factor 1. *J. Biol. Chem*., 270: 1230-1237.

Wang J, Xiong S, Xie C, Markesbery WR & Lovell MA. (2005). Increased oxidative damage in nuclear and mitochondrial DNA in Alzheimer's disease. *Journal of Neurochemistry*, 93: 953–962.

Waseda Y, Matsubara E, Shinoda K. (2011). Fundamental properties of X-rays. X-Ray diffraction crystallography: Introduction, examples and solved problems. Berlin, Heidelberg: Springer Berlin Heidelberg, pp.1-20.

Wiesner RJ, Rüegg JC, Morano I. (1992). Counting target molecules by exponential polymerase chain reaction: copy number of mitochondrial DNA in rat tissues. *Biochem. Biophys. Res. Commun*., 183: 553-559.

Willems PH, Rossignol R, Dieteren CE, Murphy MP, Koopman WJ. (2015). Redox homeostasis and mitochondrial dynamics. *Cell Metabolism*, 22: 207-218.

Winckler J. (1974). Vital staining of lysosomes and other cell organelles of the rat with neutral red. *Prog. Histochem. Cytochem*., 6: 1-91.

Wright WE., Shay JW. (2006). Inexpensive low-oxygen incubators. *Nature Protocols,* 4: 2088-2090.

Xu S, Zhong M, Zhang L, Wang Y, Zhou Z, Hao Y, Zhang W. Yang X, Wei A, Pei L, Yu Z. (2009). Overexpression of Tfam protects mitochondria against b-amyloid-induced oxidative damage in SH-SY5Y cells. *FEBS Journal*, 276: 3800-3809.

Yapici NB, Bi Y, Li P, Chen X, Yan X, Mandalapu SR, Faucett M, Jockusch S, Ju J, Gibson KM, Pavan WJ, Bi L. (2015). Highly stable and sensitive fluorescent probes (LysoProbes) for lysosomal labeling and tracking. *Sci. Rep*., 5: 8576. doi: 10.1038/srep08576.

Yoneda M, Katsumata K, Hayakawa M, Tanaka M, Ozawa T. (1995). Oxygen stress induces an apoptotic cell death associated with fragmentation of mitochondrial genome. *Biochem. Biophys. Res. Commun*., 209: 723-729.

Zapico SC, Douglas H. Ubelaker DH. (2013). mtDNA mutations and their role in aging, diseases and forensic sciences. *Aging and Disease*, 4: 364-380.

Zhang Y, McLaughlin R, Goodyer C, LeBlanc A. (2002). Selective cytotoxicity of intracellular amyloid β peptide1-42 through p53 and Bax in cultured primary human neurons. *The Journal of Cell Biology*, 156: 519-529.

Zheng L, Cedazo-Minguez A, Hallbeck M, Jerhammar F, Marcusson J, Terman A. (2012). Intracellular distribution of amyloid beta peptide and its relationship to the lysosomal system. *Translational Neurodegeneration*, 1: 1-19.

Zhu J, Aja S, Kim E-K, Park MJ, Ramamurthy S, Jia J, Hu X, Geng P, Ronnett GV. (2012). Physiological oxygen level is critical for modeling neuronal metabolism in vitro. *Journal of Neuroscience Research*, 90: 422-434.

Zigman WB, Devenny DA, Krinsky-McHale SJ, Jenkins EC, Urv TK, Wegiel J, Schupf N, Silverman W. (2008). Alzheimer's disease in adults with Down syndrome. *Int. Rev. Res. Ment. Retard*., 36: 103-145.

Other sources:

Alzheimer's Association, 2014. Alzheimer's Disease Facts and Figures, Alzheimer's & Dementia, Volume 10, Issue 2. http://www.alz.org/downloads/Facts_Figures_2014.pdf

Alzheimer's Disease International. World Alzheimer Report 2016. https://www.alz.co.uk/research/world-report-2016

https://www.carlroth.com

https://www.emdmillipore.com

http://www.mitomap.org/

http://www.seguridadypromociondelasalud.com/n134/en/article2.html

http://www.servier.com/

https://tools.thermofisher.com

www.lgcstandards-atcc.org

8. List of abbreviations

1D	one dimensional
2D	two dimensional
3D	three dimensional
Aβ	amyloid beta
AD	Alzheimer´s disease
ADP	adenosine diphosphate
APS	ammonium persulfate
ATP	adenosine triphosphate
ATRA	all-*trans* retinoic acid
Bis-Tris	2-Bis(2-hydroxyethyl)amino-2-(hydroxymethyl)-1,3-propanediol
BN	blue native
BSA	bovine serum albumin
CCCP	carbonyl-cyanid-3-chlorophenylhydrazone
CCD	charge-coupled device
ctrl	control
Da	Dalton
DCF	dichlorfluorescein
dest.	distilled
DMEM	Dulbecco's modified Eagle's medium
DMSO	dimethylsulfoxid
DNA	deoxyribonucleic acid
DNP	2,4-dinitrophenylhydrazone
DNPH	2,4-dinitrophenylhydrazine
DPBS	Dulbecco's phosphate-buffered saline
DT	doubling time
DTT	1,4-dithiotreitol
e^-	electron
eV	electronvolt
EDTA	ethylenediaminetetraacetic acid
ER	endoplasmatic reticulum
EM	emission
EX	excitation
ECL	enhanced chemiluminescence reaction
ETC	electron tranport chain
FBS	fetal bovine serum
FITC	fluoresceinisothiocyanat
FL	fluorescence channel
FSC	forward scatter
g	gravitational acceleration
g	gram
Gy	Gray
H_2O_2	hydrogen peroxide
HEK293T	human embryonic kidney cells
HEPES	2-(4-(2-hydroxyethyl)-1-piperazineethanesulfonic acid
HEPG2	hepatoma cells
HIF	hypoxia inducible factor
HMW	high molecular weight
HO_2•	hydroperoxylradical
Hsp	heat-shock protein

HRP	horse radish peroxidase
IgG	immunoglobulin G
IR	ionizing radiation
J	Joule
k	kilo
λ	wavelength
L-Gln	L-Glutamin
LMW	low molecular weight
LTR	LysoTracker® Red
µg	Microgram
µL	Microliter
µm	micrometer
M	1 mol/l, molar
MALDI	matrix-assisted laser desorption/ionisation
MCB	monochlorbimane
mg	milligram
Milli-Q-water	purified and deionized water to a high degree
min	minute
ml	milliliter
mM	millimolar
mm	millimeter
MM	MagicMark™ XP Western ProteinStandard
MTR	MitoTracker® Red
MS	mass spectrometry
mtDNA	mitochondrial deoxyribonucleic acid
n	number of replicates
N	number of independent experiments
nDNA	nuclear deoxyribonucleic acid
NFM	neurofilament M
$O_2^{\bullet -}$	superoxide radical anion
OH•	hydroxyl radical
8-OHdG	8-hydroxy-2' -deoxyguanosine
OxPhos	oxidative phosphorylation
p	p-value
p.a.	pro analysi
PAGE	polyacrylamide gel electrophoresis
PBS	phosphate buffered saline
Pi	phosphat
PI	propidium iodide
PIC	protease inhibitor cocktail
PS	phosphatidylserine
P/S	penicillin-streptomycin
RA	retinoic acid
ROS	reactive oxygen species
RT	room temperature
SDS	sodium dodecylsulfate
SEM	standard error mean
SH-SY5Y	human neuroblastoma cells
SSC	side scatter
t	time
TEMED	N,N,N',N'-Tetramethylethylendiamin
TFA	trifluoroacetic acid

TOF	time of flight
TOM	translocase of the outer mitochondrial membrane
(v/v)	volume per volume
V	voltage
(w/v)	weight per volume
wt	wild type
% C	total cross-linker concentration
% T	total acrylamide concentration
°C	degree Celsius

9. Curriculum vitae

Tamara Džinić

Date of birth: 12/09/1988
Place of birth: Tuzla, Bosnia and Herzegovina
Citizenship: Croatian

Address: Siegfriedstraße 2, D-64646 Heppenheim
Phone: +49(0)15780345926
E-Mail: dzinic.tamara@gmail.com
Skype: tamara_dzinic

Education and experience

05/2014 - **Technische Universität Darmstadt**

PhD student in the group Physical Biochemistry, Chemistry Department
Scholar of the DFG-funded graduate college (GRK 1657) "Molecular and cellular responses to ionizing radiation"
Project: "Interplay of ionizing-radiation, oxygen, ROS and age-associated diseases" supervised by Prof. Dr. Norbert A. Dencher

Occupations

Understanding of the implication of oxidative stress, created by the interplay of ionizing (X-ray) radiation, oxygen and neurotoxic amyloid beta (Aβ) peptide, in age-associated diseases, with the focus on Alzheimer´s disease (AD)
Expertise in Cell and Molecular Biology, Biochemistry and Radiation Biology
Utilizing cell culture techniques, methods of protein and DNA analysis and microscopy
Teaching in practical courses
Supervising master thesis

Data presenting at international conferences

03/2017	68. Mosbacher Kolloquium "Cell Organelles-Origin, Dynamics, Communication", Mosbach, Germany (poster)
09/2016	Dementia and Neuroscience, Los Angeles, USA (talk)
09/2015	Mitochondria at the Crossroad, Strasbourg, France (talk)
03/2015	German Peptide Symposium, Darmstadt, Germany (poster)
02/2015	Radiation Biology and Cancer, Essen, Germany (poster)

Publishing in peer reviewed journals
(DOI: 10.1080/13813455.2016.1218518)

Attending courses and workshops for professional development

09/2015 Protein Rainbow Workshop-Mass Spectrometry in Life Sciences, DDZ, Düsseldorf, Germany

2016/2017 Organization of the PhD retreat, Annweiler am Trifels

04/2013 - 05/2014 **University of Stuttgart**
Research assistant at the Institute of Cell Biology and Immunology
Occupation: Design and development of novel recombinant protein therapeutics
(DOI: 10.1080/19420862.2016.1172163)

09/2012 - 04/2013 Applying for visa, job interview, language course and moving to Germany

University of Zagreb, Faculty of Science

10/2010 - 09/2012 Master of Molecular Biology, grade average: 4.869/5.00, 122 ECTS
Thesis: "The effect of UV irradiation on Bcl-2 and Bax proteins in mouse embryonic fibroblast culture"

10/2007 - 09/2010 Bachelor of Molecular Biology, grade average: 4.483/5.00, 180 ECTS
Thesis: "On the brink of the synthetic life forms era"
Publishing in Croatian magazine for popularization of science
(ISSN 0351-0662)

09/2003 - 06/2007 **High school St.Francis, Tuzla**
grade average: 5.00/5.00

Scholarships and awards

2017 Postdoctoral support grant by the DFG within the graduate college (GRK 1657)
2014 - 2017 PhD scholarship by the DFG in the frame of graduate college (GRK 1657)
2012 Scholarship by the University of Zagreb for excellent grades in studies
2010 - 2012 Award by the Municipality of Tuzla for outstanding achievements in studies
2008 - 2011 Scholarship by the Croatian Ministry of Foreign and European Affairs
2007 Second place regional school competition in chemistry, Tuzla

Memberships

10/2015 - SciMento, networking group for women in science

05/2014 -	Gesellschaft für Biochemie und Molekularbiologie (GBM)
11/2010 -	European Association for Cancer Research

Language skills

Croatian (native) English (full professional proficiency) German (fluent, C1 level)

Software competencies

GraphPad Prism ImageJ Kaluza CloneManager Delta2D MS Office

Hobbys and interests

volunteering (humanitarian organization for children without parents)
writing (personal narratives and essays)
creating handmade postcards

Darmstadt, 15.03.2017

_____

Eidesstattliche Erklärungen

Tamara Džinić

Siegfriedstraße 2

D-64646 Heppenheim

Darmstadt, 15.03.2017

Erklärung

Ich erkläre hiermit, dass ich meine Dissertation selbstständig und nur mit den angegebenen Hilfsmitteln angefertigt habe.

Tamara Džinić

Tamara Džinić
Siegfriedstraße 2
D-64646 Heppenheim

Darmstadt, 15.03.2017

Erklärung

Ich erkläre hiermit, noch keinen Promotionsversuch unternommen zu haben.

Tamara Džinić